Towards an accurate theoretical description of surface processes

Jiri Klimes

A dissertation submitted in partial fulfillment

of the requirements for the degree of

Doctor of Philosophy

of the

University College London.

Department of Chemistry

UCL

May 16, 2011

I, Jiri Klimes confirm that the work presented in this thesis is my own. Where information has been derived from other sources, I confirm that this has been indicated in the thesis.

Abstract

Molecular modelling methods are indispensable for both helping to understand experimental results and to explore new materials. In this thesis we focus on theoretical methods that are used to study activated processes at surfaces as well as those which can account for van der Waals dispersion forces. To begin, we examine existing methods and develop a few new ones that are suitable for identifying transition states in chemical reactions. We discuss in detail how the various methods compare in efficiency for some simple chemical processes on an NaCl surface (water diffusion and HCl dissociation). The interaction of water with salt is then extended, focussing on the interaction of water clusters (up to 20 water molecules) with clean and defected salt surfaces. The aim of this part of the thesis is to understand in detail the initial stages of NaCl dissolution. In the remainder of the thesis we focus on a problem suffered by many current density functional theory methods, namely their inability to accurately account for dispersion forces. We test a recently proposed non-local functional and show how its accuracy can be dramatically improved with some simple modifications. The new functional(s) are tested on a wide variety of materials and highly encouraging results have been obtained.

Contents

1 Introduction **12**

2 Theoretical methods **16**

2.1 Introduction . . . 16

2.2 Quantum mechanics . . . 16

2.2.1 Schrödinger equation . . . 16

2.2.2 Born-Oppenheimer approximation . . . 17

2.2.3 Many electron problem – the method of Hartree-Fock . . . 18

2.2.4 Post Hartree-Fock methods . . . 22

2.3 Density functional theory . . . 23

2.3.1 Hohenberg-Kohn Theorems . . . 25

2.3.2 Exchange-correlation functionals . . . 29

2.4 Performing a calculation . . . 37

2.4.1 Basis sets . . . 37

2.4.2 Periodic boundary conditions – Bloch's theorem and k-points . . . 39

2.4.3 Core-valence electron separation . . . 39

2.4.4 Self-consistent loop . . . 41

2.5 Empirical forcefield simulations . . . 41

2.5.1 Models and parametrisations . . . 42

2.6 Transition state theory . . . 44

2.6.1 Harmonic transition state theory . . . 45

3 Methods for locating transition states **47**

3.1 Introduction . . . 47

3.2 Methods . . . 48

3.2.1 Transition state algorithms . . . 48

3.2.2 DFT computational setup . . . 51

3.3 Water molecule diffusion on NaCl(001) . . . 54

3.3.1 NEB . . . 55

3.3.2 DHS, DHS+GS, CI-DHS . . . 58

3.3.3 Constrained optimization (CO) . . . 59

3.3.4 Dimer . . . 59
3.3.5 ART . . . 60
3.3.6 OGS . . . 61
3.4 HCl dissociation on NaCl(001) . . . 62
3.4.1 NEB . . . 64
3.4.2 DHS, DHS+GS, CI-DHS . . . 64
3.4.3 Dimer . . . 66
3.5 Summary . . . 67

4 Water clusters on NaCl surfaces and the initial stages of NaCl dissolution 70
4.1 Introduction . . . 70
4.2 Computational setup . . . 72
4.2.1 Search for low energy structures . . . 74
4.3 Results . . . 75
4.3.1 Adsorption on surfaces without vacancies . . . 75
4.3.2 Adsorption on surfaces with displaced ions . . . 78
4.4 Discussion and Conclusions . . . 86

5 Optimisation of the van der Waals density functional 90
5.1 Introduction . . . 90
5.2 Reference sets . . . 92
5.2.1 S22 set . . . 92
5.2.2 Binding curves of S22 dimers . . . 94
5.2.3 Water hexamers . . . 94
5.2.4 Water monomer on NaCl . . . 95
5.2.5 Computational setup . . . 96
5.3 Tests of the vdW-DF . . . 97
5.4 Improvements of the vdW-DF . . . 99
5.4.1 Exchange part . . . 100
5.4.2 Other correlation functionals . . . 111
5.4.3 Outlook . . . 118
5.5 Summary . . . 121

6 Van der Waals density functionals applied to solids 124
6.1 Introduction . . . 124
6.2 Computational setup . . . 125
6.3 Lattice Constants . . . 126
6.4 Bulk moduli . . . 129
6.5 Atomisation energies of solids . . . 129
6.6 The effect of non-local correlation . . . 131

6.7 Discussion and Conclusions 135

7 Conclusions and Outlook **138**

Appendices

A Test of the Na^+ H_2O dimer **141**

B Tests of forcefields for the water-NaCl system **143**

C Implementation of the vdW-DF method in VASP **149**

C.1 Implementation 149

C.2 Interaction energies of the S22 dimers 150

D Comparison of VASP to all-electron calculations for the van der Waals functional **152**

D.1 All electron density based lattice constants 152

D.1.1 Convergence tests 152

D.1.2 Comparison on the whole set 155

D.2 All electron atomisation energies 156

List of Figures

1.1 STM image of Xe atoms on Ni(110). 13

3.1 Schematic illustrations of some of the transition state search methods tested. . . 52
3.2 Example of run of the ART method. 54
3.3 Equilibrium adsorption geometry and four transition state structures on NaCl(001). 56
3.4 Example of the progress of the dimer method directed towards the O-flip transition state. 60
3.5 Energy versus number of ionic steps during two OGS runs from the energy minimum towards the O-flip TS. 61
3.6 Views of the HCl dissociation process on NaCl(001). 62
3.7 Energy pathway obtained for HCl dissociation from an eight image NEB run. . . 64
3.8 Convergence of the NEB method for the HCl dissociation using different number of images. 65
3.9 Convergence of the CI-DHS method for the HCl dissociation on NaCl(001). . . . 67

4.1 Models of the different NaCl surfaces. 73
4.2 Adsorption energies for small water clusters on NaCl(001). 74
4.3 Water clusters on the NaCl(001). 76
4.4 Small water clusters adsorbed on NaCl surface with a monoatomic step. 77
4.5 Adsorption energy of water clusters on different NaCl surfaces calculated using DFT-PBE. 78
4.6 Water clusters on the NaCl surface with Cl termination. 79
4.7 Water molecules adsorbed on a NaCl surface with a Na terminated kink. 79
4.8 Displacement vacancies on flat NaCl(001). 80
4.9 Vacancy formation energies on the flat surface. 81
4.10 The “Cl near” vacancy with different number of water molecules. 82
4.11 Displacement vacancies on the NaCl surface with a monoatomic step. 83
4.12 The vacancy formation energy on a surface with a monoatomic step. 84
4.13 Monoatomic step with a “Cl near” vacancy. 85
4.14 Displacement vacancies on the NaCl surface with a Na terminated kink. 85
4.15 Vacancy formation energies on Na terminated kink. 86

4.16 Displacement vacancies on the NaCl surface with a Cl terminated kink. 87
4.17 Vacancy formation energies on the surface with a Cl terminated kink site. 88

5.1 The molecular dimers in the S22 set 93
5.2 The low energy isomers of water hexamer 95
5.3 Water monomer adsorbed on NaCl(001) 96
5.4 Interaction energies on the S22 set with LDA, semi-local DFT functionals and revPBE-vdW. 98
5.5 The difference of the revPBE-vdW and reference interaction energies on the S22 set. 99
5.6 Results of the S22 set for tested exchange functional and the vdW correlation. . 101
5.7 The exchange enhancement factors of the functionals tested on the S22 set. . . . 103
5.8 Methane benzene binding curve calculated with revPBE-vdW, PBE-vdW, and B88-vdW functionals 104
5.9 Results of the S22 set for developed exchange functional and the vdW correlation. 106
5.10 The exchange enhancement factors of the functionals optimised on the S22 set. . 108
5.11 Formation of a dimer from two monomers 110
5.12 Effect of the change of the exchange enhancement factor on the binding curve. . 111
5.13 Comparison of the binding curves of functionals optimised for vdW correlation. . 112
5.14 Binding curve of methane · benzene dimer with different vdW functionals. 113
5.15 The results of the rPW86-vdW2 functional. 114
5.16 Comparison of the binding curves of vdW functionals. 115
5.17 The effect of adding PBE correlation to the revPBE-vdW functional shown on the S22 interaction energies. 117
5.18 Binding curve of the stacked benzene dimer calculated using revPBE-vdW and revPBE-vdW-PBEc. 118
5.19 Estimation of the semi-local PBE-like correlation energy in the vdW correlation functional. 119
5.20 Binding curve of the pyrazine dimer calculated using vdW functionals with PBE correlation added. 120

6.1 Relative erros in lattice constants 127
6.2 Relative errors in bulk moduli 131
6.3 Relative errors in atomisation energies of solids for different exchange correlation functionals 132
6.4 The effect of non-local correlation on the relative errors in lattice constant 134
6.5 The effect of non-local correlation on the relative errors in atomisation energies . 135

A.1 Water molecule interacting with Na^+ ion 141

B.1 Small water cluster formation energy calculated by different methods 145
B.2 Hydrogen bond lengths of water clusters calculated by different methods 146
B.3 Formation energy of water hexamer isomers calculated by different methods . . . 147
B.4 Water clusters on NaCl(001). 148
B.5 Water clusters tested with the optB86b-vdW functional 148

D.1 Comparison of VASP and all-electron lattice constants 156

List of Tables

3.1 Summary of the transition state search methods tested. 49
3.2 Adsorption energy of a water molecule on NaCl(001) for different number of layers in the slab. 53
3.3 Summary of the main results for the four processes of water diffusion on NaCl(001). 57
3.4 The number of ionic steps needed to converge to the transition state for HCl dissociation at NaCl(001). 63
3.5 Convergence of the DHS method for the HCl dissociation process for different convergence criteria. 66

5.1 ΔCCSD(T) calculation of binding energies of water hexamers 96
5.2 Performance of different functionals with vdW correlation on the S22 set 102
5.3 Binding energies of water hexamer isomers using vdW correlation and different exchange functionals 105
5.4 Performance of different functionals using vdW correlation on the S22 reference set. 107
5.5 Binding energies of water hexamer isomers using vdW correlation and the optimised exchange functionals 109
5.6 Differences of interaction energies for dimers in different configuration. 123

6.1 Lattice constants of solids 128
6.2 Bulk moduli of the selected solids 130
6.3 Atomisation energies of solids calculated using vdW functionals 133
6.4 Summary of the results 136
6.5 Results of the AE6 test. 136

A.1 Sodium ion – water molecule binding energy 142

B.1 Several properties of the water-NaCl system calculated with different methods. . 144
B.2 Properties of the NaCl solid and surface calculated with polarisable models. . . . 144
B.3 Adsorption energies for water clusters with one, four, and five water molecules on NaCl(001). 147

C.1 Keywords for setting exchange functionals in VASP 150

C.2 Comparison of the S22 interaction energies for revPBE-vdW calculated using different methods 151

D.1 Lattice constants of Ge using different approximations for the non-local correlation energy 153
D.2 Dependence of the Ge lattice constant on the quality of interpolation 153
D.3 Lattice constant of Ge as for three values of the charge density cut-off 154
D.4 Lattice constant of Ge without the use of the soft-correction 155
D.5 All-electron calculations of the lattice constants 158
D.6 Comparison of atomisation energies from VASP and all-electron calculations . . . 159

Chapter 1

Introduction

I remember being six or seven and arguing with our teacher who was telling us about atoms, that I saw them in water while she said that they are too small to be seen. She was, of course, right and what I saw were only tiny bubbles of air. However, my wish to see atoms was stronger than the physical capabilities and resolution of a naked eye. Luckily, though perhaps not surprisingly, I wasn't the only one dreaming about watching the atoms...

Humans have been constructing devices that allow us to see smaller and smaller objects ever since the time of the magnifying glass. Using optical microscopy object with sizes around a micrometre can be observed. Electron microscopy is able to obtain even higher resolutions but at the expense of exposing the sample to high energy electrons. Only after the development of the scanning tunneling microscope (STM) and the atomic force microscope (AFM) were we able to "see" the building blocks of matter, the atoms, without affecting the sample strongly. If this wasn't enough, in the early nineties people learned not only to "see" atoms but also to manipulate them, resulting in the stunning images by Don Eigler and co-workers [1] at IBM, such as the one shown in Figure 1.1. Even after twenty years this looks like a big leap forward. Moreover, we humans like to control and decide and now the possibility to control individual atoms has appeared, although we will probably not be able to construct machines by putting individual atoms together as was once envisaged [2]. Nevertheless, the information we can obtain from STM and AFM is indispensable for understanding interactions at the nanoscale and surface processes, which in some cases can be viewed as nanomachines on their own. By utilising the experimental information we can try to design even more useful materials, for example, for energy production and storage.

Despite the lovely images and progress in experimental instrumentation, to understand what is really going on in experiments, computational modelling methods often need to be used. At the nanoscale the interactions of atoms and molecules are simulated and thus this area of science is called molecular or atomistic modelling, which is the subject of this thesis. By constructing the system from virtual atoms and letting the forces of nature, usually based on quantum mechanics, to act we can study the system and help to explain the experimental results.

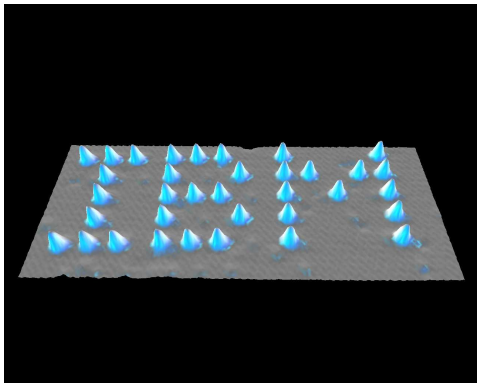

Figure 1.1: Scanning tunneling microscope (STM) image of Xe atoms adsorbed and arranged on Ni(110) to form the letters IBM [1]. Image originally created by IBM Corporation.

Moreover, for systems that are beyond the reach of experiments, such as the centre of the Earth or other planets, modelling then becomes the only tool available [3, 4]. However, the power of modelling lies in the ability of allowing us to arrange the atoms according to our will and ask the question: What if? We can explore many possibilities and study a large number of systems so that, for example, new materials with desired properties can be proposed [5]. There are several examples where modelling has been useful to accomplish this goal [6] and the future provides even bigger hope because of improving algorithms, better accuracy of the methods, and the ever increasing power of computers. In this thesis we study several aspects of theoretical methods for the nanoscale and show how they can be used to understand basic natural phenomena and processes of importance to industry. Moreover, we will show that there is still work to be done to make the methods fully reliable and thus more widely applicable. Because of the breadth of atomistic modelling methods and processes studied there are many situations which we don't discuss at all. For example, in this thesis we don't consider the interaction of systems with light which is important and widely studied. In the rest of this introduction we will discuss the relevance of the words in the title of this thesis (Towards an accurate theoretical description of surface processes) starting from the end.

There are many different applications of molecular modelling but in this thesis we concentrate on surface processes. Surfaces and interfaces are usually considered to be important, however it is often not appreciated just how crucial they are for life and technology. Everywhere around us there are interfaces, everywhere there are surfaces. They have different properties, different purposes and so it is quite difficult to pick prominent examples. Take on the one hand the basic (yet complex) interface that is formed around every living cell, the cell membrane, which blocks things from going in and out of the cell randomly and thus allows the cell to work. There are myriads of processes and reactions happening on the membrane and we are only slowly starting to understand them. On the other hand, rather different surfaces and interfaces play important roles as industrial catalysts. Catalysts are used for a simple reason: many reactions occur only slowly or result in unwanted products, by using catalysts we are able to

speed up the reactions and increase the selectivity. Two examples are the catalytic converters in cars which reduce the toxicity of the exhaust gasses, and catalysts for selective oxidation of carbohydrates that prohibit complete oxidation, *i.e.*, burning. Because of the vast importance and applications of surface processes and reactions on surfaces, to study them is one of the main tasks of computational modelling. In Chapter 3 we examine some of the methods used to study chemical reactions and reaction pathways and compare their performance in treating diffusion of a water molecule and dissociation of HCl on a NaCl surface. The methods tested allow us to discover processes likely to occur in the system and estimate the reaction rates of such processes. Ultimately, they help us to design materials with rates favourable for a specific product.

The surface studies highlight one feature of the interfaces: they are dynamic. This may not be obvious when one observes them with a naked eye but everything moves at the molecular scale. Even seemingly rigid surfaces such as those of rock salt crystals are at ambient conditions covered with water and other molecules. The molecules adsorb, move, and desorb from the surface. Not only that, the water can dissolve some of the ions which then can diffuse accross the surface, meaning that the structure of the crystal is not constant but changes over time. Overall, although the salt grains look perfectly still, they would clump together if exposed to high humidity. Chapter 4 studies the interaction of water with salt in detail and we will show what are the unexpected driving forces which cause the ions to be released from the lattice into water. This is an example where the power of current supercomputers can be exploited to study and explain natural processes.

The wide range of interfaces studied requires a wide range of computer simulation methods, some of which are described in Chapter 2. A range of methods has been developed, starting from very accurate approaches which are limited to systems with tens of atoms, to less complex methods such as density functional theory (DFT) [7], which can be applied to much larger systems [8]. For large systems methods that don't consider the electrons explicitly [9], or even group atoms together to form a coarse-grained description [10], are popular. However, one needs to be careful which method to choose, interfaces are usually large and complicated but the methods get more expensive when the size of the system is increased or when a more detailed description is required. In general, the simpler methods are less expensive and can be thus applied to larger systems or can follow the dynamics of the system for a longer time. However, being able to perform the simulation might not be useful if the method used does not describe some piece of physics or chemistry important for the system. Using more sophisticated approaches, on the other hand, usually limits the size of the system, which might disregard some effects that appear only when a large enough system is considered. For example, some surface reconstructions or adsorption structures occur over rather large surface areas [11]. One also has to keep in mind that some processes are slow and so to describe them long simulation trajectories are needed. Therefore a judicious selection needs to be done so that the method chosen is appropriate for the system of interest. For surfaces and interfaces it often becomes

necessary to consider the electrons explicitly and then DFT has proven to be extremely useful. For example, it has lead to the understanding of basic trends that govern the reactions at surfaces, ultimately giving helpful clues for the design of new catalysts [12, 6].

Modelling based on DFT has been widely used, immensely useful, and has improved the understanding of experimental observations as well as providing information about systems difficult to reach experimentally. But since approximations need to be made we often have to ask if our approach is "accurate enough" for the system studied. The phrase "accurate enough" is obviously ambiguous but we could also say "sufficient". That is, the approach we choose needs to be sufficient to describe the main characteristics of the system and of the processes that the system undergoes. Moreover, the calculated observables of interest need to agree with the experimental ones to an extent that allows us to distinguish between different processes or configurations. To say it shortly, the simulation needs to correspond closely to reality if the contribution of theory is to have some value. So how accurate is DFT? In principle, it is exact, but the problem is that the exact formula for a so-called exchange-correlation functional has not been found. So approximate DFT is sometimes "accurate enough", sometimes not, depending on the system and properties studied. For example, some well known failures relating to breaking of chemical bonds and electron self-interaction have been recently discussed in Ref. [13]. One situation which has been rather problematic for DFT are weak van der Waals forces – dispersion interactions. Although it has been clear for the last twenty years that dispersion is not described by standard functionals [14], even nowadays one can read exactly the opposite statement, appraising local functionals for the description of dispersion bonded systems such as graphite [15]. Development in this field seems to be progressing and in Chapter 5 we scrutinise one of the proposed methods, the vdW-DF functional of Dion *et al.* [16]. We show what the deficiencies are and suggest improvements that need to be made to make this method widely useful. Although we primarily use small gas phase molecular clusters for this, that is, systems different from surfaces, the example of water on the NaCl surface and especially the tests of solid state properties presented in Chapter 6, show that the results for clusters are highly relevant to the accuracy of describing surface processes.

There remains the last word in the title to be discussed: "towards". This word has probably appeared in the titles of theses about accurate methods for modelling nanoscale systems for some time and lots of computer time will be spent before it will be allowed to leave. There are accurate methods, but they require significant computational resources and can be applied only to rather small systems. They can be used for reference calculations so that less expensive yet sufficiently accurate methods can be developed. This is basically the work behind the word "towards". One of the goals for theory could be to be able to calculate adsorption energies with accuracy 5–10%, and yet perform molecular dynamics within the same approach. Although significant progress is presented in this thesis towards this goal there is still a lot of exciting work to be done.

Chapter 2

Theoretical methods

2.1 Introduction

In this part we will discuss the theories and models that are used to study matter at the molecular level. For such systems Schrödinger's equation is sufficient to describe most of the interactions. Although it looks simple, solving it for a many electron system is not and we'll discuss the theories that are used to solve it approximately. In many cases, however, the detailed knowledge of the electronic structure is not necessary and one can replace the "ab initio" interactions with simpler parametrised potentials. This much cheaper method tries to describe the effective interactions between the atoms and molecules by simple functions and we briefly discuss this approach as well.

2.2 Quantum mechanics

2.2.1 Schrödinger equation

In quantum mechanics, the Hamiltonian for matter consisting of N nuclei and n electrons can be written (using atomic units) as

$$\hat{H} = -\frac{1}{2}\sum_{i}^{n}\nabla_i^2 - \frac{1}{2}\sum_{j}^{N}\frac{1}{M_A}\nabla^2 - \sum_{iA}^{nN}\frac{Z_A}{|r_i - R_A|} + \sum_{ij}^{nn\prime}\frac{1}{|r_i - r_j|} + \sum_{AB}^{NN\prime}\frac{Z_A Z_B}{|R_A - R_B|}\,, \qquad (2.1)$$

where Z_A is the charge of nucleus A, r_i and R_A are the positions of the electrons and nuclei, respectively, and the $\prime$ sign notes that $i = j$ terms are omitted. The first two terms describe respectively the kinetic energy of the electrons and nuclei, while the electrostatic interaction of the electrons with the nuclei, the interactions between the electrons themselves, and the interactions of the nuclei are included in the last three terms. The relativistic effects leading to spin or retardation effects are not included in the Hamiltonian 2.1 but can be included approximately based on terms from Dirac's equation. Generally the importance of such terms (spin-orbit coupling or interaction of electron spin with an external magnetic field) is smaller than any of the terms in the spin-less Hamiltonian. The relativistic terms become important for example for the inner shells of heavy ions.

The time evolution of the system is given by the time dependent Schrödinger equation. For reasons that will be clear later, we are more interested in solving the time independent equation

which can be obtained for the time independent Hamiltonian by separating the wavefunction into time dependent and time independent parts. The time independent Schrödinger equation is then an eigenvalue equation for the wavefunction $\Psi(r, R)$

$$\hat{H}\Psi(r, R) = E\Psi(r, R)\,, \tag{2.2}$$

where r and R list all the electron and ionic coordinates. The system is, in principle, solved by finding the eigenstates and eigenvalues (energies) of the Hamiltonian. The solution is a wavefunction which is related to the probability density by $\varrho(r, R) = \Psi^*(r, R)\Psi(r, R)$. The lowest energy wavefunction is the ground state of the system.

Despite the simplicity of the Hamiltonian the wavefunction is a function in a $n + N$ dimensional space. That's usually a lot and it is difficult to solve even numerically except for the simplest problems. Usually the first step to reduce the complexity is to assume independence of the nuclear and electron wavefunctions and then treat the nuclei as classical particles. This is the Born-Oppenheimer approximation [17]. However, it still leaves a n dimensional equation to be solved. This is not much easier for two reasons: first, the electrons are interacting by the $1/|r_i - r_j|$ term; second, the electrons are indistinguishable. This means that the wavefunction can't be separated into single electron wavefunctions and in principle the whole wavefunction needs to be solved. Currently only a class of methods known as quantum Monte Carlo is able to try to solve the problem directly for medium sized systems [18]. Instead of the direct solution, the most widely used methods nowadays, Hartree-Fock and density functional theory, proceed by calculation of single electron orbitals and the interaction with the other electrons is accounted for in a mean field fashion, *i.e.*, the electrons interact with the density distributions of the other electrons. This crude approximation allows the problem to be solved approximately but to obtain the exact solution, or at least an approximation of it, electron correlation needs to be added. This is quite expensively done in post Hartree Fock methods and efficiently but not always accurately in density functional theory. Overall these approaches lead to methods with sufficient accuracy for many systems and properties of interest, unfortunately not for all properties of all systems. But let us now discuss the approximations and approaches more deeply.

2.2.2 Born-Oppenheimer approximation

The first approximation to the spin-less Hamiltonian divides the problem into separate equations for electrons and nuclei. The basis of the approximation comes from the fact that the nuclei are much heavier than the electrons and one can assume that the electrons follow instantaneously the nuclei. Therefore one can approximate the total wavefunction as a product of the nuclear and electron wavefunctions: $\Psi(r, R) = \Phi(R)\Psi(r; R)$, where electron wavefunction $\Psi(r; R)$ contains the nuclear coordinates only as a parameter. This Born-Oppenheimer approximation leads to

separate equations for the nuclei and electrons. The electronic Schrödinger's equation reads

$$\left(-\frac{1}{2}\sum_{i}^{n}\nabla_i^2 - \sum_{iA}^{nN}\frac{Z_A}{|r_i - R_A|} + \sum_{ij}^{nn}{}'\frac{1}{|r_i - r_j|} \right)\Psi(r;R) = E_{\mathrm{el}}(R)\Psi(r;R)\,, \tag{2.3}$$

which means that the electrons move in a potential given by the nuclei. When the positions of the nuclei change, the electrons will instantaneously follow. The electronic energy E_{el} in turn serves as a potential for the nuclei to move in. Indeed, for the nuclei one obtains

$$\left(-\frac{1}{2}\sum_{A}^{N}\frac{1}{M_A}\nabla^2 + E_{\mathrm{el}}(R) + \sum_{AB}^{NN}{}'\frac{Z_A Z_B}{|R_A - R_B|} \right)\Phi(R) = E\Phi(R)\,. \tag{2.4}$$

The crucial approximation that allowed us to obtain separate equations for electrons and nuclei was to assume that the action of the nuclear kinetic operator on the electronic wavefunction is zero. This is a good approximation in general but can be inaccurate in cases where the energy gap between ground and excited electronic states become smaller than typical energies of nuclear motion [17, 19]. This is for example violated for metals and although electron excitations caused by highly vibrationally excited molecules can be observed [20] experimentally, the approximation has proven to be accurate in a range of studies involving metals [21].

Equation (2.4) is written as an equation for the nuclear wavefunction $\Phi(R)$, the nuclei are delocalised. However, it is often sufficient to assume that the delocalisation length is small and they can be well described as point particles. This is again a very good approximation in most of the situations but can become too severe for light elements – most importantly for hydrogen for which the "quantum nuclear effects" can become important. In such cases the quantum effects can be restored using various approaches such as path integral molecular dynamics (PIMD) [22, 23, 24, 25] or the nuclear-electronic orbital (NEO) approach [26, 27, 28, 29, 30, 31].

Let us just summarise the approach that is obtained after these approximations. In the calculation we have classical point nuclei in positions R that define the potential in which the electronic wavefunction is solved and the corresponding electronic energy $E_{\mathrm{el}}(R)$ found. This can be used in several ways, for example one can systematically change the positions of the nuclei, evaluate the energy for a range of points and obtain a "potential energy surface" (PES) or a binding curve. However, from the knowledge of the wavefunction and by the virtue of the Hellman-Feynman theorem (discussed, *e.g.*, in the book of Martin [32]) the forces acting on the ions can be obtained. These forces can be used to find stationary points on the PES such as energy minima or saddle points or they can be used as an input for Newton's equations of motion to perform molecular dynamics of the nuclei [33]. Here as well the electronic wavefunction is recalculated for each position of the nuclei.

2.2.3 Many electron problem – the method of Hartree-Fock

After the BO approximation, we have to solve the time-independent Schrödinger's equation for the n-electron wavefunction $\Psi(r)$ for a given position of the nuclei R (Equation (2.3)). It is important to note that the Hamiltonian contains single particle operators that give the kinetic

energy and the interaction of the electrons with the nuclei and then the two particle electron-electron interaction term. Since this term couples two electrons, it prohibits the wavefunction from being separated exactly using single particle orbitals. The interaction between the electrons is repulsive so they will tend to "avoid each other", *i.e.*, the probability to find two electrons at the same position or close to each other will be reduced to avoid an energy penalty. Interestingly the correlations are not limited to short distances, weak correlations over the range of nanometres are caused by the same effect and both of these effects turn out to be difficult to describe.

Obtaining the exact solution would be very expensive or rather impossible and Equation (2.3) is usually solved approximately. The simplest approximate solutions of the electronic Schrödinger's equation are based on the idea that the electrons occupy orbitals. In the simplest approach by Hartree each electron occupies its own orbital[1] and the total wavefunction is then a product of the single-particle orbitals. In a simple case of two electrons this is then $\Psi(r_1, r_2) = \varphi_1(r_1)\varphi_2(r_2)$, where $\varphi_1(r_1)$ means that electron 1 occupies orbital 1. In reality, however, electrons are indistinguishable and we cannot say which electron occupies which orbital. Moreover, the Hartree product wavefunction is not antisymmetric with respect to the exchange of two particles, which is required by the fermionic nature of the electrons[2]. A simple wavefunction form that is antisymmetric is the Slater determinant, which is a combination of Hartree products. For a two particle wavefunction the Slater determinant is

$$\Psi(r_1, r_2) = \frac{1}{\sqrt{2}} \begin{vmatrix} \varphi_1(r_1) & \varphi_2(r_1) \\ \varphi_1(r_2) & \varphi_2(r_2) \end{vmatrix}, \tag{2.5}$$

the single particle orbitals are normalised which leads to the prefactor. In this simple case the terms can be written out:

$$\Psi(r_1, r_2) = \frac{1}{\sqrt{2}} \left(\varphi_1(r_1)\varphi_2(r_2) - \varphi_1(r_2)\varphi_2(r_1)\right), \tag{2.6}$$

and we see that the wavefunction is indeed antisymmetric and a combination of Hartree products. The determinantal wavefunction is written shortly as $\Psi(r_1, r_2) = |\varphi_1(r_1)\varphi_2(r_2)\rangle$ where by convention the diagonal elements are written out. When we add more electrons we can simply write the wavefunction in the form of (normalised) determinant and the antisymmetry will be preserved.

The form of the determinant based on orbitals is useful since the expectation value of the electronic Hamiltonian can be easily evaluated. For example, the kinetic term is

$$\begin{aligned} T &= \langle \Psi(r) | \hat{T} | \Psi(r) \rangle \\ &= -\frac{1}{2} \langle \varphi_1(r_1)\varphi_2(r_2)\ldots\varphi_n(r_n) | \sum_{i=1}^{n} \nabla_i^2 | \varphi_1(r_1)\varphi_2(r_2)\ldots\varphi_n(r_n) \rangle . \end{aligned} \tag{2.7}$$

[1] More accurately each electron occupies its own spin-orbital.

[2] The Hamiltonian is invariant upon exchange of two particles which implies that the wavefunction can be either symmetric or antisymmetric. Particles with a symmetric wavefunction are bosons, fermions have antisymmetric wavefunctions.

This looks like a very complicated formula at first sight: we have a sum over the kinetic energy terms for each dimension, and then two Slater determinants which are by themselves sums over $n!$ Hartree products. However, because the orbitals are orthogonal, many of the terms will be strictly zero. If we consider the kinetic operator acting on the electronic coordinate r_1, then the expectation value will be zero unless the Hartree products are identical on both sides. This leaves $n!$ terms left corresponding to the $n!$ terms in the determinant. Since the operator acts only on the coordinate r_1, the integration over the $r_2 \dots r_n$ coordinates can be performed. This will give $(n-1)!$ identical terms for each orbital. This leads to

$$T(r_1) = -\frac{1}{2n}\left(\varphi_1^*(r_1)\nabla_1^2\varphi_1(r_1) + \dots + \varphi_n^*(r_1)\nabla_1^2\varphi_n(r_1)\right) . \tag{2.8}$$

If we sum all the terms for all the electronic coordinates and realise that we can swap the electronic coordinates without changing the value we find

$$T = -\frac{1}{2}\sum_{i=1}^{n}\langle\varphi_i(r_1)|\nabla_1^2|\varphi_i(r_1)\rangle = \sum_{i=1}^{n}\langle\varphi_i(r_1)|t(r_1)|\varphi_i(r_1)\rangle\,, \tag{2.9}$$

where we have defined the kinetic energy Hartree-Fock operator. Therefore we can write the expectation value of the kinetic energy operator as a sum of expectation values of single particle orbitals. This is true in general for any single particle operator. A similar calculation can be done for the Coulomb operator. However, this is a two particle operator and the expectation value can be in fact written as a sum of expectation values of two electron Slater determinants. This means that not only the term

$$\varphi_1^*(r_1)\varphi_2^*(r_2)\frac{1}{|r_1 - r_2|}\varphi_1(r_1)\varphi_2(r_2) \tag{2.10}$$

appears, which gives the Coulomb interaction of two electron densities $|\varphi_1(r_1)|^2$ and $|\varphi_2(r_2)|^2$ and is called the Hartree term, but also a term which originates from the antisymmetry of the wavefunction

$$-\varphi_1^*(r_1)\varphi_2^*(r_2)\frac{1}{|r_1 - r_2|}\varphi_2(r_1)\varphi_1(r_2)\,. \tag{2.11}$$

Because on the right hand side the two orbitals are exchanged it is called the exchange term. The negative sign comes from the antisymmetry of the wavefunction. It is important to note that for two identical orbitals the exchange and Coulomb term cancel. Furthermore, when we consider spin, the exchange term can be only non-zero when the spins of the two orbitals are parallel. Lastly the term can be viewed as describing an electrostatic interaction between electron densities given by the product of the orbitals. Therefore it will be nonzero only when the two orbitals overlap. Overall we can write the expectation value of the electron-electron interaction for one Slater determinant as

$$E_{\text{el}} = \frac{1}{2}\sum_{ij}^{nn}\int \mathrm{d}r_1\mathrm{d}r_2\left(\varphi_i^*(r_1)\varphi_j^*(r_2)\frac{1}{|r_1 - r_2|}\varphi_i(r_1)\varphi_j(r_2) - \varphi_i^*(r_1)\varphi_j^*(r_2)\frac{1}{|r_1 - r_2|}\varphi_j(r_1)\varphi_i(r_2)\right) . \tag{2.12}$$

Being able to calculate the expectation value we can now ask which Slater determinant gives the lowest energy, that is we want to find which set of orthonormal orbitals minimises

the energy $E = \langle\Psi|\hat{H}|\Psi\rangle$. This is the idea of the Hartree-Fock (HF) method. The energy minimisation can be done by the method of Lagrange undefined multipliers minimising $L[\varphi_i] = E = \langle\Psi|\hat{H}|\Psi\rangle - \sum_{ij}\varepsilon_{ji}(\langle\varphi_i|\varphi_j\rangle\delta_{ij})$ where the second term keeps the single particle orbitals orthonormal. By performing a functional minimisation with respect to the orbitals and unitary transformation to diagonalise the matrix of the Lagrange multipliers one obtains the Hartree-Fock equations

$$(h(r_1) + \sum_j (J_j(r_1) - K_j(r_1)))\varphi_i(r_1) = \varepsilon_i\varphi_i(r_1)\,, \tag{2.13}$$

for n orbitals $i = 1, \ldots, n$. The $h(r_1)$ operator is a sum of the kinetic energy operator $t(r_1)$ and electrostatic interaction with the nuclei. The $J_j(r_1)$ and $K_j(r_1)$ are respectively the Coulomb and exchange operators which are defined by the action on the orbital $\varphi_i(r_1)$ as

$$J_j(r_1)\varphi_i(r_1) = \int \mathrm{d}r_2 \frac{\varphi_j^*(r_2)\varphi_j(r_2)}{|r_1 - r_2|}\varphi_i(r_1)\,, \tag{2.14}$$

$$K_j(r_1)\varphi_i(r_1) = \int \mathrm{d}r_2 \frac{\varphi_j^*(r_2)\varphi_i(r_2)}{|r_1 - r_2|}\varphi_j(r_1)\,, \tag{2.15}$$

and come from the electron-electron interaction described by 2.12.

Thus we have an eigenvalue equation for the single particle HF orbitals φ_i. By observing Equation (2.13) and the form of the operators one can see that in the Hartree term the electrons interact with the potential formed by the electron densities of the other electrons. This means that the HF method is a mean field method and the correlations of the electrons are accounted for only partially. Indeed, the electrons with opposite spins have non-zero probability to occupy the same position in space [34]. Although this probability is zero for the electrons with parallel spins, these correlations are still local and non-local correlations are missing from HF completely. This can be understood from the fact that the long range two electron interaction is described as an interaction of two charge densities.

We will discuss the general approach to solving electronic structure equations in more detail in Section 2.4 but let us just outline some of the computational points concerning the HF method. The usual way to find the lowest energy orbitals is to represent them using some basis set and reformulate the problem into finding the expansion coefficients. This then leads to algebraic equations for the coefficients, Roothaan's equations (the derivation can be found in Ref. [34]). It is also important to note that we have obtained a set of coupled non-linear equations, *i.e.*, the solution cannot be obtained directly since the operators J and K depend on the solution. The equations need to be solved iteratively starting from some suitable guess for the set of orbitals which is then refined in each step. Since when convergence is reached the new interaction operators are identical to the previous ones, the procedure is known as a self-consistent-field (SCF) method.

The HF theory is quite useful and captures many of the general features of the electronic structure but its accuracy is limited. Further problems arise when the ground state is far from a single determinant, which occurs for some molecules or for stretched bonds [35, 36]. Nevertheless

HF is widely used as a starting point for more complicated computational methods that describe the electron-electron correlations more accurately and which will be discussed now.

2.2.4 Post Hartree-Fock methods

The Hartree-Fock energy E_{HF} given by the single determinant is an upper limit of the exact non-relativistic electronic energy E_0. The limit can be approached or reached when the energy is minimised using not a single determinant but when a wavefunction formed by many determinants is used instead. Combining the determinants will lead to a better description of the electron correlations and of the exact wavefunction. For this reason the difference $E_0 - E_{\mathrm{HF}}$ is called the correlation energy. It's important to understand that the correlation energy is a rather arbitrary quantity that occurs only by our inability to solve Schrödinger's equation directly. In the following we briefly discuss the methods used nowadays to obtain the correlation energy, there are several good references where the methods are discussed in depth, for example the book by Szabo and Ostlund [34].

The methods that add correlation to HF (post-HF methods) usually follow the idea of adding more determinants by assuming some prescribed form for the wavefunction. For example the configuration interaction (CI) method adds determinants where one or more of the occupied orbitals are replaced by an orbital higher in energy than the highest occupied HF orbital – "excited" orbital. When determinants containing single and double excitations are added to approximate the total wavefunction the method is called CISD. If all the possible determinants are added (within the given basis set) the approach is called full-CI (FCI) which is exact within the basis set. However, it is usually not possible to perform an FCI calculation because the number of determinants rises quickly with the size of the basis.

One of the problems of the CISD approach is that it is not size extensive: the sum of the CISD energies of two species calculated separately differs from the CISD energy calculated for a dimer in infinite separation. One popular method that does not suffer from this deficiency is the coupled cluster (CC) approach (see Ref. [37] for a recent review). Here the wavefunction is written as $\Psi_{\mathrm{CC}} = \exp(T)\Psi_{\mathrm{HF}}$, where T is an operator that includes single, double, triple, ... excitations. Because the cost increases quickly with the number of excitations included, single and double excitations are most often used with the effect of triple excitations accounted for perturbatively. This is the CCSD(T) method [38] which has become the "gold standard" for quantum chemistry reference calculations. However, because of the high cost the method is limited to small systems and is often used only to obtain reference data which are used to assess more approximate approaches.

It's also possible to use perturbation theory starting with the HF Hamiltonian and wavefunction. The perturbation is chosen to replace the mean field HF electron interaction term with the Coulomb operator. The cost of this approach increases with the order of the perturbation included and most often second order energy corrections are evaluated, referred to as second order Møller-Plesset theory (MP2) [39]. The MP2 method is used for many reference calculations

since it's cheaper than CCSD(T). However, it's less accurate, for example for stacked systems such as two benzene molecules in a sandwich configuration [40, 41, 42]. Even more seriously, it fails for systems with zero band-gap such as metals where the energy correction diverges [43, 44].

The most serious problem of the post-HF methods is their computational cost caused by unfavourable scaling with the size of the basis set. For example MP2 scales as $O(m^5)$, CCSD(T) as $O(m^7)$ with m being the number of basis set functions. Although computational algorithms are being constantly improved and new methods developed (see Refs. [45, 46] for up to date reviews), the size of systems that can be tackled using method such as CCSD(T) is limited to tens of atoms. A class of methods that has a more favourable scaling with the size of the system and can be, in principle, used to find the wavefunction is called quantum Monte Carlo (QMC) [18]. As the name suggests the wavefunction is found by a stochastic procedure. As with other stochastic methods the error decreases only slowly with the length of simulation which usually makes the methods very expensive. A good parallelisation, on the other hand, means that the method has been used to obtain reference interaction energies for systems too large for traditional quantum chemistry approaches [47]. In an interesting recent approach the stochastic QMC approach has been used to obtain the FCI wavefunction [48, 49] for systems larger than traditional approaches based on diagonalisation have achieved.

One of the details to notice is that in principle one doesn't have to use the HF wavefunction as the initial guess. Indeed, if we used a different starting determinant and performed an FCI calculation then we would obtain the same exact wavefunction and energy. Since the energy of the original determinant is different from the HF energy, the correlation energy would differ from the post-HF correlation energy. In the context of the DFT, the HF-like total energy is often referred to as "exact exchange", although there are reasons for this name, they should correspond to the fact that the form of exchange cancels the electron self-interaction and not to the value of the energy. In fact, the exchange energy in a multideterminantal wavefunction comes not only from the HF wavefunction but from all the determinants. The exchange energy is then the part of the electron-electron interaction that comes from the exchange of two particles and a portion of it is basically a part of the correlation energy.

2.3 Density functional theory

Not only is the full wavefunction difficult to calculate, it's also big to store in computer memory. Studying realistic systems without a large amount of memory is just not feasible. Trying to use the electron density, only a three dimensional function, instead has been a popular idea already since the days of early quantum mechanics (*e.g.*, the Thomas-Fermi model and subsequent developments discussed in the book by Parr and Yang [50]). However, only after developments made by Hohenberg, Kohn, and Sham [51, 52] did the approach become accurate enough to be applied to realistic systems. Moreover, the much better scaling with the system size than the post-HF method has lead to a tremendous increase of the size of the systems that can be treated with a sufficient accuracy. We discuss the developments in this section.

The idea of using the electron density instead of the full wavefunction to evaluate the terms in the Hamiltonian 2.3 comes out naturally. Consider for example the interaction of the electrons with the nuclei which is defined as

$$\begin{aligned} E_{\text{nuc}} &= -\langle\Psi| \sum_{iA}^{nN} \frac{Z_A}{|r_i - R_A|} |\Psi\rangle \\ &= -\int \mathrm{d}r_1 \dots \mathrm{d}r_n \Psi^*(r_1 \dots r_n) \sum_{iA}^{\mathrm{nN}} \frac{Z_A}{|r_i - R_A|} \Psi(r_1 \dots r_n)\,. \end{aligned} \tag{2.16}$$

The sum over the electrons can be written explicitly

$$\begin{aligned} &-\int \mathrm{d}r_1 \dots \mathrm{d}r_n \Psi^*(r_1 \dots r_n) \sum_{A}^{\mathrm{N}} \frac{Z_A}{|r_1 - R_A|} \Psi(r_1 \dots r_n) - \dots - \\ &-\int \mathrm{d}r_1 \dots \mathrm{d}r_n \Psi^*(r_1 \dots r_n) \sum_{A}^{\mathrm{N}} \frac{Z_A}{|r_n - R_A|} \Psi(r_1 \dots r_n)\,. \end{aligned}$$

Now we have n terms where in each the electron with coordinate r_i interacts with the potential of the nuclei. However, because of the antisymmetry of the wavefunction if we swap, e.g. r_1 and r_2 in Ψ, the only change will be in the sign. Since the wavefunction is present two times in the integration, there will be no change in the sign. Therefore the terms are identical and we can sum them as

$$-n \int \mathrm{d}r_1 \dots \mathrm{d}r_n \Psi^*(r_1 \dots r_n) \sum_{A}^{\mathrm{N}} \frac{Z_A}{|r_1 - R_A|} \Psi(r_1 \dots r_n)\,. \tag{2.17}$$

The integration can be now split into an integral over r_1 and over the rest of the coordinates:

$$-\int \mathrm{d}r_1 \sum_{A}^{\mathrm{N}} \frac{Z_A}{|r_1 - R_A|} n \int \mathrm{d}r_2 \dots \mathrm{d}r_n \Psi^*(r_1 \dots r_n) \Psi(r_1 \dots r_n)\,. \tag{2.18}$$

The term in the integration over the $r_2 \dots r_n$ coordinates is just the definition of the electron density

$$\varrho(r_1) = n \int \mathrm{d}r_2 \dots \mathrm{d}r_n \Psi^*(r_1 \dots r_n) \Psi(r_1 \dots r_n) \tag{2.19}$$

and therefore we finally obtain

$$E_{\text{nuc}} = -\int \mathrm{d}r \sum_{A}^{\mathrm{N}} \frac{Z_A}{|r - R_A|} \varrho(r)\,, \tag{2.20}$$

where we have dropped the index for the electron coordinate. The sum over nuclei gives rise to the Coulomb potential $v_{\text{nuc}}(r) = -\sum_j^{\mathrm{N}} Z_j/|r - R_j|$ so that the energy becomes simply

$$E_{\text{nuc}} = \int \mathrm{d}r v_{\text{nuc}}(r) \varrho(r)\,. \tag{2.21}$$

The Coulomb interaction is just one example of a single particle local potential, and the formula for some local external potential $v_{\text{ext}}(r)$ can be generally written as

$$E_{\text{ext}} = \int \mathrm{d}r v_{\text{ext}}(r) \varrho(r)\,. \tag{2.22}$$

This formula shows us that the energy of the interaction of the electrons with the external potential can be written as a simple functional of the electron density $E_{\text{ext}}[\varrho]$. Similarly the classical Coulomb energy of electron density can be written as[3]

$$E_{\text{class}} = \int \mathrm{d}r_1 \mathrm{d}r_2 \frac{\varrho(r_1)\varrho(r_2)}{|r_1 - r_2|}\,. \tag{2.23}$$

Therefore the electron density is clearly a useful variable that looks promising for evaluation of the energy. However, not all terms in the electron Hamiltonian can be easily written as a functional of the density. First of all, the kinetic energy, otherwise a straightforward expectation value when single particle orbitals are available, is problematic to obtain as a functional of the density. The first kinetic energy functionals due to Fermi, Thomas and others based on the non-interacting uniform electron gas (UEG) model completely fail when applied to atoms and molecules. It is well known that they lead to atoms without a shell structure and molecules that don't bind. Only recently has progress been made and a non-local kinetic energy functional was devised that was able to bind simple molecules [53]. It is, however, far from being generally applicable.

There is another term where the coordinates of all except one electron can't be integrated out to obtain an explicit functional of the electron density and that is the electron electron interaction. Here the procedure leads to an equation

$$E_{\text{el}} = \int \mathrm{d}r_1 \mathrm{d}r_2 \frac{\gamma_2(r_1 r_2, r_1 r_2)}{|r_1 - r_2|}\,, \tag{2.24}$$

where $\gamma_2(r_1 r_2, r_1 r_2)$ is the second order spin-less reduced density matrix (2-RDM). This, in analogy to the electron density $\varrho(r_1)$ is obtained by integrating out all the electron (and spin) coordinates of the product $\Psi^*(r'_1, \ldots r'_n)\Psi(r_1, \ldots r_n)$ except for the first two. Note that Equation (2.24) is exact and includes any problematic effect that burdens single particle theories (HF or DFT) that use the electron density [54, 55, 56] such as strong and weak correlations. However, a direct minimisation of the energy using Equation (2.24) for the electron-electron energy leads to energies that are lower than the exact values [57, 58, 59, 60]. This is because 2-RDMs that don't correspond to any n-particle wavefunction, and thus should not be included, are also considered in the search. Although the problem has been recognised a long time ago [61] only recently has progress been made in finding and defining non trivial n-representability conditions as well as reducing the computational effort [62, 63].

2.3.1 Hohenberg-Kohn Theorems

Since it is difficult to apply the post-HF methods to larger systems, a large effort has been put into using the electron density as the main variable. The main impulse to this development is due to two theorems of Hohenberg and Kohn who have shown that, in principle, the electron density is sufficient to obtain the exact solution and can be used as the optimisation variable.

[3] Note that this formula gives the charge-charge interaction where individual electrons interact with themselves. Although exactly the same formula appears in the HF theory, the self-interaction is removed there exactly by the exchange term.

Furthermore Kohn and Sham reintroduced the orbitals in the theory which allows one to obtain the kinetic energy rather accurately as well as resulting in independent particle equations. This leads to equations which are less computationally demanding than the HF method and can achieve similar or better accuracy for a wide range of systems. We now discuss this in a more detail.

We start with the two Hohenberg and Kohn theorems. First we consider a Hamiltonian in the form given by the Schrödinger's equation for the electrons:

$$H = T + V + U\,, \tag{2.25}$$

which contains the kinetic operator T, V gives the interaction of the electrons with an external potential v_{ext}, and U is the electron-electron interaction operator. The first Hohenberg-Kohn theorem proves that for some n-electron system the local external potential v_{ext} is uniquely determined by the electron density and vice versa. The way from the potential to the density is straightforward: since we know the v_{ext} and the number of electrons we can solve the Schrödinger's equation and obtain the all-electron wavefunction Ψ. From Ψ we obtain the density ϱ by a simple integration. (Here we have assumed that the solution is non-degenerate.) Thus the external potential leads to a unique density. Now we want to prove that given the density there can be only one external potential v_{ext} that generated it. This can be done in a rather surprisingly simple way and proceeds by *reductio ad absurdum*. Suppose that we have v'_{ext} an external potential that differs from v_{ext} by more than a constant and yet it leads to the same density ϱ. Now we calculate the all-electron wavefunctions corresponding to the two external potentials. The solutions Ψ and Ψ' must differ since they correspond to different Hamiltonians H and H'. From the variational principle we know that Ψ minimises the energy of H and therefore

$$E = \langle\Psi|H|\Psi\rangle < \langle\Psi'|H|\Psi'\rangle\,. \tag{2.26}$$

Since the Hamiltonians differ only in the external potential, we can use $H = H' - V' + V$ and write

$$E = \langle\Psi|H|\Psi\rangle < \langle\Psi'|H|\Psi'\rangle = \langle\Psi'|H' - V' + V|\Psi'\rangle = E' + \langle\Psi'| - V' + V|\Psi'\rangle\,. \tag{2.27}$$

Since we assumed that the external potential is a local single particle operator, we can rewrite the expectation value as

$$\langle\Psi'| - V' + V|\Psi'\rangle = \int \mathrm{d}r(v(r) - v'(r))\varrho(r)\,. \tag{2.28}$$

Overall we have obtained that

$$E < E' + \int \mathrm{d}r(v(r) - v'(r))\varrho(r)\,. \tag{2.29}$$

Now we can repeat the procedure starting from E' which will only change the primes and we obtain

$$E' < E + \int \mathrm{d}r(v'(r) - v(r))\varrho(r)\,. \tag{2.30}$$

Finally the equations can be summed giving

$$E + E' < E + E' \,, \tag{2.31}$$

which is false. This implies that we can't obtain exactly the same density for different v_{ext}, *i.e.*, for different systems. That is the v_{ext} is uniquely determined by the electron density. This means that also the all-electron wavefunction is uniquely determined by the electron density. This, in principle, is a very powerful finding. Anything for which Ψ is needed can be obtained only from the electron density. This, of course, means that also the total energy can be obtained from the electron density, since that's just the expectation value of the Hamiltonian using Ψ. Specifically, the sum of the kinetic and electron-electron energies can be written as a functional of the density

$$F[\varrho] = \langle \Psi | T + U | \Psi \rangle \,, \tag{2.32}$$

since the Ψ is given by ϱ. The functional $F[\varrho]$ is a general functional that can be used with any external potential and gives us the exact kinetic and electron-electron energies. Therefore the total energy can be written as a functional of the electron density

$$E[\varrho] = \int \mathrm{d}r v_{\text{ext}}(r)\varrho(r) + F[\varrho] \,. \tag{2.33}$$

This way we have basically rewritten E using density while the dependence on Ψ is kept via Equation (2.32). Therefore for some external potential v_{ext} the energy given by correct density ϱ will be just the ground state energy given by ground state Ψ. However, not only that, we can use the density as the optimisation variable since $E[\varrho]$ has a minimum when evaluated on the ground state density. (Among all v-representable densities, *i.e.*, densities corresponding to some external potential.) This follows easily when one realises that this variational principle holds for the ground state wavefunction Ψ. Indeed, if we evaluated $E[\varrho]$ using a ground state density ϱ' corresponding to a different external potential v'_{ext}, we would have to use the ground state wavefunction Ψ' which must give higher energy than Ψ and therefore $E[\varrho] < E[\varrho']$ which is the second HK theorem.

Overall the Hohenberg-Kohn theorems allow us to search for the ground state using only the density as the variational variable and a universal functional $F[\varrho]$. There is, of course a well known problem: although we know the form for $F[\varrho]$ (Equation (2.32)), this is an equation which uses the all-electron wavefunction. The electron density is involved only in the sense that Ψ is uniquely determined by ϱ. Obtaining an explicit formulation for $F[\varrho]$ in terms of density is much more difficult and does not seem to be possible for realistic systems with some approximations needed to be used instead. The functional $F[\varrho]$ contains the Coulomb interaction of the electron density which is written separately to obtain

$$E[\varrho] = \int \mathrm{d}r v_{\text{ext}}(r)\varrho(r) + \int \mathrm{d}r\mathrm{d}r' \frac{\varrho(r)\varrho(r')}{|r - r'|} + G[\varrho] \,, \tag{2.34}$$

where $G[\varrho]$ now describes the kinetic energy and the difference between the exact electron-electron interaction and the electrostatic interaction given by the electron density ϱ. Therefore $G[\varrho]$ has to include the electron correlations and the effects arising from the exchange term.

As we have mentioned before, it is very difficult to obtain a kinetic energy density functional that leads to a good description of molecular systems. In 1965 Kohn and Sham introduced an auxiliary system of non-interacting electrons which has the same density as the real system. For this system the kinetic energy is calculated exactly (similar to HF). Therefore the functional $G[\varrho]$ is rewritten as $G[\varrho] = T_s[\varrho] + E_{xc}[\varrho]$, where T_s is the kinetic energy of the non-interacting electrons and E_{xc} sums all the other terms, the subscript "xc" is a abbreviation for exchange and correlation. The point of the Kohn-Sham scheme is that the equations for the orbitals are identical to Schrödinger's equation applied to a system of non-interacting electrons with an external potential

$$v_{\text{ext}}^{\text{KS}}(r) = v_{\text{ext}}(r) + \int \mathrm{d}r' \frac{\varrho(r')}{|r - r'|} + \frac{\delta E_{xc}[\varrho]}{\delta \varrho(r)} \,. \tag{2.35}$$

The last term is the unknown exchange correlation potential μ_{xc}. The equations are analogous to the Hartree-Fock equations but the Fock exchange term is not written explicitly but rather included in E_{xc}. Still at this point we face the problem of finding an accurate form for the exchange-correlation functional. Kohn and Sham proposed a form for the exchange correlation functional which is exact for the UEG system, the local density approximation (LDA). This choice not only gives a local potential but also is a local functional. Although exact for the UEG, it completely ignores the non-locality of the interactions and is exact only because of the symmetry of the problem. If we split the UEG into two halves (together with its positive background) with an infinite barrier and increased the separation, the energy using LDA would be independent of the separation which is not correct [64]. Despite the crude approximations the KS equations using LDA made possible to tackle solid state systems with cost much lower compared to HF or even post-HF methods and with comparable accuracy [65, 66]. On the other hand there are many systems where LDA gives terrible results [67, 68, 69, 70, 71] and functionals have been developed that try to improve upon LDA, some of which we discuss in the next Section.

However, before discussing the various functionals we need to mention one general point. The E_{xc} functionals are meant to describe the exchange correlation effects correcting for: i) the self interaction of the electrons; and ii) terms originating from the difference between description using a single determinant and the exact wavefunction (which we can think of as a weighted sum of a large number of determinants). This latter part contains both Coulomb and exchange energy integrals. Therefore, one could try, in principle, to fit the exchange functionals to all the exchange energies coming from all the determinants. However, this is not the case in DFT and a different approach is used that the exchange fitted to HF energies. This originates from the formula for the exchange-correlation energy calculated using the adiabatic-connection fluctuation-dissipation theorem (ACFDT). In this method the exact exchange-correlation energy can be written as $E_{\text{xc}} = E_{\text{x,HF}} + E_{\text{c}}$, where the first term is the HF-like electron exchange interaction evaluated using the KS orbitals. The second term is the correlation energy which, however, requires knowledge of an unknown exchange-correlation kernel to be obtained exactly.

In DFT the exchange energy has been defined to be the first term and exchange functionals are fitted or tested on reproducing the single determinant energy. On the one hand this is a clear definition and the functionals developed seem to work, on the other hand it is hard to imagine that this makes sense when the reference atom or molecule have some other determinant of comparable importance to the HF determinant in the exact wavefunction. This effect might not lead to "obvious" changes in the density which would have to be captured by the correlation functional. Furthermore, the correlation part effectively needs to cancel part of the HF-like exchange term to reduce its importance in the final energy.

2.3.2 Exchange-correlation functionals

As was shown in the previous part the problem of finding the many-body wavefunction for some external potential can be recast in a variational problem using solely the electron density. Furthermore, this approach would be exact if the exact form for the exchange-correlation functional was known. Since this is not available for realistic systems, the form of E_{xc} needs to be approximated. A large number of approximations have been proposed that differ in the amount of information they need. Traditionally they are classified into functionals that use only the local electron density (*i.e.*, LDA), local gradient of the density (generalised gradient approximation (GGA) functionals), or local Laplacian of the density (or orbital kinetic energy), these functionals are called meta-GGAs. The effectively local treatment of the intrinsically nonlocal interactions leads to several issues with these functionals which have varying severity depending on the system studied. The local exchange leads to improper cancellation of the self-interaction coming from the Hartree term. This, for example, causes too strong delocalisation of charge in some chemical reactions [72, 73, 74] or in systems with the electron detached from molecules [75, 76]. It can also lead to an incorrect description of radicals [77]. Self-interaction correction schemes [69, 78, 77] are one way of improving the description of the systems in such cases. Further problems arise because the non-local electron interaction is described as a Coulomb interaction of two electron densities which completely fails to describe the non-local correlations (dispersion) interactions. Attempts to alleviate problems in both exchange and correlation have been made by introduction of the KS orbitals into the form of E_{xc}. For the exchange part the Fock exchange term can be included leading to "hybrid" functionals while adding an energy term analogous to MP2 or other post-HF method leads, for example, to doubly hybrid functionals. In the last step, the calculations become analogous to a post-HF procedure. We discuss briefly some of the functionals in the following.

Let us first discuss the simplest approximation for the E_{xc}, the LDA. Here the exchange-correlation energy is written as

$$E_{\mathrm{xc}}^{\mathrm{LDA}} = \int \mathrm{d}r \varrho(r) \varepsilon_{\mathrm{xc}}^{\mathrm{LDA}} \,, \tag{2.36}$$

where $\varepsilon_{\mathrm{xc}}^{\mathrm{LDA}}$ is the exchange-correlation energy density of the UEG. The exchange part of LDA uses the HF exchange energy of the UEG which can be evaluated analytically. Thus for this

system the LDA gives the DFT exchange energy exactly. Furthermore the UEG system can be solved to a high accuracy using approaches such as quantum Monte Carlo, and therefore the correlation energy between the non-interacting and interacting systems can be obtained. This is usually done for a range of densities and interpolated with a suitable functional form. Parametrisations of LDA devised by Ceperley and Alder [79], Perdew and Zunger [69], Perdew and Wang [80], or Vosko, Wilk, and Nusair [81] are often used in functionals that build on LDA and try to achieve a better accuracy.

Already in the paper of Kohn and Sham it was noted that the worst performance can be expected from LDA when applied to atoms and molecules. Indeed, while description of structural properties of solids is acceptable [82], atomisation energies of molecules are too large [70] (and in fact, they are too large for solids as well). The simplest recipe that was devised consists of including a dependence on the gradient of the electron density in the form of E_{xc}. This gradient correction originally comes from studies of a slowly varying electron gas. For this system the exchange energy density was found to depend on the density gradient as $\varepsilon_{\mathrm{x}} = \varepsilon_{\mathrm{x}}^{\mathrm{LDA}}(1 + \mu s^2)$, where $\mu = 10/81$ and s is the reduced density gradient $s = |\nabla \varrho|/2(3\pi^2)^{1/3}\varrho^{4/3}$. In a similar manner functional forms that depend on the s, so-called enhancement factors, multiply the LDA exchange and correlation forms to make the functional more accurate for atoms and molecules. This leads to so-called generalised-gradient approximation (GGA) functionals. However, as it turns out, when one tries to use the slowly varying electron gas gradient correction the errors of the atomisation energies are only halved compared to LDA. Still this is not surprising since even this model is far from a typical atom. It has been found empirically that using μ twice as large leads to much better results for molecular atomisation energies and values similar to 2μ are used in many functionals for small s (below $\approx$1). Overall, there is a large number of various GGA functionals since the physical requirements for the enhancement factors are insufficient to obtain a unique functional. The most popular functional for surface calculations is the Perdew-Burke-Ernzerhof (PBE) [83] which is based on the Perdew-Wang (PW91) [84] functional. For molecular calculations, the exchange functional of Becke (B88) [85] coupled with correlation functionals of either Lee-Yang-Parr (LYP) [86] or Perdew (P86) [87] are used.

It has been realised recently that the empirical values of μ that give good atomisation energies give lattice constants and bond lengths that are on average too long. For these properties the original slowly varying electron gas value of μ seems to be more appropriate. Since only one value of μ can be used in a GGA functional, there has been an interest in so-called meta-GGA functionals which add the dependence on the orbital kinetic energy or the Laplacian of the density. This way it can be used to "distinguish" between areas which are molecule-like and areas which are solid-like. The latest proposed form, revTPSS [88] functional tries to follow both the limits and seems to give promising results for both the lattice constants and the atomisation energies.

The local treatment of the exchange and correlation gives good results for many systems.

However, this has been attributed to a cancellation of errors which does not always work [89, 90]. Moreover, non-local correlations are omitted so that electron dispersion forces are not included, and the exchange formula fails to correct for self-interaction of electrons. While we will discuss the first problem in the following part, it has been argued that including some Fock-like exchange will reduce the self-interaction problem. This is because the Fock term cancels exactly the electron interaction with itself in HF theory. The resulting functionals are called hybrid functionals since one might view them as hybrids between KS and HF theories. Viewed from the side of HF theory, adding some exchange and correlation terms to it can, to some extent, mimic the expensive post-HF procedures and thus improve the results. The hybrids were found to improve atomisation energies [91] and reaction barriers and are widely popular in codes using atomic-centered orbitals, especially the B3LYP [92] formulation. However, there is a problem for extended systems, especially for metals, since in reality the exchange is screened at long range which is not properly done with normal correlation functionals [93]. Thus adding Fock exchange is problematic for a large class of problems. Nevertheless, the hybrids are useful for cluster calculations or for solid state calculations with strong self-interaction errors. In the solid state modifications of the PBE form known as PBE0 [94] and HSE [95, 96] (where the long-range Fock part is screened) are commonly used. Let us mention that there is also an interesting idea of using non-local density functionals for exchange without invoking the Fock term [97]. This seems to be a good idea since the Fock-like exchange term cancels only the self-interaction of the KS orbitals and not the self-interaction of the other determinants when one uses the point of view of the post-HF methods.

Let us close this part by mentioning a problem of the classes of functionals presented: there is no systematic improvement upon making the functionals more complex. For example lattice constants of diamond, silicon and germanium are very accurate when LDA is used and all the GGAs lead to worse results. This is in a stark contrast with the HF and post-HF methods where the properties approach the exact non-relativistic limit when more and more determinants are added and the basis set size is increased.

2.3.2.1 Including electron dispersion in density functional theory

As we have stressed previously, most of the exchange-correlation functionals used nowadays approximate the energy from local information such as the value of the density and its derivative. This form ignores non-local effects such as electron dispersion (also called London dispersion or van der Waals dispersion) which is caused by non-local electron correlations and gives rise to a well known $1/r^6$ long range interaction. In times when DFT was used to treat condensed matter, this was not a big problem[4]. However, growing interest in systems where dispersion is important such as biomolecules or physisorbed molecules on surfaces has lead to a growth of interest in methods able to describe dispersion. Because the local functionals give contributions

[4] Although the form of description of electron correlation that would be appropriate for surface energy calculations of UEG relevant to metals was discussed in 1970's [98, 64, 99, 100, 101].

from regions of electron density overlap, they will be only able to give exponentially decaying interaction energies. Although there are constant attempts to construct local functionals for dispersion [102, 103], they are ultimately doomed to fail, this can be seen for example in Ref. [104]. Here we describe and discuss some of the methods available that correct this behaviour.

Probably the most popular approach approximates the missing dispersion interaction by an attractive energy term acting on the nuclei

$$E_{\text{disp}} = \sum_{ij}^{NN}{}' C_{ij}^{\text{AB}} \frac{f(r_{ij})}{r_{ij}^6}\,, \tag{2.37}$$

which is added to the total energy calculated using standard exchange-correlation functionals. In the formula r_{ij} represents the distance of the atoms, C_{ij}^{AB} is a dispersion coefficient for a pair of elements A and B. The function $f(r_{ij})$ is a damping function which removes the divergence of the $1/r^6$ function for small separations. It is interesting to note that this correction was originally proposed to correct the HF method (which also fails for dispersion) [105]. The good point about this approach is that the evaluation of E_{disp} is very fast compared to the rest of the DFT calculation. Therefore corrections of this type are quite popular and several have been proposed [106, 107, 108, 109, 110]. The dispersion coefficients are the main weakness of the method since they are usually kept constant for each pair of elements. This, however, can be a severe approximation since the actual coefficients change due to the environment or depending on the hybridisation of the atom [111]. More recently methods that try to rectify this have been proposed [111, 112]. They reduce the empiricism by the use of reference polarisability data. The polarisability is important since the leading isotropic long range dispersion interaction coefficient can be calculated by a Casimir-Polder integral [113]

$$C^{\text{AB}} = \frac{3}{\pi}\int_0^\infty \mathrm{d}\omega \alpha_{\text{A}}(i\omega)\alpha_{\text{B}}(i\omega)\,, \tag{2.38}$$

where $\alpha_{\text{A}}(i\omega)$ is the polarisability of atom or molecule A at an imaginary frequency $i\omega$. Two recent approaches that build upon this formula are those by Tkatchenko and Scheffler [111] and by Grimme *et al.* [112]. The first method uses a database of accurate reference coefficients and scales them according to the change of the volume occupied by the atom. This reflects the dependence of the polarisability on the change of the volume: atoms that are "squeezed" are less polarisable and thus interact less than more free atoms. The approach of Grimme *et al.* [112] calculates the polarisabilities from time-dependent DFT (TDDFT) data to obtain the dispersion coefficients. The effect of the environment is approximated by making the dispersion coefficient depend on the number of neighbouring atoms. This again tends to decrease the errors compared to coefficients that are constant. Despite this development, there are several weak points of these approaches. First of all, the interaction does not come directly from the density and large changes in density are difficult to address (*e.g.*, the change from Na to Na^+). Furthermore, although the dispersion coefficients can be very accurate, the $1/r^6$ interaction needs to be removed for small separations by using the damping function $f(r)$. This damping

is made in the part of the binding curve where the effect of repulsion is strong and thus the damping function affects the position of the minimum on the binding curve. This also means that if one wants to obtain similar binding minima with PBE or BLYP functionals, the damping function needs to differ considerably for the two functionals since they give quite different binding curves [108, 114]. Furthermore, as one can observe, the E_{disp} term is always attractive and the binding will always increase. Therefore the E_{disp} should be used with a functional which does not overbind without the dispersion correction, this is not always done and for example the PBE functional is often used. This means that for systems such as small water clusters [114] where PBE overbinds the absolute errors are increased. For such a choice of functional the method becomes much more sensitive to the choice of the damping function [115].

An interesting approach to include the non-local correlations is to add them explicitly as correlations between the KS orbitals using some formula analogous to a post-HF method. The short range effects are then treated using some DFT functional which means that less effort is needed to describe short-range correlations than if a post-HF approach was used. The short- and long-range separation can be done rigorously by creating a range separated functionals [116] where the Coulomb operator is divided into a short- and long-range part. For the short-range a range separated LDA-sr functional was derived [117, 118] and for the long-range part Fock-like exchange is used [119] while the correlation energy can be obtained using formulae analogous to MP2 [120], coupled cluster [121], or the random phase approximation [122, 123]. A similar way, often called "double hybrid functionals" [124, 125] adds the non-local correlation of the orbitals using the long-range Coulomb interaction. The exchange part usually uses a hybrid functional, hence the name. The amount of Fock-like exchange, (semi-)local correlation, and non-local correlation is given by parameters which are fitted on a range of properties such as atomisation energies or barrier heights. The inclusion of the non-local effects with an explicit orbital correlation formula makes the method much more expensive than a standard GGA calculation or even than a hybrid functional calculation of the same system.

Let us now briefly discuss a promising approach that we have mentioned before which is based on the adiabatic-connection fluctuation-dissipation theorem [100, 126, 101]. This approach is, in principle, exact and the E_{xc} can be written using the KS orbitals. The formula is derived by considering the fully interacting system and a system with no electron-electron interaction. The two systems are adiabatically connected by a set of intermediate systems where the strength of the electron-electron interaction is increased adiabatically from zero to the full value using a coupling constant λ. That is, the interaction is scaled as $V_{\text{el}}(\lambda) = \lambda V_{\text{el}}$. Importantly, the electron density is kept at the density of the fully interacting system. Using this approach the total electron-electron interaction can be then written as an integral over the coupling constant

$$E_{\text{el}} = \int_0^1 \mathrm{d}\lambda \langle \Psi_\lambda | V_{\text{el}} | \Psi_\lambda \rangle \,, \tag{2.39}$$

where the $|\Psi_\lambda\rangle$ is the ground state wavefunction of a system with the scaled electron-electron interaction but V_{el} is the full interaction. The constant density is achieved by altering the local

potential v_λ acting on the electrons. This means that for $\lambda = 1$ the potential corresponds to the external potential $v_1 = v_{\text{ext}}$ but for $\lambda = 0$ (since the density is the same) $v_0 = v_{\text{KS}}$, the KS potential. Using the exact relation for the electron-electron interaction (Equation (2.24)) one can use the fluctuation-dissipation theorem to replace the two electron density matrix by a combination of the single electron density matrix and a density-density response χ at imaginary frequency $i\omega$[5]. This leads to a formula that contains the Coulomb interaction of the electron density (the Hartree term) E_{H}, the Fock exchange term evaluated at the KS orbitals $E_{\text{x}}[\psi_{\text{KS}}]$, and the correlation energy calculated from the response functions of the KS system χ^0 and system with appropriate λ:

$$E_{\text{el}} = E_{\text{H}}[\varrho] + E_{\text{x}}[\psi_{\text{KS}}] - \int_0^1 \mathrm{d}\lambda \int_0^\infty \frac{\mathrm{d}\omega}{2\pi} \mathrm{Tr}\left[V_{\text{el}}\left(\chi^\lambda(i\omega) - \chi^0(i\omega)\right)\right] , \tag{2.40}$$

here the trace represents a two spatial integrations over the coordinates of the response functions. This formula is exact but there are several issues with its application. First the response function χ^λ could be evaluated from the KS response only if an exchange-correlation kernel f_{xc} was known. And even if it was known, the evaluation of the correlation energy would be extremely expensive. Currently, a so called random phase approximation (RPA), which sets $f_{xc} = 0$ has been used to study properties of several systems. These include total energies [127], binding energies of molecules [128, 129] or crystals [130, 131, 132]. The most exciting feature of the ACFDT or RPA methods is that dispersion is seamlessly included and a correct asymptotic behaviour for different materials [133, 134] is obtained. However, the results presented so far suggest that RPA tends to underestimate the strength of the binding. This is still to be confirmed because current calculations are not done self-consistently and the dependence on the input KS orbitals is considerable. Nevertheless, this seems to be true for weakly bonded dimers [135] or solids [136, 137, 138]. There have been developments which suggest that more accurate methods could be obtained by including some classes of correlation diagrams [139] or by devising approximate forms for the f_{xc} [140]. Let us mention lastly one more positive thing about the RPA: it works well also for metals where MP2 completely fails. For example, RPA was recently successfully applied to a long standing problem of CO adsorption on metal surfaces [141, 142].

The largest problem of the ACFDT formula or the RPA is computational cost. For example, the evaluation of the density-density response functions requires a sum over both occupied and unoccupied orbitals. Therefore methods have been devised that try to approximate some part of the calculation to make it more tractable. For example, we have already mentioned the range separated RPA approach where DFT functionals are used at short range [122, 123]. In a different approach Dobson [143] approximated the χ using a formula analogous to a uniform

[5] It is a slightly philosophical question how to deal with the fact that the same energy can be obtained from the knowledge of the full wavefunction as an expectation value on one side and from the interaction of density oscillations of the other side. However, one can view the coupled density oscillation as some determinant which alters the wavefunction with a correlated non-local electron moves.

electron gas and obtained an energy expression

$$E_{\mathrm{disp}} = -\frac{3\hbar}{32\pi^2}\int \mathrm{d}r_1 \mathrm{d}r_2 \frac{1}{r_{12}^6}\frac{\omega_1\omega_2}{\omega_1+\omega_2}\,, \tag{2.41}$$

where $\omega = \sqrt{4\pi e^2 \varrho(r)/m}$ is the local plasma frequency. Similar formulae were derived by other authors [144, 145, 146, 147]. They all represent one approach in the sense that a non-local dispersion formula is constructed which is based solely on the electron density. Similar to the empirical dispersion methods, this approach requires also the interaction to be cut at short distances.

A similar development done in the groups of Langreth and Lundqvist is the van der Waals density functional for general geometries (vdW-DF) [16, 148] which we use in this thesis. This again starts from the ACFDT correlation energy and proceeds by several approximations. These lead to a double space integral where only the electron density and its gradients are used, *i.e.*, there is no reference to the orbitals. Parts of the derivation can be found in Refs. [149, 150, 151, 16, 152, 153] and here we present only the main steps. In the ACFDT formalism the correlation energy is obtained as

$$E_{\mathrm{c}} = -\int_0^1 \mathrm{d}\lambda \int_0^\infty \frac{\mathrm{d}\omega}{2\pi}\mathrm{Tr}\left[V_{\mathrm{el}}\left(\chi^\lambda(i\omega)-\chi^0(i\omega)\right)\right]\,, \tag{2.42}$$

this is just the last term of Equation 2.40. The intermediate response χ^λ (we omit the ω dependence for brevity) is rewritten using response to the full potential $\tilde{\chi}^\lambda = \chi^0 + \chi^0 f_{\mathrm{xc}}^\lambda \tilde{\chi}^\lambda$ which allows χ^λ to be rewritten as $\chi^\lambda = \tilde{\chi}^\lambda + \tilde{\chi}^\lambda \lambda V_{\mathrm{el}} \chi^\lambda$. Although there has been no approximation so far, evaluation of $\tilde{\chi}^\lambda$ would require the knowledge of the exchange correlation kernel f_{xc}^λ. Now an approximation is made setting $\tilde{\chi}^\lambda = \tilde{\chi}^1$, so-called full potential approximation (FPA). This enables the integration over λ to be performed to obtain

$$E_{\mathrm{c}} = \int_0^\infty \frac{\mathrm{d}\omega}{2\pi}\mathrm{Tr}\left[\ln\left(1-\tilde{\chi}^1 V_{\mathrm{el}}\right)+\chi^0 V_{\mathrm{el}}\right]\,. \tag{2.43}$$

In the next step the dependence on the orbitals is removed for the first term [151]. This is done by using the formula for the electron density response $\delta\varrho$ to an external potential Φ_{ext}, $\delta\varrho = \chi\Phi_{\mathrm{ext}} = \nabla\chi\Phi$, where Φ is the screened potential. The density response can be also written in terms of polarisation and the dielectric function $\delta\varrho = \nabla\cdot\alpha\nabla\Phi$, where the polarisability $\alpha = (\epsilon-1)/4\pi$. The correlation energy can be then written as

$$E_{\mathrm{c}} = \int_0^\infty \frac{\mathrm{d}\omega}{2\pi}\mathrm{Tr}\left[\ln\left(1-\nabla\cdot(\epsilon-1)/4\pi\nabla V_{\mathrm{el}}\right)+\chi^0 V_{\mathrm{el}}\right]\,. \tag{2.44}$$

Approximate formulae that use the electron density are later used to obtain ϵ. Therefore expensive evaluation of χ from the orbitals as is done in, for example, RPA, is not required but the details of the chemical bonding are basically lost. For interaction of distant molecules such details might not be important. However, a more detailed approach would be needed to describe bonding with a very high accuracy. In the next step Equation 2.44 is written for UEG where the first term simplifies because ∇ comutes with ϵ leading to

$$E_{\mathrm{c}}^{\mathrm{UEG}} = \int_0^\infty \frac{\mathrm{d}\omega}{2\pi}\mathrm{Tr}\left[\ln\left(\epsilon\right)+\chi^0 V_{\mathrm{el}}\right]\,. \tag{2.45}$$

Finally, the non-local correlation energy is defined as

$$E_{\mathrm{c}}^{\mathrm{nl}} = E_{\mathrm{c}} - E_{\mathrm{c}}^{\mathrm{UEG}} = \int_0^\infty \frac{\mathrm{d}\omega}{2\pi} \mathrm{Tr}\left[\ln\left(1 - \nabla\cdot(\epsilon-1)/4\pi\nabla V_{\mathrm{el}}\right) - \ln\left(\epsilon\right)\right] . \tag{2.46}$$

That is, the non-local correlation energy is defined with respect to the UEG reference and therefore is zero for UEG, however strange this may seem. In the next step Equation 2.46 is approximated to a second order in terms of a polarisation operator $S = 1 - \epsilon^{-1}$ leading to

$$E_{\mathrm{c}}^{\mathrm{nl}} = \int_0^\infty \frac{\mathrm{d}\omega}{4\pi} \mathrm{Tr}\left[S^2 - \left(\nabla S \cdot \nabla \frac{V}{4\pi}\right)^2\right] . \tag{2.47}$$

This equation is transformed to reciprocal space where S is approximated subject to several constrains (Equation (5) in Ref. [16]). A form inspired by a plasmon-pole model is used which employs a suitable dispersion relation for the plasmon peak frequency (Equation (6) in Ref. [16]). As shown in Ref. [151], the chosen form allows one to transform the formula back to real space to take the form of

$$E_{\mathrm{c}}^{\mathrm{nl}} = \int \mathrm{d}r_1 \mathrm{d}r_2 \varrho(r_1)\phi(d(r_1), d(r_2))\varrho(r_2)\,, \tag{2.48}$$

where $\phi(d(r_1), d(r_2))$ is a correlation kernel. Therefore, the non-local correlation energy can be evaluated as a simple double space integral. The function $d(r)$ entering the kernel is defined as $d(r) = |r - r'|q_0(r)$, where $q_0(r)$ is a continuous function related to the length scale which switches between different behaviours of the dispersion relation. For the model chosen, $q_0(r)$ is directly related to the local exchange-correlation energy ϵ_{xc}^0 obtained with the help of Equation 2.45. Because more accurate approximation for local exchange-correlation energy are available, the correlation energy given by Equation 2.45 is not used and gradient corrected LDA is used instead. Therefore, $q_0(r)$ is written as $q_0(r) = k_F(r)F_{\mathrm{xc}}^0(\varrho(r), s(r))$, with $k_F^3 = 3\pi^2\varrho$, and $F_{\mathrm{xc}}^0 = 1 + \lambda s^2 - (4\pi/3k_{\mathrm{F}})\epsilon_{\mathrm{c}}^{\mathrm{LDA}}$, an enhancement factor with $\lambda = 0.09434$. The choice of the enhancement factor is to some extent arbitrary but turns out to be quite important in the evaluation of the energy. That is because changing the formula for $q_0(r)$ will change the value of the kernel function $\phi(d(r_1), d(r_2))$ that enters the double space integral and thus the final energy. Indeed, an offspring of vdW-DF, termed vdW-DF2, was proposed [154] where $\lambda \approx 0.2096$. This change was supposed to make the functional more appropriate for molecules (in opposite analogy of the change made to PBE to make it more accurate for solids via the PBEsol functional). Although justifiable, the alteration made the C_6 coefficients too low [147]. The reason for this is probably that the change increases the values of $q_0(r)$ leading to larger values of $d(r)$. By observing Figure (1) in Ref. [16] it is clear that larger values of $d(r)$ lead to lower values of $\phi(d(r_1), d(r_2))$ for $d(r)$ large enough (corresponding to long-range interactions). Therefore, smaller $E_{\mathrm{c}}^{\mathrm{nl}}$ as well as smaller C_6 coefficients are obtained. In a functional called vdW-DF-09 by Vydrov and van Voorhis [152] another approximation of $q_0(r)$ was used and it is not clear which one of the proposed forms should be better.

One of the good points of the vdW-DF method is that it is "seamless": although the interaction has $1/r^6$ asymptotic behaviour, it does not diverge for small distances. For this,

however, a suitable form for E_c^{UEG} is required, for which LDA is used. Moreover, the correlation part needs to be used with some exchange functional, in the work of Dion *et al.* [16], the revPBE [155] functional was used so that the total exchange-correlation energy in vdW-DF reads:

$$E_{\mathrm{xc}} = E_{\mathrm{x}}^{\mathrm{revPBE}} + E_{\mathrm{c}}^{\mathrm{LDA}} + E_{\mathrm{c}}^{\mathrm{nl}} \,. \tag{2.49}$$

The dispersion interaction given by this functional seems to be overestimated and further refinements of the method have been proposed [152, 156]. The overestimated correlation energy means that the method does not give accurate results when used with HF exchange [157, 158] and a functional that corrects for this needs to be used.

Although the vdW-DF is a non-local correlation functional and includes the dispersion seamlessly, there are approximations that limit its scope. For example, the convenient two point integration leads to a method that does not describe higher order effects or long wavelength excitations, which can be important in metals. Indeed, as Dobson *et al.* [133, 159] showed, how the asymptotic interaction behaviour of metals, insulators, and graphite differs. Any method based on the $1/r^6$ summation will not capture this and will give the same decay for metals and insulators. This is not true for RPA and ways how to devise methods less expensive than RPA but able to capture the correct behaviour are currently being sought.

2.4 Performing a calculation

The equations discussed in the previous sections, *i.e.*, Schrödinger's, Hartree-Fock, and Kohn-Sham, can be solved analytically only for simple systems and they are usually solved numerically. In this part, we will discuss some of the details that need to be addressed when one wants to study systems using some quantum mechanical method such as DFT.

2.4.1 Basis sets

In any method that we want to use, we ultimately need to represent the real space shape of the wavefunction, most commonly, the shape of the single particle orbitals. This is done usually by representing the orbital ψ_σ is some basis set of well-defined functions $\{\varphi_i\}$:

$$\psi_\sigma = \sum_i c_{\sigma i} \varphi_i \,, \tag{2.50}$$

where $c_{\sigma i}$ are the expansion coefficients. There are several rather distinct basis sets used which are favoured depending on what kind of problem one is interested in. The two main types are localised basis sets, which have been traditionally used in programmes for HF and post-HF calculations of molecules and clusters, and plane waves, which are widely used for solid state calculations; we start with the first type. In the localised basis sets the basis functions are chosen to resemble the electronic orbitals so that a small basis set is needed. For example, one can use hydrogen atom-like functions which are then called Slater-type orbitals (STO). However, it turns out that the terms in the HF Hamiltonian are difficult to evaluate using the STO basis functions. For this reason the STO form is often replaced by a sum of Gaussian

functions for which all the terms in HF equations can be evaluated analytically. More recently, especially for DFT calculations, other forms such as splines or numerical radial functions have been used [160, 161, 162]. Another point which needs to be considered concerning the localised basis set is its size. Although one electron in an isolated hydrogen atom is well described by one $1s$ orbital, this is not enough when the hydrogen binds to another atom. For this reason, more basis set functions are added so that the orbitals can be represented accurately. There are standard basis sets which are tabulated, for example the basis sets due to Pople or Dunning. Although smaller basis sets require less computational time, the can increase the errors of the calculations. Moreover, the binding energy of molecular dimers is overestimated because of a so called basis set superposition error (BSSE). The BSSE occurs since upon forming the dimer (A+B) the basis functions on species B represent an additional optimisation space for orbitals of species A which lowers the total energy and results in the overestimation. Although this error is sometimes neglected and even more sometimes considered beneficial [104], a proper approach is to extrapolate results to a complete basis set (CBS) limit [163, 164, 165, 166]. Let us finally mention some issues with the localised basis sets from the point of view of surface studies. First, when the atom moves, the basis set function moves as well which needs to be considered in the numerical formulae. Second, it's difficult to describe an electron detached from an atom since, unless explicitly specified, there are no basis set functions in the "vacuum". Last, while it is advisable to use basis functions with slow decay ("diffuse") for molecular calculations, in condensed phase these cause a poor conditionality of the overlap matrix and often lead to numerical instabilities.

For solid state calculations a completely different type of basis set functions is popular: plane waves [167] which because of their periodicity make a natural representation of the orbitals. That is the electronic orbitals are expanded using a set of functions $\mathrm{e}^{iG\cdot r}$, where G is a vector of the reciprocal lattice. Thus we are basically using the Fourier representation of the orbitals and storing the Fourier coefficients. The size of the basis is then controlled by the highest momentum of plane wave that is included. There are several good points about the plane wave basis set, for example, they are orthogonal and thus several terms in the electronic Hamiltonian are simple to evaluate. Moreover, they describe the whole cell in the same way and thus there is no BSSE. However, the homogeneous description of the cell is very inefficient when one wants to study molecules since a lot of effort is spent on describing vacuum. The most serious problem arises when one wants to describe the fast oscillations of the electronic orbitals close to the nuclei since these would require very high plane-wave cut-offs. We discuss later in section 2.4.3 the approaches that are used to avoid this problem and keep the calculation efficient. Let us close by stating that compared to the localised orbitals, evaluation of the Fock exchange term is computationally expensive and also a divergence in the energy needs to be addressed [168].

The GTOs and plane-waves are not the only types of basis sets used. This is partially caused by the growing interest into large systems and linear scaling codes [169, 170]. Because

the calculations are implemented as parallel programmes, there is a need to reduce the communication between individual processes. There are several codes using different approaches, for example codes using grids [171], various localised basis sets [160, 161, 162], or wavelets [172]. One example which reduces the communication is to replace the calculation of density derivatives (needed for example to obtain the exchange correlation energy) which is done using FFT in plane wave codes by finite differences which can be evaluated locally. For systems with thousands of atoms and more these methods seem indispensable and the development in the field offers a promise for future applications.

2.4.2 Periodic boundary conditions – Bloch's theorem and k-points

As we mentioned before, the calculations using plane wave basis set are usually done using periodic boundary conditions. That means that a single computational cell is periodically repeated in the whole space. Now one could think that if we want to represent orbitals in metals where the electrons are delocalised we would have to use a very large computational cell so that the orbitals "fit" into the cell. Fortunately, this is not the case as can be shown using Bloch's theorem. This states that for a periodic potential the eigenfunction can be written as a product of a function φ with the same periodicity as the potential and a plane wave $\exp(ik \cdot r)$:

$$\psi_{n,k}(r) = \exp(ik \cdot r)\varphi_{n,k}(r)\,. \tag{2.51}$$

Here the index n enumerates the eigenfunctions for a given k, over the whole k-space states with identical n form so-called bands. The energy eigenvalues are periodic in the reciprocal space $\varepsilon_n(k) = \varepsilon_n(k + G)$, where G is a vector of the reciprocal lattice. This means that we can consider k only from the first Brillouin zone, and instead of simulating a large supercell we can solve the equations for a set of k-points instead. For an infinite crystal, the k-space is smooth but in a calculation it needs to be discretised. While the use of k-points can be viewed as a way to simulate large supercells, to evaluate some variables requires integration over the k-space and here the sampling is used to perform the integration. In any case one needs to find what is the necessary sampling that gives converged variables of interest. This convergence test can be done once for a given system using, *e.g.*, the primitive cell. When a larger cell is required the number of k-points can be reduced accordingly to the increase of the increase of the size. A widely used k-space sampling procedure was devised by Monkhorst and Pack [173].

2.4.3 Core-valence electron separation

We now turn to the main problem of the plane wave representation of the orbitals, it is inefficient in describing the rapid oscillations of the electron orbitals close to the nuclei. The two main ideas to overcome this issue are to: (i) replace the core electrons by an effective potential (pseudopotential) acting upon the valence electrons; or (ii) to treat the core and valence electrons or regions separately. The latter is represented, *e.g.*, by the linear augmented plane wave (LAPW) method [32] where the electron orbitals are represented with a combination of a radial grid and spherical harmonics inside atom-centered spheres. Between the spheres a plane wave

basis set is used. Similar ideas are used in the projector augmented plane wave (PAW) method which also builds upon the pseudopotential methods and we thus discuss it after them.

The idea to divide the electrons in an atom into valence electrons which are involved in the chemistry and the core electrons which are not notmally involved in bonding is rather natural and has a long history [32]. The pseudopotential method replaces the interaction of the core electrons with the valence electrons by a pseudopotential requiring that the scattering properties are not changed. The pseudopotential is localised around the nucleus within some radial cut-off and thus the potential acting on the valence electrons is not affected for distances larger than the cut-off. The real valence orbitals with rapid oscillations are replaced by pseudo-orbitals without these oscillations so that a lower plane-wave cut-off is generally required. However, for larger distances the pseudo-orbitals are identical to the real orbitals. There are various approaches to constructing pseudopotentials but we briefly mention two methods. First, norm conserving pseudopotentials lead to pseudo-orbitals with the same norm as the real orbitals only removing the rapid oscillations near the nuclei. A second widely used method is ultrasoft pseudopotentials [174]. Here the norm of the pseudo-orbitals inside the cut-off radius is not preserved which leads to smoother pseudo-orbitals than for the norm-conserving pseudopotentials and thus lower required basis-set cut-off. To correct the norm additional charge density is added inside the cut-off radius.

One important issue about the use of pseudopotentials is the question of their transferability. Since the pseudopotential involves a cut-off radius below which the pseudo orbitals differ from the real orbitals, one needs to consider if a given pseudopotential is sufficient for their calculation. That is, if this approximation has an effect on the calculation and how large this effect is. With the reduced radial cut-off the pseudopotential will be more transferable (*i.e.*, applicable in more situations) but a higher plane-wave cut-off will be generally required. Moreover, since the core and valence electrons are strictly divided, the number of valence electrons needs to be sufficient for a given problem. Again, a larger number of valence electrons will generally increase the transferability but also the computational cost will be increased.

As a formal unification of the ideas introduced in the ultrasoft pseudopotentials and LAPW methods the PAW method is able to keep the small plane-wave cut-off while being an all-electron method at the same time. The PAW calculation is basically divided in two parts [175, 176]: a calculation using the pseudo-wavefunction which is by itself very similar to an ultrasoft pseudopotential calculation. Afterwards, the real wavefunction is obtained from the pseudised one and used to remove the terms calculated approximately by the pseudo-wavefunction inside the atomic spheres. This calculation is done on radial grids. In this way the energy is evaluated effectively on the all-electron density.

Although the PAW method is all-electron, the core orbitals are usually not allowed to change during the calculation ("frozen core" approximation). However, this is not a restriction of the method and due to recent developments the core orbitals can be relaxed [177]. The

PAW method is implemented in the VASP code which has been almost exclusively used in this thesis. Apart from standard DFT capabilities VASP is also able to calculate the Fock exchange integrals and thus perform a hybrid functional calculation within the PAW method. The more complex RPA method is available as well.

2.4.4 Self-consistent loop

The problem of finding eigenfunctions and eigenvalues of a Hamiltonian with functions represented using some basis set usually translates into matrix diagonalisation. As we have mentioned before the HF and KS-DFT Hamiltonian depends on the orbitals. This is a problem: we don't know the Hamiltonian we want to solve since it's defined by the solution. Therefore an iterative procedure needs to be used starting with a guess of the orbitals. The guess Hamiltonian is solved which leads to improved orbitals and the procedure is repeated. Usually the new solution is combined with the previous ones which helps to avoid oscillations in the orbital coefficients and thus improves the convergence to the solution. The solution is found when several criteria are met: the density, orbital coefficients, and the total energy differ less than a given threshold from the variables obtained at the previous step. The required convergence needs to be considered, it does not have to be stringent when only the total energy is required since the error in the energy is of the second order. Accurate forces on the other hand require a well converged wavefunction. Better convergence of course means more iterative steps and thus higher computational effort.

We can close this part with a statement that there are nowadays reliable implementations of the KS-DFT approach suitable for a wide range of studies available in several programmes; for example, for surface studies VASP [178], CASTEP [179], CP2K [180], or QUANTUM ESPRESSO [181]. In many cases the programmes are reliable enough to be used almost as "black boxes" whatever the consequences of this are.

2.5 Empirical forcefield simulations

Let us now leave the quantum theory methods and discuss an approach that makes no attempt to describe the electrons directly – forcefield simulations (see Ref. [9] for a more in-depth discussion). This method, instead of calculating the energy and forces from the wavefunction, prescribes the interaction between atoms by simple and sound functional forms. Using this parametrisation standard procedures such as molecular dynamics or geometry optimisation can be performed. Since the interactions are prescribed by a simple functions, the computational requirements are much smaller than for a DFT based molecular dynamics approach.

The forcefields are often useful and sufficient to obtain an idea about the system studied. For example, the interaction between noble gas atoms can, to a high accuracy, be described by a combination of an attractive van der Waals potential and a short range exponentially decaying repulsive potential. Since this captures most of the interactions, it is a completely appropriate model. Moreover, the parameters can be fitted to the experimental data which for a species such as noble gas is simple. For more complicated systems with chemical bonds, more terms

need to be added to describe the system realistically and we discuss them in the following. It is important to note that to obtain such terms requires a considerable effort and there are several sets of parametrisations available, at least for biologically important systems.

2.5.1 Models and parametrisations

The total energy in the empirical potential methods is calculated as a sum of effective terms that try to describe the various interactions:

$$E = E_{\text{elstat}} + E_{\text{LJ}} + E_{\text{bond}} \,. \tag{2.52}$$

The E_{elstat} describes the electrostatic interaction of the ions. Usually the charge of an ion is an effective charge, *i.e.*, a sum of the nuclear charge and the charge of the proximate electron cloud. Therefore ions such as Na^+ have an effective charge $+1$, while the hydrogen atom in a water molecule will have charge $\sim$0.42. The E_{LJ} term is the Lennard-Jones (LJ) term which is given by

$$E_{\text{LJ}} = \varepsilon \left(\frac{\sigma^{12}}{r^{12}} - \frac{\sigma^6}{r^6} \right) , \tag{2.53}$$

and describes both the Pauli repulsion and dispersion attraction. The ε and σ parameters are related to the equilibrium distance and binding strength of the attractive minimum. The values are different for different elements but differ also depending on the bonding environment of the atom. Therefore there are several "types" of, say carbon atoms with different strength of the interaction depending on, *e.g.*, to which amino-acid they belong. Although the repulsion part should have an exponential decay and not $1/r^{12}$-like decay since it is caused by electron density overlap, there are at least two reasons for the preference of the latter. First, it is computationally simpler and second, the potential described by a function (called Buckingham potential)

$$E_{\text{Buckingham}} = A \exp(-Br) - \frac{C_6}{r^6} \tag{2.54}$$

goes to $-\infty$ for $r \to 0$. That is, for small enough separations the Buckingham potential becomes attractive. This is not true for the LJ potential which is repulsive for all separations smaller than the equilibrium distance. Although this might not seem as a strong point, for bad initial guesses of the atomic positions, unphysical small separations can occur during the optimisation. The electrostatic and LJ terms are simple and rather straightforward to understand physically. The bonding energy E_{bond} terms are much more complicated. The simplest term describes the chemical bond as a function of the distance of the atoms and usually takes the form of $E^2_{\text{bond}} = \kappa(x - x_0)^2$. Therefore we describe every chemical bond using a parabolic potential with parameters giving the stiffness and equilibrium bond length. Apart from being simple it is also a good first approximation of the bond.[6]

[6] Of course a problem would be if the bond would have to be broken. If bonds break then one can try to use a "reactive" potential which allows bonds to be broken. There are also methods such as generalised valence bond [182], tight binding [183], or other semi-empirical quantum mechanical methods such as AM1 or PM3 [184]. In these methods the simplifications allow to study systems with computational costs between that of DFT and empirical potentials.

For large molecules bonded terms that involve three or four atoms need to be considered and parametrised. The three body terms are essential to describe bond angles and have a form $E^3_{\text{angle}} = C_\theta(\theta - \theta_0)^2$, which is similar to the two body term but now describes the deformations of an angle θ from its equilibrium position θ_0. Again the stiffness of the angle is given by the parameter C_θ. Four body terms are more complicated and are applied to describe for example energy dependence of torsions. For such complicated parameters it is usually necessary to employ some reference quantum mechanical calculations.

Despite the popularity of the models based on the simple parametrisations just described, they fail to include one important effect and that is polarisability. A bond can become more or less polarised depending on the environment but the effective charges on the atoms are usually kept constant. Since this can become a problem, it has been addressed in several ways. For example potentials were devised where a charged particle is added to the atom and the change of the position of the particle with respect to the atom mimics the polarisation [185, 186]. Other approach allows the charges to fluctuate during the simulation [187]. It needs to be noted that including polarisation is more computationally demanding than using non-polarisable forcefields.

There is one material for which hundreds, if not thousands, of potentials exist – water. The large number is caused by the importance of water in biological and technological processes and the need to describe these accurately. The simplest models use three charge centres in the positions of the atoms and one LJ interaction centre at the oxygen position. Widely used models of this type are SPC/E (simple point charge/extended) [188] or TIP3P [189], although they perform poorly for some bulk properties of water such as melting point [190]. Despite a presence of better water models it is not straightforward to replace a (worse) water model by a better one. This is because the forcefield parameters were obtained by fitting to some experimental properties (such as solvation free energies) using the worse water model. Replacing the water model with an improved one might improve the description of the water part but will probably increase the errors on the fitted properties. Improved water models usually increase the number of interaction sites: TIP4P [191] moves the negative charge site from oxygen to a bisector site; TIP5P [192] adds two charge sites in the direction of the lone electron pairs. Models with more interaction sites have also been devised. All the models mentioned so far are non-polarisable, but there are several polarisable models available as well (see, *e.g.*, Refs. [193, 194, 195, 196, 197, 198]) and despite the development the quest for a good water potential is not over. In a completely different approach to constructing the water model a large number of accurate quantum mechanical data can be used to build an interaction potential for water dimer [199, 200]. The crucial difference is these parametrisations don't include quantum nuclear effects as opposed to models such as SPC/E which includes them effectively. (For SPC/E one wants them to be included since one wants to simulate "real" water.) This is not a problem since the quantum nuclear effects can be added using, *e.g.*, path integral molecular dynamics and their importance can be studied [201, 202].

2.6 Transition state theory

In this part we briefly introduce the theory developed to study chemical reactions and other processes where the system changes states. This is to introduce concepts that will be discussed later in Chapter 3 where we study computational methods which are used to search for the low energy path between reactants and products. To study a chemical reaction it is usually not sufficient to set up the simulation and perform a molecular dynamics run. This is because the time scale needed for the reaction to occur is usually longer than the time scale available in a simulation. For example, molecular dynamics based on DFT is limited to tens or hundreds of ps; and although simulations using empirical forcefields can span a length scale of approximately a few microseconds [7], this is still shorter than the time needed for a medium sized protein to fold. In short: when one observes a long simulation, usually not much happens. Therefore to study reactions, methods need to be devised that either reformulate the problem or force the system to undergo the change. The reason it takes a long time for a system to undergo a change is because it spends most of the time around an energy minimum. Only after a sufficiently large fluctuation in the right direction occurs it might overcome an energy barrier and fall into a different energy basin. There it will stay for some time before some other fluctuation occurs. Therefore there are many approaches which try to force the system from one minimum to another (see, *e.g.*, Ref. [205]) and thus explore different states. There are also approaches that calculate what is the rate of transfer over a barrier which we will discuss in the following.

We consider an ensemble of systems with two energy basins A and B separated by an energy barrier. If the system is in basin A it is called reactant, basin B is the product side. If we initially have only reactants they will change into products with an initial reaction rate $k^{\mathrm{AB}}[A]$ where k^{AB} is the reaction constant and $[A]$ is the concentration of the reactants. Eventually a dynamical equilibrium will occur where parts of the ensemble will belong to both the reactants and products. The products may react to form the reactants with a rate $k^{\mathrm{BA}}[B]$ but the ratio of the concentrations of both species will be preserved (for a large ensemble). An empirical law that describes the dependence of the reaction constant on the temperature has been found:

$$k^{\mathrm{AB}} = A \exp(-E_{\mathrm{act}}/kT)\,, \tag{2.55}$$

this is the Arrhenius law (discussed, *e.g.*, in Ref. [206]). The E_{act} is the activation energy and A is some prefactor which is determined experimentally. In the following we discuss how these values are determined theoretically.

One way to calculate reaction constants from an atomistic theory is by using transition state theory. Given an energy basin of reactants A and of products B, there is a dividing (hyper-)surface between them that all the reactive trajectories have to pass. The idea is that we can calculate all the trajectories crossing this surface to obtain the reaction constant. First,

[7] One of the longest simulation of biomolecule needed 3 months of supercomputer time to obtain a trajectory of 10 microseconds [203]. On a special purpose hardware 1 millisecond simulation was recently performed [204]

the probability for a system to occur in the transition state (denoted by †) can be written as

$$P_{\mathrm{TS}} = \langle \delta(r - r^\dagger) \rangle_{\mathrm{R}} \,, \tag{2.56}$$

where the subscript R denotes that the ensemble average is done over the reactant space. The rate with which the reaction occurs can be obtained when we include the velocity of the system in the transition state in Equation (2.56):

$$k_{\mathrm{TST}} = \frac{1}{2} \langle |v| \delta(r - r^\dagger) \rangle_{\mathrm{R}} \,, \tag{2.57}$$

where the factor $1/2$ selects only the trajectories that cross from the reactant side to the product side. For a system with particles of identical mass m the average momentum is constant and the velocity is $\langle |v| \rangle = \sqrt{2kT/\pi m}$ so that the reaction constant is

$$k_{\mathrm{TST}} = \frac{1}{2} \sqrt{\frac{2kT}{\pi m}} \langle \delta(r - r^\dagger) \rangle_{\mathrm{R}} \,. \tag{2.58}$$

The reaction constant given by this formula will be overestimated, mainly for two reasons. First, in principle any surface can be used as the transition state but surfaces will differ in the estimated reaction constants. Taking a surface too close to the reactant basin will lead to increased P_{TS} and thus higher rate. However, one consequence of this is that the position of the transition state surface can be optimised so that it crosses through the energy bottlenecks between the reactants and products so that P_{TS} is minimised. This is the idea of variational TST [207]. Second, even when the transition state is found so that the reaction rate is the smallest possible, the reaction rate will be overestimated because some of the trajectories that cross the transition state will recross it back and some of them even might cross it several times before finally falling into either the reactant or product energy basins. To correct for this a dynamical correction factor needs to be found which will lower the k_{TST} rate [208, 209, 210, 211].

2.6.1 Harmonic transition state theory

To obtain the reaction rate we need to calculate the probability of the system to be in the transition state P_{TS}. The probability can be written also as the ratio of the partition functions

$$P_{\mathrm{TS}} = \frac{q^\dagger}{q_{\mathrm{A}}} \,, \tag{2.59}$$

which can be used to obtain the reaction rate. The partition functions can be approximated if we assume that the potentials are harmonic around the minimum A and the saddle point [212]. The saddle point is the lowest energy point on the transition state dividing surface and we implicitly assume that all the reactive trajectories pass through the transition state in a vicinity of the saddle point. The harmonic approximations gives this approach its name: harmonic transition state theory (hTST) [212]. The partition function can be then written using a partition function of a classical harmonic oscillator

$$q_{\mathrm{A}} = \exp(-E_{\mathrm{A}}/kT) \Pi_{i=1}^{3N} \frac{kT}{\hbar \omega_i} \,. \tag{2.60}$$

A similar expression is used for $q^{\dagger}$ and inserting both expressions into 2.58 leads to the final expression for the rate constant

$$k_{\mathrm{hTST}} = \frac{\Pi_{i=1}^{3N} \omega_i^{\mathrm{min}}}{\Pi_{i=1}^{3N-1} \omega_i^{\dagger}} \exp\left(\Delta E / kT\right). \tag{2.61}$$

This expression then agrees with the empirical Arrhenius law (Equation (2.55)). Within the hTST the saddle point is often referred to as the transition state and this is a convention that we are going to use in Chapter 3.

Chapter 3

Methods for locating transition states

3.1 Introduction

Elementary processes at solid surfaces, such as molecular adsorption/desorption and diffusion are of the utmost importance to a wide variety of disciplines including heterogeneous catalysis and the semiconductor industries. To be able to accurately determine the rates of these processes using the formulae introduced in Section 2.6 is an important challenge to current computational materials modelling. Mainly this is because it requires not only determination of the initial and final state minima on the potential energy surface (PES) through which the reaction proceeds but also a determination of the relevant low energy transition state(s) (TS) that connect these local minima. Almost since the outset of computational materials modelling, methods have been developed to efficiently determine such transition states and the minimum energy pathways (MEPs) that connect them to the initial and final states (see, *e.g.*, [213] or [214] for a review).

Here we test a selection of the methods popular in treating processes at surfaces using pathways where only one TS is present between the initial and final state. The methods considered include the nudged elastic band (NEB) [215, 216, 217], Dewar, Healy, and Stewart (DHS) [218], dimer [219, 220, 221], constrained optimization (CO), activation-relaxation technique (ART) [222, 223] as well as novel one-side growing string (OGS) and combinations of the DHS with growing string (DHS+GS) and DHS plus climbing image (CI-DHS). We selected water diffusion on NaCl(001) and HCl bond breaking on NaCl(001) as processes with which to test the various algorithms. These processes represent two distinctive classes of surface events: diffusion with a relatively low barrier (<0.2 eV); and dissociation with a high barrier (>1 eV). NaCl(001) is the lowest energy NaCl surface, the main surface exposed of salt crystals and as such plays an important role in atmospheric chemistry [224]. Water adsorption on this surface has been studied previously at various levels of theory [225, 226, 227, 228, 229, 230, 231, 232, 233, 234, 235, 236, 237] and experimentally [238, 239, 226, 240, 241, 242, 243, 244]. In this work we restrict ourselves to the low coverage water monomer regime. In contrast to the widely studied water/NaCl system, the interaction of HCl with NaCl has not received any attention.

Although studies comparing different TS search methods have been previously pre-

sented [213, 245, 220, 246, 247], many of them used empirical potentials for the evaluation of the energy and forces. Use of these potentials lacks one important feature of the *ab initio* calculations, namely the self-consistent field (SCF) procedure for determining the ground state electronic density. This iterative procedure has an impact on the calculation of the forces: while the forces are accurate and readily available using empirical potentials, in *ab initio* methods their accuracy depends on the convergence tolerance of the SCF procedure. A tighter convergence tolerance delivers more accurate forces but requires more computational time. Moreover, large changes in geometry between successive steps are no more costly than small changes with the empirical potentials but in the electronic structure calculations they can require many more SCF iterations to update the electron density. Finally, for some especially poor initial guesses of the geometry the SCF procedure can even fail. Thus it is worthwhile to evaluate the performance of the various TS search methods directly within an electronic structure framework, which is what we do here.

In this Chapter we study the performance of a number of methods for locating TSs with density functional theory (DFT). Aside from several popular techniques we also developed three new algorithms: the "DHS+GS" and "CI-DHS" algorithms that are based on the DHS method, and a simple OGS technique. A key conclusion is that the NEB method is relatively fast, especially when just a single (climbing) image is used. Indeed, for our set of processes, using NEB with more images is an unnecessary computational expense. The performance of the dimer method depended strongly on the corrugation of the underlying PES: convergence towards the TSs was slow and problematic for the diffusion processes whereas it was fast for the dissociation reaction. The DHS+GS algorithm improves over the original DHS scheme and can be used to quickly establish an approximate MEP and TS. The guess of the TS can then be refined with the novel CI-DHS method. Overall, this scheme gives similar performance to the single image NEB in cases where the initial guess for the TS is poor, such as for the HCl dissociation and some of the diffusion processes.

3.2 Methods

3.2.1 Transition state algorithms

There are many methods for searching TSs and minimum energy pathways. Here we test several popular algorithms and combine some of them to produce new schemes. Specifically the NEB, dimer, DHS, ART, and CO methods are examined and two new techniques based on the DHS method, DHS+GS and CI-DHS, are presented. We also present an OGS method which is somewhat similar to the constrained optimization walk [248] and growing string methods [220].

In general, the various approaches considered here can be classified according to the amount of information they require in order to perform a search, specifically if they require a predefined final state geometry or a guess of the TS. The particular requirements for the techniques tested are summarized in Table 3.1. All methods considered here proceed by modifying the real force,

$\mathbf{F}_{\text{real}}$, acting on the system by, for example, flipping the component of the force parallel to some direction $\mathbf{N}$:

$$\mathbf{F}_{\text{mod}} = \mathbf{F}_{\text{real}} - 2\mathbf{N}\mathbf{F}_{\text{real}} \cdot \mathbf{N} \,. \tag{3.1}$$

The modified force, $\mathbf{F}_{\text{mod}}$, then maximizes the energy along $\mathbf{N}$ and minimizes it in all other directions. Therefore, when $\mathbf{N}$ is aligned with the direction of the lowest frequency mode near to the TS, the force leads the system to the TS. The lowest frequency mode can, in principle, be obtained from the Hessian matrix. However, in practice the methods considered here approximate it in some way. A convenient approximation is to set $\mathbf{N}$ equal to the vector between two states that lie at the bottom of the potential energy valley. In this case the more proximate the points are, the more accurately the minimal mode is obtained. We give the ranges of the length scales on the PES used for $\mathbf{N}$ in Table 3.1.

Table 3.1: Summary of the methods used in this study compared by the information they require, namely the need for a predefined final state geometry or guess of the reaction path or TS geometry. The "Range for $\mathbf{N}$" gives the length scale that is used to approximate the direction of the minimal mode. Approximation by, *e.g.*, the vector between the initial and final states is labelled "Global". Information obtained from $\leq$0.5 Å of the position of the image is labelled "Local". The NEB and DHS methods are described as "Global – Local" because the former depends on the number of images used, and the latter becomes more local as the run progresses. We also show what methods are designed to converge to the TS geometry accurately. The acronyms for the methods listed are (CI-)NEB: (Climbing image-) Nudged elastic band; DHS(+GS): Dewar, Healy, and Stewart (+Growing string); CO: Constrained optimization; ART: Activation-relaxation technique; OGS: One side growing string.

Method	Range for $\mathbf{N}$	Final state	Guess of Pathway	Converges to TS	Reference
NEB	Global – Local	Yes	Yes	No	[215]
CI-NEB	Global – Local	Yes	Yes	Yes	[249]
DHS	Global – Local	Yes	No	No	[218]
DHS+GS	Global – Local	Yes	No	No	This work
CI-DHS	Local	Yes	No	Yes	This work
CO	Global	Optional	No	No	[250]
Dimer	Local	No	Optional	Yes	[219]
ART	Global	No	Optional	Yes	[251]
OGS	Local	Optional	No	No	This work

Let us now briefly describe the double ended methods, namely NEB, DHS and CO. The NEB method (Figure 3.1(a)) takes a set of images of the system between the initial and final states and optimizes them simultaneously in a subspace perpendicular to the imaginary line connecting the images. Additional forces keep the images evenly distributed along the pathway between the initial and final states. The TS can be located with the NEB method using the

climbing image (CI) procedure, where the highest energy image is moved according to the Equation (3.1). When only a single image is used and let to climb (*i.e.*, CI-NEB(1)) the method is equivalent to the force inversion method of Tateyama *et al.* [222] with N in Equation (3.1) taken as a fixed vector between the initial and final states.

The DHS method uses two images starting from the initial and final states, with the lower energy image shifted towards the higher energy one in each step. Geometry optimization using only the component of the force perpendicular, $\mathbf{F}_\perp$, to the vector between the images is then performed. A few initial steps of this method are shown in Figure 3.1(b), where it can be seen that the main idea is to bracket the TS from both sides. A typical problem with a DHS run is that it will fail if both images get on the same side of the TS during the optimization. To avoid this a smaller step must be used near the TS, which can lead to slow convergence towards the TS. Here we have improved the DHS method in two simple ways: first, we provide it with more information by using a sum of the regular DHS vector and a vector connecting the two previous images on the same side of the TS. This scheme which we dub "DHS+GS" is schematically illustrated in Figure 3.1(c). Second, we avoid the slow last stage of the DHS method near the TS and terminate the run when the distance of the two images drops below a predefined value. The last two frontier images and a third image made through their linear interpolation are then used as the initial, final and guess of the TS in a CI run from which the TS can be accurately identified. We call this scheme CI-DHS.

The CO method is one of the simplest approaches and because of this is widely used (see, *e.g.*, Ref. [252]). In this approach some reaction coordinate (*e.g.*, the distance between two atoms, the Cartesian coordinates of an individual atom) is chosen and the entire system is optimized subject to this constrain. After the forces converge a step is made along the reaction coordinate and a new optimization initiated. Here we start from the initial state and use the distance to the final state as the reaction coordinate. The optimization is then performed using only the forces perpendicular to the vector between the current and final states. The CO procedure is well known to suffer hystereses problems in some cases when approaching the TS from either the reactant or the product states (see, *e.g.*, Ref. [213]).

The single ended methods try to locate the TS without any reference to the final state. Usually they follow an energetic valley leading out of the energy minimum in the hope that a TS is located at the end of the valley. Some methods require the Hessian matrix but this is unnecessary when only the minimal (softest) mode is to be followed. Methods from this class include the "dimer", OGS techniques and ART. In the ART and the dimer methods the system follows $\mathbf{F}_{\mathrm{mod}}$ with different approximations of the minimal mode $\mathbf{N}$ employed. For the ART we use a vector between the current geometry and geometry in a local minimum as $\mathbf{N}$. The initial geometry is taken as a structure close to the minimum geometry but displaced slightly along a predefined direction. The method then follows the force given by Equation (3.1) away from the minimum. The dimer method uses two images of the system with similar structures to

find the minimal mode (Figure 3.1(d)). The latter also calculates the curvature of the surface in the direction of the dimer and uses this as a switch in the modification of the force. When the curvature is positive, the system is driven only by the force parallel to the dimer, the full modified force is used in regions with negative curvature to find the TS. In the OGS method discrete steps are made towards the TS (Figure 3.1(e)) which are followed by optimization using the component of the force perpendicular to the vector to the mean of the two previous images. The very first step in this procedure is obtained by displacing the initial geometry along a predefined direction and the initial guess for each subsequent point is taken as a linear extrapolation of the geometries of the two previous images.

We note one final point that is particularly relevant to the ART method, but also to the OGS and dimer techniques. Using just $\mathbf{F}_{\mathrm{mod}}$ means that *each* atom of the system is pushed away from its fixed reference. For the surface processes examined here, large moves of all surface atoms are not desirable. To avoid this a subset of atoms is defined and only the atoms in this subset are acted upon by $\mathbf{F}_{\mathrm{mod}}$. This procedure is known as weighting and is equivalent to performing the search with a restricted set of reaction coordinates.

3.2.2 DFT computational setup

The calculations were performed using the DFT plane-wave approach within the PAW method [175, 176], as implemented in the VASP code [253, 178]. The Perdew, Burke, and Ernzerhof (PBE) [83] generalized gradient approximation (GGA) has been used throughout. A 400 eV plane-wave cut-off has been used and the NaCl surface was modelled as a two layer slab with the bottom layer held fixed. A Monkhorst-Pack k-point mesh equivalent to $4 \times 4 \times 1$ per c(1×1) surface cell was used. This setup was found to give water adsorption energies (E_{ads}) converged to within 15 meV of those obtained with an eight layer thick slab or increased number of k-points or PW cut-off of 600 eV (Table 3.2). The fact that this is such a benign system, converging rapidly with respect to the number of layers used, has been seen before [235, 254]. Aside from the convergence tests summarised in Table 3.2, which were performed in a c(1×1) cell, a c(2×2) surface cell was used throughout, corresponding to a water coverage of 0.125 ML, where one monolayer (ML) corresponds to one water per surface NaCl pair. For this coverage the adsorption energy, E_{ads}, is -370 meV. This value is similar to those reported before using PBE and the PW91 exchange-correlation functionals [234, 235, 236]. However, it is less than the ~ -500 meV obtained recently by Li *et al.* using accurate quantum chemistry methods and embedded cluster approaches [244]. There could be at least three reasons for such a discrepancy. First is related to the exchange functional which has the GGA form. This leads to wrong asymptotic behaviour of the exchange potential and generally too small electronic gap. The consequences of this are, for example, too large polarisability which can affect the binding energies of water [255]. Often such problems can be alleviated by using a hybrid functional. However, as was shown by Li *et al.* [244], the PBE and PBE0 (hybrid version of PBE) functionals give adsorption energies that differ by less than 10 meV ($E_{\mathrm{ads}}^{\mathrm{PBE}} = 326$ meV, $E_{\mathrm{ads}}^{\mathrm{PBE0}} = 317$ meV

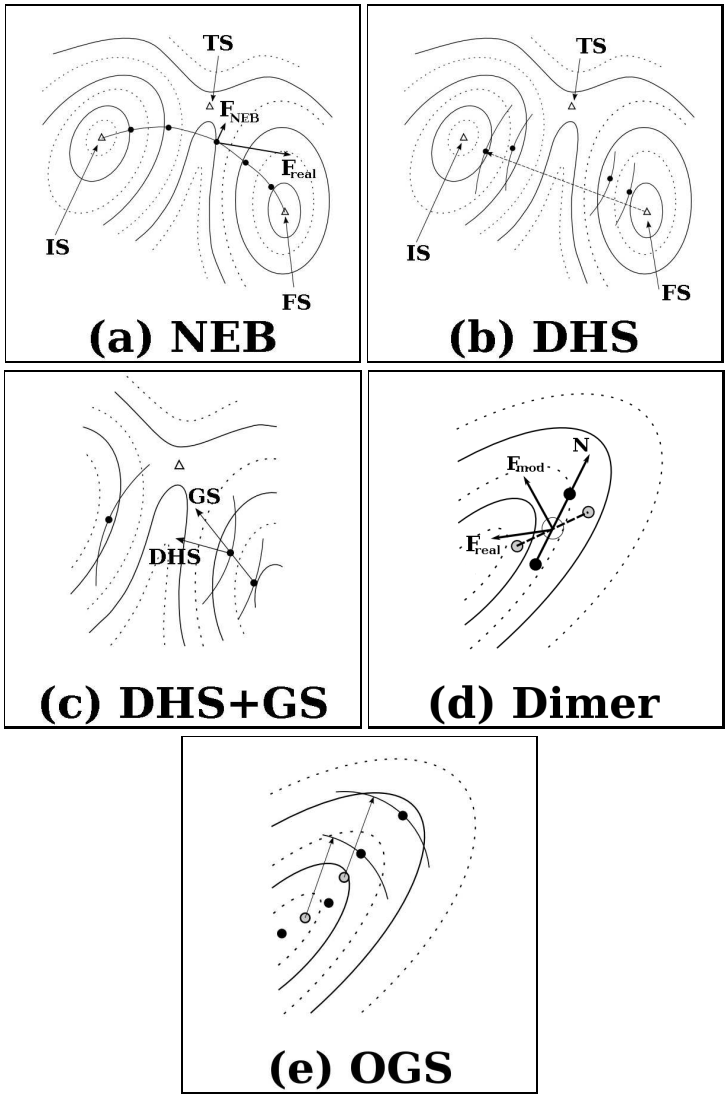

Figure 3.1: Schematic illustrations of some of the methods employed: (a) The NEB method is shown after a few steps with images connecting the initial and final states represented by black circles. The real force $\mathbf{F}_{\mathrm{real}}$ (shown for one image) is replaced by optimization of the force, $\mathbf{F}_{\mathrm{NEB}}$, in a subspace perpendicular to the imaginary line that connects the images. (b) The DHS method tries to confine the TS from both sides using two images. During the procedure the image with lower energy makes a step towards the other image with subsequent constrained optimization. Here we show four initial steps. (c) In the DHS+GS method the step is not made directly towards the image on the other side of the TS (DHS arrow) but is combined with the vector connecting two previously converged images on the same side (GS arrow) in a defined ratio. (d) The dimer rotates (from gray circles to black circles) to find the direction that minimizes the sum of the energies of both images. The component of the real force $\mathbf{F}_{\mathrm{real}}$ that is parallel to the direction of the dimer $\mathbf{N}$ is then inverted to produce a modified force, $\mathbf{F}_{\mathrm{mod}}$, that is used in the geometry optimization procedure. (e) In the OGS method discrete steps are made followed by constrained optimization. Linear extrapolation of two previous images is used to supply a guess for the subsequent optimization which is performed with the distance constrained to the mean of two previous images.

in the structures of Li *et al.*). Second, the PBE functional could be just too repulsive for the interaction of water with the ions. To test this, we calculated the interaction energies of water binding to Na^+ ion in gas phase. The results of these tests are summarised in Appendix A and show that PBE as well as PBE0 give very good agreement with the reference data. The third possible cause of the too weak E_{ads} could be missing long-range electron correlation in PBE. This, in fact, seems to be the most important reason and we will discuss this in depth in the following Chapters.

Table 3.2: Adsorption energy of a water molecule on NaCl(001) for different number of layers in the slab. The adsorption energy, E_{ads}, is calculated according to: $E_{\mathrm{ads}} = E_{m+\mathrm{NaCl}} - (E_m + E_{\mathrm{NaCl}})$, where $E_{m+\mathrm{NaCl}}$ denotes the total DFT energy of the slab with the adsorbed molecule, and E_m, E_{NaCl} give the energy of a free molecule in the simulation cell and free slab, respectively. In each slab the bottom NaCl layer was held fixed and all other atoms allowed to relax. The tests reported here have been performed in a c(1×1) cell.

Number of layers	1	2	3	4	6
E_{ads} [meV]	-359	-341 $(-353)^{\mathrm{a}}$	-343	-338	-345

[a] Using a $6 \times 6 \times 1$ k-point mesh and a 600 eV plane-wave basis energy cut-off.

A similar setup was used for the calculation of HCl adsorption and dissociation. Additional convergence tests for this system established that the HCl adsorption energy and dissociation barrier were converged to within 10% of the values obtained on a four-layer slab. Since this process is examined merely as an example of one with a high barrier ($\sim$1.5 eV) this precision is sufficient for the present purposes.

The values obtained for the activation energies, E_{a}, are defined as

$$E_{\mathrm{a}} = E_{\mathrm{TS}} - E_{\mathrm{IS}}\,, \tag{3.2}$$

where E_{TS} and E_{IS} are the adsorption energies of the TS and initial states, respectively.

The TSs used for reference purposes have been converged with extreme accuracy settings (forces $<$0.001 eV/Å) with either the CI-NEB or the dimer method and confirmed with vibrational frequency analysis. When the performance of the different TS search methods in identifying the reference TSs is compared a more practicable $<$0.01 eV/Å convergence tolerance is used. To aid comparison between the various methods we define the approximation of the TS for methods that do not converge to the reference TS as the point with the highest energy and $\mathbf{F}_\perp$ converged to a given criterion (for DHS, OGS, and CO) or, for ART, as the first geometry with the real force pointing in the same direction as $\mathbf{N}$. Approximate TS structures are compared by determining the Euclidean distance[1] of the approximate TSs from the reference TSs.

[1]The difference between two structures A and B is determined from $\Delta_{\mathrm{geom}} = \sqrt{\sum_i (x_i^{\mathrm{A}} - x_i^{\mathrm{B}})^2}$, where the sum runs over all coordinates, x_i^{A} and x_i^{B}, in the structures A and B, respectively.

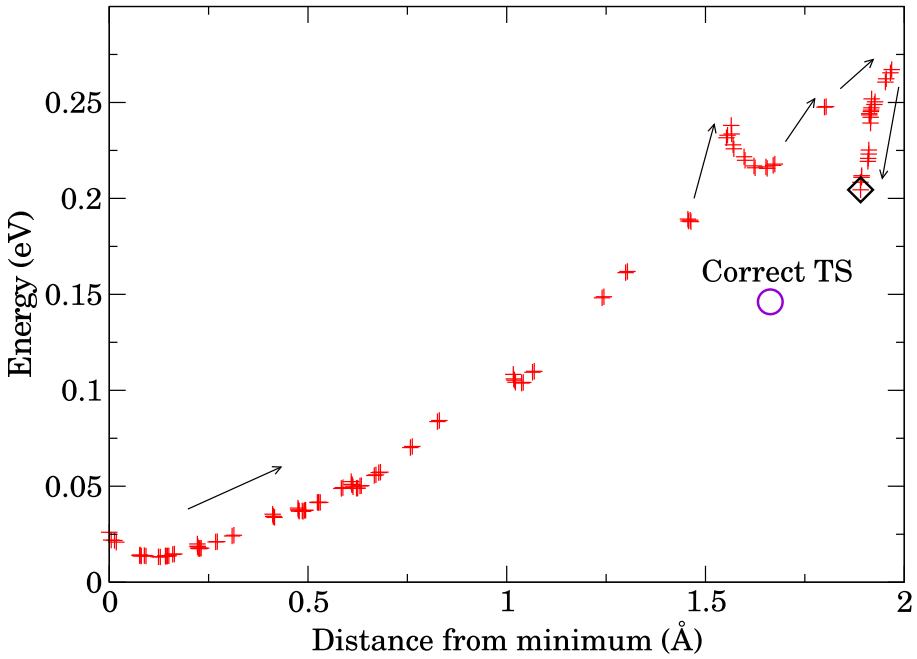

Figure 3.2: Energy versus distance from the minimum during an ART run towards the O-flip TS. The system follows a force inverted along the vector to the minimum and the progress of the method is illustrated by the arrows. The estimate of E_a is 228 meV after 120 steps (black diamond) compared to the NEB or dimer converged value of E_a = 145 meV (violet circle). Continuation of the run beyond 120 steps (not shown) did not lead to convergence to the correct TS.

We find that distances up to 0.2 Å give a good representation of the geometry of the TSs and errors of only a few meV in E_a, whereas distances of ∼1 Å give bad geometries and energies. The general approach adopted in this study is illustrated by Figure 3.2. The evolution of the total energy is shown for one TS algorithm (ART). The final structure identified is indicated by the black diamond, which resides about 83 meV above and 0.88 Å away from the reference TS (violet circle) which was previously identified with NEB and confirmed with vibrational analysis.

The NEB method is implemented in VASP and some additional algorithms are available with the TSTools[2] package. The other techniques tested or introduced here, which are not part of TSTools, have been implemented in a similar manner. The TSTools package also contains force based optimisers that are suitable for use with the methods compared here.

3.3 Water molecule diffusion on NaCl(001)

The most stable geometry for water adsorption is shown in Figure 3.3(a). The oxygen atom of the water molecule is located approximately above a Na site, with the two OH bonds directed at adjacent Cl sites. This geometry is similar to the one observed in previous DFT calculations [234, 235, 236]. The location of the oxygen above the Na matches the adsorption site suggested on the basis of helium scattering experiments for 1 ML coverage [226]. Due to symmetry there

[2]See: http://theory.cm.utexas.edu/henkelman/code/

are four equivalent orientations of the water adsorption geometry from the perspective of Na (and eight from the perspective of Cl). One can thus imagine many possible ways for water to move from one site on this surface to another. The question is which ones are relevant, *i.e.*, what diffusion processes have low energy barriers. Three processes have been identified before by Cabrera-Sanfelix *et al.* [235] and in this study a fourth has been determined[3]. We label the three previously identified processes according to Ref. [235] and call the newly found mechanism "Higher O-flip". All the initial, transition and final states for the four processes are depicted in Figure 3.3(b)–(e). Two of the processes involve only reorientation around the Na adsorption site (OH-flip and Parallel Rotation) whereas in the other two the water molecule moves from one Na site to another (O-flip and Higher O-flip). All processes involve molecular diffusion across a relatively static substrate. The E_a for each process is quite small: 50 meV for the OH-flip and 82 meV for the Parallel Rotation, in which the water molecule moves only around the Na site; 145 meV for the O-flip and 166 meV for the Higher O-flip, which lead to changes in the Na adsorption site. Similar values were obtained by Cabrera-Sanfelix *et al.* [235] where the OH-flip, Parallel Rotation, and O-flip processes were first identified and the small differences (22 meV for OH-flip, 9 meV for Parallel Rotation and 5 meV for O-flip) can most likely be attributed to slightly different computational set-ups.

Using these established TSs, we then sought to see which methods could identify them or approximate them and how quickly this could be done. The main conclusion from these water diffusion studies, to be discussed in more detail below, is that the NEB method using a single climbing image was the most efficient algorithm at identifying the TSs. However, when only a poor guess of the TS geometry is available, the CI-DHS method introduced here was competitive. We now consider the results of each method separately, starting with those that require both initial and final state configurations.

3.3.1 NEB

The performance of the NEB approach in combination with the climbing image procedure is now discussed, dealing specifically with how the efficiency depends on the number of images[4]. The NEB method is known to be sensitive to the initial guess of the reaction pathway [220]. Here, in order to be as unbiased as possible, the initial guesses of the pathways go through TSs that have been obtained through a linear interpolation of IS and FS structures, with the water molecule then adjusted to have a H-O-H angle of 180°. Overall, NEB proved to be robust and quite efficient at locating the TSs and mapping each MEP. Indeed, three out of four TSs were

[3]We find here that one of the previously identified processes (H-flip) [235] goes through a stationary point with two imaginary frequencies.

[4]Tests with various geometry optimisers were also performed for a single image NEB run. These were largely in agreement with the results of Ref. [247]. Two of the TSTools optimisers (conjugate gradients (CG) and limited memory Broyden-Fletcher-Goldfarb-Shanno (L-BFGS) methods) converge in fewer steps (*e.g.*, for the OH-flip CG needs 200 steps and L-BFGS 127 steps) than the default VASP optimisers (CG (278 steps) and modified Newton-Raphson scheme (>500 steps)) and than the other TSTools optimisers (Fire: 493 steps).

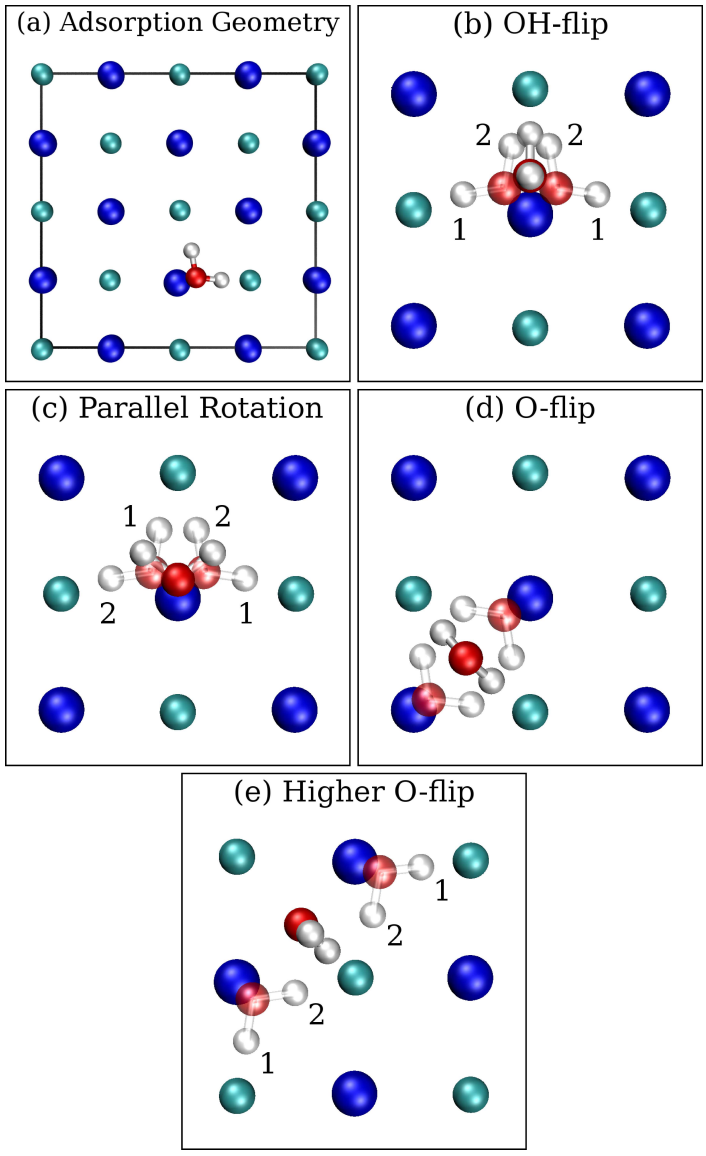

Figure 3.3: Equilibrium adsorption geometry (a) and four TS structures for water on NaCl(001). In (b) to (e) the initial and final states for each transition are shown in pale colours. The unit cell shown in (a) has been used for all studies, only a small portion of it is shown in (b)–(e) for clarity. Similarly, labels have been added to the hydrogen atoms in the initial and final states. The initial guesses of the pathways for the NEB method go through geometries with the position of oxygen obtained by a linear interpolation of IS and FS structures and the hydrogen atoms added to form an H-O-H angle of 180° which makes such structures less biased. Na, Cl, O, and H ions are coloured blue, green, red, and white, respectively. This colour scheme is used throughout.

Table 3.3: Summary of the main results obtained for the four water diffusion processes considered, reporting the number of ionic steps (energy and force evaluations) needed to converge the geometry of the various TSs with a force accuracy of 0.01 eV/Å or for the approximate methods (DHS, DHS+GS, ART, OGS, CO) to reach the highest energy point on the path. Also reported are the activation energies, E_a, in meV and the Euclidean distance, Δ_{geom}, in Å of the approximate TSs from the reference TSs. The failure of a method to converge even approximately to a given TS is indicated by "F". Diffusion processes not considered with a given method are indicated with a dash. Results for the DHS+GS method are shown for two levels of accuracy.

Method	OH-flip			Parallel Rotation			O-flip			Higher O-flip		
	Steps	E_a	Δ_{geom}	Steps	E_a	Δ_{geom}	Steps	E_a	Δ_{geom}	Steps	E_a	Δ_{geom}
CI-NEB(1)	127	50		68	82		34	145		470	166	
CI-NEB(3)	579	50		210	83		132	145		–	–	–
CI-NEB(8)	1216	50		608	82		656	145		–	–	–
Dimer	F			F			337	145		600	166	
DHS[a]	272	90	0.67	126	112	0.71	147	146	0.14	375	196	0.66
DHS+GS[a] (H)[b]	250	80	0.66	111	109	0.67	136	149	0.23	249	180	0.44
DHS+GS[a] (M)[b]	255	74	0.58	88	108	0.70	105	140	0.19	333	178	0.46
CI-DHS[a]	302	50	0.04	179	82	0.08	155	145	0.02	433	166	0.06
ART	400	170	1.37	F			120	228	0.88	F		
OGS[a]	164	67	0.87	F			81	285	1.36	F		
CO[a]	251	107	1.00	62	150	0.81	73	181	0.53	291	280	1.00

[a]Convergence criterion of 0.05 eV/Å for perpendicular forces and stepsize of 0.2 Å used.

[b]Medium (high) settings in VASP correspond to an accuracy set to medium (high), wavefunction convergence criterion 10^{-5} eV (10^{-6} eV), and the use of real (k-space) projectors. The computational cost is decreased by about a factor of three when medium compared to high accuracy settings are used.

identified in a relatively small number of steps (<130 steps).

Assessing the effect of the number of images on the total performance, we give results for the NEB with one, three and eight images in Table 3.3[5]. All three set-ups converge to an identical TS and E_a. However, the main thing we find is that the total number of energy/force evaluations needed to converge the climbing image increases with the number of images used. Surprisingly, this also almost always involves a slight increase in the number of steps per image when more than one image is used. For example, for the OH-flip the number of steps needed to identify the TS increases from 127 to 579 to 1216 upon going from 1 to 3 to 8 images. The increase in the number of steps per image arises because more images must be simultaneously converged to a certain value to let the climbing image converge to the TS. Of course, increasing the number of images is not entirely detrimental since more images generally improve the approximation of the full MEP. However, when only the TS structure and energy are of primary interest, using multiple images represents an unnecessary computational burden.

3.3.2 DHS, DHS+GS, CI-DHS

In the DHS method two images of the system climb towards each other to meet at the TS. This technique performed reasonably well, approximately identifying all TSs. For the O-flip it performed particularly well, obtaining a TS within 1 meV of the reference one in 147 steps. However, the other activation energies are somewhat overestimated (up to 40 meV for the OH-flip) since the method does not always converge accurately to the precise TS structure. To improve the performance of DHS we developed two new algorithms: DHS+GS and CI-DHS.

In the DHS+GS algorithm more information about previous geometries is retained and used in order to improve the quality of the extrapolations made at each subsequent step. Specifically, as mentioned in section 3.2.1, we base the extrapolations on a sum of the regular DHS vector and a vector connecting the two previous images on the same side of the TS (see Figure 3.1(c)). To test the influence of the GS-like step on the performance we ran several simulations for the OH-flip process with the DHS and GS contributions combined in proportions from 10:0 to 1:9. The optimal performance, which resulted in a 20% decrease in the number of steps was achieved for a 1:1 mixing ratio[6]. For all the other processes we therefore used a 1:1 mixing of the DHS and GS-like vectors which decreases the number of required steps by 10 to 30% and, with the exception of the O-flip, improves the final geometry.

In the CI-DHS method we combine the appealing features of the CI-NEB and the DHS methods: the ability of the DHS to confine the TS by walking from minima; and reliable

[5]A short NEB initial run with the QuickMin optimizer was performed and subsequent optimization using the climbing image used the global L-BFGS method (except for the three image Parallel Rotation run, where the CG method had to be used).

[6]Increasing the GS part over this value leads to a decrease in performance because the images are more likely to end up in the same energy valley leading from the TS. We expect the 1:1 mixing to perform well in most situations, though there might be no improvement or even a decrease in performance compared to DHS for highly curved MEPs.

convergence to the transition state using two fixed images to approximate the transition mode. As shown in Table 3.3 this combined method locates precisely the same TSs as the CI-NEB method. In the DHS part we found it expedient to use the DHS+GS variant just described and the CI procedure was started once the Euclidean distance of the frontier images was <1 Å. The total number of steps required is larger than that for the CI-NEB(1) method with the exception of the Higher O-flip where the CI-DHS performs the best out of all of the methods considered. In this case the CI-DHS needed 433 steps whereas CI-NEB(1) required 470 steps. The CI-DHS is superior to CI-NEB for this process because the method does not require a guess of the TS geometry – something which strongly influences the performance of the NEB method.

3.3.3 Constrained optimization (CO)

We now briefly discuss the CO technique where the system makes steps from the initial to the final state with subsequent optimization in the direction perpendicular to the vector between the current and final states. Although this method, by construction, found pathways from the initial to the final states for each process, the overall performance was poor with the TS structures and energies identified differing significantly from the reference TSs. For all processes the errors in the geometry were in the range of 0.5–1.0 Å and the activation energies were off by as much as 114 meV. As for the DHS scheme the best result was obtained for the O-flip process with the TS error being 0.53 Å and the barrier 36 meV higher than the accurate E_{a}. The poor performance of this method for water diffusion compared to, *e.g.*, diffusion of a single atom across the surface or cleavage of a single covalent bond, where the CO method has been shown to offer adequate performance, is attributed to the greater complexity of the water diffusion PES. Specifically the processes examined here involve substantial rotations and reorientations of the water molecule going through TSs that are poorly described by a linear interpolation of the initial and final states. For example, in the TS for the OH-flip the water molecule is upright (along the surface normal) whereas in the IS and FS the molecule is almost flat (parallel to the surface).

3.3.4 Dimer

Turning our attention to the single ended approaches, we start with the dimer method. The dimer is a rather popular approach, however, for this particular system it exhibited variable or poor performance. When started from the adsorption geometry, it failed to locate two of the four TSs: the OH-flip and Parallel Rotation. In addition, it only located the O-flip TS after a very large number of steps (337 compared to 34 with CI-NEB(1)) and with a "restrictive" choice of parameters[7]. This particular search is shown in Figure 3.4 where it can be seen that ∼50% of the steps are spent on lowering the force from 0.1 to 0.01 eV/Å with energy already converged to within 1 meV. However, a very positive feature of the dimer method was that it was able to identify the Higher O-flip TS, a TS that had not been identified before. Nonetheless this again required a very large number of steps (600), and, in general, for the water diffusion

[7]The system converged only when the maximum step size was reduced to 0.1 Å, more rotations were allowed (6) and a tighter torque criterion was set (0.5 eV).

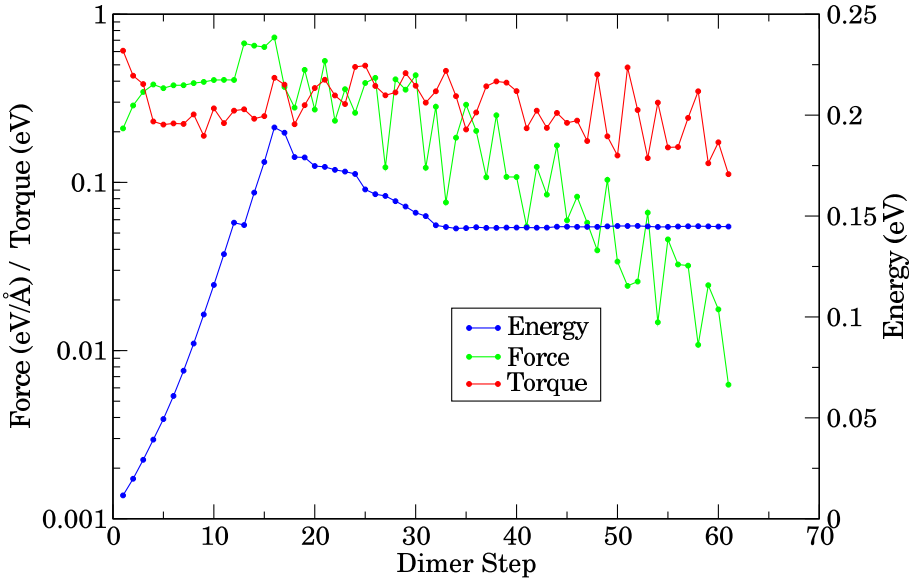

Figure 3.4: Energy (blue), force (green), and torque (red) acting on the dimer during the O-flip TS search. During the first part of the run where the energy profile seems to be parabolic, the curvature is positive and the system only maximizes its energy along the minimal mode. When the curvature becomes negative, the system also minimizes energy in every other direction. The method converged to 0.01 eV/Å after 61 dimer steps (337 energy/force evaluations).

processes examined here the dimer method was thus rather inefficient.

In the original dimer paper [219] it was suggested that the dimer could be used as a scheme for refining the geometry of the TS from a preconverged NEB run with, for example, forces that are on the order of 0.1 eV/Å. To this end we ran several dimer calculations starting from (CI-)NEB-preconverged geometries. These calculations converged for the O-flip and Parallel Rotation with default dimer parameters and for the OH-flip when a higher number (6) of rotations per step and smaller geometry step (0.1 Å) were used. However, we found that the dimer method was actually slower in converging to the TS for water diffusion than a simple continuation of the CI-NEB run. Although the real force is modified in the same way in both methods using Equation (3.1), the mode **N** is refined in each step in the dimer whereas in CI-NEB the **N** is given by the geometries of the images adjacent to the CI.

3.3.5 ART

Moving to the simpler single ended methods, we begin with the ART. Overall, this technique showed poor performance not converging to any of the TSs and only approximating the OH-flip and O-flip TSs with large errors in geometry and energy. The inversion of the force along the vector between the reference and actual geometries causes the force to point upwards towards the transition ridge independent of which side of the ridge the system is on. Therefore, when the system reaches the transition region, it simply hops back and forth. Figure 3.2 shows the energy versus distance from the minimum for an ART run directed towards the O-flip TS[8].

[8]The weighting procedure was used here so that only the force acting on the water molecule was modified.

Although the method approximated this particular TS, continuation of the run did not lead to convergence with the estimate of the TS structure being 0.88 Å away from the reference TS.

3.3.6 OGS

Finally, we discuss the performance of the OGS method, another new technique tested here. This approach was more successful than ART, decreasing the number of steps needed to approximate the TS and obtaining more accurate activation energies. However, as with ART, only two of the TSs were approximately located: the O-flip and the OH-flip TSs. Given that the other TSs (Parallel Rotation and Higher O-flip) have higher activation energies and lie in a similar direction to the approximated TSs, we conclude that the ART and OGS methods preferably find lower lying transitions in a given direction. As an example of the OGS procedure, we show in Figure 3.5 the evolution of the energy during two OGS runs directed towards the O-flip TS. The simulations are the same except for one the weighting procedure is applied. Without weighting (red) the surface atoms tend to shift from their equilibrium positions which artificially increases the E_a. Weighting eliminates this problem lowering the estimate of E_a for this process from 293 to 178 meV.

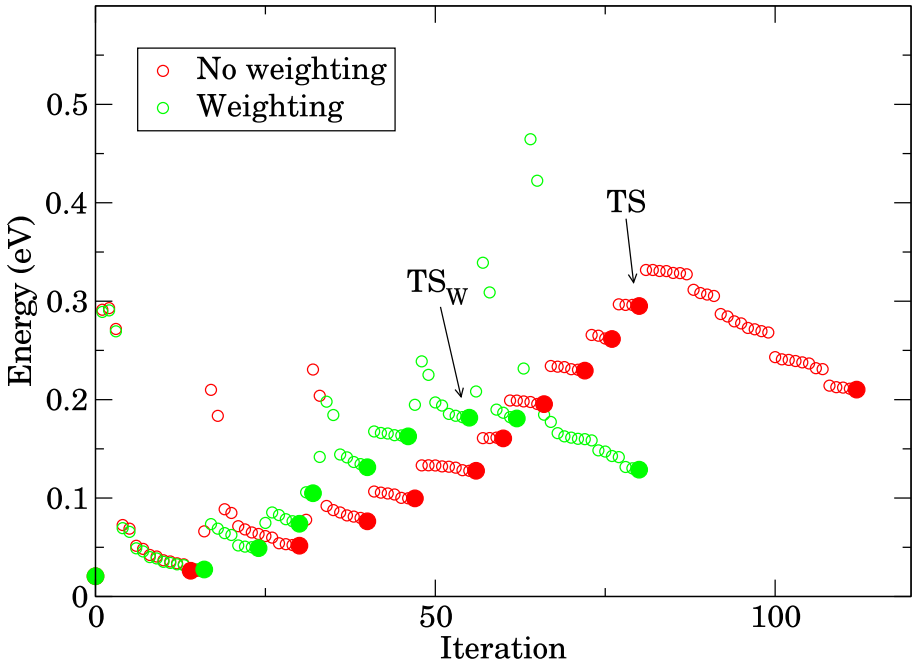

Figure 3.5: Energy versus number of ionic steps during two OGS runs from the energy minimum towards the O-flip TS (only parts of the runs are shown). In one run the weighting procedure (*i.e.*, only the force acting on the water molecule is changed) was used (green) whereas in the other the modified force was applied to all atoms (red). The filled circles show the points at which the perpendicular forces $F_\perp$ are converged with a convergence criterion of 0.05 eV/Å. The estimate of E_a was 293 meV and 178 meV, after 80 and 55 steps, without and with weighting, respectively. The NEB or dimer converged value of E_a is 145 meV. The location of the transition state estimates without (TS) and with weighting (TS$_W$) are also indicated.

3.4 HCl dissociation on NaCl(001)

So as to broaden the scope of this study and to evaluate the performance of some of the methods for a rather different surface process, in particular one with a considerably higher barrier, HCl bond breaking on NaCl(001) was examined. The initial and final states for this process, obtained through an extensive set of structure optimizations, are shown in Figure 3.6. The initial state is a weakly adsorbed molecular state with an adsorption energy of −230 meV. In this structure the tilted HCl molecule rests along a surface NaCl pair with the hydrogen end down. The final state is 1.45 eV higher in energy than the initial state and has the hydrogen inserted between two surface Cl ions with a neighbouring Na being considerably displaced upwards from its ideal lattice position. The pathway connecting these two states, obtained at first by NEB using 8 images, is depicted in Figure 3.7. With these initial and final states we then considered the efficiency with which the different methods identified the TS that separated them. The lowest energy TS identified for this process (Figure 3.6) has an activation energy of 1.70 eV relative to the initial state. The main results of the various methods tested are summarised in Table 3.4.

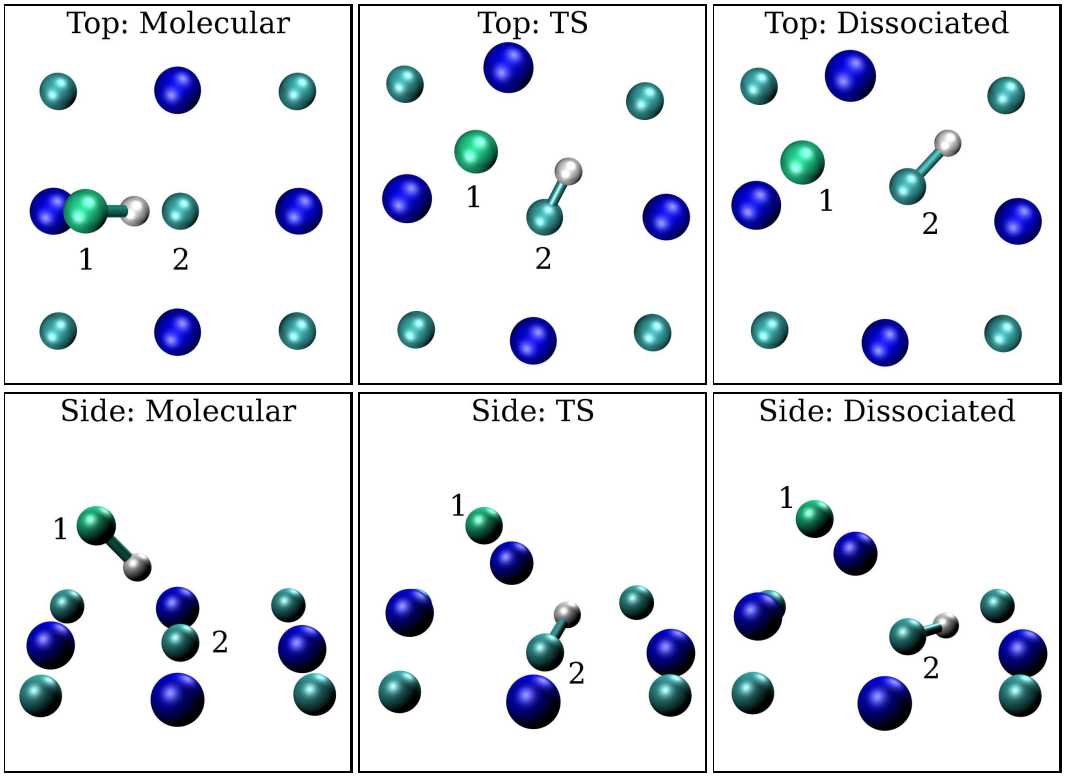

Figure 3.6: Top and side views of molecularly adsorbed (left), TS (middle) and dissociated (right) states for HCl on NaCl(001). The process involves the cleavage of the H-Cl(1) bond followed by the formation of the H-Cl(2) bond and the ejection of a Na from the lattice which then forms a new bond with Cl(1). Note that only part of the surface is shown.

Table 3.4: Number of ionic steps needed to converge to the TS for HCl dissociation at NaCl(001) with a force tolerance of 0.01 eV/Å. The errors in the geometry and energy estimates compared to the dimer method with forces converged to 0.001 eV/Å are given. Two data sets for the DHS and DHS+GS methods refer to different accuracy settings. The data for the CI-DHS method is divided into the DHS and CI parts of the calculation.

Method	CI-NEB(1)	CI-NEB(4)	CI-NEB(8)	Dimer	DHS (M/H)[a]	DHS+GS (M/H)[a]	CI-DHS
Number of steps	187	432	1040	192	188/262	182/228	121 + 52
Δ_{geom} [Å]	0.15	0.16	0.12	0.06	0.65/0.62	0.63/0.63	0.45
ΔE_{a} [meV]	<1	<1	<1	<1	11/6	7/7	<1

[a]Medium (high) settings in VASP correspond to an accuracy set to medium (high), wavefunction convergence criterion 10^{-5} eV (10^{-6} eV), and the use of real (k-space) projectors. Moreover, $\mathbf{F}_{\perp} = 0.05$ eV/Å for "M" and $\mathbf{F}_{\perp} = 0.01$ eV/Å for "H".

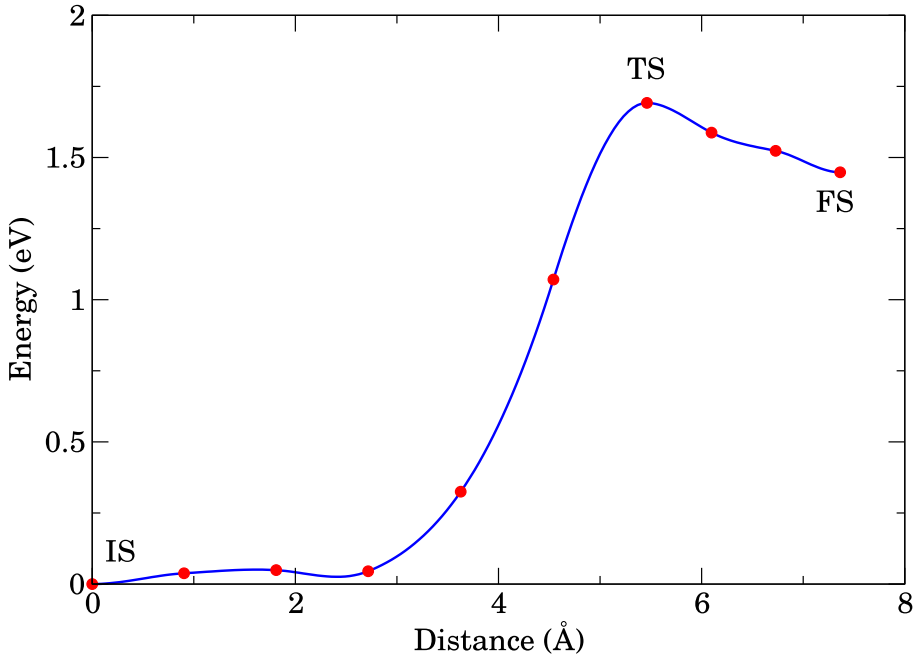

Figure 3.7: Energy pathway obtained for HCl dissociation from an eight image NEB run, with the climbing image converged to the TS. Each image is depicted by a red circle and the blue line was obtained by spline interpolation and should be regarded as a guide to the eye. The distance along the reaction coordinate was calculated by integration of the length along this spline.

3.4.1 NEB

For HCl dissociation we compare again NEB with one, four and eight images between the initial and final states[9]. In each case an equivalent TS was identified. However, we find again that extra images do not offer improved performance compared to a single image. Although the forces drop more smoothly for NEB runs with more images (Figure 3.8), the single image NEB run again converges in the least number of steps: 187 steps for one image compared to 432 and 1040 steps for four and eight images, respectively. Of course multiple images can also be used to obtain the full MEP rather than the TS alone (see Figure 3.7). Nonetheless, if one is only interested in the height of the barrier using multiple images represents an unnecessary computational burden.

3.4.2 DHS, DHS+GS, CI-DHS

For this reaction the DHS algorithm was rather rapidly able to identify an approximate TS structure. Specifically the DHS method identified the TS after 145 steps with an error of 18 meV and Δ_{geom} of 0.72 Å. We explored in detail how the quality of the $\mathbf{F}_\perp$ determinations

[9]To allow for a comparison of the methods, the same procedure was used with each number of images. First a linear interpolation was used to obtain the initial guess of the images and only after 25 steps was the climbing image procedure switched on. In addition, we note that a similar number of steps to converge was found for the CG and L-BFGS optimisers for four and eight images. However, the L-BFGS optimizer seems to require higher wavefunction accuracy (one order) and the CG optimizer performs better when the system starts further from the TS.

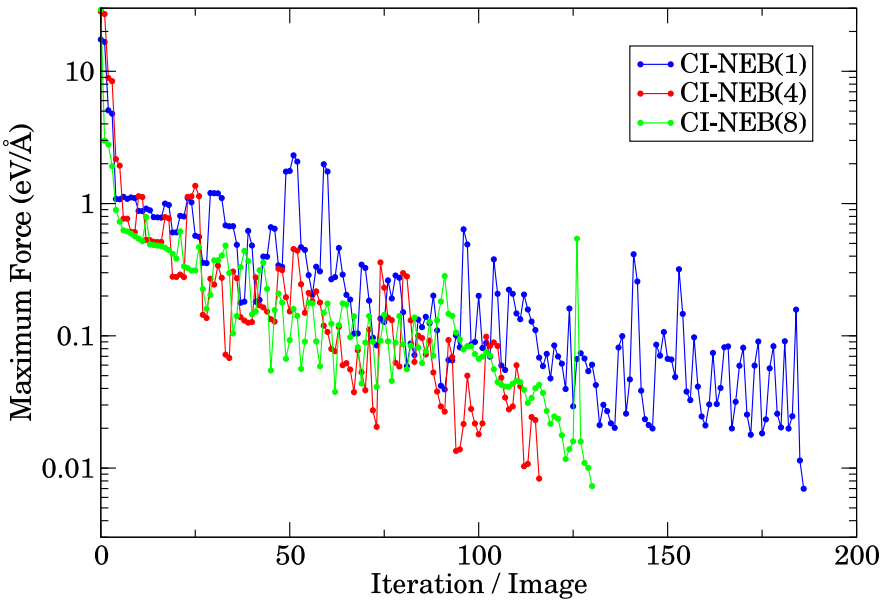

Figure 3.8: Maximum atomic force in the climbing image for one (blue), four (green) and eight (red) image NEB calculations for the HCl dissociation process. A conjugate gradient optimizer was used for the CI-NEB(1) and CI-NEB(4), whereas the global L-BFGS optimizer was used for CI-NEB(8).

and convergence criteria impacted upon the results obtained with a series of calculations at different $\mathbf{F}_\perp$ values (0.05, 0.02, and 0.01 eV/Å) and convergence settings. However, as can be seen from Table 3.5, reducing the value of $\mathbf{F}_\perp$ does not have a significant impact on the quality of the TS estimate, whereas it does have a big impact on the number of steps required to reach convergence. For this process, it is therefore not worthwhile to reduce the $\mathbf{F}_\perp$ convergence tolerance below 0.05 eV/Å. The DHS+GS approach was also considered and exhibited similar performance to the original DHS scheme (Table 3.4). The CI-DHS method was again superior to conventional DHS leading to convergence to a much better quality TS after 173 steps. As can be seen from Figure 3.9, the energy profile is also well reproduced compared to the NEB data (Figure 3.7). Although the error in the geometry is rather large ($\Delta_{\text{geom}} = 0.45$ Å), the quality of the TS can readily be improved by using a tighter force convergence criterion during the CI procedure. For example a 0.001 eV/Å convergence criterion leads to $\Delta_{\text{geom}} = 0.004$ Å after about another 150 steps, *i.e.* essentially the reference TS is located.

Table 3.5: Number of ionic steps needed to converge the DHS method for the HCl dissociation process and the resulting errors in energy and geometry for three values of $\mathbf{F}_\perp$ at two different levels of accuracy (see Table 3.4).

Accuracy	High[a]			Medium[a]		
$F_\perp$ [eV/Å]	0.05	0.02	0.01	0.05	0.02	0.01
Number of steps	145	204	262	188	294	431
ΔE_{a} [meV]	18	1	−6	11	6	−3
Δ_{geom} [Å]	0.72	0.67	0.62	0.62	0.65	0.58

[a]Medium (high) settings in VASP correspond to an accuracy set to medium (high), wavefunction convergence criterion 10^{-5} eV (10^{-6} eV), and the use of real (k-space) projectors.

3.4.3 Dimer

For HCl dissociation the dimer method performed much better than it did for H_2O diffusion. Indeed the number of ionic steps required to identify the TS was comparable to the CI-NEB(1) method. We note however, that since the energy profile is asymmetric, the number of steps needed to reach the TS depends on whether the run starts from the initial or the final state. Whereas 192 ionic steps were needed to reach the TS from the final state, from the initial state 479 steps were required[10] Interestingly, although the dimer run that started from the final state needed slightly more ionic steps than the CI-NEB(1), each individual SCF optimization was completed in fewer steps and so less time overall was needed for the dimer to converge.

For the HCl dissociation reaction the dimer could also be used just to refine a guess of a TS obtained with one of the approximate methods. As a test of this approach we used the

[10]The default set of parameters for the dimer was used in each case and the initial geometry was directed slightly towards the TS (by 0.15 Å).

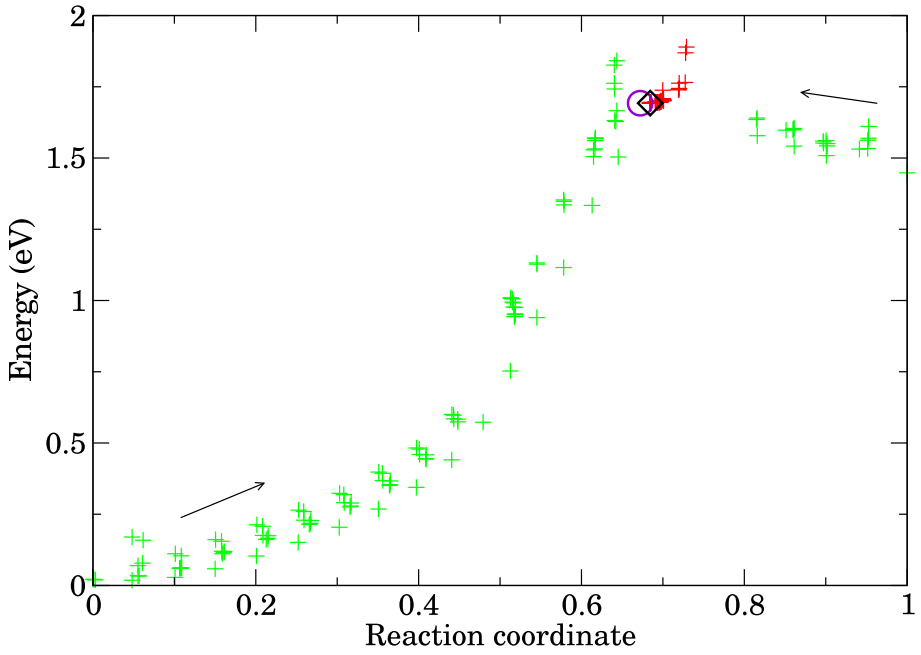

Figure 3.9: Energy versus reaction coordinate (distance from the initial state as a proportion of the total distance between the initial and final states) for the CI-DHS method for the HCl dissociation process. The DHS part is shown with green crosses with the two arrows indicating the progress of the two images. The subsequent climbing image part is shown in red. The TS identified is shown with a black diamond and the accurate (with a tighter convergence criterion) TS position with the violet circle.

DHS+GS method to supply a suitable TS guess. The dimer run required a further 117 ionic steps to converge to the TS with a force tolerance of 0.01 eV/Å. Overall, this combination of DHS+GS followed by a dimer run required ∼10% less computer time than a regular dimer run. Moreover, contrary to a single dimer run information about the whole pathway was obtained.

3.5 Summary

Let us now discuss in a broader context the performance of the various algorithms tested here. Overall, the NEB method with a single climbing image is superior to the other techniques when a suitable guess of the TS is available. Indeed for the processes examined here it was not necessary to use multiple NEB images. Of course using multiple images provides additional information about the shape of the MEP, however, if the TS alone is sought multiple images may be unnecessary. Nevertheless, in cases where interpolation between the IS and FS can be easily made, running a short NEB run with multiple images is a useful means to obtain a guess of the TS. The TS can then be refined using a CI-NEB(1) run with the highest energy image and the adjacent images used as the TS, IS, and FS, respectively [216, 246][11].

[11]For example, in the HCl dissociation case we used the first part of the NEB(8) run with 25 steps to approximate the pathway and then the highest energy image and its neighbors to perform the CI-NEB(1) run. This second calculation needed 71 steps to converge giving 271 steps in total and an error in the geometry of

In cases when only a poor initial guess of the TS is available and when both the initial and final states are known, then the modified DHS schemes presented here provide a means to approximate the MEP relatively quickly (DHS+GS) and to subsequently converge to the TS (CI-DHS). Indeed, in such cases the CI-DHS required less steps to converge to the TS than the CI-NEB(1) method. Moreover, the DHS method does not require as accurate forces as NEB (or dimer) and can therefore be used with lower accuracy settings that require less time to converge the SCF procedure. Overall the CI-DHS scheme offers some potential for further investigations given that it is a relatively simple technique, easy to implement and competitive with CI-NEB.

Performance of the ART and OGS methods was found to be unsatisfactory since both methods failed to identify the TS of the HCl bond breaking process and only some of the TSs were approximately identified for water diffusion. Selecting only some atoms to move according to the modified force (weighting) is essential for ART and improves the performance of the OGS method. However, application of the weighting procedure is less straightforward for processes that involve large displacements of the surface atoms, such as the HCl dissociation. The CO method had problems with reorientations of the water molecule which resulted in poor performance for water diffusion. The conclusion that the reaction coordinate driven methods (ART and CO) essentially fail for some processes is in agreement with previous studies [213].

The overall performance of the dimer method was rather poor for water diffusion. This is probably caused by the flat PES with several low energy modes of, *e.g.*, translation. On the other hand, we have some positive remarks: i) a new TS was found with this method (the "Higher O-flip" process); ii) unlike other methods the dimer correctly did not identify the "H-flip" stationary point which has two imaginary frequencies with our setup and was previously suggested to be a TS [235]. For HCl dissociation, the dimer could easily align with the bottom of the deep PES valley and its performance was better than that of the NEB with any number of images. Thus, a clear conclusion of this study is that the dimer method is considerably more efficient when the PES to be explored is highly corrugated.

Let us conclude with a few more comments of the effects that arise in the TS search because of the SCF procedure used to evaluate the DFT energy. With each SCF iteration the values of the energy and forces are (usually) improved until a predefined convergence criterion is achieved. Therefore methods that rely on accurate forces, such as the dimer, in general require more SCF iterations than methods that do not converge accurately to the TS, such as DHS or OGS. Specifically, since forces and energies in two proximate points are compared in the dimer method, it needs a more tightly converged wavefunction with ΔE between two successive SCF steps at least one order lower than is required by the NEB method. Similarly for structure optimizations, the accuracy of the forces required by the NEB method increases as the converged MEP and TS are approached. A computationally efficient scheme to account for this is therefore to use a relatively poor SCF convergence criterion in the initial stages of the

---

$\Delta_{\text{geom}} = 0.19$ Å.

TS search followed by more accurate settings as the quality of the MEP improves and the TS is approached. A final aspect of the SCF procedure that is relevant here is the quality of the trial structures used. The structure interpolation used in some methods can lead to initial structures with very distorted geometries. For example for the OH-flip process, interpolation of the initial and final states leads to an initial guess of the TS in which one of the OH bond is only 0.3 Å long. First ten geometry optimizations need twice as many SCF steps than optimization of a structure near the adsorption minimum. Even worse, linear interpolation for the Higher O-flip process puts the hydrogen atoms in the same place and running SCF would be meaningless. Similarly, the efficiency of the NEB with multiple images is also reduced by the fact that in typical NEB implementations within electronic structure framework all images of the system are optimized in parallel and must wait for the slowest image to converge the SCF procedure. Therefore, initial structures that are far from the initial and final states can take many more SCF steps to become converged. In each of these cases an algorithm such as the DHS method will not suffer from such deficiencies.

Chapter 4

Water clusters on NaCl surfaces and the initial stages of NaCl dissolution

4.1 Introduction

We will now continue to study the interaction of water with the NaCl surface but with an increased number of water molecules. The consequences of exposing salt to water are rather well-known: it dissolves. However, it is not understood how this process is initiated and how it proceeds on the molecular scale. For example, defects such as steps or kinks are expected to be more prone to release the ions than terraces but their relative importance is not known. And although it is obvious that during the dissolution all the ions are released from the lattice, it has not been established if the dissolution proceeds via single ions or ion pairs. While experiments [256] suggest that at low humidities Cl ions could be the first to become solvated it is not clear if the Na ions leave as well or if they tend to stay. It is also interesting to ask what actually is the number of water molecules required so that the release of the ions becomes energetically favourable. These are the questions that we address in this Chapter by studying small water clusters on different rock salt surfaces.

The dissolution process has been subject to a number of experimental studies using a wide range of techniques, which we discuss here briefly. Infrared spectroscopy measurements [242, 257, 258] performed at different temperatures and humidities have found adsorbed water films of varying thickness depending on the humidity. When the coverage reached about 3 monolayers at ambient temperature the spectrum changed from one resembling bulk water to one resembling a brine spectrum suggesting an onset of dissolution of the surface. This work and previous ultraviolet photoelectron spectroscopy experiments [259] stressed the importance of defects for the dissolution process. However, as information averaged over the whole surface of the sample is obtained a detailed molecular scale picture is missing. Much more detailed information has been obtained using atomic force microscopy (AFM) and scanning force microscopy (SFM) (or scanning polarisation force microscopy (SPFM)) techniques in experiments of Dai *at al.* [243], Shindo *et al.* [260, 261], and others [262, 256, 263]. The measurements revealed that the surface geometry starts to change when the humidity is increased above $\sim 40\%$. The SPFM experiment

also observed that before a water film covers the terraces, water molecules adsorb at defects [256] such as steps. At humidities of ∼35% this leads to an increase in SPFM contrast which was explained by the release of the ions from the step and their solvation. An observed decrease of the contact potential has been explained by assuming that the Cl ions are released first from the steps. Similar conclusions were presented based on experiments combining AFM and ambient pressure X-ray photoelectron spectroscopy of Verdaguer *et al.* [263]. However, it is not clear why the Cl should be released first since when cations are present as impurity on the step, they seem to be solvated first [256].

Since the experimental measurements are often unable to obtain molecular level information, molecular simulations have been widely used to gain information about the dissolution process. So far, mainly two rather distinct approaches have been used: the first uses accurate post-Hartree-Fock (post-HF) methods to study binding energies of small water clusters containing Na and Cl ions. The use of post-HF approaches limits the size of the systems that can be studied and also zero temperature is implied, as post-HF molecular dynamics (MD) studies are extremely rare. Several studies have been published where adsorption of water molecules on a small cluster was studied and the energy needed to displace one of the ions from the ideal lattice position calculated [264]. In a related study [265] it has been claimed that six water molecules are sufficient to break a single NaCl molecule into a separated ion pair, however, the omission of temperature effects could be a severe approximation. The rather small size of the systems that can be treated using post-HF method seems to be rather limiting for obtaining general conclusions and trends valid for realistic surfaces.

Most studies of the salt dissolution process use a different approach where a molecular dynamics (usually employing forcefields (FF)) method is applied. From the several studies performed [266, 267, 268], a recent one of Yang [269] has found a higher probability for corner Cl ions to leave the crystal first. Although during this simulation the dissolution process is directly addressed, the simple forcefields employed don't account for effects such as polarisation or possible dissociation of the water molecule. Only recently have studies appeared where density functional theory (DFT) is used to study the interaction of liquid water films with a flat salt surface [270, 271] and the dissolution process into a liquid water film [272].

In this Chapter we focus on calculating the vacancy formation energy for different vacancies on several types of NaCl surfaces with increasing defectivity. The vacancy formation energy is just the cost to displace an ion or a pair of ions to a less coordinated position and the surface models employed here are a flat surface, a surface with a step and a surface with a kink. Most importantly we study the energy cost as a function of the number of water molecules present on the surface using up to ∼20 water molecules. This range should correspond to the humidities for which water adsorbs at defects and some ions might be released. By using a small number of water molecules and different surfaces we hope to learn about the initial stages of dissolution and the factors that influence the release of ion(s). Specifically we hope that we will be able

to gain a more detailed understanding of the roles that the various interactions play in the dissolution process than the methods which use large coverage of water. Moreover, although the small number of water molecules has been used in the cluster studies here we use realistic models of the surface which occur on a real NaCl crystal. As we will show in this Chapter the chosen conditions allow us to confirm the release of Cl ions from steps suggested from experiments. However, the major surprise to come is that the release is only a "byproduct" of the stronger interaction of water and Na ions. The stronger interaction leads to the release of Cl ions so that more Na sites on the surface are exposed.

In the following Section we discuss the technical details of the methods employed to simulate the systems and to obtain representative structures. This is followed by study of adsorption on the different surfaces in Section 4.3.1. The dependence of the energy required to displace the ions is studied in Section 4.3.2 which is followed by discussion and conclusions in Section 4.4.

4.2 Computational setup

The surfaces were modelled using a slab geometry with periodic boundary conditions. We have studied flat NaCl(001), a surface with a monoatomic step (NaCl(017)), and surfaces with a kink, either Na or Cl terminated. The models as well as the simulation cells are depicted in Figure 4.1. In the NaCl(001) case we used three atomic layers of NaCl and a large 4×4 supercell. Four atomic layers were used to model the NaCl(017), the layers were tilted to create a step on the surface. A similar strategy was employed to create the kinks, which leads to one side of the surface having a Na terminated kink while the other side has a Cl terminated kink.

Our strategy is to compare the difference in energies of water clusters on a surface with vacancies and the lowest energy water cluster on a surface without a vacancy. Therefore we study the vacancy formation energy, which we define as

$$E_{\mathrm{vac}} = E(\mathrm{vac} + \mathrm{wat}) - E(\mathrm{wat})\,, \tag{4.1}$$

where $E(\mathrm{vac} + \mathrm{wat})$ is the total energy of the system with the water cluster adsorbed on the surface with a vacancy (displaced ion or ions). The $E(\mathrm{wat})$ is the total energy of the lowest energy adsorbed water cluster on the surface. Thus positive E_{vac} means that the vacancy is not stable with respect to the non-defected surface while negative E_{vac} means that energy is released by displacing ions from the lattice. Displacement vacancies were formed by moving an ion or an ion pair (Na-Cl) to a suitable position in the ad-layer (*i.e.*, Na on top of Cl and vice versa). Because of the very large number of possible structures for water on the various surfaces a forcefield molecular dynamics based approach has been employed to generate the plausible structures. These structures then were used for subsequent DFT/PBE calculations from which the vacancy formation energies are obtained.

The adsorption energy E_{ads} is calculated using

$$E_{\mathrm{ads}} = (E_{\mathrm{surf+wat}} - nE_{\mathrm{wat}} - E_{\mathrm{surf}})/n\,, \tag{4.2}$$

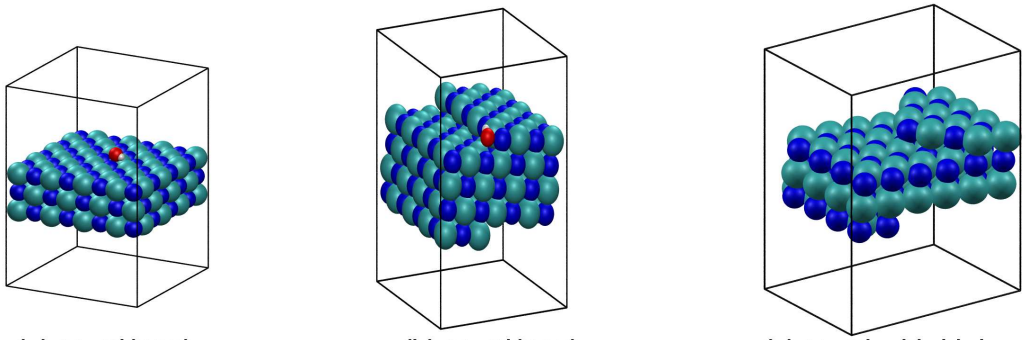

Figure 4.1: Simulation cells used in the study: (a) flat surface, (b) surface with a monoatomic step, and (c) surface with a kink. Each of the cells shown is repeated in three dimensions using periodic boundary conditions. In the case of the flat and stepped surfaces, one adsorbed water molecule is shown as well.

where $E_{\mathrm{surf+wat}}$ is the total energy of the system with a water cluster adsorbed on the surface, E_{wat} is a reference total energy of an isolated water molecule in the gas phase, E_{surf} is the total energy of a relaxed surface without any water molecules adsorbed. n is the number of adsorbed water molecules.

The forcefield (FF) calculations were performed using the Gromacs suite of programmes [273, 274]. The AMBER parameters [275, 276] were used for Na and Cl and water was modelled using the TIP4P [191] potential. We have also performed some simulations with the TIP4P2005 [190] model for comparison. These parameters were selected since they give the best agreement with PBE data for various properties of interest from the forcefields available in GROMACS. We discuss our choice more in Appendix B. The TIP4P water model is simple and when combined with AMBER gives similar adsorption energies to PBE for water on salt (see Figure 4.2). It should be noted that the vacancy formation energies are overestimated with the AMBER parameters. Although this could be improved when polarisable potentials were used, none of the tested "charge-on-spring" [185, 186] polarisable models for Na and Cl [277, 278] and water [197, 279, 280] lead to an improved description of both the water-water and water-salt interactions. Although more accurate forcefields would be definitely useful, the AMBER/TIP4P combination is sufficient for this study. This is because our final method of choice is DFT, and we require only a large number of different structures to be generated using FF and a decent accuracy within one class of vacancies.

For the DFT calculations VASP 4.6 [253, 178] was used with the PBE exchange-correlation functional [83]. A plane wave basis set with a cut-off of 400 eV and Γ point k-space sampling were employed. The core electrons in VASP are treated within the PAW method [175, 176]. The geometry optimisations were run with maximal atomic force criterion of 0.02 eV/Å. Recently it has been shown that the monomer adsorption energy is somewhat underestimated by the PBE functional [244], and since the system is in between chemisorbed and physisorbed, the dispersion

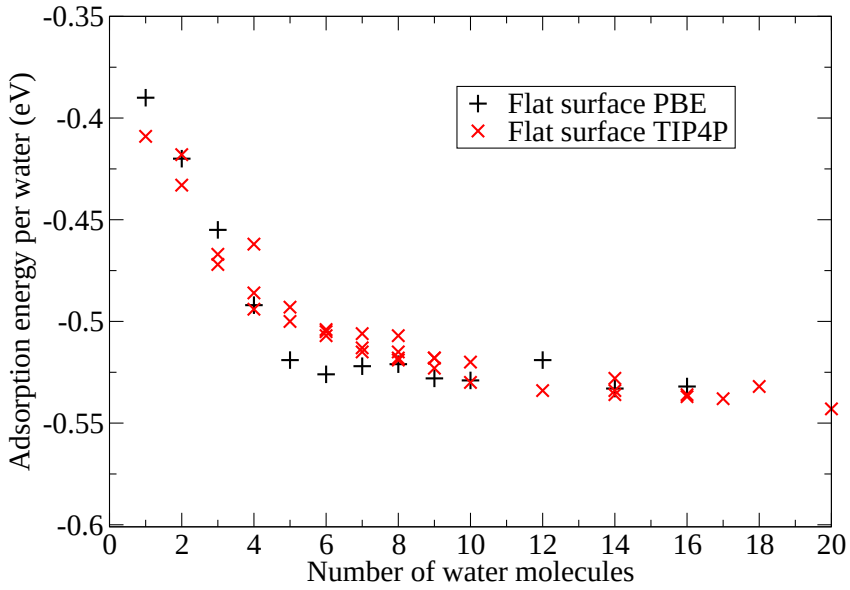

Figure 4.2: Adsorption energies per water molecule on flat defect-free NaCl(001) as calculated with DFT-PBE and FF-TIP4P/AMBER parametrisation. The two methods are in good agreement and show that for small clusters, up to six water molecules, the adsorption energy quickly decreases. The adsorption energy stays rather constant for a larger number of water molecules.

contribution can be expected to be important. We will show in next Chapter that indeed the adsorption energy can be improved when a non-local correlation functional [16] is used with a compatible exchange part. The absolute adsorption energies are affected by the choice of functional and the inclusion of dispersion. However, we have tested on several structures that the relative differences, mostly governed by stronger electrostatic contributions, do not change so as not to alter the conclusions drawn with the PBE functional. We show several examples in the second part of Appendix B.

4.2.1 Search for low energy structures

Since our goal is to compare the energy of a cluster adsorbed on the intact surface with the energy of a cluster on a surface where one or two of the ions have been displaced, we need to have a sufficient (*i.e.*, large enough) sample of representative low energy structures for each case. There are several approaches suitable for producing a large number of distinct clusters such as simulated annealing or various Monte Carlo based approaches [281]. We opted for a relatively simple and mostly automated procedure where for a given number of water molecules and type of vacancy we perform 2 ns of FF-MD simulations at 200, 230, 260, and 300 K. From each of these runs we select a large number (>200) of structures and perform geometry optimisation using Gromacs. By ordering the structures according to their energy we obtain low energy structures for each specific water cluster, and for some of them we then perform geometry optimisations

using VASP. This gives us several DFT optimised structures from which we select the lowest energy one. For some vacancies, such as the Na ion vacancy with a small number of water molecules, the ion quickly returns to the surface layer during the FF-MD. In such cases we use low energy structures from the FF-MD equilibration period, in which the vacancy ion(s) are fixed, as an input for the DFT optimisation.

Our selection procedure is able to give us a representative set of low energy structures. However, we cannot claim that we always identify the lowest energy PBE-DFT cluster. This is especially true when there is a large number of water molecules and consequently there are many possibilities for water to arrange. However, given the large number of tested clusters the trends should be recovered correctly. One needs to have in mind that we are interested in smaller clusters and the relative ease of dissolution. For large clusters where the dissolution is more probable to occur, free energy calculations are the method of choice. Although some initial steps have been performed in our group in this direction [272] using DFT, a large scale application as presented here[1] is not yet possible with DFT. In a separate study on a similar system using FF we have compared the vacancy formation free energies with the energy differences of the lowest energy clusters and found a rather good agreement [282].

4.3 Results

4.3.1 Adsorption on surfaces without vacancies

4.3.1.1 Flat surface

First we study how water molecules adsorb on the selected surfaces trying to understand the general features of the water substrate interactions. The lowest energy structure of a water monomer ($E_{\text{ads}} = -390$ meV) is found to be almost flat with O on top of a Na ion with the water hydrogens directed towards adjacent Cl ions [234, 235, 236, 244] (see Figure 4.3(a)). The water molecule can also bind to the Cl ion via a hydrogen bond, although less strongly [234, 236] ($E_{\text{ads}} = -160$ meV). A dimer (Figure 4.3(b)) can form from these two structures when a new hydrogen bond is formed involving the hydrogen of the Na-adjacent water and the oxygen of the Cl-adjacent water. The dimer structure contains one more hydrogen bond with a typical energy gain of >200 meV which increases the relative stability of the dimer and even more for larger clusters. The formation of hydrogen bonded clusters causes a progressive decrease in the adsorption energy when the number of water molecules is increased up to six (see Figure 4.2, black + data). These clusters have been studied previously in the literature, and we find the same minimum for the monomer and dimer as those reported in Refs. [234, 236, 235, 283] and a similar lowest energy structure for the trimer (Figure 4.3(c)) as in Ref. [234]. The adsorption energies in these studies don't agree that well with each other, for the monomer Park *et al.* [234] and Cabrera-Sanfelix *et al.* [235, 283] found −330 meV while Yang *et al.* [236] found −400 meV.

[1] Overall we have performed full geometry optimisation using DFT of hundreds of clusters containing around 200 atoms each in the simulation cell.

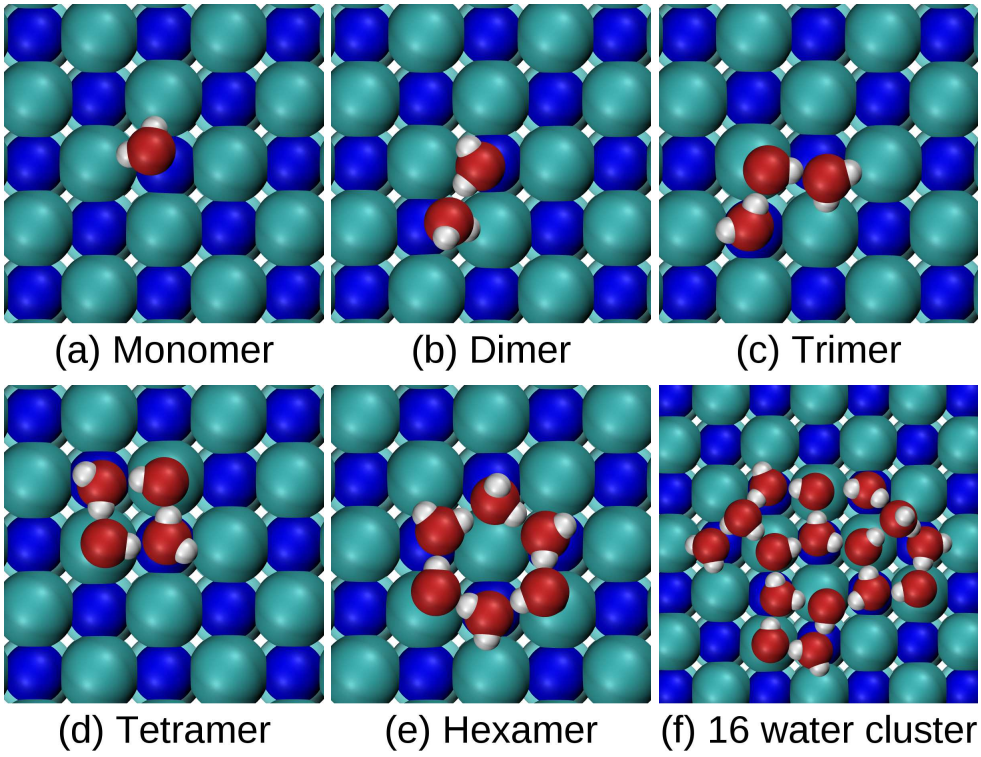

Figure 4.3: The lowest energy water clusters found on a flat surface containing 1, 2, 3, 4, 6, and 16 water molecules. The water molecules tend to bind to Na ions but adsorption on Cl is possible because such water molecules can accept hydrogen bonds. This leads to the formation of loops containing four or more molecules. For large clusters, some of the molecules can occupy positions in a second layer, and are not in direct contact with the surface.

Furthermore, while Cabrera-Sanfelix *et al.* predicts the dimer to be almost 100 meV per water more stable ($E_{\text{ads}} = -423$ meV) than the monomer, Park *et al.* found no energy gain upon forming the dimer. With adsorption energies of -390 meV and -420 meV for the monomer and dimer we obtain similar stabilities to those reported by Yang *et al.* and we find the same lowest energy structure for the tetramer ($E_{\text{ads}} = -492$ meV, Figure 4.3(d)).

When the number of water molecules is increased the clusters become more stabilised by allowing a larger number of hydrogen bonds per water molecule to form. However, once the water molecule can't form more hydrogen-bonds, its contribution to the total adsorption energy reaches some limit. In large water clusters many of the water molecules are close to this limit so that the total adsorption energy stays almost constant. This can be seen in Figure 4.2 where the PBE adsorption energy per water molecule is very similar (around -530 meV) once more than six water molecules form the cluster. It is also interesting to look at the structure of the large clusters, an example of the optimised lowest energy cluster for 16 water molecules can be seen in Figure 4.3(f). The larger clusters are generally similar to the one shown, the water molecules tend to form small connected rings with four to six water molecules that are bonded to the surface.

4.3.1.2 Stepped surfaces

Let us now focus on the defective (non-flat) surfaces where a step or a kink is present. Although such surface features will invariably be present in a real crystal, water adsorption on such surfaces has not been widely studied in the case of NaCl [284]. The most favourable adsorption site for water is next to the step where two Na ions are exposed: one Na ion is below the water molecule and a second is in the step (see Figure 4.1(b)). The adsorbed water molecule can bind to both ions which results in a much more favourable adsorption energy (−625 meV) when compared to the flat surface. In our simulation cell four such sites are present and four water molecules can adsorb strongly in these sites. When we add more waters, they occupy the Cl step sites and connect the water molecules already adsorbed on the Na ions. For eight water molecules this results in a formation of a water chain along the step shown in Figure 4.4, the most stable adsorption structure for this model (see Figure 4.5, blue ×). Additional water molecules have to adsorb on the less favourable terrace sites and they need to distort the chain structure which leads to a less stable average adsorption energy.

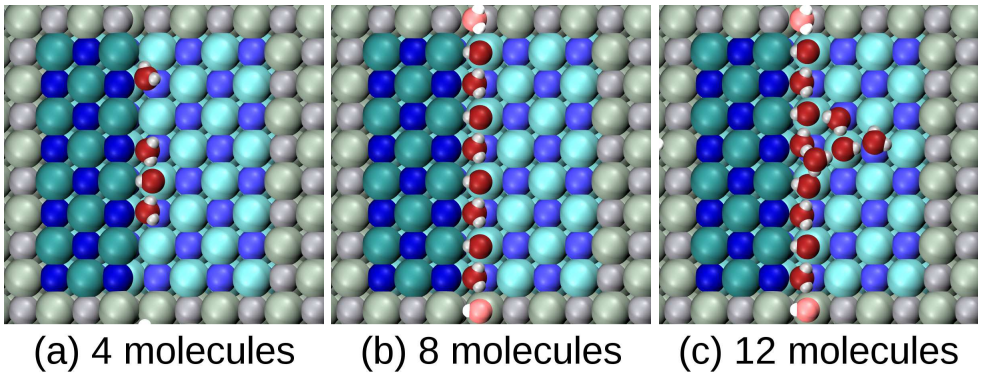

Figure 4.4: Water clusters with four, eight, and twelve molecules on the surface with a monoatomic step. The upper terrace is shown with darker colours, the lower with pale colours to highlight the step. The periodic cells are shown with light colours and this colouring scheme is used throughout. Adsorption at the step is favourable compared to adsorption on a flat surface due to the presence of sites with two adjacent Na ions exposed. The waters adsorbed to these sites can then be linked with molecules adsorbed to Cl ions that also accept hydrogen bonds from the Na-adsorbed waters.

The surface with a kink can have either Na or Cl termination and although the adsorption is much stronger on the kink than on the flat surface for both terminations, it is somewhat sensitive to the terminal ion. Specifically in the case of the Cl terminated kink the adsorption energy increases monotonically when water molecules are added. Although a chain similar to the one on the step can be formed, the corner site with three Na ions does not seem to facilitate a favourable connection of the two chains (see Figure 4.6). The water molecules that adsorb after the step sites are occupied tend to adsorb in the area between the kinks. A rather different situation appears on the Na terminated kink (Figure 4.7) where, again because of the periodicity

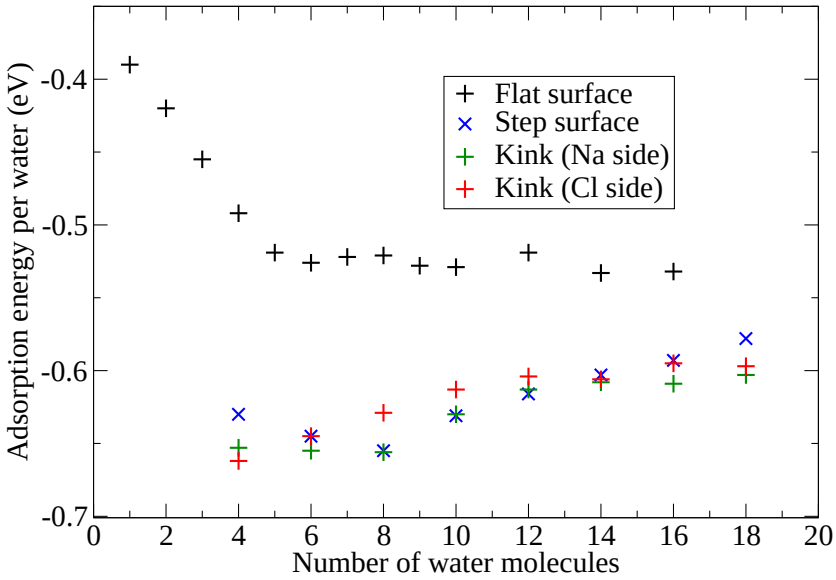

Figure 4.5: Adsorption energy per water molecule in eV for the four surfaces studied: Flat (001), monoatomic step (017), and two surfaces with a Na or Cl kink. The surface defects lead to a lower adsorption energy. However, as the number of water molecules present on the surface increases the adsorption strength for the defective surfaces weakens since the most strongly binding sites are occupied and only terrace-like sites are available.

of our model, eight water molecules can form a chain structure with very low adsorption energy. As can be seen in Figure 4.5 the adsorption energy follows closely the one on the stepped surface between 8 and 14 water molecules. The adsorption seems to be more favourable on the Na terminated kink for 16 and 18 water molecules since on this surface the clusters occupy the corner area between the two periodic kinks and thus can form more compact structures.

4.3.2 Adsorption on surfaces with displaced ions

Let us now present the results for vacancies, starting with the flat surface. Although this surface is not expected to be the easiest place to start dissolution, it turns out that many things generally relevant to the defective surfaces can be learnt. Let us just repeat that we study how the vacancy formation energy E_{vac} for different vacancies depends on the number of water molecules adsorbed. This gives us the cost in energy to displace the ion and form the vacancy and how this is affected by the presence of water. When the E_{vac} is positive, the water cluster is more stable, when E_{vac} is negative it is favourable to release the ion from the lattice position and form the vacancy.

We compare the energy cost to create various types of vacancies: single Cl or single Na ions or a NaCl ion pair, shown in Figure 4.8. For the flat surface we create different Cl vacancies by placing the ion two lattice positions away ("Cl far", Figure 4.8(c) or one lattice position away

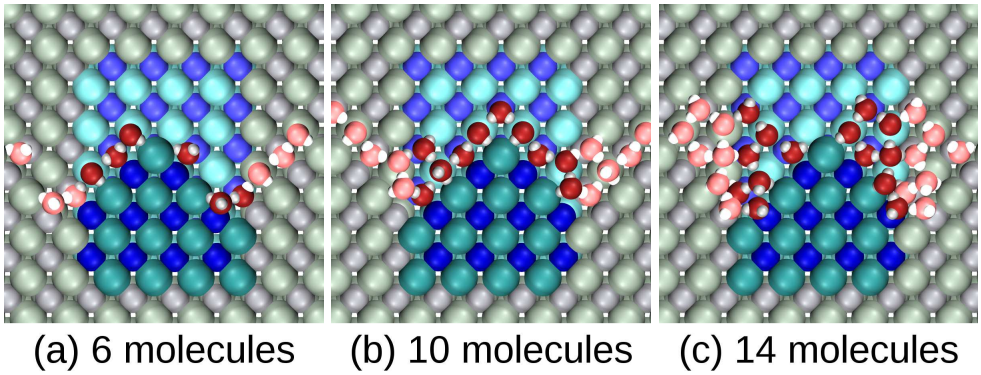

Figure 4.6: Water clusters with six, ten, and fourteen molecules on the Cl terminated kink. Although the favourable adsorption sites are present on this surface, the corner site with three Na ions does not facilitate a smooth connection of the water chains which leads to less favourable adsorption compared to the surfaces with a step or the Na terminated kink.

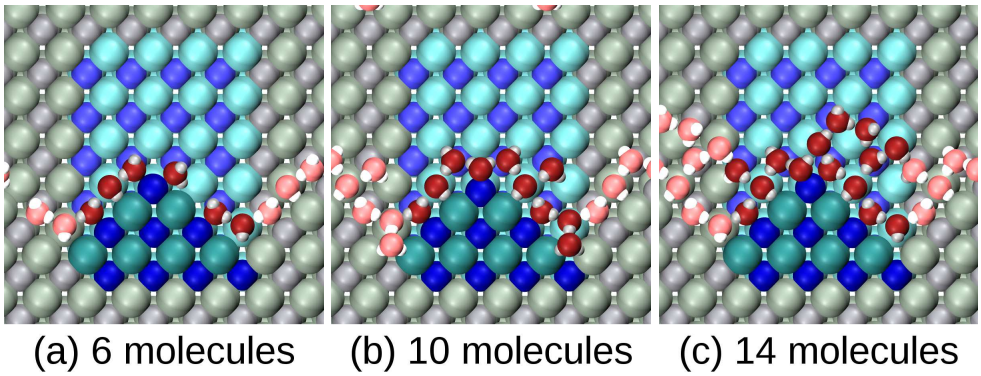

Figure 4.7: Water clusters with six, ten, and fourteen molecules adsorbed on the Na terminated kink. Similar to the surface with a step, this surface exposes the favourable adsorption sites with two adjacent Na ions. Moreover, the surface can also support a formation of a water chain.

("Cl near") from the lattice. The "Cl near" can form a "Na half out" (Figure 4.8(b)) vacancy by displacing an adjacent Na ion from the vacancy. The last Cl vacancy "Cl above" (Figure 4.8(a)) is formed when the Cl ion occupies the position above the vacancy but the vacancy itself is occupied by a water molecule. The Na ion can form a "Na near" vacancy (Figure 4.8(d)). It doesn't form a structure corresponding to the "Cl above" for reasons we will discuss later and the "Na far" vacancy becomes stable in the FF-MD simulations only for a large number of water molecules. The ion pair can be removed and displaced to a position closer or farther from the vacancy leading to "NaCl near" and "NaCl far" structures, shown in Figures 4.8(e) and (f), respectively. The vacancy formation energies are quite high, ranging from 1.7 eV for a single Cl vacancy to 2.2 eV for the ion pair vacancy. These energy costs correspond to the vacancy formation energies for zero water molecules in Figure 4.9.

Let us now discuss how the vacancy formation energies change when a small number of water

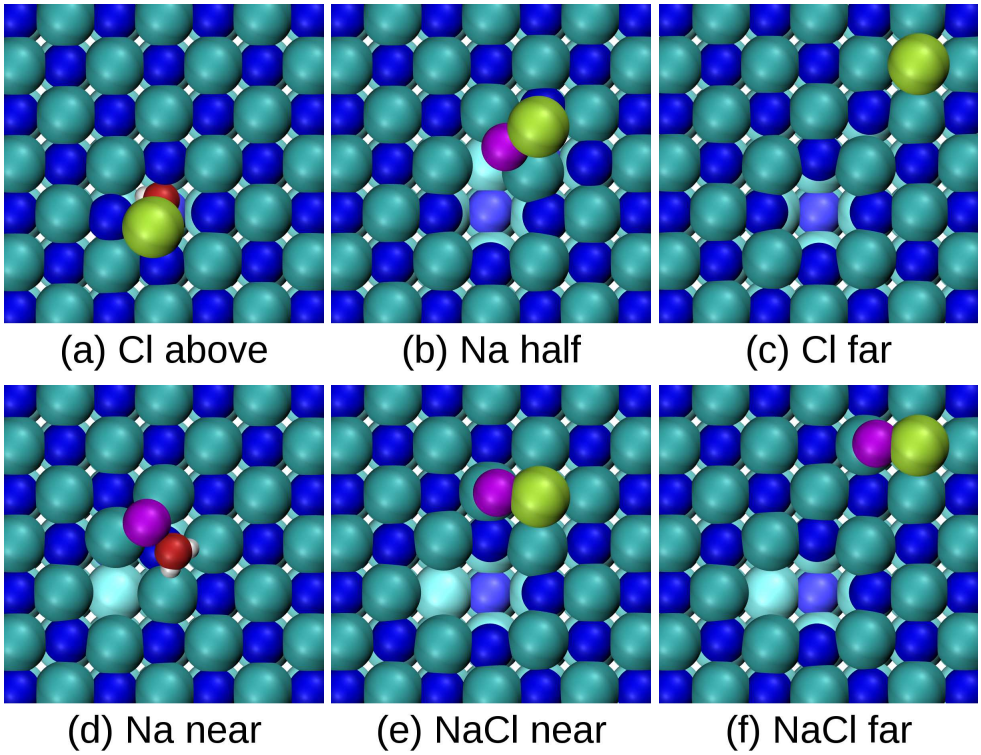

Figure 4.8: Displacement vacancies on flat NaCl(001): (a) "Cl above" where one water molecule prevents the displaced Cl from returning to its original lattice site, (b) "Na half out" which is a Cl ion vacancy where the Cl ion displaces an adjacent undercoordinated Na ion, (c) "Cl far" with the Cl ion far from the vacancy, (d) "Na near" where the Na ion has been taken out, (e) "NaCl near", an ion pair vacancy proximate to the hole, and (f) "NaCl far" with the ions taken farther. Although "Cl above" is the least costly initially (∼0.5 eV), this cost almost doesn't change when water molecules are added. In contrast, the ion pair vacancies are very costly in the absence of water molecules (>2 eV) but this energy cost is quickly reduced as water molecules can adsorb at the many favourable adsorption sites exposed.

molecules (<8) is adsorbed. As can be seen in Figure 4.9, adding water molecules decreases the vacancy formation energy significantly. This is simply caused by the fact that the surface with the vacancy offers more favourable adsorption sites for water molecules, *i.e.*, sites where the absolute value of E_{ads} is larger than on the flat surface. In the case of a Cl ion vacancy, the water molecule adsorbs into the vacancy where many Na ions are exposed, in the case of the Na vacancy the water adsorbs preferentially at the adatom, which in both cases is caused by stronger water adsorption on Na ions. This leads to an interesting situation where in the case of the Cl vacancy the water can prevent the ion from coming back into the vacancy, forming the "Cl above" structure. In the case of the Na ion vacancy the water molecules adsorb at the displaced ion. The vacancy is not "screened" by water molecules and the ion can return. Therefore although the "Na near" vacancy is less costly to create than the corresponding "Cl near" vacancy, the Cl can form the "Cl above" type of structure which has lower E_{vac}. From

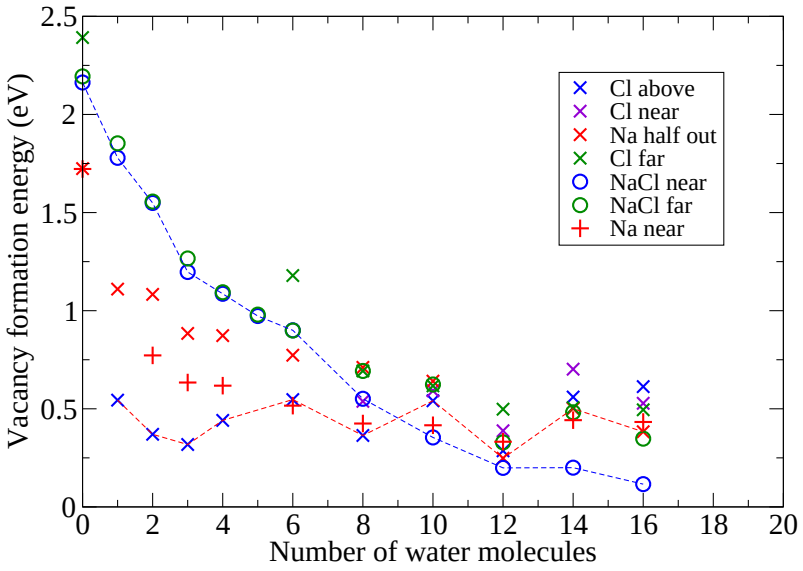

Figure 4.9: The vacancy formation energy in eV for different vacancies and number of water molecules on the flat surface. The value represents the energy cost between the lowest energy water cluster adsorbed on a flat surface and the lowest energy structure identified for a cluster with the same number of water molecules plus a vacancy. We show data for a single Cl vacancy, ion pair vacancy and single Na vacancy. The red (blue) dashed curves connect the lowest energy single ion (ion pair) vacancies.

the costs of the single ion vacancies it's clear that there is a competition between the ion-ion and ion-water interactions. The water molecules interact strongly with Na ions but the Na ions also seem to be less "stable" when removed from the lattice site.

When we look at E_{vac} for more than 8 water molecules we note that the energy cost needed to create the single ion vacancy basically does not change. This can be again simply understood from Figure 4.10, where a "Cl near" vacancy with 8, 12, and 16 waters is shown. Once the vacancy and adatom are covered by water molecules, the water molecules adsorbing next see an environment similar to adsorption on a flat surface without any vacancy. That is, the displaced ion or vacancy decrease the adsorption energy only for the water molecules directly in contact. The adsorption energy can be therefore decreased only when not a single ion but an ion pair is displaced. This requires more energy initially since the surface is more deformed, on the other hand more sodium ions are exposed to the water molecules, presenting more favourable adsorption sites. In the case of the "NaCl near" vacancy the energy gain is sufficient to bring the energy cost of the ion pair vacancy below the cost of single ion vacancies once ∼10 water molecules are adsorbed. The cost drops to just 100–200 meV for the largest clusters we have studied, this is a major reduction and just 5–10% of the vacancy formation energy computed

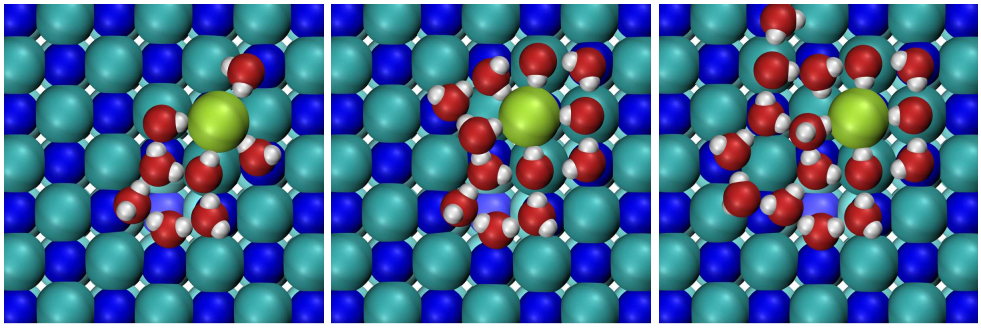

Figure 4.10: The "Cl near" vacancy on the flat surface with 8, 12, and 16 water molecules. The water molecules occupy the most energetically favourable adsorption sites. Initially, the exposed sites in vacancy are covered. For 12 water molecules also the positions adjacent to the displaced Cl ion are occupied. Now all the defects induced by creating the vacancy are covered with water molecules and water molecules adsorbing next can only occupy a site not directly connected with the defect. Their adsorption energy is basically not affected by the defect and is similar to water molecules adsorbing on the flat surface without any vacancy.

in the absence of water. However, since all the favourable sites are covered by water molecules, the energy cost does not decrease when more water molecules are added.

Thus on the flat surface we have not observed a situation where it would be energetically favourable for the ion to leave the lattice. From the trends observed we can conclude that for a given number of water molecules, structures where all the favourable adsorption sites created by the displaced ions are covered with water molecules should be the most stable. Structures with fewer displaced ions will have many water molecules adsorbed on non-favourable sites whereas configurations with more displaced ions won't have enough water molecules to cover all the adsorption-favourable positions. Therefore the ion pair vacancies become less costly than the single ion vacancies once the number of water molecules is high enough.

We now focus on the surface with a monoatomic step, where some of the ions are less coordinated. As with the flat surface we have compared the energy cost to create a single Na or Cl vacancy near or further, and ion pair vacancies. The different vacancies are shown in Figure 4.11 and are analogous to the ones on the flat surface with the removed ion either near to or far from the vacancy as well as ion pair vacancies. Moreover, we use a vacancy that we call "Cl contact" (Figure 4.11(c)) which is similar to the "Cl above" on the flat surface. That is the Cl ion is close to the vacancy which is hindered by a water molecule. As can be seen from Figure 4.12 the vacancy formation energy first rises when water molecules are added. This can be understood with the help of Figure 4.5 and the fact that the system with eight water molecules without any vacancy is very stable. For more than eight water molecules the step without any vacancy does not represent such a favourable adsorption site and the vacancy formation energy quickly decreases. One particularly stable structure is formed by the "Cl near" vacancy where

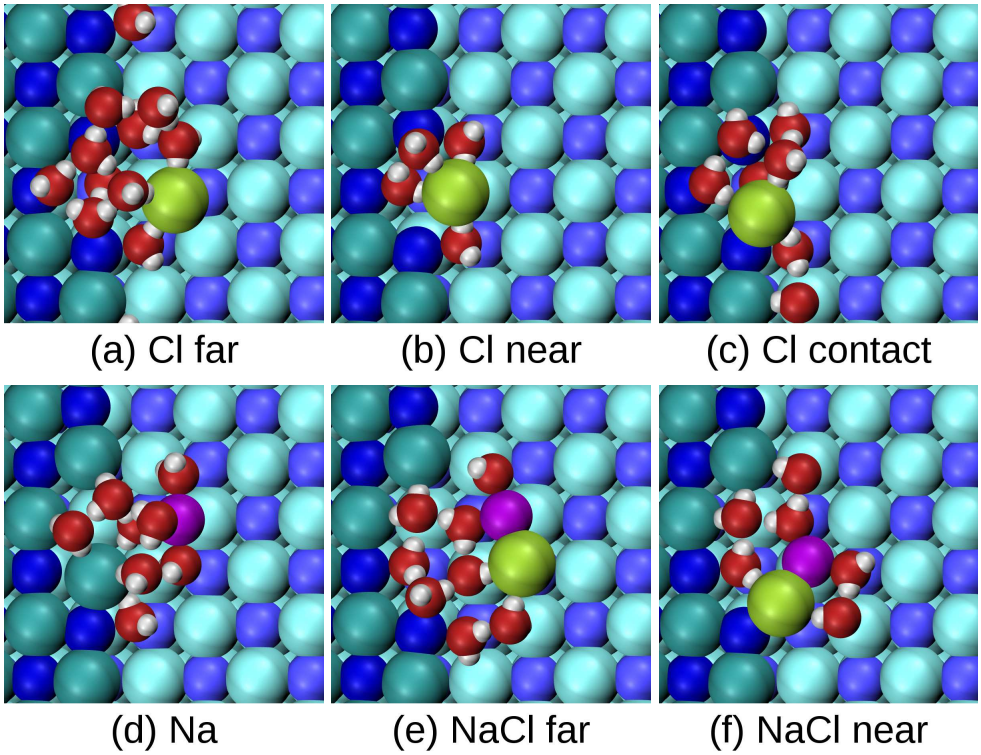

Figure 4.11: Displacement vacancies on the NaCl surface with a monoatomic step. The Cl ion can reside far ("Cl far") from the vacancy, or can sit in a hydration shell ("Cl near"), or it can come into contact with a Na ion adjacent to the vacancy site ("Cl contact"). The Na ion vacancies are less stable and we show data for the "Na" vacancy, which is equivalent to the "Cl far". We displace the ion pair to a "NaCl far" position, and also structures denoted as "NaCl near" occurred during the molecular dynamics, in these structures the Cl ion is raised above the step. As is shown in Figure 4.12 the ion pair vacancies have rather similar energy cost to the single Cl vacancies and all have a small cost (<0.2 eV) for a large number of water molecules.

the Cl ion is taken out of the step and partially hydrated by water molecules that bind to the exposed Na ions at the same time. We show several structures of this vacancy for increasing number of water molecules in Figure 4.13. Interestingly, the Cl ion is not in contact with a Na ion but rather above another Cl ion and surrounded by six water molecules, each of which is adsorbed to a Na ion. This represents favourable adsorption sites for the water molecules. And even more, for 16 water molecules the cost to create this vacancy becomes negative, *i.e.*, it is energetically favourable to release the Cl ion. Although energy is lost by creating the vacancy, the gain obtained by adsorbing water molecules to favourable Na sites is able to bring the total energy below the energy of the lowest energy cluster adsorbed on a step which has only a limited number of favourable Na sites.

The ion pair vacancies are less costly to form than on the flat surface with the cost being similar to that of the single Cl vacancies. It seems plausible from the trend that the NaCl pair will become favourable for more water molecules. However, because of the large number

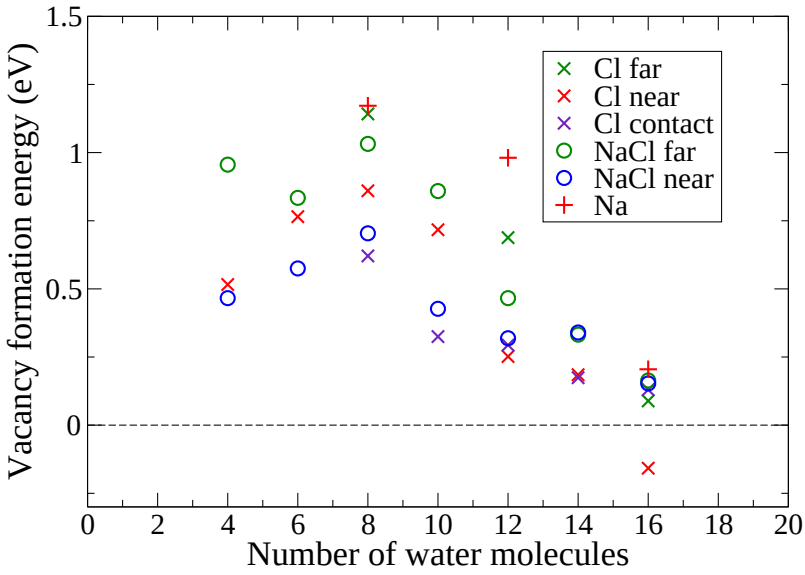

Figure 4.12: The vacancy formation energy on a surface with a monoatomic step. We show data for a single Cl or Na vacancy in different arrangements and data for two types of NaCl dimer vacancies. As can be seen for 16 water molecules it is more favourable to form the "Cl near" vacancy than to form a cluster on the step. The cost initially increases because a favourable structure is formed on the step without a vacancy for 8 water molecules.

of water molecules it's difficult with our approach to obtain a number of water molecules when this will happen. Nevertheless, if the ions are to diffuse on the surface, both Na and Cl need to be released. The Na vacancy by itself is not favourable to form, even with respect to the ion pair vacancies. This agrees with our former findings, indeed, when Na is displaced from the step, a site packed with Cl ions is exposed which does not yield favourable adsorption sites for water.

Let us now move to the surfaces with either Na or Cl terminated kink sites. As with the flat and stepped surfaces we calculate the vacancy formation energy for a single ion or ion pair vacancies and various numbers of water molecules. In the case of a Na terminated kink the single ion vacancy is a Na ion, which upon displacement exposes two Cl ions, shown in Figure 4.14(a). As we have already learnt from the previous surfaces such a structure is not favourable for water adsorption and one would not expect the Na vacancies to be preferred. Figure 4.15 shows that this is indeed the case and in fact it is easier to create the ion pair vacancies. However, even for the pair vacancies E_{vac} for a large number of water molecules is quite high, above 300 meV. The apparent increase in the vacancy formation energy seen in Figure 4.15 for 14–18 water molecules is partially caused by a lower adsorption energy on the kink visible in Figure 4.5, another reason could be insufficient sampling of the lowest energy clusters.

The last surface model we have considered is the Cl terminated kink structure and we show

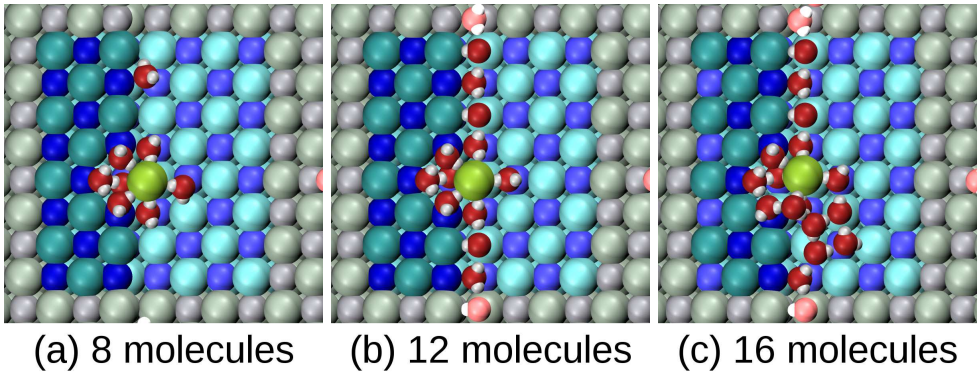

Figure 4.13: The hydrated Cl ion vacancy ("Cl near") on the monoatomic step with eight, twelve, and sixteen water molecules. This vacancy represents a very stable structure and becomes favourable for 16 water molecules.

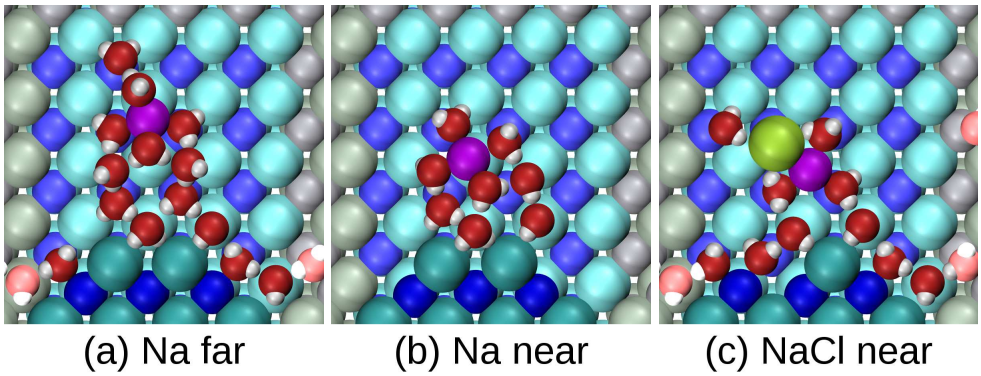

Figure 4.14: Displacement vacancies on the NaCl surface with a Na terminated kink. We show data for structures where the Na ion is either far ("Na far") or close ("Na near") to the vacancy. As with the ion pair vacancies can occupy a position near or far from the vacancy.

the different vacancies in Figure 4.16. The displacement of Cl ions exposes favourable adsorption sites for water molecules and thus one would expect that: i) the release of the ions could become favourable for a large number of waters; and ii) the cost of single ion vacancies will be initially lower than the cost of ion pair vacancies (as opposed to the situation on the Na terminated kink which we just discussed). The latter point is indeed observed: the single Cl ion vacancy in the "Cl near" configuration (Figure 4.16(b)) has a lower vacancy formation energy than the "NaCl near" vacancy (see Figure 4.17). Moreover, the structure "Cl contact" (Figure 4.16(c)), where the Cl ion is only slightly displaced has an even lower energy cost. However, it seems that this vacancy does not expose enough Na ions to become favourable compared to the kink surface without a defect. Although the final vacancy formation energies for most of the vacancies are quite low, around 200 meV, we haven't found any vacancy structure that would be favourable compared to the surface without any vacancy. This is also true for the "Cl near" structure which cannot form the very compact and favourable structure as on the step. There could be one more reason why we don't observe a favourable release of the ion from the lattice which

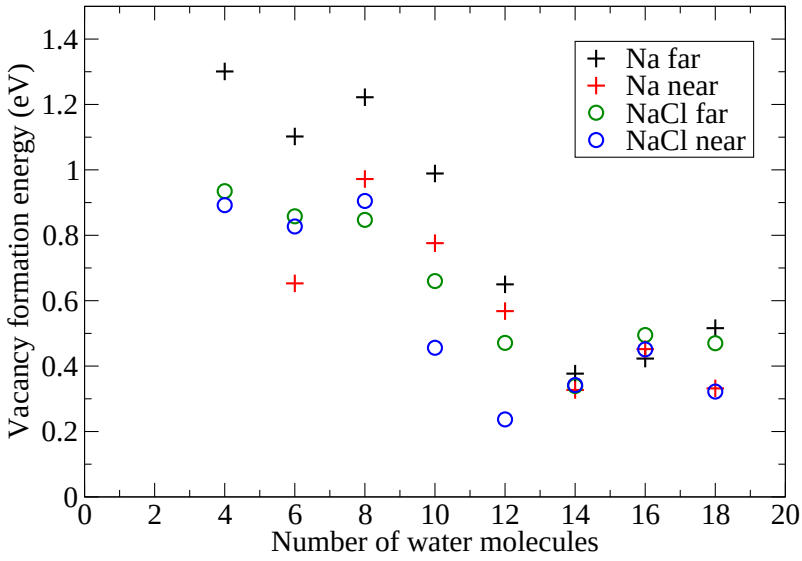

Figure 4.15: The vacancy formation energy on a Na terminated kink surface for Na ion and NaCl ion pair vacancies in two positions. The Na ion vacancy is less favourable than the NaCl pair vacancy. This is because such a vacancy uncovers two adjacent Cl ions at the terminal position which are unfavourable adsorption sites.

relates to the models chosen. On the kink structure the water molecules can form clusters in the corners between the terraces. The adsorption in such clusters seems to be quite strong as can be inferred from Figure 4.5. Between 12 and 18 water molecules the adsorption energy on the kink is almost constant while there is a progressive loss on the step. Thus it can be expected once the space between the steps on the kinks are full of water clusters, the adsorption of subsequent water molecules will be destabilised. This would then help to increase the relative stability of the vacancies.

4.4 Discussion and Conclusions

We have performed a large scale study aiming to elucidate the intimate details of the initial stages of salt dissolution in water. The different surface models used enabled us to find basic principles which govern the process and we discuss our findings in more detail in the following.

Let us start with the behaviour of water on surfaces without vacancies. As observed previously water molecules bind more strongly to the Na ion than to the Cl ion. Furthermore the binding is even stronger when two adjacent Na ions are exposed, for example on the step. The adsorption on Cl is favourable only when the adjacent Na ions are occupied in which case the Cl adjacent water forms a hydrogen bond with the Na adjacent molecule. This leads to formation of clusters on the flat surface and molecular chains that run along the steps for the defected surfaces. As can be seen in Figure 4.5 the chains have much lower adsorption energy than the

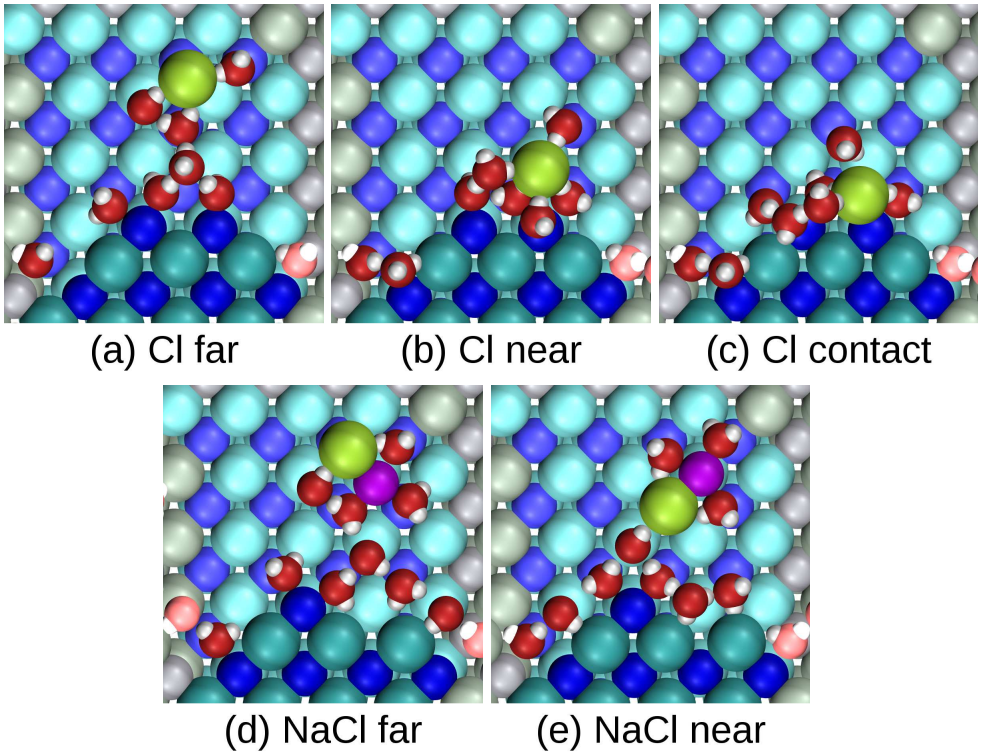

Figure 4.16: Displacement vacancies on the NaCl surface with a Cl terminated kink. The single ion vacancies are represented by "Cl far", "Cl near", and "Cl contact" structures where the ion resides either far, near in a hydration shell, or near in a contact with a Na ion adjacent to the vacancy, respectively. The ion pair vacancies can similarly occupy a position far and near. Although the "Cl near" structure is similar to the one on the step, the lack of one Na ion leads to a less favourable structure.

clusters formed on the flat surface. However, once water covers the favourable sites on the step, further water molecules need to adsorb at the less favourable sites and the average adsorption energy decreases in magnitude.

We have found that the energy cost required to release an ion from the lattice is governed by two competing forces: i) the energy cost to create a defect (breaking ionic bonds); and ii) the energy gain of adsorbing water on the favourable defect sites. The cost to create a defect is high, about 1–2 eV, but the adsorption energy of water is enhanced by ∼0.2 eV (this value can be inferred from the plot of adsorption energies on the flat surface and on the step in Figure 4.5). Thus the release is not favourable but adding water molecules reduces the cost through the stronger binding to the defect. However, as we have seen before for adsorption on the step, once the defects are covered the adsorption is no longer favourable to lower the vacancy cost. This can be clearly seen for the flat surface single ion vacancy formation energies in Figure 4.9. In a situation where there is more water molecules than available favourable defect adsorption sites more ions can be released so that more defect sites are present. This leads to a preference for the ion pair vacancy on the flat surface for more than 10 water molecules and one could expect

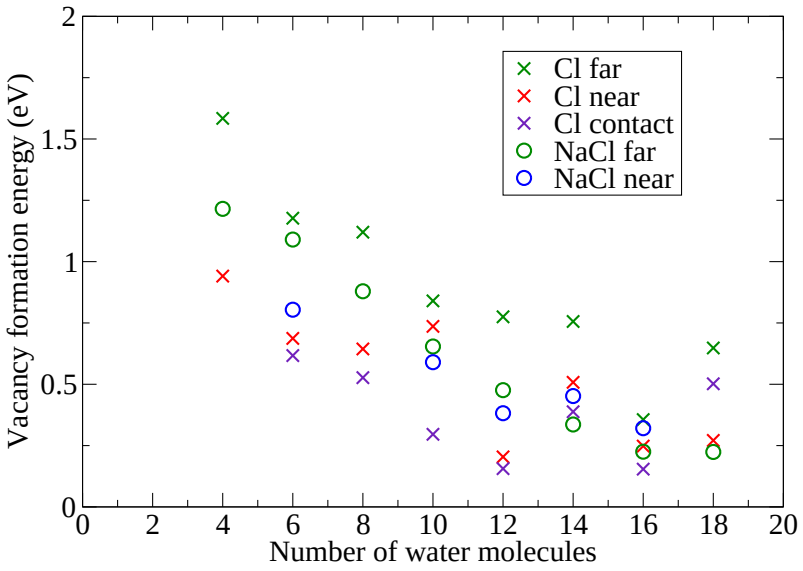

Figure 4.17: The vacancy formation energy for the surface with a Cl terminated kink site for single Cl ion or NaCl ion pair vacancies. As with the step the "Cl near" or "Cl contact" vacancies cost little energy to create although we haven't found a structure for which enough energy is gained to create the vacancy. For a large number of water molecules the ion pair vacancy seems to, like on the flat surface, give the most preferred structure.

that this trend will continue. That is for even larger numbers of water molecules more ions will be released leading ultimately to dissolution.

A major surprise to come out of this study is the role the Na ions play in dictating the issue of which ion will leave the lattice first. As we have stressed before the water molecules adsorb more strongly to the Na ions than to the Cl ions, however, the Na ions also seem to be less "stable" when removed from their lattice sites. This together leads to the conclusion that the Cl ions are released first for two main reasons: i) when the Cl ion is released favourable adsorption sites with Na ions are exposed; and ii) the Cl ion is more "stable" as a vacancy since the created defect (hole) is blocked by water molecules. Thus the first dissolution step seems to be unexpectedly governed by a rather inverse logic: it is not the energy gained from removal and hydration of the Cl ion that drives the release of the ion but rather the energy gained by exposing more favourable Na adsorption sites. These conclusions explain the experimental observations from Ref. [256], namely if there are some impurities present on the surface, Na ions will be the first to be hydrated; on the steps Cl ions will be released first.

Let us briefly discuss the question of where the dissolution will start: at the kink or the step? When we compare the vacancy formation energies on the step and kink with Cl termination we see that they are quite similar and very small. It can even become energetically favourable for the single Cl ion vacancy on the step to be released. While we don't see this happening on

the kink, the trends would suggest that the Cl will be released for a similar number of water molecules as on the step. Even more the kink site could be thought of as the one where the Cl ion will be released first because of its smaller coordination. On the other hand the very favourable Cl ion vacancy that is formed on the step seems to be less stable on the kink, where less water molecules can adsorb favourably. On both the step and kink we observe that the ion pair has a very low vacancy formation energy. The pair does not require a precise structure to be formed as the Cl ion on the step and it seems plausible that the pair becomes favourable with a larger number of water molecules. To dissect this exactly a larger model for the kink would be required but also free energy calculations would be helpful.

To conclude we have used density functional theory to elucidate the details of the initial stages of NaCl dissolution. We have found that the release of ions is possible at defects even with a relatively low number of water molecules. This agrees well with the experiments where similar conclusions are drawn for relative humidities below $\sim$40 %. The process is initially driven by the stronger affinity of water molecules towards Na ions and defects exposing Na ions. This causes the Cl ions to be released first so that more Na ions are exposed. This conclusion explains why the Cl ion is the first despite the common sense which would argue that Na ion will be first because of its stronger interaction with water molecules. This seems to be a rather general conclusion and we expect it to be valid for similar systems.

Chapter 5

Optimisation of the van der Waals density functional

5.1 Introduction

From this chapter on we will spend more time on the method that has been mostly used in this thesis: density functional theory (DFT). As has been discussed in Chapter 2, DFT is exact in principle because for any density there is only one external potential and one wavefunction and thus energy can be calculated as a functional of the density. However, this is not very useful in practice since the problem is reformulated from solving an n-dimensional Schrödinger equation to a problem of finding the exchange-correlation functional $F_{\rm xc}^{\rm exact}$, a beast, that solves the many-body problem implicitly from the electron density. Therefore without the knowledge of the $F_{\rm xc}^{\rm exact}$ some approximate $F_{\rm xc}$ needs to be used. As it turns out even probably the simplest $F_{\rm xc}$, the local density approximation (LDA) gives quite good results, especially for solid systems. Inferior performance for molecules, already expected in the Kohn-Sham paper, and transition states has lead to a plethora of exchange-correlation functionals, semi-local or with non-local Fock exchange (hybrids). All this development has, because of the (semi-)locality of the functionals and mean-field nature of DFT, omitted one important piece of physics namely non-local electron-electron correlations. This is an important issue since such correlations give rise to London dispersion forces, part of the van der Waals interactions which contribute to binding in many systems. Although there have been approximate schemes that add dispersion interactions as a sum of $1/r^6$ dispersion energy terms for some time, the non-local correlation functionals have appeared only recently.[1] We discuss our contributions to the development of one of such schemes in this and the following chapter.

Let us stress the vast importance of including dispersion in today's approximate DFT functionals. With the increasing power of computers and algorithm development systems with thousands of atoms can be studied routinely. These include biomolecules [285], systems impor-

[1] One reason for the slow development probably was that LDA gives some binding in dispersion bonded systems. Despite the fact that this binding occurs for the wrong reason, the views that LDA describes dispersion and is thus appropriate for systems such as graphite still appear.

tant for future energy production such as (large) organic molecules and frameworks of those adsorbed on surfaces [286], or sieve-like materials such as metallo-organic frameworks or zeolites for gas separation and storage [287, 288]. The common important point of such systems is that their structure is, at least partially, far from being densely packed. They contain parts that are not held together by chemical bonds; weak electrostatic interactions and dispersion are important for such systems to be stable and perform their function. Therefore to accurately describe dispersion within DFT is becoming increasingly important. The two oldest ideas are: i) to add a sum of pairwise atom-atom dispersion terms with $-C_6/r^6$ asymptotics to the energy with C_6 obtained either empirically or from isolated atom calculations [106, 108, 109, 110, 111, 112]; and ii) construct a range-separated double-hybrid functional by adding a second order many-body perturbation theory (MBPT2) or coupled cluster (CC) term [289]. While the first one is fast but usually needs to be heavily parametrised, the second approach is very expensive. One of the most promising new methods is the van der Waals density functional (vdW-DF) [16] from the groups of Langreth and Lundqvist which was described in Chapter 2. Let us only repeat that the exchange-correlation energy in this method is calculated as

$$E_{\rm xc} = E_{\rm x}^{\rm GGA} + E_{\rm c}^{\rm LDA} + E_{\rm c}^{\rm nl}\,, \tag{5.1}$$

where $E_{\rm x}^{\rm GGA}$ is the exchange energy calculated using the revPBE [155] functional, $E_{\rm c}^{\rm LDA}$ is the local density approximation (LDA) to the correlation energy. The $E_{\rm c}^{\rm nl}$ is the non-local correlation energy term which is evaluated using a fully non-local correlation functional where the dispersion is estimated based on a model response function.

The vdW-DF method has been applied to a wide variety of systems where dispersion is important [290]. However, little attention has been given to comparison with accurate reference data to assess the general accuracy of the method [157, 158]. This is an important point since not only the accuracy of the method is assessed, such comparisons often lead to further developments and improvements of exchange-correlation functionals. With the increasing availability of accurate reference data, the accuracy of vdW-DF has begun to be scrutinised [291, 292] and it has been observed that in many important circumstances the current vdW-DF is simply not accurate enough. For example, for the widely used S22 dataset [41] (a set of 22 weakly interacting dimers mostly of biological importance) it yields a mean absolute deviation (MAD) of $\sim$60 meV [292] compared to coupled cluster reference data. This is outside the so-called "chemical accuracy" of 1 kcal/mol or $\sim$43 meV and inferior performance to other DFT-based dispersion corrected schemes [108, 110, 111]. Water clusters, important for atmospheric chemistry and liquid water, are another example where vdW-DF substantially underbinds (by $\sim$20% compared to accurate reference data) and in terms of absolute dissociation energies is worse than a regular GGA such as PBE [291, 114].

In this chapter we focus on testing the accuracy of vdW-DF and finding ways to improve it. For this we use available reference sets which are introduced in Section 5.2. After scrutinising the original vdW-DF formulation in Section 5.3 we explore the possibility of improving vdW-DF by

using alternative exchange functionals to the original revPBE in Section 5.4.1. Since it is known that vdW-DF correlation is not compatible with Hartree-Fock (HF) exact exchange [157, 158] and the original revPBE exchange functional was just one of many possible choices, we search for alternative exchange functionals that yield more reliable interaction energies than revPBE. Following this we test our methods on two complex systems where dispersion interactions are crucial: water hexamers [114] and water adsorbed on NaCl(001) [244]. To deepen the understanding of the advantages and disadvantages of the method we use the binding curves of the S22 dimers where reference data have become recently available [104]. From these studies we propose new exchange functionals, that when incorporated within vdW-DF offer vastly improved interaction energies compared to those from the original vdW-DF. In Subsection 5.4.2 we focus more on the correlation part of the functional. This has become a rather debated part with several new forms proposed [152, 156, 147, 154]. In such a situation, assessing the accuracy and finding ways to improve it to make a generally applicable method seems to be more important than applying the method to any system.

5.2 Reference sets

5.2.1 S22 set

Dispersion interactions are crucially important in biology and contribute to hold molecules such as proteins or DNA together. Although such molecules are currently too big to be treated as a whole, it is possible to study interactions of the constituent molecules such as DNA bases or amino acids. In this regard the most established reference is the S22 set of Jurečka *et al.* [41] which contains 22 weakly bonded molecular dimers and provides a tough test for molecular simulation methods. The dimers are close to their optimal position and their interaction energies have been mostly estimated using the ΔCCSD(T) approach extrapolated to the complete basis set (CBS) limit[2]. The set is divided into three subsets which contain dimers bonded predominantly by hydrogen bonds (HB), dispersion (DB), and a mixture of both (MB). Note that this division is partially arbitrary since, for example, dispersion is ubiquitous and contributes to binding of each dimer, a more detailed analysis of the contributions can be found in Ref. [293]. The dimers of the three subsets are shown in Figure 5.1. The accuracy measures used for this set are the mean absolute deviations (MAD) for the whole set and the three subsets. Furthermore, we define "Range" as the difference between the highest error and the lowest one, *i.e.*, it gives the spread of errors. We also calculate a quantity $\Delta^{\mathrm{H-D}}$ which gives the difference of the mean deviations of the HB and DB subsets (*i.e.*, $\Delta^{\mathrm{H-D}}$=MD(HB)−MD(DB)). Recently the interaction energies have been recalculated by two groups using larger basis sets [294, 295] which improved the reliability of the reference. Some of the functionals developed in the following text used the old interaction energies as a reference, however in the following we compare

[2]The smaller dimers were optimised using CCSD(T), the larger using MP2 using large basis sets. The interaction energies were extrapolated to the CBS limit either directly from the CCSD(T) data or, in most of the cases from MP2 data with a CCSD(T) correction (Δ). The details can be found in Ref. [41].

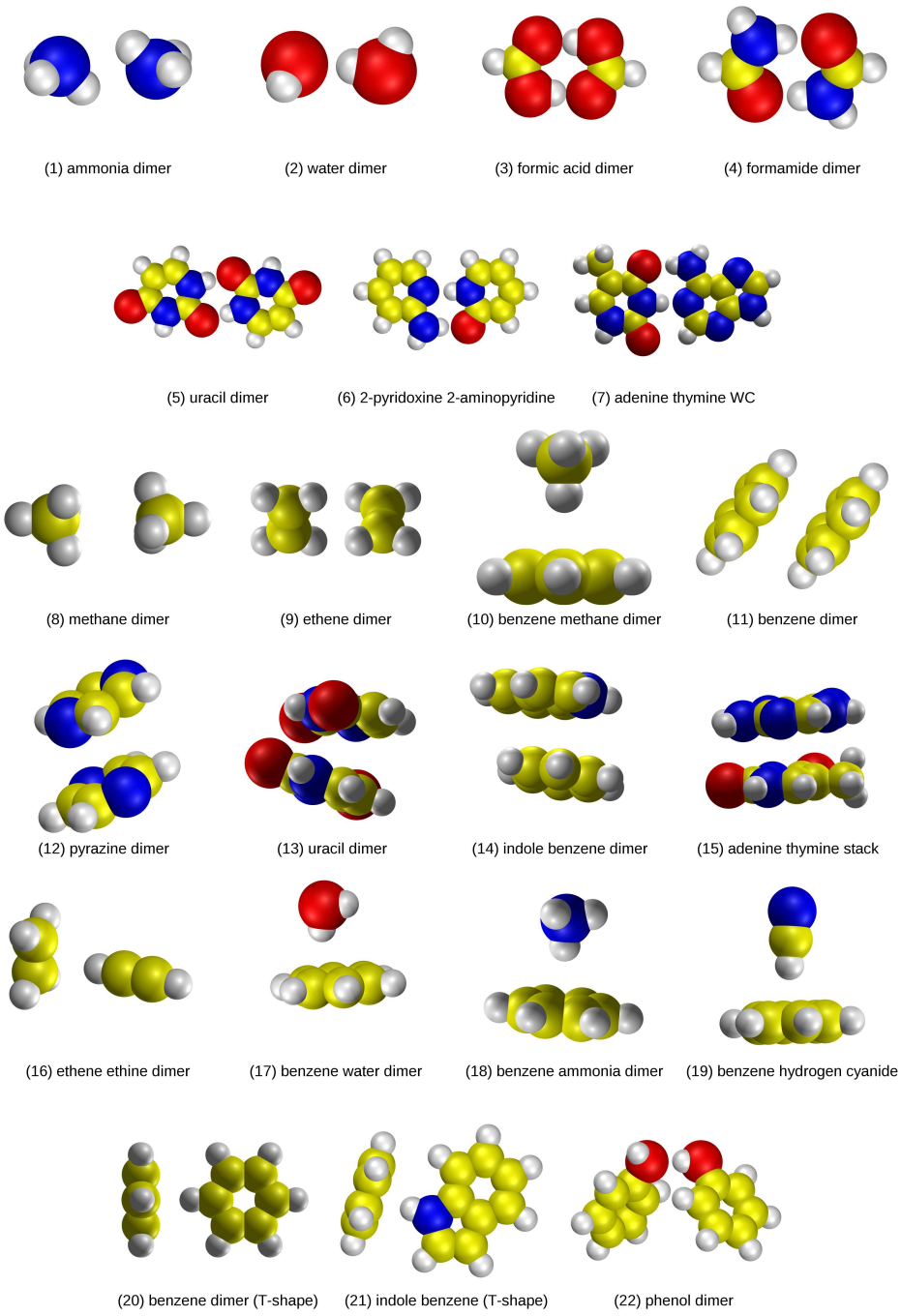

Figure 5.1: The molecular dimers in the S22 set of Jurečka *et al.* [41]. Nitrogen atoms are in blue, oxygen in red, carbons in yellow, and hydrogens in white.

to the new reference energies. The change of the total MAD when the old and new reference is used is ∼3 meV. Since we are interested in establishing precisely how the methods tested perform compared to the accurate reference data, interaction energies were computed on the reference structures and geometry optimizations were not performed. Moreover, the geometry optimisation is not recommended since most of the dimers are not in their optimal positions.

5.2.2 Binding curves of S22 dimers

In most cases we are not only interested in how well a method can reproduce the interaction energy at the minimum of a binding curve but also how well it can reproduce the whole binding curve. This is again an important point since fitting DFT functionals to a single point of a binding curve does not necessarily mean that the total shape of the binding curve will be correct as well. This is especially true when dispersion is the dominant part of the interaction in the long range.[3] Although the S22 test offers quite a variety of structures that decrease the possibility of such a failure, it does not contain structures far from the optimal distance. Such geometries are especially important to assess the asymptotics of the dispersion interaction. There are now two tests available using the S22 dimers, one containing 15 points on the binding curve from Molnár *et al.* [104], the other containing 5 points for each dimer [293]. Although ΔCCSD(T)/CBS has been used in both, the extrapolation has been made in smaller basis set than the recent S22 interaction energies, and the binding curves represent a less reliable reference. There are other good quality reference binding curves, for example for benzene dimers [40], H_2S benzene dimer [296], and others [297, 298] but generally the behaviour of the functionals is similar to the S22 binding curves.

5.2.3 Water hexamers

Water is one of the themes of this thesis and there are some tests available for water. Here we use one highly relevant test: water hexamers. There have been several accurate calculations of the water hexamer binding energies [299] but here we use the data from Ref. [114]. This test contains four low energy isomers that are shown in Figure 5.2. It was shown in Ref. [114] that although many exchange-correlation functionals give binding energies within ∼20 meV of the reference, they completely fail in reproducing the correct ordering of the clusters. While wavefunction methods give "prism" or "cage" as the lowest energy structure, all GGA, meta-GGA, or hybrid GGA functionals tested in Ref. [114] point to the "book" or "cyclic" clusters as the most stable ones. However, the correct ordering can be recovered when dispersion corrections are included in the calculations. This makes the test highly suitable for assessing vdW-DF and modifications of it and indeed the vdW-DF method was tested by Kelkkanen *et al.* [291]. We have used the reference MP2 optimised geometries of Santra *et al.* [300, 114] and further improved the binding energies by obtaining CCSD(T) energies using an aug-cc-pVTZ basis set (instead of the original aug-cc-pVDZ). The results and final reference energies are summarised in Table 5.1. The results

[3]This has, for example, been shown in Ref. [104] for the M06-L functional [102] which does not include dispersion.

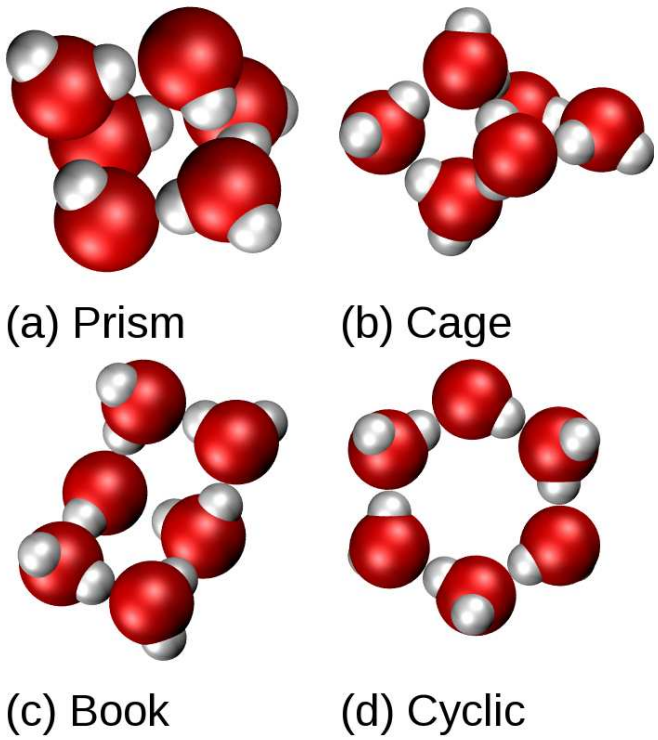

Figure 5.2: Four low energy isomers of the water hexamer. While the "prism" and "cage" isomers are preferred by wavefunction methods, standard DFT functionals tend to give the "book" and "cyclic" clusters as the ones with lower energy. It was shown in Ref. [114] that the correct ordering can be recovered when dispersion corrections are included in the calculations.

presented in this chapter have been calculated using the MP2 optimised geometries. However, performing a geometry optimisation changes the binding energies by less than 5 meV.

5.2.4 Water monomer on NaCl

The importance of dispersion for adsorption systems has been known and debated for some time [301, 302], however for systems with strong chemisorption it usually can be neglected. Of course the complete opposite is true for systems which are physisorbed or systems chemisorbed but with important physisorption. Such systems are represented by systems such as organic molecules on metal or semiconductor surfaces which are becoming more popular as a subject of theoretical studies, for example as models of dye sensitized solar cells [303, 304]. Although important, reliable reference data are very scarce as large surfaces are difficult to treat with wavefunction methods. (One approach gaining popularity has been quantum Monte Carlo, used to study, *e.g.*, interaction of water with graphene [47].) Therefore, one important contribution was establishing the interaction energy of a water molecule with NaCl(001) surface by Li *et al.* [244] (shown in Figure 5.3) . The reference value -487 ± 60 meV without geometry relaxations of the substrate reveals the inaccuracy of standard generalised-gradient approximation (GGA) exchange-correlation functionals for this system. For example PBE [83] gives adsorption energy

Table 5.1: Reference values in meV for the binding energies of the water hexamers. The MP2 values extrapolated to the complete basis set limit obtained by Santra *et al.* [114] were improved by evaluation of the CCSD(T) energy with the aug-cc-pVTZ basis set (shown as 3ζ in the table). The difference between the MP2 and CCSD(T) (Δ) calculations was then added to the MP2/CBS energies to estimate the ΔCCSD(T)/CBS binding energies.

Isomer	MP2/(3ζ)	CCSD(T)/(3ζ)	Δ	MP2/CBS	ΔCCSD(T)/CBS
Book	−343.1	−341.6	1.5	−330.2	−328.7
Cage	−346.0	−346.0	0.0	−331.9	−331.9
Cyclic	−335.2	−332.2	3.0	−324.1	−321.2
Prism	−346.5	−348.0	−1.4	−332.3	−333.8

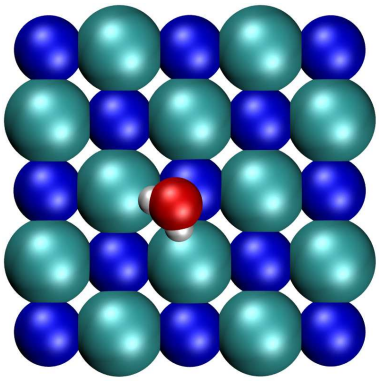

Figure 5.3: Water monomer adsorbed on NaCl(001). While the reference adsorption energy obtained from wavefunction based methods is ∼−500 meV, the PBE value is ∼−330 meV.

of only ∼−330 meV. For this system the effect of non-local correlations is expected to be considerable.

5.2.5 Computational setup

The vdW-DF energies have been calculated in two ways: for the tests using the vdW correlation most of the data are based on a non-self-consistent post-processing approach. The binding curves and data for the vdW2 correlation functional have been obtained using a self-consistent implementation of the vdW method in VASP which uses the algorithm of Román-Pérez and Soler [305]. The latter approach gives basically identical results to the post-processing evaluation (see Appendix C). In both cases calculations were done with VASP 5.2 [253, 178]. The post-processing approach works in two steps: first, calculations with a given exchange functional[4] and PBE correlation functional are performed. Second, the electron density is used to determine the vdW correction using JuNoLo [306] code. We find that the magnitude of the vdW correction is rather insensitive to the underlying density used[5]. Therefore, density from B86 (exchange)

[4]The exchange functionals that were not already in VASP were implemented by the author.

[5]For the entire S22 set the vdW corrections to the interaction energy are within 2 meV of each other, irrespective of whether density obtained with B86 [70], PBE, or revPBE exchange functional is used.

and PBE (correlation) calculations was used for all functionals except PBE and revPBE, where density from the respective exchange-correlation functional was used. Care was taken with the VASP calculations to ensure that converged energies were obtained, which involved the use of hard projector-augmented wave (PAW) [175, 176] potentials, an 800 to 1000 eV cut-off, dipole corrections, and 20 to 25 Å^3 unit cells for the S22 set and water clusters. We have checked that the self-consistency does not affect the results significantly using the GPAW code [171]. For the S22 dataset the non-self-consistent and self-consistent interaction energies are within 1.5 meV, except for the large dispersion bonded dimers (dimers 11–15) where the differences are $\leq$4 meV.

5.3 Tests of the vdW-DF

Here we compare the results of the original formulation of vdW-DF to the reference sets presented in the previous part. Since vdW-DF contains the revPBE exchange functional we will refer to it as revPBE-vdW for reasons that will be clear later, we retain vdW-DF for designation of the method in general. However, before showing the data, let us first convince the reader that dispersion has to be accounted for if DFT is to give qualitative agreement with the S22 reference data. As Figure 5.4 shows, when standard GGA such as revPBE (green line) is used on the S22 set, the DB dimers are either bound very weakly or even repel instead of being bound by ∼300 meV. This is not solved by using more attractive GGAs such as PBE or PBEsol (blue and red lines in Figure 5.4). The results of LDA, which gives even more attractive binding, for the DB dimers are consternating and shockingly accurate. There are, however, two main points which one needs to keep in mind against the use of LDA. First, the binding energy of the HB dimers is terribly wrong, for example the water dimer is bound by 340 meV instead of the reference 217 meV (relative error over 50%). Second, the asymptotic behaviour of LDA or any GGA will not recover the correct $1/r^6$ shape but will decay exponentially instead. However, when the non-local correlations are included as in the revPBE-vdW method (violet dashed line in Figure 5.4) an improved description of the interaction energies is observed. Although the method improves substantially the DB subset, it is clearly worse than either PBE or PBEsol for HB dimers where it strongly underbinds. In fact, most of the interaction energies on the whole set are underestimated. This becomes more apparent when the differences between the revPBE-vdW and reference energies are calculated. The differences for each of the dimers in the S22 dataset are shown in Figure 5.5. One can see that with revPBE-vdW most of the dimers are substantially underbound. The MAD is 65 meV (Table 5.2), which is in good agreement with the MAD of 60 meV in Gulans *et al.* [292] where interaction energies for geometry optimised structures were presented. The agreement is even better with the recent calculations of Vydrov and van Voorhis [307] where no geometry optimisations were done (see Appendix C.2). The errors for the individual HB, DB, and MB subsets are all quite large at 106, 52, and 38 meV, respectively. Furthermore, this functional yields a very large "Range" of errors of 163 meV. The rather large value of $\Delta^{\mathrm{H-D}}$ for revPBE-vdW of 57 meV reveals that on average the HB dimers are underbound compared to the DB dimers, an effect that comes from a potential that is too

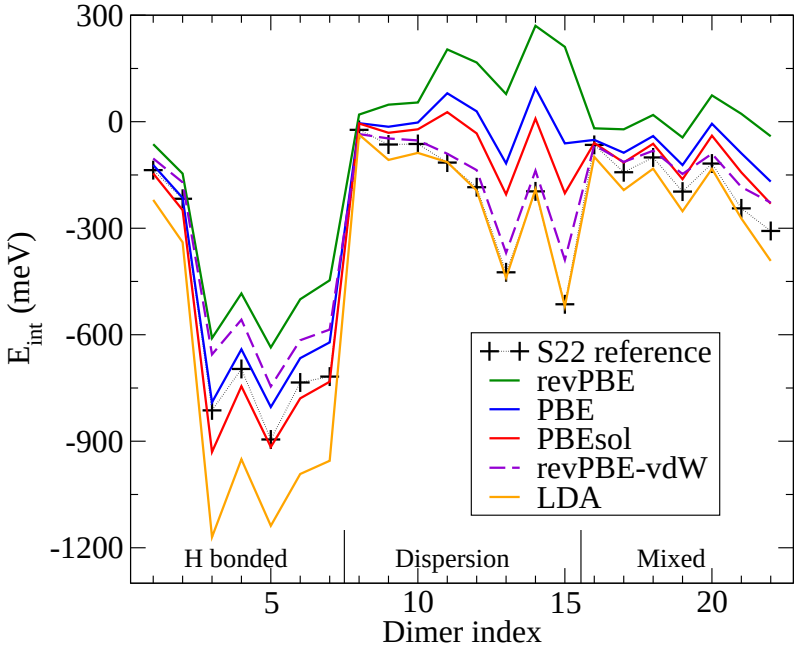

Figure 5.4: The total interaction energies of the S22 dimers calculated using different exchange-correlation functionals: LDA, revPBE, PBE, PBEsol, and revPBE-vdW. The reference values from Ref. [295] are shown and the division of the set into three subsets is indicated. As can be seen, the interaction strengthens upon going from revPBE to PBE to PBEsol to LDA. While for the hydrogen bonded subset PBE and PBEsol give reasonably satisfactory results, all the semi-local functionals severely underestimate the interaction energies of the dispersion bonded dimers and dimers in the mixed subset. Although LDA gives surprisingly accurate results for the dispersion bonded subset, the interaction energies for the hydrogen bonded dimers are largely overestimated. The overall agreement is dramatically improved when the revPBE-vdW functional is used since it includes a description of dispersion.

repulsive for short separations. Therefore, the original revPBE-vdW does not deliver chemical accuracy for either systems held by dispersion or hydrogen bonds, it yields a large range of errors, and on average underbinds the HB dimers compared to the DB systems.

Before discussing the results for the water hexamers let us point out that one of the S22 dimers, number 2, is the water dimer. revPBE-vdW gives an interaction energy which is too small (-173 meV), an underestimation by 44 meV. This presages what the result for the hexamers will be. And indeed, our calculations, which agree with previous calculations of Kelkkanen *et al.* [291], show that although the energy ordering of the hexamers is improved, the binding energy per water molecule is underestimated by $\sim$50 meV (see Table 5.3).

As a final test we have applied the revPBE-vdW method to the adsorption of water on NaCl(001). Using the post-processing approach and direct evaluation of the vdW integral this

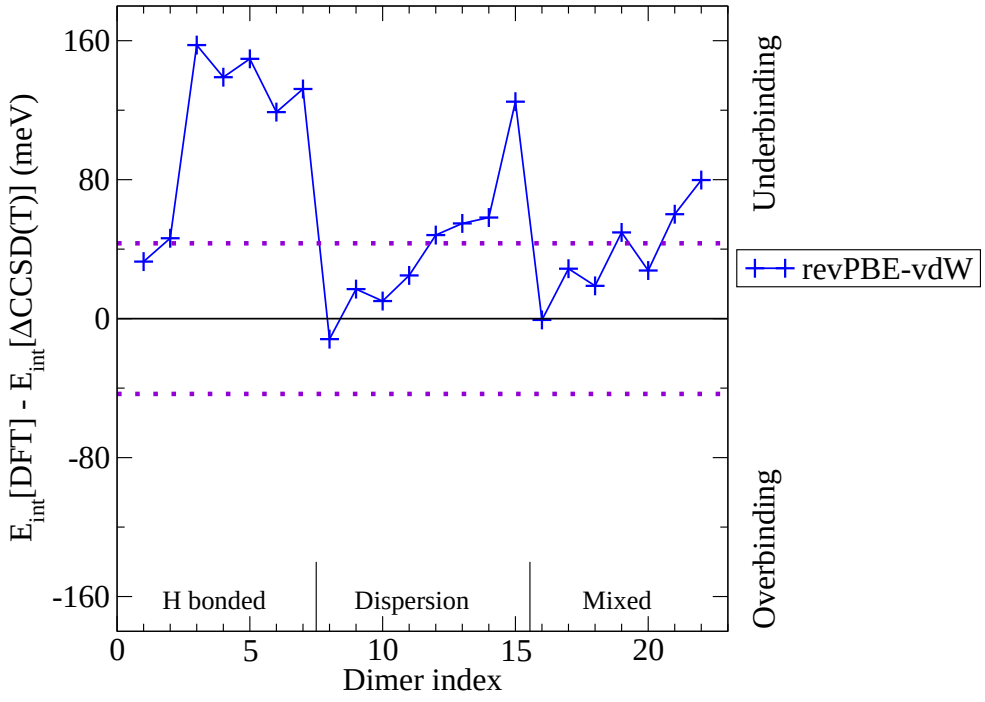

Figure 5.5: The difference of the revPBE-vdW and reference interaction energies on the S22 set. The interaction energies are underestimated for almost all of the dimers.

system requires much more computational resources than a standard GGA calculation. Despite this tremendous increase in required time, the value of $E_{\mathrm{ads}} = -334$ meV for revPBE-vdW is a negligible improvement compared to PBE ($E_{\mathrm{ads}} = -328$ meV). Both methods recover only $\sim$2/3 of the reference adsorption energy ($E_{\mathrm{ads}} = -487 \pm 60$ meV).

Overall, we have shown that although the revPBE-vdW method leads to a qualitative agreement with accurate reference data, the accuracy is inferior to standard GGA functionals when systems bound by hydrogen bonds are considered. In the rest of this chapter we will discuss ways that improve the accuracy and thus make this method more useful.

5.4 Improvements of the vdW-DF

As we have shown in the previous section, on the one hand revPBE-vdW yields promising results but on the other hand fails for several systems, most importantly for hydrogen bonded systems. In this Section we focus on improving the accuracy of revPBE-vdW. This can be done in several ways and we first discuss improvements which are achieved by changing the exchange functional while keeping the correlation part intact. This is followed in Subsection 5.4.2 by tests of different correlation functionals. Let us note that a straightforward improvement is hindered by the fact that in DFT exchange and correlation are in principle defined together[6]. Of course, they need

[6]In fact, not only in DFT, but also in post Hartree Fock methods. In post-HF calculations, the correlation energy is defined as the difference between the energy of the exact solution of the N-electron Schrödinger equation and energy in the HF approximation. If one used, *e.g.*, the natural orbitals, the correlation energy would change

to be explicitly defined as a DFT functional and the problem is what reference to use for the exchange functional and what for the correlation part.

5.4.1 Exchange part

As stated previously the vdW-DF E_{xc} (Equation (5.1)) is given as a sum of semi-local exchange, local correlation, and non-local correlation functionals. The revPBE exchange functional was chosen since it gives negligible binding for rare gas dimers compared to, *e.g.*, PW91 exchange [84]. However, revPBE is not the only exchange functional that does not bind rare gas dimers [308]. The problem becomes more severe by noting that the vdW correlation functional is not compatible with Hartree-Fock exchange [157, 158]. Thus a functional that is compatible with the vdW correlation cannot be fitted to HF binding curves or other properties.

5.4.1.1 Tests of exchange functionals

To try to improve the accuracy of the vdW-DF method we have implemented several exchange functionals in VASP and used them instead of the original revPBE. We again calculate the interaction energies of the S22 dimers, binding energies of water hexamers and the adsorption energy of the water molecule on NaCl(001). The considered functionals are all of the GGA form and they are PBE, Becke86 (B86) [70], Becke86 with modified gradient correction (B86b) [309], Perdew-Wang86 (PW86) [310], Becke88 (B88) [85], RPBE [311], PBEα [312][7], PBEsol [313]. As with the revPBE exchange we denote the combination of an exchange functional "X" with the vdW correlation as a X-vdW.

The results for the S22 set are shown in Figure 5.6 and summarised in Table 5.2. As can be seen, except for PBEsol, all functionals yield smaller MADs than revPBE-vdW (*i.e.*, the original vdW-DF). The overall performance is also qualitatively different, for example, in contrast to revPBE-vdW, PBE-vdW systematically overbinds all the dimers. Although the MAD of B88-vdW is only marginally smaller (60 meV) than that of revPBE-vdW, the $\Delta^{\mathrm{H-D}}$ is reduced from 70 to 29 meV. And of most interest, B86-vdW, yields an overall MAD of just 28 meV. This is the lowest MAD obtained from all published functionals considered and a substantial improvement over revPBE. We note that exchange functionals shown [308, 314, 315] to closely reproduce asymptotic HF binding curves such as PW86 and B86b, when incorporated within vdW-DF do not perform especially well for the S22 dataset (see Table 5.2). This confirms that the correlation contribution to vdW-DF is not exact and thus to obtain accurate binding energies with vdW-DF some cancellation of errors is required.

By comparing the data in Figure 5.6 to the exchange enhancement factors in Figure 5.7 a clear correlation between the two can be made. The trends in relative binding can be attributed to the steepness of the F_{x} for small values of the reduced density gradient s. For example, the most steeply rising functionals, revPBE and RPBE give the smallest binding for the HB dimers,

accordingly to the change of the HF-like energy

[7]This functional contains one free parameter α. Setting $\alpha = 2$ gives good results on the S22 set and we refer to this functional as PBE$\alpha = 2$.

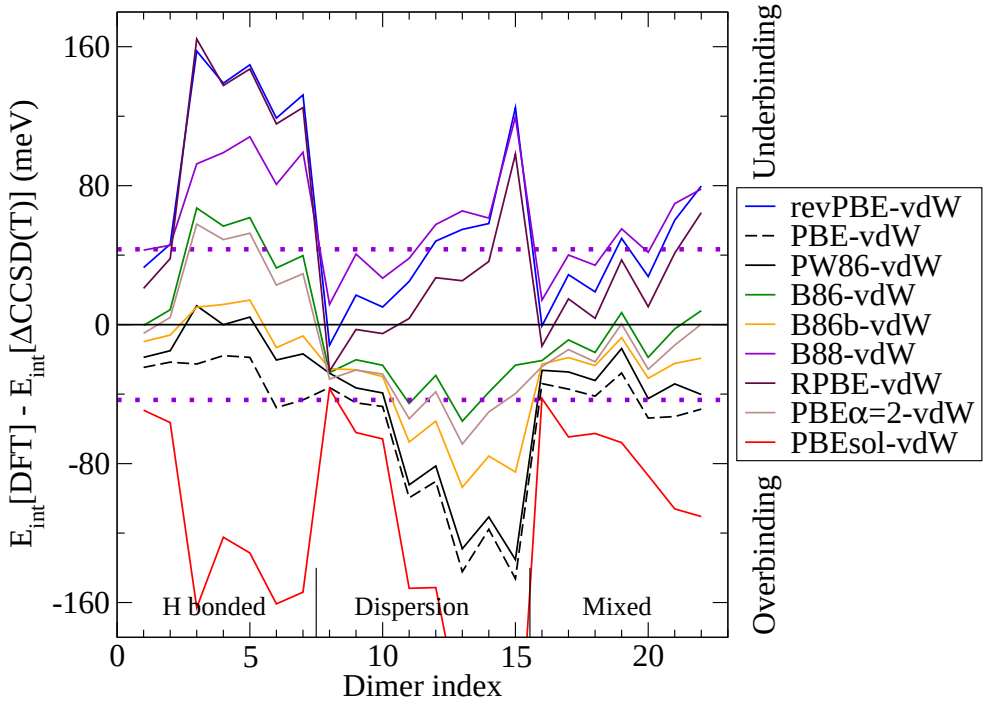

Figure 5.6: Difference from the reference interaction energies for vdW correlation using different published exchange functionals. As can be seen results from complete underbinding (B88-vdW) to complete overbinding (PBE-vdW or PBEsol-vdW) are obtained.

while PBEsol gives binding which is too strong. For the DB dimers where the optimal distance is larger, the steepness of F_x for larger s seem to be more important. This is supported by the fact that B88 gives more repulsion for this subset than either revPBE or RPBE. A similar conclusion can be made based on the data presented in Figure 5.8 which shows the binding curves of revPBE-vdW, PBE-vdW, and B88-vdW for the methane benzene dimer. Although none of the functionals reproduces closely the reference data, PBE-vdW is clearly less repulsive than either revPBE-vdW or B88-vdW for small separations. In the tail of the binding curve, $\sim$2 Å beyond the optimum, the asymptotic behaviour of F_x is dominant; revPBE-vdW and PBE-vdW give almost identical behaviour and B88-vdW reduces the binding due to the rising F_x. We will discuss this point more in Section 5.4.1.3.

As can be seen in Figure 5.6 the interaction energy of the water dimer (dimer 2) is improved when alternative exchange functionals such as B86, B86b, or PBEα = 2 are used. Table 5.3 shows that the binding energies of water hexamers are improved as well, for example, B86-vdW gives energies which are all within 8 meV from the reference values and with the correct ordering. Therefore also here the alternative choice leads to much improved results. Let us now mention one related point, the PBE functional is often used in connection with dispersion corrections in the $1/r^6$ fashion. The water hexamer test reveals that although the ordering can be improved, the absolute values can be only worsened [114]. When the PBE correlation is replaced with the

Table 5.2: Mean absolute deviations from the reference data [41, 295] for the S22 set for vdW-DF with various exchange functionals ("Method"). MADs are given for the whole set ("MAD Total"), the hydrogen bonded ("MAD HB"), dispersion bonded ("MAD DB"), and mixed bonding subsets ("MAD MB"). For each functional we also report the difference between the largest and smallest deviations from the reference in column "Range" and the difference in the mean deviations of hydrogen bonded and dispersion bonded subsets (column "$\Delta^{\mathrm{H-D}}$").

Method	MAD				Range	$\Delta^{\mathrm{H-D}}$
	Total	HB	DB	MB		
revPBE-vdW	63	111	44	38	169	70
PBEsol-vdW	117	120	148	77	249	29
B88-vdW	60	81	53	48	108	29
RPBE-vdW	53	107	28	26	191	88
PBE-vdW	55	28	91	42	128	62
PW86-vdW	43	12	82	31	146	74
B86b-vdW	31	10	57	21	108	57
PBE$\alpha = 2$-vdW	30	32	42	14	127	72
B86-vdW	28	38	33	12	123	71

vdW correlation, the absolute dissociation energies increase as well and also in this case PBE leads to worse agreement with the reference.

5.4.1.2 New exchange functionals

In the previous part we have shown that using the B86 exchange functional with the vdW correlation functional leads to the smallest errors of all the functionals tested. However, B86 was constructed empirically and does not seem to be used nowadays[8]. The range of errors is also quite high for B86-vdW, being 112 meV. Therefore there doesn't seem to be any strong reason to choose B86 over PBE$\alpha = 2$ or B86b as the alternative exchange functional since all of them obey similar constraints. In this situation we have tried to find an exchange functional that further improves the results on the S22. Although it is better in general when a functional is "non-empirical", there are not enough constraints for such a construction to be made. Let us remind the reader that PBE and RPBE functionals obey the same constraints and yet, as can be seen in Figure 5.6 they give completely different results on the S22 set. This is because given the known limits, a rather arbitrary function needs to be chosen to connect them in the end. PBE, revPBE, or B88 are quite widely used but no theoretical case can be made to argue which one is "better".

[8]Rather amusingly, most of the 50 or so citations that cite the paper of Becke from 1986 use it incorrectly as a citation for B3LYP or BP86. The first one should cite two later Becke's papers [85, 91]. And although the name could suggest that the latter reference is right, it is again Becke's 1988 exchange functional that is part of BP86 [87].

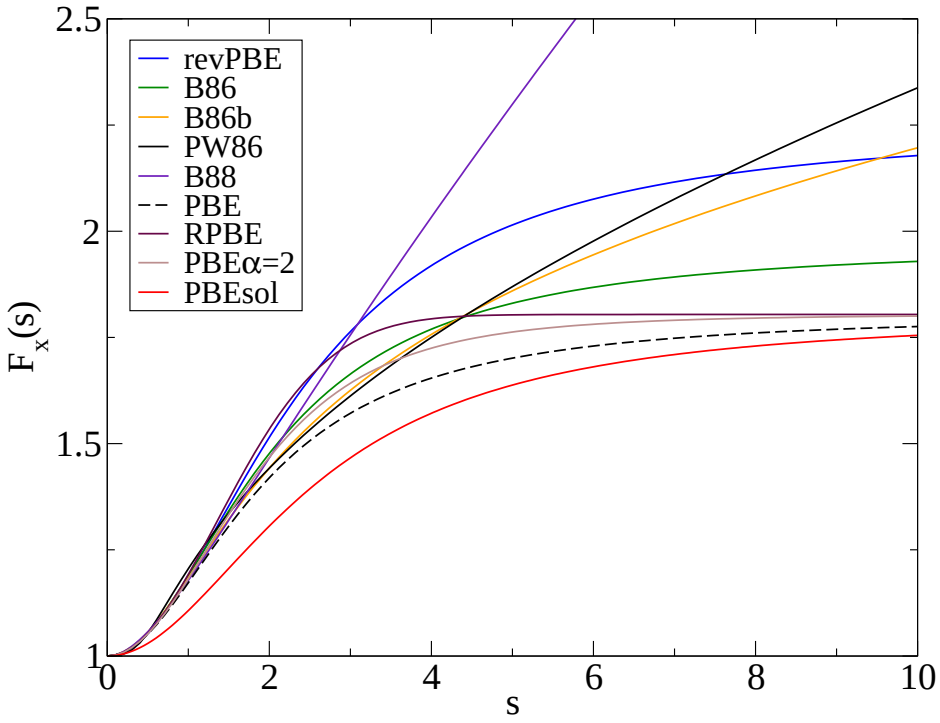

Figure 5.7: The exchange enhancement factors F_{x} for the tested functionals. In principle, they are a function which depends on the reduced density gradient s. This function then multiplies the LDA energy density to obtain the GGA energy density which is integrated to obtain the GGA exchange energy. The value for $s = 0$ is fixed by the requirement to recover LDA for the uniform electron gas. Small s behaviour is similar for most of the functionals shown, where they behave like $1 + \mu s^2$ with $\mu \approx 0.22$. This leads to good atomisation energies but also gives too long lattice constants. PBEsol has $\mu \approx 0.1234$ which is the slowly varying electron gas limit, leading to, for example, stronger interaction energies. The behaviour for large s is debated, effectively it influences the amount of repulsion or attraction in the tails of binding curves.

How can one decrease the errors further? In the following we will explore several possibilities starting from simple adjustments of the PBE form before turning to optimising the B88 and B86b functionals on the S22 set. The contrasting performance of different functionals such as PBE-vdW and revPBE-vdW provides the necessary physical insight needed to identify improved exchange functionals. As we know, the exchange enhancement factors of PBE and revPBE have the same form:

$$F_{\mathrm{x}}^{\mathrm{PBE}}(s) = 1 + \kappa - \kappa/(1 + \mu s^2/\kappa)\,. \tag{5.2}$$

The parameter μ is also the same and so the functionals differ only in the value of the parameter κ. revPBE has a larger value of κ than PBE (κ^{revPBE}=1.245, κ^{PBE}=0.804), which causes F_{x} to rise more rapidly with revPBE than PBE (see Figure 5.7 to see the enhancement factors). As a consequence, regions with large reduced density gradients are stabilised more with revPBE than PBE, which in turn leads to weaker interactions with revPBE (see Ref. [311] and Section 5.4.1.3

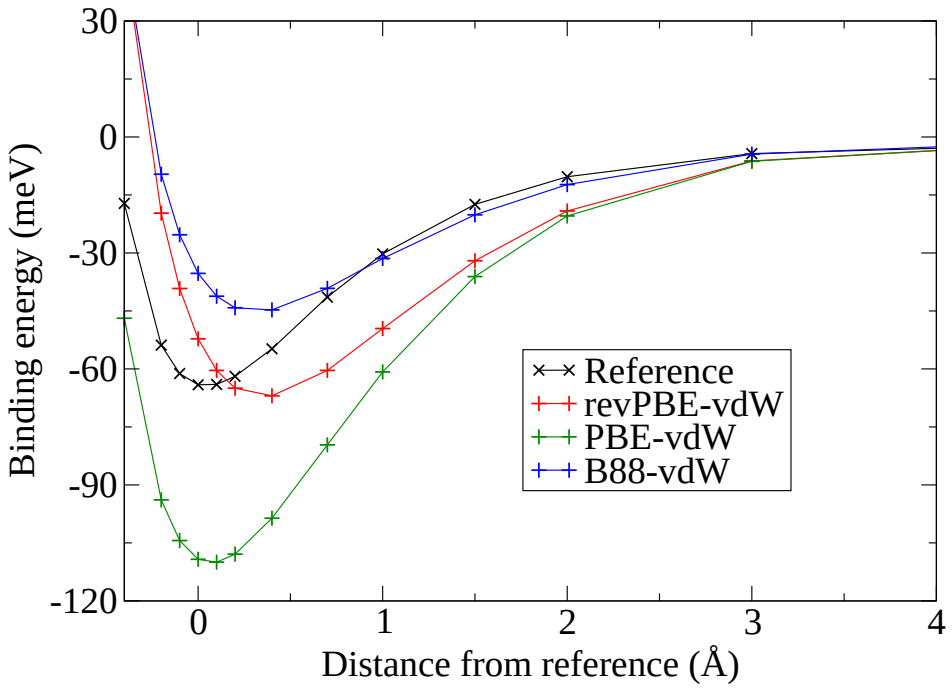

Figure 5.8: The binding curve of the methane benzene dimer calculated using the revPBE-vdW, PBE-vdW, and B88-vdW functionals. Since the correlation part is the same, the differences come solely from the different exchange functionals. For revPBE-vdW the combination of overestimated binding in long range and too strong repulsion in short range leads to overestimation of the optimal distance, and a slight overestimation of the binding energy (by $\sim$3 meV). Although PBE and revPBE give very different results for distances around the energy minimum, for separations larger than 2 Å beyond the optimal distance, PBE and revPBE give similar binding. We attribute this to the similar behaviour of the exchange enhancement factor for large s. The B88 exchange leads to less binding in this range because of the steeply rising exchange enhancement factor and follows closely the reference curve. However, for small separations it becomes too repulsive.

Table 5.3: The binding energies of the water hexamer isomers calculated using vdW correlation and different exchange functionals. We show also the results for PBE, which gives a good absolute binding energies but prefers more open "cyclic" and "book" isomers. The vdW correlation gives good agreement with the correct trend.

Method	Prism	Cage	Book	Cyclic
ΔCCSD(T)	−334	−332	−329	−321
PBE	−333	−335	−341	−339
revPBE-vdW	−267	−268	−269	−264
PBEsol-vdW	−450	−448	−438	−421
B88-vdW	−284	−286	−286	−281
RPBE-vdW	−274	−274	−275	−270
PBE-vdW	−379	−377	−370	−357
PW86-vdW	−375	−372	−364	−349
B86b-vdW	−364	−362	−357	−345
PBEα = 2-vdW	−335	−333	−330	−320
B86-vdW	−327	−326	−322	−313

for a more detailed discussion on this issue). Therefore, in principle, a simple strategy for obtaining improved interaction energies while keeping the PBE form is to identify an exchange functional intermediate between PBE and revPBE. To this end we varied κ from the PBE to revPBE values (in 0.05 increments) and calculated interaction energies within vdW-DF for the complete S22 dataset. A value of κ=1.00 resulted in the smallest MAD of only 26 meV. We dub this new exchange functional "PBEκ = 1" and show the results in Figure 5.9. Although this form improves largely upon both PBE-vdW and revPBE-vdW, it gives qualitatively very similar results to B86-vdW.

As a next step we have considered a combination of the RPBE and PBE functional forms and varied both μ and κ. RPBE by itself gives results very similar to revPBE but the different functional form gives us increased flexibility. (For RPBE the exchange enhancement factor reads $F_{\mathrm{x}}^{\mathrm{RPBE}} = 1 + \kappa(1 - \exp(-\mu s^2/\kappa))$.) The μ parameter changes the behaviour for small s which is known to influence lattice constants and atomisation energies. We have performed an optimisation of the total MAD using a simple steepest descent algorithm. After the calculations, we obtained an exchange functional "optPBE" that yielded a MAD of only 20 meV (see Table 5.4). This functional turned out to be a $x = 94.5268\%$ PBE and $(100 - x)\%$ RPBE combination with $\mu = 0.175519$, and $\kappa = 1.04804$. Although this functional has been obtained by fitting to the S22 dataset it can be seen from Figure 5.10 that it varies smoothly over the entire s range shown. It has one new parameter, simply the mixing ratio of PBE and RPBE. From Figure 5.9 it can be seen that this functional decreases the relative underbinding of the HB subset relative to the DB subset. This is confirmed in Table 5.4 by $\Delta^{\mathrm{H-D}}$= 50 meV as well as by lower Range

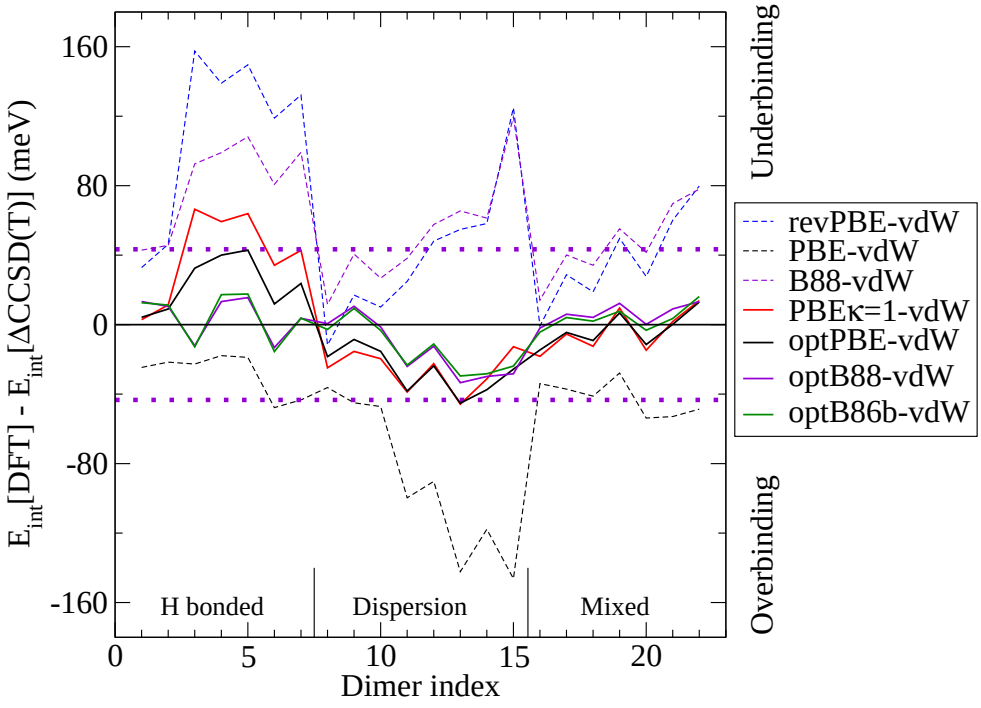

Figure 5.9: Results of the optimised functionals on the interaction energies of the S22 set. We show the results for PBE$\kappa = 1$, optPBE, optB88, and optB86b exchange functionals with the vdW correlation part and compare them to the results of revPBE-vdW as well as PBE-vdW and B88-vdW.

of errors of 88 meV.

The two PBE-style functionals introduced above offer substantial improvement over revPBE-vdW. However, they still exhibit large errors $\Delta^{\mathrm{H-D}}$ and overbind the methane dimer (dimer 8, by 25 meV or 108% with PBE$\kappa = 1$ and 19 meV or 85% with optPBE). It can be seen from Table 5.2 that B88-vdW is free from these deficiencies and we decided to explore optimised versions of it. The B88 exchange enhancement factor can be written as

$$F_{\mathrm{x}}^{\mathrm{B88}}(s) = 1 + \mu s^2/(1 + \beta s \,\mathrm{arcsinh}(cs))\,, \tag{5.3}$$

where $c = 2^{4/3}(3\pi^2)^{1/3}$, $\mu \cong 0.2743$, and $\beta = 9\mu(6/\pi)^{1/3}/(2c)$. As B88 underbinds the dimers, we modified the ratio μ/β to lead to increased binding, resulting in an optimal μ/β of 1.2 and a μ of 0.22. The new exchange functional, which we dub "optB88", yields a MAD of only 12 meV, an accurate binding energy for the methane dimer, and similar mean deviations for all three subsets.

It has been discussed several times in the literature [308, 314, 315] that the exchange enhancement factor should have asymptotic behaviour $F_{\mathrm{x}} \sim s^{2/5}$ for large s to give binding curves similar to HF[9]. Such form then prohibits any spurious binding from the exchange part,

[9] Although this might give the same shape of the interaction curve as HF does, one could say that, in analogy to correlation, it is for the wrong reason since non-local exchange effects are modelled by semi-local functionals.

Table 5.4: Mean absolute deviations from the reference data [41, 295] for the S22 set for vdW-DF with different exchange functionals ("Method") optimised on the S22 set. MADs are given for the whole set ("MAD Total"), the hydrogen bonded ("MAD HB"), dispersion bonded ("MAD DB"), and mixed bonding subsets ("MAD MB"). For each functional we also report the difference between the largest and smallest deviations from the reference data ("Range") and the difference in the mean deviations of hydrogen bonded and dispersion bonded subsets ($\Delta^{\mathrm{H-D}}$).

Method	MAD				Range	$\Delta^{\mathrm{H-D}}$
	Total	HB	DB	MB		
revPBE-vdW	63	111	44	38	169	70
B86-vdW	28	38	33	12	123	71
PBE$\kappa = 1$	26	40	26	11	112	66
optPBE	20	23	27	9	88	50
optB88	12	12	18	7	49	19
optB86b	12	13	16	6	47	19

a problem of functionals that converge to a constant for large s such as PBE (and PBEsol, revPBE, RPBE, B86, ...) or, in fact, LDA[10]. In our test there are two exchange functionals that have the correct asymptotics: PW86, and B86b. Although better than revPBE-vdW, both of them give substantial errors. We have selected B86b for optimisation since it has a smoother functional form and one parameter less than PW86. There are in fact two parameters in the exchange enhancement factor, μ and κ: $F_{\mathrm{x}}^{\mathrm{B86b}} = 1 + \frac{\mu s^2}{(1+\mu s^2/\kappa)^{4/5}}$. While the ratio μ/κ changes the slope of the F_{x} and thus affects the total magnitude of binding, the value of μ can be related to the strength of repulsion for shorter separations. We will show this explicitly in the following part but it can be understood from the results of the PBE and PBEsol functionals for lattice constants. In that case PBE gives on average larger lattice constants than PBEsol does, an effect ascribed to the parameter μ [313]. Similarly for the S22 dimers, larger μ and steeper F_{x} for small s lead to too strong repulsion for shorter binding distances. In the hope of duplicating the less steep small s behaviour of optPBE and optB88 which can be seen in Figure 5.10, we have fixed $\mu = 0.1234$. This is the same value derived from the slowly varying electron gas that is used in PBEsol. We then optimised the value of κ and found that $\kappa = 1.00$ leads to results which are very similar to the optB88-vdW ones. We call the final exchange functional optB86b, and as shown in Table 5.4 the MAD for the whole S22 and the different subsets differ only by 2 meV at most from the optB88-vdW values. Specifically, the overall MAD is 12 meV, the same as for optB88-vdW. As can be seen in Figure 5.9 the results are very similar when optB88-vdW and optB86b-vdW are compared on the S22 geometries, however, there are differences when

[10]From the behaviour of different F_{x} we can understand that the LDA F_{x} which is just 1, independent of s, leads to a small repulsion and a considerable binding of dimers. This is the reason behind the statement that "LDA is able to describe dispersion".

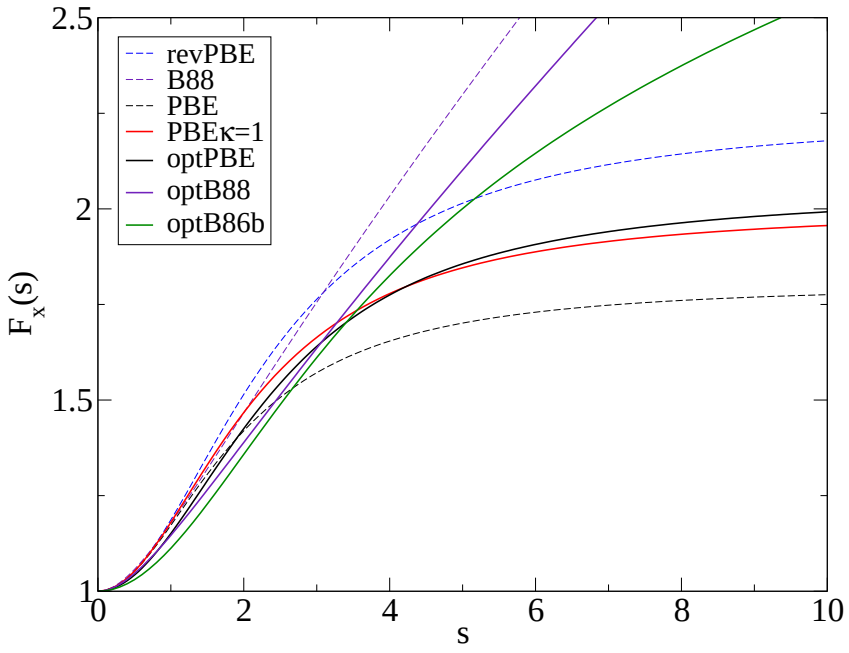

Figure 5.10: The exchange enhancement factors of the PBE$\kappa = 1$, optPBE, optB88, and optB86b exchange functionals optimised on the S22 set with the vdW correlation. We show the forms of revPBE, PBE, and B88 for comparison as well. As can be seen the optimised functionals rise less steeply for small s than the parent functionals which decreases repulsion for hydrogen bonded dimers. Furthermore, the optB88 and optB86b keep rising for large s which increases the repulsion for dispersion bonded dimers. It also decreases the overestimation of the binding caused by the vdW correlation.

geometries away from minimum are considered since optB86 exchange is less repulsive than optB88 at long range.

We now briefly consider whether the improved performance of the optimised functionals carries over to the other systems in our test. For the water hexamers, all the functionals lead to improvement over revPBE-vdW, and as can be seen in Table 5.5 the dissociation energies given by optPBE-vdW are essentially identical to those obtained with ΔCCSD(T). The optB88-vdW and optB86b-vdW functionals tend to overbind but are still within 15 meV of the accurate reference. Turning to the adsorption energy of water on NaCl(001), the optimised functionals, again, improve upon the revPBE-vdW values with all the functionals predicting the adsorption energy in a range from -413 meV (PBEκ = 1-vdW) to -424 meV (optB88-vdW). Although this is still below the lower end of the error bar on the reference, it represents an improvement by 90 meV or almost 1/5 of the adsorption energy.

5.4.1.3 Binding curves

At this point, after presenting the improved results and before showing the binding curves, it seems useful to briefly discuss how the shape of the F_x affects the binding curves. This will hopefully make the alterations to the exchange functionals clearer. We will discuss two parts of

Table 5.5: The binding energies of the water hexamer isomers calculated using vdW correlation and the exchange functionals optimised on the S22 set. Compared to revPBE-vdW the agreement with the reference data is much improved. The optPBE-vdW method gives values that are almost identical to the reference data. The optB88-vdW and optB86b-vdW functionals slightly overbind the hexamers but the binding energies are still within 15 meV of the reference data.

Method	Prism	Cage	Book	Cyclic
ΔCCSD(T)	−334	−332	−329	−321
PBE	−333	−335	−341	−339
revPBE-vdW	−267	−268	−269	−264
PBEκ = 1-vdW	−324	−323	−321	−312
optPBE-vdW	−335	−334	−332	−323
optB88-vdW	−347	−347	−344	−334
optB86b-vdW	−346	−347	−344	−336

F_{x}: the behaviour for small s and the behaviour for large s – asymptotics. Small s regions are located around the centres of bonds, or around regions where two molecular densities overlap when a dimer is formed; large s regions are located in density tails with s growing with increasing distance from the core.

Let us first show the effect of the large s behaviour of F_{x}. For this we consider two atoms (*e.g.*, of noble gas) in positions far apart and forming a dimer with some parts of the density tails overlapping as shown schematically in Figure 5.11. The s in overlapping regions changes from large values to small values, for simplicity we suppose that in the overlapping region $s = 0$. Now consider two exchange functionals with different F_{x}: $F_{\mathrm{x}}^{\mathrm{high}}$ that rises (such as optB86b, left column in Figure 5.11) and the other $F_{\mathrm{x}}^{\mathrm{low}}$ that converges to a constant for large s (*e.g.*, PBEsol, right column in Figure 5.11). In the overlapping region both functionals will yield the same energy density since $s = 0$ and thus $F_{\mathrm{x}} = 1$ and the LDA energy density is recovered. However, for the monomers, the functional with $F_{\mathrm{x}}^{\mathrm{high}}$ will have a higher absolute energy density (since that is just $\varepsilon_x = F_{\mathrm{x}}(s)\varepsilon_{\mathrm{x}}^{\mathrm{LDA}}$). Since $\varepsilon_{\mathrm{x}} < 0$ by creating the overlap the energy will increase more for F_x^{high} than for F_x^{low}. This means that the binding curve of the functional with $F_{\mathrm{x}}^{\mathrm{high}}$ will be above the curve of functional with $F_{\mathrm{x}}^{\mathrm{low}}$, *i.e.*, the first functional will give a more repulsive behaviour. Indeed, optB86b exchange is more repulsive than PBE, PBEsol or LDA. The situation for small s seems to be quite analogous, however, it appears for shorter distances such as bond lengths or lattice constants of solids.

The effect of the F_{x} can be demonstrated on the binding curves of the S22 dimers. In Figure 5.12 we show the binding curve of the methane benzene dimer calculated using the optB86b-vdW functional and functionals where the F_{x} was changed to be more or less steep either for small s or large s. We do this by altering the parameters μ and κ in the $F_{\mathrm{x}}^{\mathrm{B86b}} = 1 + \frac{\mu s^2}{(1+\mu s^2/\kappa)^{4/5}}$. The parameter μ was set to 0.1234 in the optB86b functional to follow the

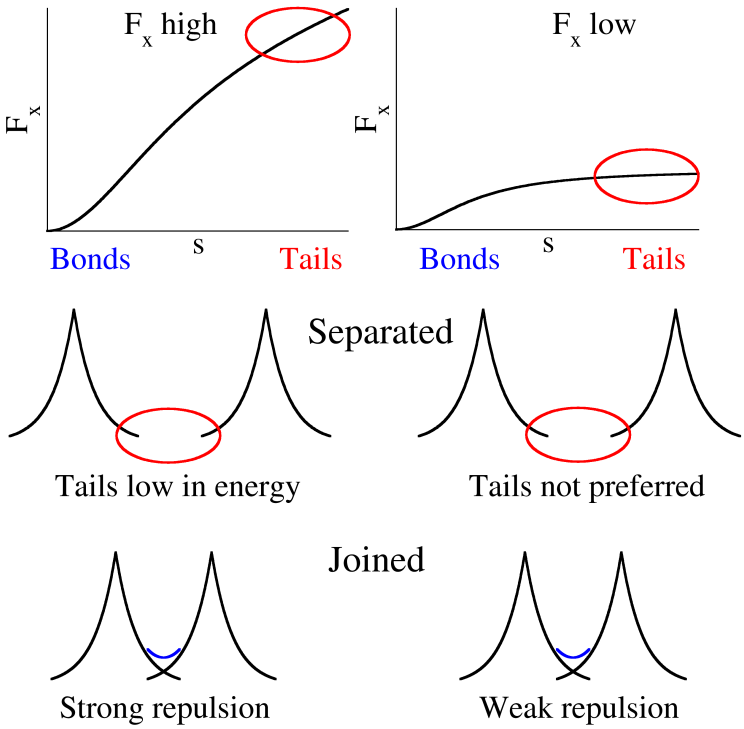

Figure 5.11: A schematic illustration of the effect of the density tails on the energy change upon formation of a dimer for two exchange functionals. In the left column an exchange functional with F_x high for large s (*e.g.*, optB86b) and second on the right exchange functional with F_x small for large s (*e.g.*, PBEsol). When two atomic densities are brought together to form a dimer, the values of s in the regions of the overlap (shown with blue line) decrease to values $\sim$0. Since the functionals with high F_x prefer energetically the configurations with high s, forming the overlap requires more energy than for the functionals with F_x small. Overall this leads to a more repulsive binding curve for the first kind of functionals compared to the second.

slowly varying electron gas limit and the behaviour is known to affect the short range repulsion. This change of short range behaviour for changing μ can be seen by comparing the violet curve of optB86b-vdW with the curves (red lines) of functionals with μ changed to either 0.09 (less repulsive) or 0.15 (more repulsive). By changing the μ parameter the position of the repulsive wall can be clearly shifted to smaller or larger distances. Simultaneously to changing the μ parameter we have changed κ so that the large s behaviour is unaffected. Indeed, the binding curves are almost identical for separations larger than 1 Å beyond the minimum. The long range behaviour is affected when the κ is changed. Here larger κ will increase the steepness of the F_x and smaller κ will make the functional more attractive. As can be seen the different asymptotic behaviour of F_x induced by different κ makes the binding curves differ already for large separations.

With this reasoning we can expect that the optB86b-vdW functional will be the least repulsive for small dimer separations, followed by optB88-vdW and optPBE-vdW. In the asymptotic

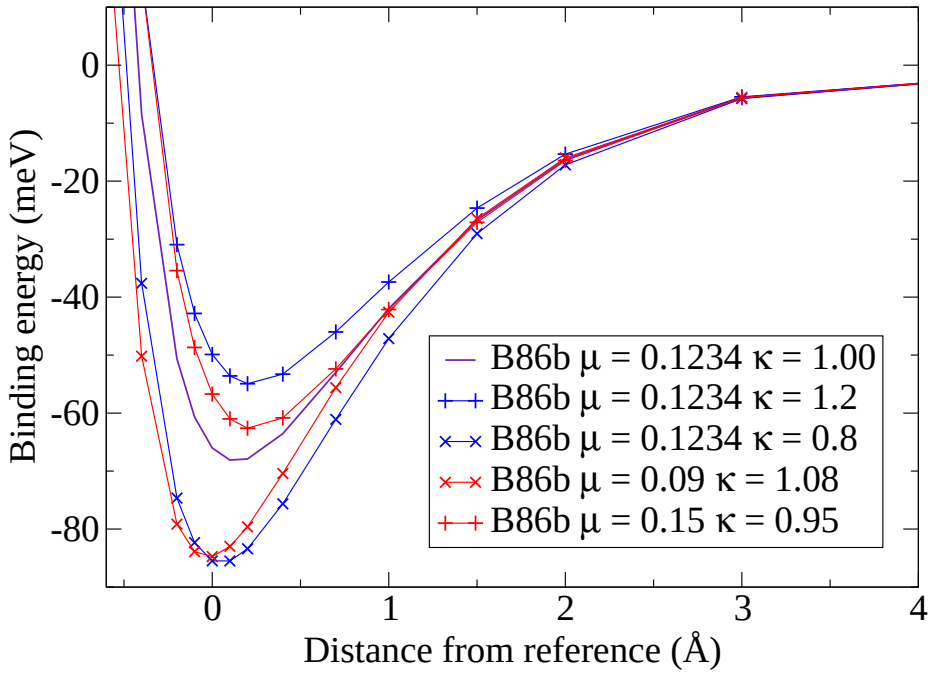

Figure 5.12: The effect of the small and large s behaviour of the exchange enhancement factor on the shape of the binding curve. The violet curve shows the binding curve of the methane benzene dimer obtained with the optB86b-vdW functional which behaves like $1 + 0.1234s^2$ for small s, parameter κ, set to 1 in this functional influences the steepness for large s. Changing the μ to 0.09 or 0.15 while keeping the long range behaviour intact (red curves) affects the position of the repulsive exchange well which changes the position of the binding minimum. When μ is kept constant and κ is altered to make the F_x more or less steep, the binding curve changes already for distances smaller than ∼3 Å beyond the minimum. The position of the minimum changes as well. For even smaller distances the same value of μ will lead to a very similar behaviour, not much dependent on the value of κ.

region, optPBE-vdW will be more attractive than optB86b-vdW, and optB88-vdW will give the smallest interaction. Since the vdW correlation overestimates the interactions for long range, the optB88 exchange will tend to decrease this effect. This is indeed the case as can be seen in Figure 5.13 where the binding curves for the formamide, indole benzene, and T-shape benzene dimers are shown.

5.4.2 Other correlation functionals

We have shown that the accuracy of the vdW-DF method can be improved when alternative exchange functionals are used. However, despite the fivefold improvement in average errors there are still problems left which can be traced back to the form of the correlation functional. One reason is that the two point form of the vdW-DF correlation is a simplification of the exact correlation functional. However, as was shown in Ref. [156], the vdW functional overestimates

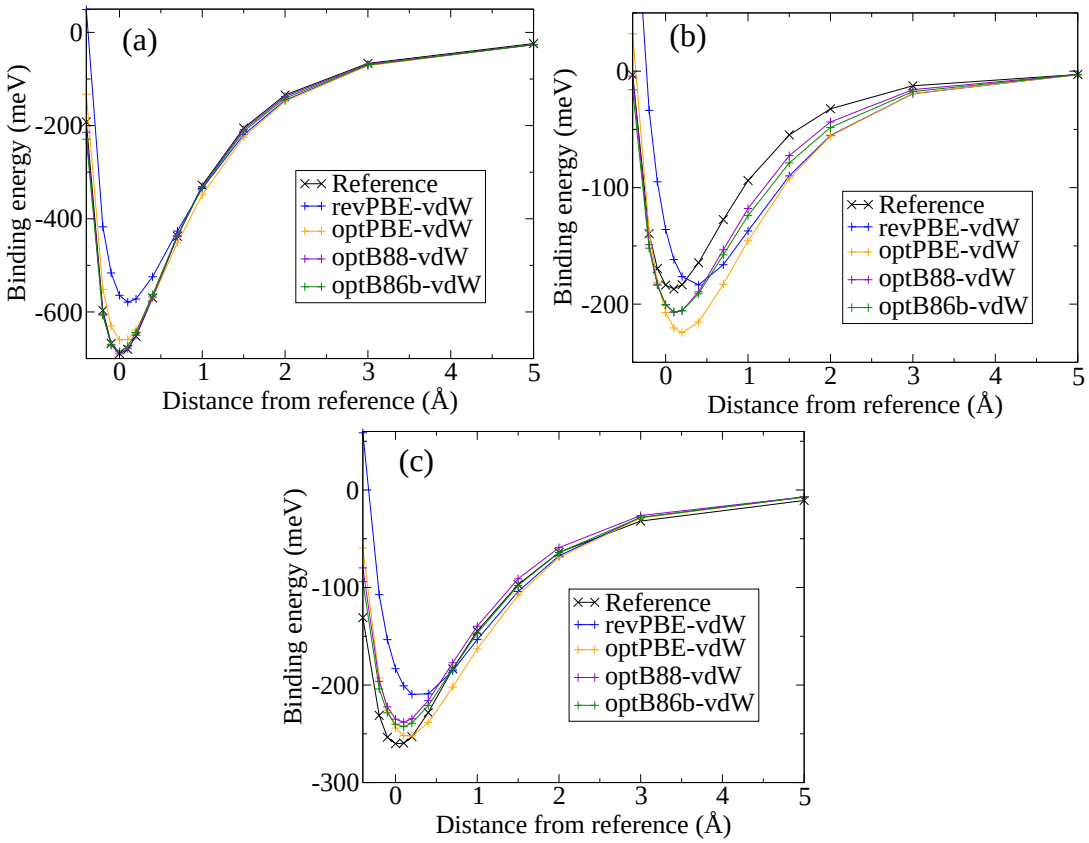

Figure 5.13: The binding curves of three dimers of the S22 set calculated using the original revPBE-vdW, and three functionals optPBE-vdW, optB88-vdW, and optB86b-vdW where the exchange part was optimised on the S22 data. We show the data for (a) formamide dimer, (b) pyrazine stacked dimer, and (c) indole · benzene T-shape dimer. As can be seen the short range repulsive behaviour of revPBE-vdW is largely improved. The optB88-vdW and optB86b-vdW also lead to less overbinding in the asymptotic region.

on average the dispersion interaction (given by the C_6 coefficient) and there is a possibility for improvement. In this part we will first look at non-local correlation functionals proposed to improve the overbinding of vdW in the long-range. After this we briefly discuss an alternative way to improve the vdW results for smaller distances by addition of a semi-local correlation term.

5.4.2.1 Correlation functionals of Vydrov and van Voorhis

The vdW functional was implemented by Vydrov *et al.* [316] for a Gaussian basis set. Following this work, several non-local correlation functionals were proposed by Vydrov and van Voorhis [152, 156, 147]. They focused on obtaining improved C_6 coefficients, although this again needs to be taken in a statistical manner, that is some of the C_6 coefficients still have large errors. However, trying to obtain accurate asymptotic behaviour is a good approach since in this regime non-local correlation can be clearly defined. Their functionals are not simple to use in the reciprocal space evaluation scheme of Román-Pérez and Soler [305], but they can

be implemented in the JuNoLo code [306] which performs the double integral. We have done this for the vdW09 functional [152] and tested it with the functionals implemented in VASP. However, the original work used a range separated hybrid and the results are discouraging when GGAs are used. Although there is one parameter which should be adjustable to the exchange functional, this does not lead to improvement.

5.4.2.2 The vdW2 correlation functional

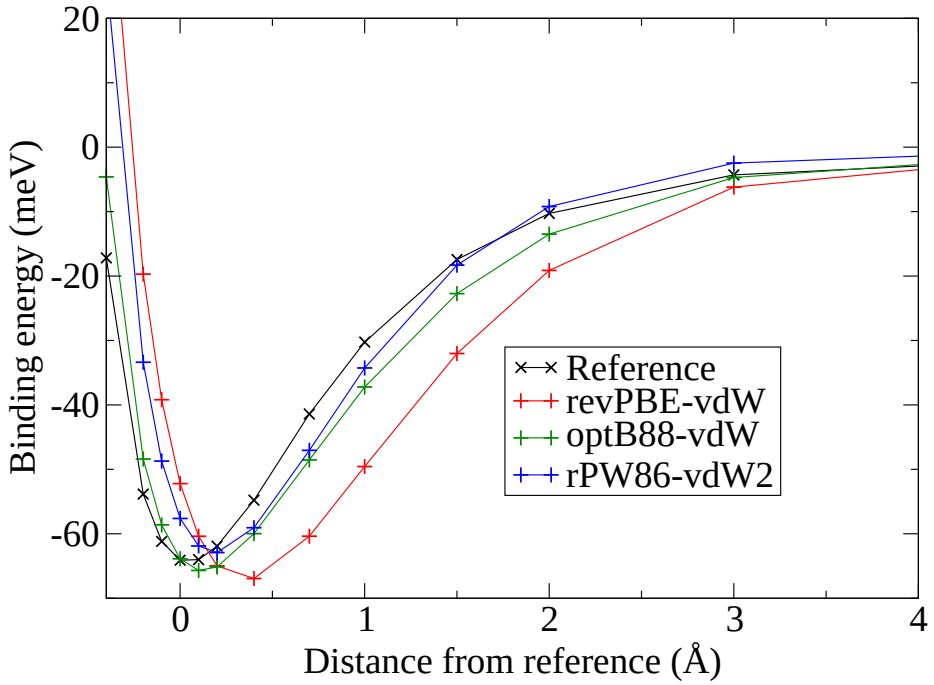

Figure 5.14: Binding curve of the methane · benzene dimer calculate with the revPBE-vdW, optB88-vdW, and rPW86-vdW2 functionals. Although rPW86-vdW2 improves over revPBE-vdW in several ways, the dispersion at long range is severely underestimated. It can be seen that 3 Å away from the S22 geometry rPW86-vdW2 underestimates the interaction and only for smaller distances the vdW contribution starts to be stronger.

Let us now turn to a functional that has been proposed by the authors of the original vdW scheme (Langreth and Lundqvist groups), as an improvement of the original method. This functional, called vdW-DF2 in the work of Lee *et al.* [154], uses the same non-local kernel as vdW, only modifies the s dependence of the internal functional F_{xc}^{0} defined in Section 2.3.2.1. Recall that this was originally defined as $F_{\mathrm{xc}}^{0} = 1+\lambda s^{2}-(4\pi/3k_{\mathrm{F}})\epsilon_{\mathrm{c}}^{\mathrm{LDA}}$. The value of λ, originally corresponding to the slowly varying electron gas limit was changed to twice of that, which is supposedly more appropriate for molecules. Effectively this increases the values of d used for the calculation of the vdW energy. By observing the kernel shown in Ref. [16], larger values of d decrease the value of the kernel, this then leads to lower long-range binding. The exchange part was taken to be a modified PW86 functional, called rPW86 [315], therefore we refer to

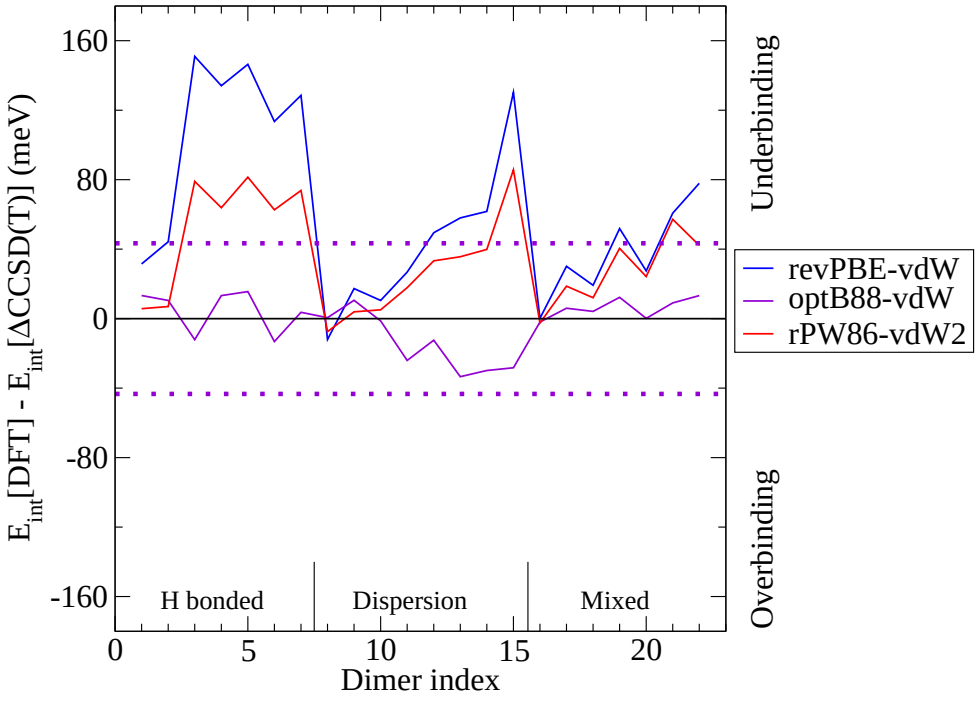

Figure 5.15: The differences from the S22 reference for the rPW86-vdW2 method proposed in Ref. [154] (and called vdW-DF2 therein) compared to the results of the original revPBE-vdW and the optimised optB88-vdW. Although rPW86-vdW2 decreases the errors, especially the HB dimers are still strongly underbound. This can be attributed to the choice of the exchange functional which rises steeply for small s.

this functional as rPW86-vdW2. Although the rPW86-vdW2 form improves upon revPBE-vdW, it is at the expense of severe underestimation of the C_6 coefficients. This can be inferred from Figure 5.14 where the binding curve of the methane benzene dimer is shown. Clearly for distances larger than 2 Å beyond the minimum the rPW86-vdW2 gives too little binding; only for shorter distances it starts to increase the interaction becoming more attractive than the reference around 1.7 Å away from the minimum. The interaction is then too strong before exchange repulsion becomes dominant. The C_6 coefficients have been calculated explicitly by Vydrov and van Voorhis [147] and they show that the C_6 coefficients evaluated using the vdW2 correlation functional are only 40% of the accurate reference values.

We now summarise the results of our tests for the rPW86-vdW2 functional. Figure 5.15 compares the differences from the S22 dataset for revPBE-vdW, optB88-vdW, and rPW86-vdW. One can see that rPW86-vdW indeed improves the interaction energies upon revPBE-vdW, most notably for the HB subset where the MAD changes from 111 meV for revPBE-vdW to 53 meV for rPW86-vdW2. The total MAD, however, is decreased only to 36 meV, and especially the error for the HB dimers is substantial.

The most significant change should be observed for larger separations. This is indeed the

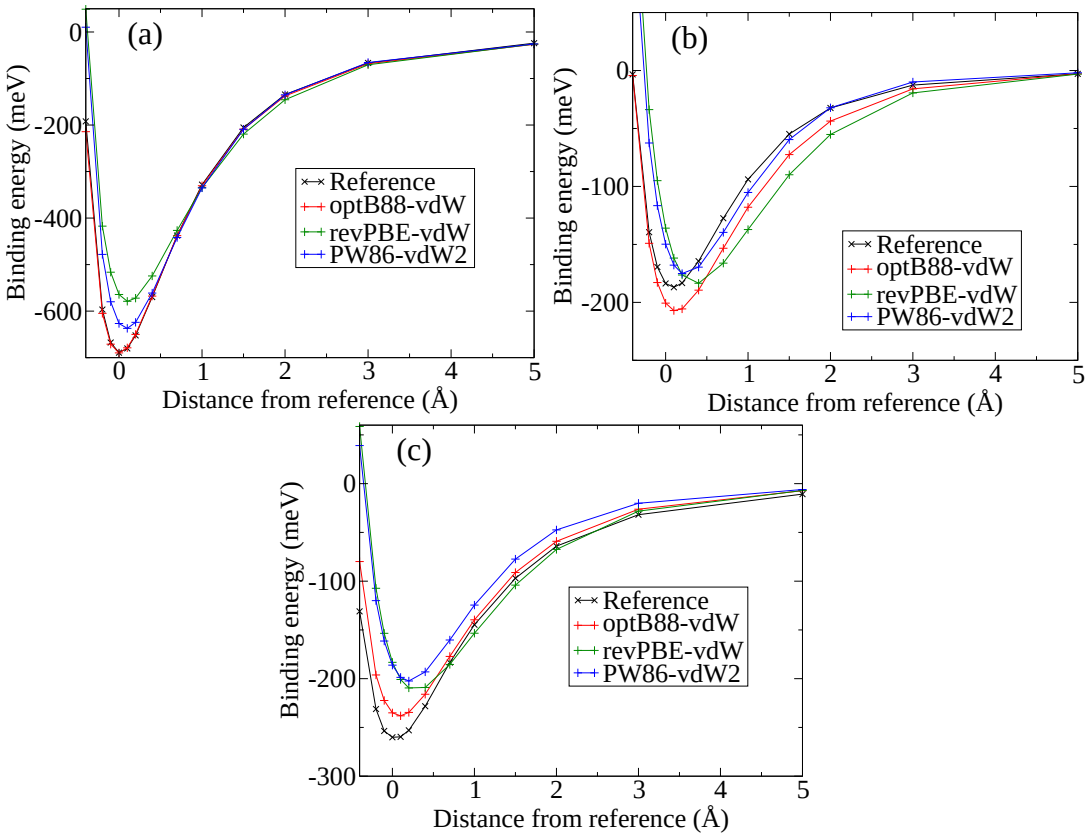

Figure 5.16: The binding curves of three dimers of the S22 set calculated using revPBE-vdW, optB88-vdW, and rPW86-vdW2. We show the data for (a) formamide dimer, (b) pyrazine stacked dimer, and (c) indole · benzene T-shape dimer. The rPW86-vdW2 decreases the overestimated correlation in long range, although too much in the case of the pyrazine dimer. For small distances it is still repulsive which leads to the overestimation of equilibrium distances and underestimation of the interaction energies in the S22 geometries.

case for dimers where dispersion plays an important role. This is clearly seen from the binding curve of the stacked pyrazine dimer in Figure 5.16(b) where rPW86-vdW2 follows the reference most closely for separations >0.5 Å away from the minimum. However, as can be seen from Figure 5.16(a,c), rPW86-vdW2 gives similar behaviour to revPBE-vdW for smaller separations, which we attribute to the exchange enhancement factor. That is, it is too repulsive for short separations which leads to overestimation of the equilibrium distances, although to a smaller extent than revPBE-vdW. The optB88-vdW functional describes the binding curves better for separations smaller than 0.5 Å from the minimum for all the dimers shown.

Let us now mention the results for the water hexamers and adsorption. The binding energies of the water hexamers are, rather surprisingly, very accurate and underestimate the reference energies by 6 meV (without performing geometry optimisation). Finally, the adsorption energy of water on NaCl(001) turns out to be −402 meV, which is a significant improvement over revPBE-vdW, and worse by only ∼20 meV than optB88-vdW.

Overall, the method seems to achieve improvements at long range but not in the ideal

manner: the correlation part is too weak for large separations and too strong at mid-range. A more appropriate solution would be to decrease the long-range as well as the mid-range interaction slightly. The large repulsion at short distances seems to be partially improved, but not enough, as we will show in the next Chapter in the case of lattice constants.

From the improvements of the revPBE-vdW method it is clear that the simplest step needed to improve the accuracy of the rPW86-vdW2 method without affecting the vdW2 correlation part is to make the exchange functional less repulsive at short range. The rPW86 functional is quite a reasonable choice, however, in the functional form $F_{\mathrm{x}}^{\mathrm{rPW86}} = (1 + as^2 + bs^4 + cs^6)^{1/15}$, the parameter b was obtained from a fit to a model exchange hole [310]. While the a was chosen so that the slowly varying electron gas limit is followed, the choice of b causes F_{x} to depart from the small s limit and to rise too steeply. This also leads to the too strong short-range repulsion. The way to decrease the repulsion and thus to improve the S22 results is to lower the value of b. Indeed, choosing $b = 3.5$ leads to a substantial improvement on the S22 with the MAD being only 8 meV, negligible $\Delta^{\mathrm{H-D}}$= 2 meV and all the individual errors within 17 meV of the reference. Although this is the best functional form found so far, the errors at long range are expected to be very similar to the rPW86-vdW2 ones. We refer later to the modified rPW86 functional as rrPW86.

5.4.2.3 Including semi-local correlation in the vdW correlation functional

After we have shown that the results can be improved by changing the exchange functional, and the non-local correlation functional, we will discuss the last term remaining in the definition of the vdW functional: the local correlation (cf. Equation (5.1)). The non-local correlation term includes some semi-local correlation and thus only the LDA correlation term was chosen to avoid a double counting of the semi-local correlation. Although this, in principle, is a sensible approach, there is the possibility that not all the appropriate semi-local correlation is accounted for. Indeed, it has been suggested that adding full PBEc[11] semi-local term leads to improved binding energies of metals [317]. We will discuss solids in the next chapter but let us show here what the results for the S22 dataset would be. As shown in Figure 5.17, the functional, which can be called revPBE-vdW-PBEc leads to better interaction energies of HB dimers but dramatically overbinds the dimers of the DB subset.

The effect of adding the PBE correlation can be seen in Figure 5.18 where the binding curves of revPBE-vdW and revPBE-vdW-PBEc are shown for the stacked benzene dimer. Adding PBEc indeed leads to increased binding and the minimum is shifted more towards the reference. Unfortunately, it also amplifies the overbinding at mid-range. It therefore does not seem appropriate to add more attraction to binding curves which are already overestimated.

The most problematic question, however, concerns the double counting of semi-local corre-

[11] There is, again, a plethora of choices for semi-local correlation functionals, but we will explore the suggested PBE. A more appropriate approach would probably be to find a functional form that gives the same asymptotics for large s as PBE correlation, but with different small s behaviour.

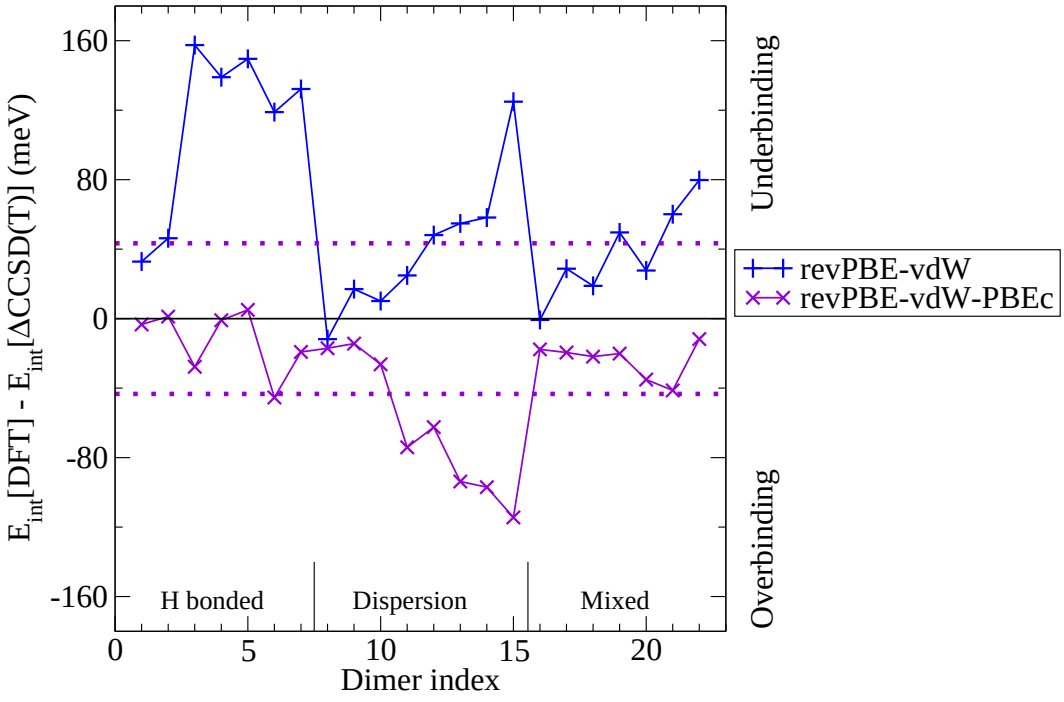

Figure 5.17: The results of the revPBE-vdW-PBEc functional for the S22 set. In contrast to the usual revPBE-vdW, the PBE semi-local correlation is kept in the revPBE-vdW-PBEc functional. By comparison with the revPBE-vdW data, one can see that this results in a more attractive behaviour. Although the HB subset is in a good agreement with the reference, the DB dimers are overbound by a similar amount that revPBE-vdW underbinds.

lation. While the vdW correlation is constructed to recover some semi-local correlation, it is not clear to what extent. With not many options available, we have performed a simple estimation. We take the electron densities (pseudo-valence) of the S22 dimers and monomers and calculate the semi-local correction of the PBE correlation functional, *i.e.*, the difference between LDA and PBE correlation energies. We then took the E_c^{nl} energies calculated using the JuNoLo code on the same densities and compared them to the PBE semi-local part. As can be seen in Figure 5.19, the ratio E_c^{nl}/E_c^{PBE} is almost constant for all the monomers, being 0.465 on average. This changes to 0.462 when the dimers are also included showing that the non-local correlation is smaller than the semi-local contribution. Therefore it seems that if one wants to reproduce the PBE correlation energies, $\sim$0.55 of E_c^{PBE} should be added to the vdW calculation. Since PBE correlation will increase the binding and many exchange functionals with vdW correlation give already overestimated binding, there is just a handful of choices left to test. By using the data obtained before, we found that adding 0.55 of PBE correlation to B88-vdW interaction energies leads to a MAD of only 16 meV, although Δ^{H-D} of 16 meV shows that the HB dimers are slightly underbound and DB dimers overbound. We note that adding more semi-local correlation will increase the binding in the mid-range and from this point modification of the non-local

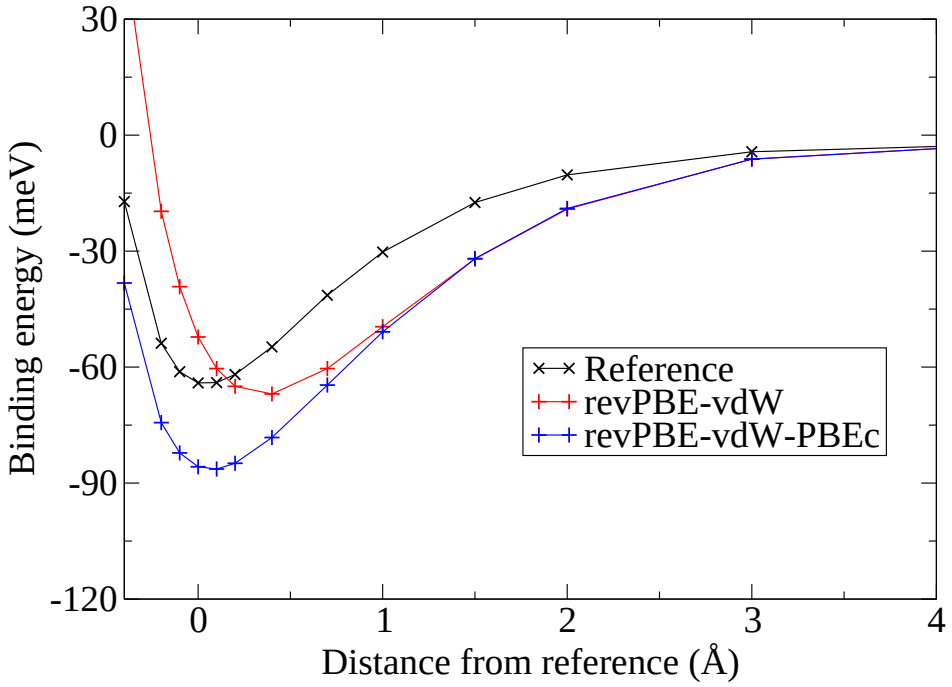

Figure 5.18: The binding curve of the stacked benzene dimer calculated using revPBE-vdW and revPBE-vdW-PBEc where the full PBE correlation is used instead of LDA correlation only. The PBE correlation leads to more binding for small separations and improved position of the energy minimum. This, however, is at the expense of a too strong binding.

correlation seems necessary.

The semi-local PBE correlation can, of course, be added to functionals using the vdW2 correlation as well. However, the long-range underbinding will not be improved by this procedure but the short range underbinding will be improved. A simple test reveals that adding 0.43% of PBE correlation to the rPW86-vdW2 functional leads to MAD = 13 meV, similar to that of optB88-vdW. However, the DB dimers become overbound relative to the HB dimers with $\Delta^{\mathrm{H-D}} = 22$ meV.

5.4.3 Outlook

Looking at the development from a broader perspective, the non-local correlation functionals seem indispensable for DFT studies in the medium to long term. Not only because dispersion interactions are becoming more and more important in the contemporary systems being studied, but mostly for physical reasons. Unlike LDA, non-local correlation functionals try to describe non-local correlation by a non-local functional. The development continues at a fast pace and there are now several proposed non-local density correlation functionals, as well as simpler functionals based on summation of $1/r^6$ terms. The validity of the forms will need to be tested, the importance of which we try to stress in this and the next Chapter.

The optimised vdW functionals which were obtained to increase the accuracy of the method

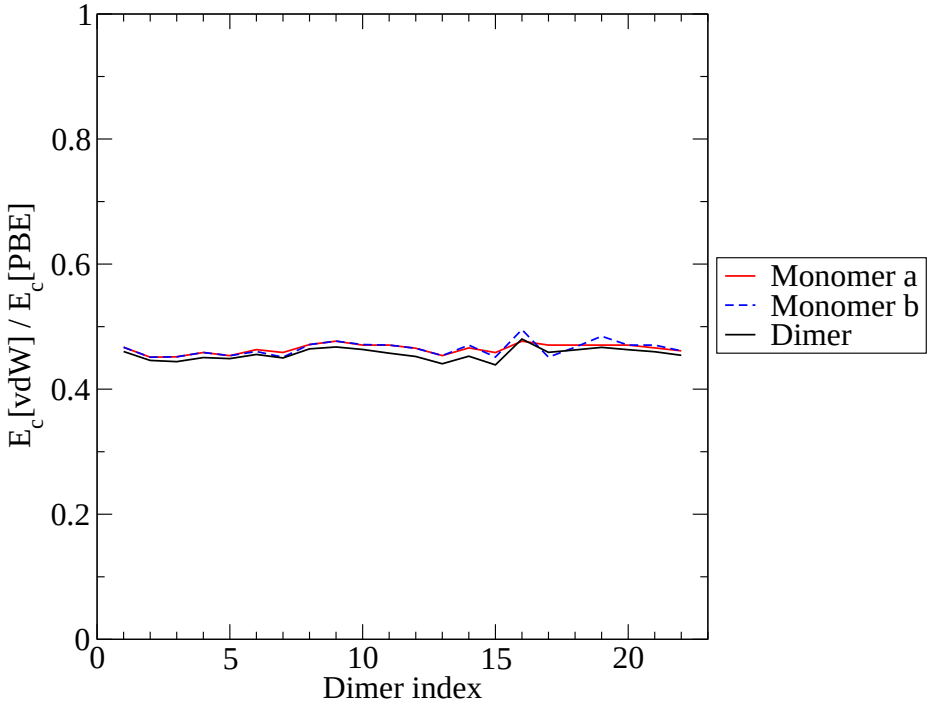

Figure 5.19: The ratio of the PBE and vdW corrections to LDA correlation energies on the monomers and dimers of the S22 set. This gives some idea on how much PBE-like correlation is included in the vdW functional. Clearly the ratio is rather constant with the average value equal to 0.462 and does not depend strongly on whether the energies of monomers or dimers are used.

have demonstrated successes for several systems. As an example, we can mention the long standing problem of surface wetting where small energy differences decide what the water behaviour on the surface will be. Experimentally water ice-like overlayers on different metal surfaces such as Cu(110) [318] are found despite standard DFT functionals (*e.g.*, PBE) predicting that ice should not wet the surfaces. That is, the lattice energy of ice is found to be lower than the adsorption energy per water molecule on the surface. While revPBE-vdW doesn't change this conclusion, the optimised functionals are the first functionals that prefer the experimentally observed structures while giving a good lattice formation energy of ice at the same time [319]. This and other applications support the need and importance of accurate vdW functionals. However, there are some outstanding issues relating to the two point form of the functionals. This leads to the fact that screening is accounted for only effectively and even the lowest order three body Axilrod-Teller-Muto term [320, 321] is not recovered. If, or how, severe this problem is is difficult to assess, but we show some estimations in the next part. The two body form also leads to incorrect asymptotic behaviour for systems where long wavelength excitations are important [133, 322].

The real question is what exchange and what correlation functionals to use and against

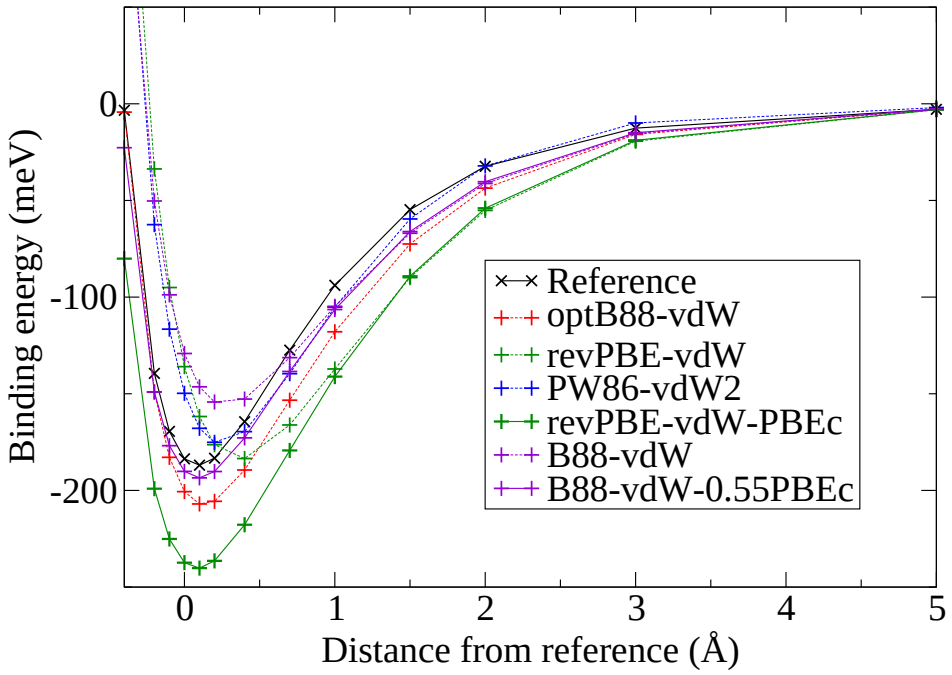

Figure 5.20: The binding curve of the pyrazine dimer calculated using different vdW functionals with different amount of PBE correlation added. We show the reference binding curve and the binding curves obtained with optB88-vdW, revPBE-vdW, and rPW86-vdW2. The effect of adding full PBEc is shown on the revPBE-vdW data. The PBE correlation affects the binding for distances smaller than ∼1.5 Å beyond the minimum and leads to a stronger binding. Although the position of the optimum is shifted to the correct distance, the binding strength is overestimated by ∼50 meV. We estimated the amount of missing PBE-like correlation in vdW to 55% and adding this amount to the B88-vdW calculations gives a binding curve in a much better agreement than any other calculation. The interaction in the tail is still overestimated because of the overestimated vdW correlation.

what to benchmark them. The idea to start from ACFDT, and use the HF-like exchange for exchange and to include the rest of the energy in correlation does not, in fact, differ qualitatively from doing a HF calculation followed by post-HF wavefunction reconstruction [323]. And even quantitatively, the HF-like exchange curves using DFT orbitals don't differ much. However, obtaining an exchange functional that gives results like HF is more difficult (setting aside the question if this is a real necessity) [315]. Moreover, as we have mentioned earlier, in analogy to the dispersion being treated by a semi-local functional, the exchange is also non-local, albeit more short ranged. Therefore constructing an approximate non-local exchange functional could lead to some developments.

5.4.3.1 Three body contribution

The next step beyond two point contributions are three point contributions, with the leading term known as the Axilrod-Teller-Muto (ATM) [321, 320] term. Although the energy contribution of this term seems to be difficult to calculate and translate into the atom-centered summation, there have been two estimations recently. The work of von Lilienfeld and Tkatchenko [324] has estimated that the three point contribution is large for several materials, *e.g.*, graphite. Moreover, they estimate the contribution for the dimers in the S22 to be as high as 1.6 kcal/mol or almost 70 meV in some cases. This contribution is destabilising and largest for the DB dimers. It indeed seems plausible when observing the data in Figure 5.9 that this contribution can have an effect since it has the same trend as the overestimation of optB88-vdW data. To show this explicitly, we compare in Table 5.6 the errors in the energy differences between two isomers from the S22 set to the three body correction from Ref. [324]. We show that the errors in the isomer energy differences could be, at least partially, attributed to the three body terms. For different correlation functionals (vdW, vdW2, VV09), and different exchange parts (optB88, rrPW86, HF, rPW86) the errors and corrections have the same sign and have a similar magnitude. This is true especially for the optB88-vdW functional. Note that the data from Ref. [324] are crude estimates and they depend on the cut-off function which is necessary to apply to remove the divergence of the $1/r^6$ function. Whether indeed the three body contributions are the main reason for the relative overbinding is not clear, for example tests by Murray *et al.* [315] show that the differences for the benzene dimer could be explained by overestimation of the repulsion part relative to the HF repulsion. Similarly, some of the differences might be caused by a simple overestimation of the non-local correlation. In any case, the terms beyond two body contributions deserve some attention.

5.5 Summary

To summarise we have shown that the vdW functionals are an important step in the development of DFT exchange-correlation functionals but a thorough testing is needed to establish their applicability. Specifically, we have used the vdW-DF method and explored the possibility of using an exchange functional other than the original revPBE. Several promising functionals have been introduced (optB88-vdW, optPBE-vdW, and optB86b-vdW) which offer up to a five-fold improvement on the S22 dataset while improving the results for the isomers of the water hexamers and for water adsorbed on NaCl(001). However, since the vdW correlation functional overestimates the interaction the form of the functional needs to be addressed. The attempt to improve the asymptotic interaction by the Langreth and Lundqvist groups with the rPW86-vdW2 functional reduces the interaction between fragments too much. Other non-local correlation functionals which try to obtain accurate asymptotics in the first place seem to be promising. We have also found how the semi-local correlation (such as in the PBE correlation functional) affects the binding and discussed how the importance of the higher-order terms. In

the next Chapter we will focus on how some of the functionals perform for more general and widely used test of solids.

Table 5.6: Errors in interaction energies in meV for several functionals shown for four dimers which appear in the S22 set two times in two different configurations. The dimers are: uracil dimer (dimers 5 and 13 in the S22), adenine-thymine dimer (7, 15), benzene dimer (11, 20), and indole-benzene (14, 21). The functionals are optB88-vdW, the vdW2 correlation with the exchange rrPW86 functional where one of the parameters was decreased to reproduce more the slowly varying electron gas limit compared to the parent rPW86 functional. Furthermore, two functionals with the VV09 [156] correlation and either HF or rPW86 exchange are used (data from Ref. [307]). The "(1) error" and "(2) error" columns show the error in the interaction energy with respect to the reference data for the first and second configuration, respectively. The difference between these two errors is shown as Δ and is basically the error in the energy difference between the two isomers. In the last column "ATM (vL-T)" we show the difference between the estimated three body term from Ref. [324] for the same isomers. This therefore gives an estimate of difference between the isomer energies that could be attributed to the three-body effects. Despite the scatter of the data, there is a correlation between the estimated ATM contribution and the errors of the various methods. This is true for all three model non-local correlation functionals and also holds when either HF or rPW86 exchange are used with the VV09 correlation. We show only two isomers for the other functionals for brevity.

Method	Dimer	(1) error	(2) error	Δ	ATM (vL-T)
optB88-vdW	(5, 13)	16	−33	49	45
	(7, 15)	4	−28	32	69
	(11, 20)	−24	0	−24	−17
	(14, 21)	−30	9	−39	−35
rrPW86-vdW2	(7, 15)	10	−3	13	69
	(11, 20)	−12	5	−17	−17
HF-VV09	(7, 15)	−19	−184	165	69
	(11, 20)	−39	−20	−19	−17
rPW86-VV09	(7, 15)	113	14	99	69
	(11, 20)	−5	30	−35	−17

Chapter 6

Van der Waals density functionals applied to solids

6.1 Introduction

In the previous chapter we discussed the results of various density functional theory (DFT) exchange-correlation functionals devised to describe the van der Waals (vdW) dispersion interactions. We focused on non-local correlation functionals and our test set included mostly molecular dimers, although we applied the methods to adsorption as well. As we have shown, the revPBE-vdW method as formulated by Dion *et al.* [16] leads to binding energies that are too low and we have studied how this can be improved by different modifications. Other alterations of the approach both in the exchange and correlation parts have been suggested [156, 147, 325, 154, 326]. With several functional forms proposed, it is important to test the methods on general reference test sets to uncover strengths and weaknesses and help further development. To this end we assess here the functionals using a test set of solid state properties of materials. Apart from method assessment, this is also important since many of the applications of vdW functionals lie outside of "soft matter", involving, for example, adsorbates on solid surfaces. Such calculations will require a good description of the solid structural parameters to accurately describe the systems of interest [327]. The PBE lattice constant is usually employed in studies using revPBE-vdW, however, as we show here, the PBE and revPBE-vdW lattice constants can differ by several percent.

There is at least one more reason to perform these tests: non-local correlations are thought to be important for solid state materials where the core electron densities have large polarisability. For example, copper and gold have been subject to several studies [328, 329, 330], with the non-local core-core correlation contribution to binding estimated to be 0.2–0.6 eV for Cu and 0.6–1.2 eV for Au. There are only a handful of studies concerning heavy alkali metals [331], but here too dispersion is important and has been shown to be key to the stabilisation of the bcc structure. More recently, the necessity of including non-local correlations in DFT semi-local functionals has been discussed [332] for the heavy alkalis.

In this chapter we test the performance of several vdW functionals using a standard test

of lattice constants, bulk moduli, and atomisation energies of solids. Our test is similar to the test of Csonka *et al.* [333] and includes metals, ionic, and covalent materials. We include the original revPBE-vdW, the recently proposed rPW86-vdW2 [315, 154], and three of the vdW functionals presented in Chapter 5, optPBE-vdW, optB88-vdW, and optB86b-vdW. We compare the results of the vdW functionals to the results obtained with the PBE [83] and PBEsol [313] generalised-gradient approximation functionals (GGA). By using a test set which does not involve weak hydrogen or dispersion bonds but rather strong interactions we hope to obtain an insight about the strengths and deficiencies of the vdW functionals that will hopefully lead to further developments.

The main results of the tests presented in this chapter are: the revPBE-vdW and rPW86-vdW2 largely overestimate the lattice constants for most of the materials and the average absolute error is more than twice that of the optB88-vdW and optB86b-vdW functionals. The optB88-vdW and optB86b-vdW functionals give errors between that of PBEsol and PBE. This is caused by the fact that the exchange enhancement factor (F_x) of the optB88-vdW and optB86b-vdW functionals is between the F_x of PBEsol and PBE for small reduced density gradients (s). The optB88-vdW and optB86b-vdW functionals also almost halve the errors of PBE in atomisation energies. The optPBE-vdW improves over revPBE-vdW but not as much as optB88-vdW does. This behaviour for the lattice constants is similar to that of binding curves and bond lengths, where in all three cases the functionals with rapidly growing enhancement factor give on average longer equilibrium distances.

This chapter is organised as follows: in the next section we discuss the details of the computational setup. The results are summarised in Sections 6.3, 6.4, 6.5 for lattice constants, bulk moduli, and atomisation energies, respectively. We study the differences between local, semi-local, and non-local correlation models in Section 6.6. And finally in Section 6.7 we discuss the implications of the results for further development of the vdW density functional (vdW-DF) methods.

6.2 Computational setup

We have used VASP [253, 178] with our implementation of the vdW correlation functional of Dion *et al.* [16] using the efficient algorithm of Román-Pérez and Soler [305] which is discussed briefly in Appendix C. Although our implementation involves some approximations, as we show in Appendix D the error in lattice constant is usually below 0.1%, slightly higher for materials with very small bulk moduli. Likewise, the error in atomisation energies is below 1% of the total atomisation energy. Such differences are much smaller than the intrinsic errors of the exchange-correlation functionals themselves and smaller or comparable to differences between different codes [93, 334, 333, 138] or potentials [335].

We employ a standard approach to calculate the solid properties. The energy is calculated for a set of lattice constant values and for each functional at least seven points around the lowest energy are used to fit the Murnaghan equation of state. The plane-wave basis set cut-off

is set to 750 eV or 900 eV for solids containing C and F. To reduce the errors, we have used the latest hard PAW potentials supplied with VASP [336] with the highest number of valence electrons. For semiconductors and ionic solids (metals) a 8×8×8 (16×16×16) Monkhorst-Pack k-point grid is used in the conventional unit cell. Our PBE lattice constants agree well with the VASP calculations of Paier *et al.* [93] as well as the all electron reference PBE and PBEsol values of Haas *et al.* [334]. The reference calculations for atoms were performed in a large $12 \times 14 \times 16$ Å^3 rectangular box; for spin polarised atoms we evaluate the E_c^{nl} term on the sum of the two spin-densities. We define the atomisation energy as the energy per atom required to infinitely separate the atoms of a given solid. The experimental reference values, corrected for zero point energy effects in the case of lattice constants and atomisation energies, are taken from Refs. [333] and [88]. The statistical values that we use to quantify the errors of the functionals are the mean error (ME) and the mean absolute error (MAE), as well as the relative versions of these quantities, namely mean relative error (MRE) and mean absolute relative error (MARE).

6.3 Lattice Constants

The lattice constants calculated with VASP are given in Table 6.1 and shown as relative errors in Figure 6.1. For comparison we also give the errors of LDA, PBE, and the PBEsol functional, one of the GGA functionals [337, 338, 312, 313] devised for solid-state calculations. We also include the results of the adiabatic-connection fluctuation-dissipation theorem (ACFDT) in the random phase approximation (RPA) approach taken from Ref. [138], which represents the state-of-the-art for solid state calculations. Before discussing the results in detail, let us just point out the most striking feature of the results: the errors are not random and clear periodic trends are observed. All methods shown tend to give larger lattice constants for the transition metals, ionic solids, and semiconductors while the alkali and alkali earth lattices are too short. This seems to correspond to the tendency of functionals to give larger lattice constants when going from left to right in the periodic table [334]. This behaviour does not seem to be improved by hybrid functionals [93] and is also present to some extent in the RPA lattice constants, although from the alkali and alkali earth metals only the data for Na has been published [138]. In fact, the functionals designed for solids don't lead to a qualitative improvement of the lattice constants. For example, the difference between the largest and the smallest relative errors is similar for LDA, AM05, PBEsol, or PBE [334].

Let us now discuss the results of the vdW functionals. The two vdW functionals proposed by the Langreth and Lundqvist groups (revPBE-vdW and rPW86-vdW2) tend to give larger lattice constants (ME = 0.105 Å for revPBE-vdW and ME = 0.088 Å for rPW86-vdW2). While revPBE-vdW overestimates all values, rPW86-vdW2, rather surprisingly, underestimates the lattice constants of the alkali and alkali earth metals. The errors are as large as 5.0% (6.8%) for revPBE-vdW (rPW86-vdW2) in the case of Ag and large for other transition metals included as well as for Ge and GaAs. The large errors are similar to the overestimation of the binding distance that has been observed before for many systems [16, 157, 339, 340]. As was

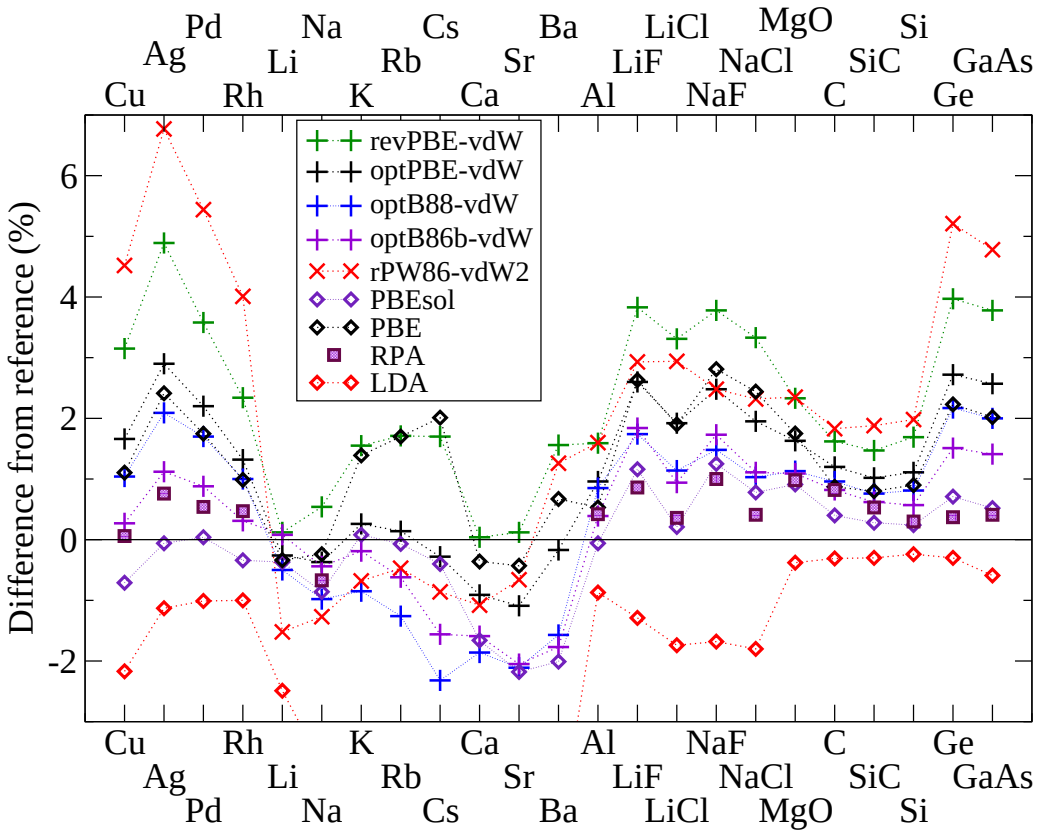

Figure 6.1: Comparison of the relative errors in the lattice constants calculated with different vdW functionals, LDA (from Ref. [333]), PBE, PBEsol, and recent data using the RPA [138]. All the methods overestimate the lattice constants for ionic solids and semiconductors and tend to give shorter lattices for alkali and alkali earth metals. As with the S22 set, both the revPBE-vdW and rPW86-vdW2 yield equilibrium distances that are too long in most of the cases. This is improved by the functionals with optimised exchange: optPBE-vdW, optB88-vdW, and optB86b-vdW.

discussed in the previous chapter, this can be related to the too steep behaviour of the exchange enhancement factor for small reduced density gradients. Although originally both revPBE and rPW86 exchange functionals were selected because they give similar binding to Hartree-Fock for some gas phase dimers, at short separations these functionals are too repulsive [315], which is important in hydrogen bonding and here, for lattice constants.

The repulsion is largely decreased by utilising an exchange functional that has less steeply rising F_x and thus is less repulsive for short interatomic separations, such as the optimised exchange functionals presented in Section 5.4.1.2. The optPBE-vdW is based on the PBE functional and it gives similar lattices to PBE for all the systems except for the alkali and alkali earth metals. For these metals, the vdW correlation term gives better agreement with the reference than the semi-local PBE correlation. The average errors are further reduced by using the optB88-vdW or optB86b-vdW functionals. However, for the alkalis the lattice constant

Table 6.1: Lattice constants in Å of different solids calculated using VASP for different vdW functionals and two GGA functionals: PBE and PBEsol calculated in this work using the same settings. In addition, we show the LDA values taken from Ref. [333]. The values are compared to the experimental values corrected for zero-point energy effects (indicated by "ZPEC") also taken from Ref. [333]. While both optPBE-vdW and optB88-vdW give mean absolute errors similar to those of PBE, the MAE of the optB86b-vdW functional is between those of PBE and PBEsol. The original revPBE-vdW gives lattice constants that are too large.

Exchange	revPBE	rPW86	optPBE	optB88	optB86b	LDA	PBEsol	PBE	Exp.
Correlation	vdW	vdW2	vdW	vdW	vdW	LDA	PBEsol	PBE	(ZPEC)
Cu	3.708	3.757	3.655	3.632	3.605	3.517	3.569	3.635	3.595
Ag	4.254	4.331	4.174	4.141	4.101	4.010	4.059	4.154	4.056
Pd	4.014	4.086	3.960	3.941	3.909	3.836	3.876	3.943	3.875
Rh	3.882	3.945	3.843	3.831	3.805	3.755	3.780	3.830	3.793
Li	3.453	3.396	3.440	3.432	3.452	3.363	3.436	3.437	3.449
Na	4.233	4.156	4.195	4.169	4.191	4.054	4.174	4.200	4.210
K	5.293	5.177	5.225	5.168	5.202	5.046	5.216	5.284	5.212
Rb	5.672	5.550	5.584	5.506	5.541	5.373	5.572	5.671	5.576
Cs	6.141	5.987	6.022	5.899	5.945	5.751	6.015	6.160	6.039
Ca	5.555	5.493	5.502	5.450	5.465	5.328	5.461	5.533	5.553
Sr	6.052	6.005	5.979	5.917	5.921	5.782	5.913	6.019	6.045
Ba	5.073	5.058	4.987	4.917	4.906	4.747	4.894	5.028	4.995
Al	4.084	4.084	4.058	4.054	4.036	3.985	4.018	4.041	4.020
LiF	4.116	4.080	4.067	4.033	4.037	3.913	4.010	4.068	3.964
LiCl	5.223	5.204	5.153	5.114	5.103	4.968	5.067	5.152	5.056
NaF	4.752	4.693	4.693	4.647	4.658	4.502	4.636	4.708	4.579
NaCl	5.750	5.694	5.673	5.622	5.627	5.465	5.609	5.701	5.565
MgO	4.281	4.282	4.252	4.231	4.230	4.168	4.222	4.257	4.184
C	3.600	3.608	3.585	3.577	3.572	3.532	3.557	3.574	3.543
SiC	4.406	4.424	4.386	4.375	4.369	4.329	4.354	4.377	4.342
Si	5.507	5.523	5.476	5.460	5.447	5.403	5.429	5.465	5.416
Ge	5.864	5.934	5.793	5.762	5.725	5.623	5.680	5.766	5.640
GaAs	5.851	5.908	5.783	5.751	5.717	5.605	5.667	5.752	5.638
ME (Å)	0.105	0.088	0.050	0.012	0.010	−0.100	−0.006	0.061	
MAE (Å)	0.105	0.116	0.064	0.066	0.049	0.100	0.033	0.067	
MRE (%)	2.3	2.0	1.1	0.4	0.3	−2.0	−0.1	1.3	
MARE (%)	2.3	2.6	1.4	1.4	1.0	2.0	0.7	1.4	

becomes too short and this worsens progressively as the ion size increases. This might be caused by overestimation of the dispersion energy in the vdW functional [147] or by the lack of higher order terms [324]. The optB88-vdW functional yields a mean error of 0.012 Å. The mean absolute error of 0.066 Å is comparable to the error of optPBE-vdW (MAE = 0.064 Å). The optB86b-vdW which, like PBEsol, follows the limit of slowly varying density for small s, further improves the agreement with the reference (MAE = 0.049 Å) and performs in between PBEsol (MAE = 0.033 Å) and PBE (MAE = 0.067 Å).

Although it might be surprising at first sight that functionals optimised on interaction energies of gas phase dimers give very good lattice constants, it just highlights the connection between the influence of the exchange part on lattice constants, molecular bonds, and intermolecular binding curves [341, 342]. In all these cases the small s behaviour is able to alter the properties, and by following the slowly varying electron gas limit all these three measures tend to be improved.

6.4 Bulk moduli

It is known that the behaviour of a given functional for bulk moduli is inversely related to errors in lattice constants. The shorter the predicted lattice constant, the higher the bulk modulus. The vdW functionals tend to follow this trend as can be seen from the data in Table 6.2 and the relative errors shown in Figure 6.2. The revPBE-vdW and rPW86-vdW2 functionals give too soft lattices, with the bulk moduli smaller by more than 30% for Ag, Pd, Ge, and GaAs. This correlates well with the overestimation of the lattice constant by more than 3% for these materials with revPBE-vdW and rPW86-vdW2.

There are several trends that one can observe, perhaps the most clear is the tendency of PBE and PBEsol to underestimate the bulk modulus with the increase of the ion size. This is most prominent for semiconductors, where it is clear that none of the vdW functionals alter this trend. On the other hand the RPA results don't suffer this deficiency. Importantly, this softening trend for alkali metals is improved by the vdW functionals. The reference values don't include zero point energy effects which would slightly increase the reference values (up to ∼3% in the case of Li [333]). Let us then conclude that here again the optimised vdW functionals improve upon the original methods and they follow the trend expected from the errors in the lattice constants. Specifically, the average absolute errors increase in order PBEsol < optB86b-vdW < optB88-vdW ≈ PBE ≈ optPBE-vdW < revPBE-vdW < rPW86-vdW.

6.5 Atomisation energies of solids

The calculated atomisation energies for our selection of solids are presented in Table 6.3, and the relative errors are shown in Figure 6.3. Again we include for comparison LDA, PBE, PBEsol, and RPA data in Figure 6.3. As can be seen the revPBE-vdW and rPW86-vdW2 functionals underestimate the atomisation energies with average relative errors of −11.0% and −15.9%, respectively. This underestimation is similar to the overestimation of LDA (MRE = 15.1%).

Table 6.2: Bulk moduli in GPa of the selected solids using different exchange correlation functionals with the LDA values taken from Ref. [333]. The experimental data are shown as well, these are not, however, corrected for zero point energy effects which would lead to a slight increase of the values (see Ref. [333]).

Exchange	revPBE	rPW86	optPBE	optB88	optB86b	LDA	PBEsol	PBE	Exp.
Correlation	vdW	vdW2	vdW	vdW	vdW	LDA	PBEsol	PBE	
Cu	111	97	129	138	149	190	165	139	142
Ag	67	61	85	95	104	139	116	89	109
Pd	137	119	161	172	187	227	203	168	195
Rh	221	193	248	258	276	320	295	256	269
Li	13.7	14.7	13.9	13.8	13.4	15.2	13.6	13.9	13.3
Na	7.39	7.96	7.73	7.81	7.65	9.50	7.86	7.71	7.5
K	3.58	3.97	3.80	3.95	3.79	4.60	3.71	3.56	3.7
Rb	2.82	3.14	3.02	3.21	3.05	3.54	2.93	2.79	2.9
Cs	2.07	2.28	2.04	2.30	2.01	2.58	2.00	1.98	2.1
Ca	16.4	17.7	16.9	17.6	17.3	19.1	17.4	17.2	18.4
Sr	11.4	12.5	12.3	13.2	13.0	14.8	12.9	11.5	12.4
Ba	9.04	9.77	9.59	9.92	9.64	10.9	9.33	8.95	9.3
Al	66.5	60.1	71.9	70.6	77.0	83.8	82.1	78.6	79.4
LiF	63.4	68.9	68.2	71.7	70.2	86.5	72.6	66.9	69.8
LiCl	30.3	32.3	32.9	34.5	34.3	40.8	35.0	31.6	35.4
NaF	43.6	48.8	46.9	49.4	47.5	61.2	48.0	44.6	51.4
NaCl	23.6	26.0	25.7	27.0	26.2	32.4	25.8	22.8	26.6
MgO	148	148	153	157	156	172	159	148	165
C	404	395	418	424	431	467	446	429	443
SiC	200	191	208	212	215	225	221	212	225
Si	82.8	79.6	86.9	88.7	91.2	96.8	93.8	88.3	99.2
Ge	48.7	42.8	54.7	57.3	61.5	72.6	67.0	58.6	75.8
GaAs	51.4	47.1	57.3	60.2	63.6	74.2	68.9	60.2	75.6
ME (GPa)	−15.9	−19.5	−9.4	−6.2	−3.2	10.3	1.6	−7.4	
MAE (GPa)	15.9	19.8	9.5	6.7	4.5	10.9	4.8	7.4	
MRE (%)	−13.8	−12.2	−7.2	−3.1	−2.7	14.5	0.2	−7.8	
MARE (%)	14.0	16.2	8.8	7.6	5.1	15.3	4.8	8.4	

The optimised optPBE-vdW, optB88-vdW, and optB86b-vdW functionals give much improved results with the average relative errors of −3.0%, −1.3%, and 2.1%, respectively. In most cases the optimised functionals tend to give larger atomisation energies and increase in the order optPBE-vdW, optB88-vdW, and optB86b-vdW. Only in the case of the alkali metals does

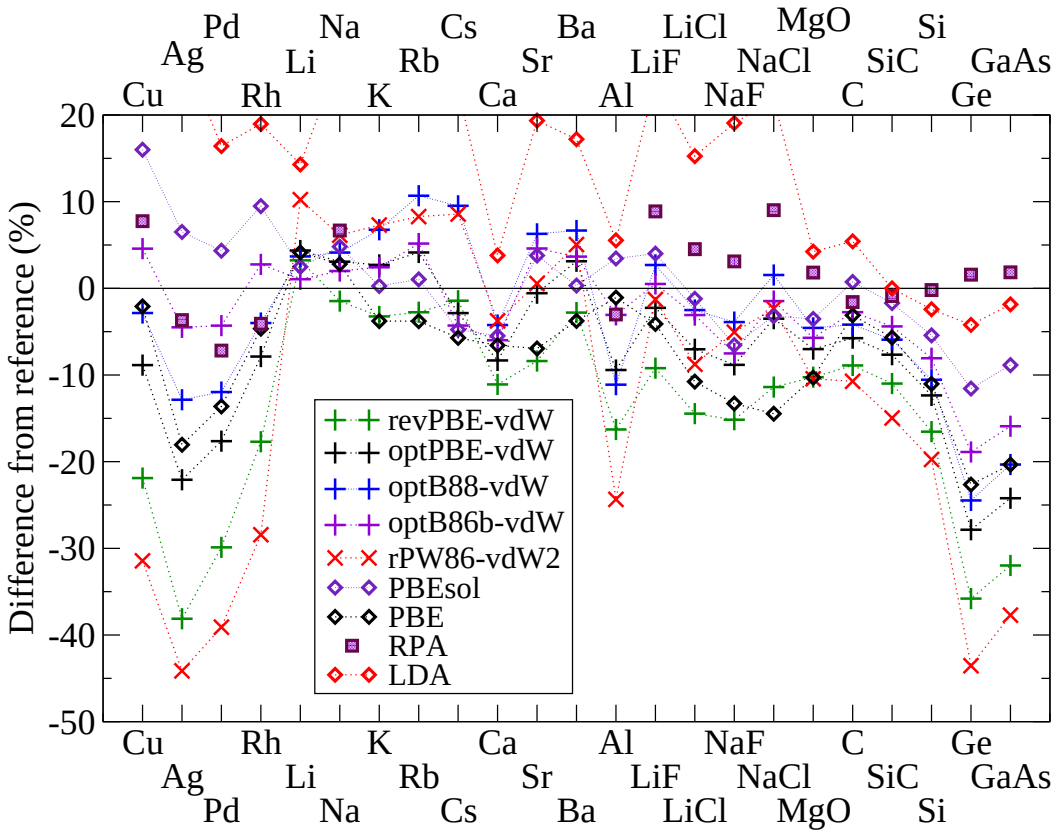

Figure 6.2: Relative errors in the bulk moduli for the methods considered in this study. The original revPBE-vdW and rPW86-vdW2 methods underestimate the moduli by up to 45% and the optimised vdW functionals reduce the errors.

optB88-vdW give less binding than optPBE-vdW which for these materials agrees well with the reference values.

Interestingly, when one compares the semi-local and non-local correlation, there seems to be some systematic improvement as well, most notably for the alkali metals. While the PBE atomisation energies get progressively worse with the increase of the ion size, all the vdW functionals give errors of a similar magnitude. While one can observe a similar trend for PBE atomisation energies of semiconductors, which is decreased by the optimised vdW functionals, PBEsol seems to improve over PBE as well. The atomisation energies of the alkali halides calculated using the optimised vdW functionals are also in better agreement with the reference data than either PBE or PBEsol. The effect of different correlation functionals will be discussed more in the next section.

6.6 The effect of non-local correlation

Although we know that the vdW-DF correlation form is only approximate, it is interesting to see what changes occur when semi-local correlation such as PBEc is replaced by the non-local form of vdW. To study this change we have calculated the lattice constants using the PBE exchange functional and LDA, PBE, and vdW correlation functionals. This way we can directly

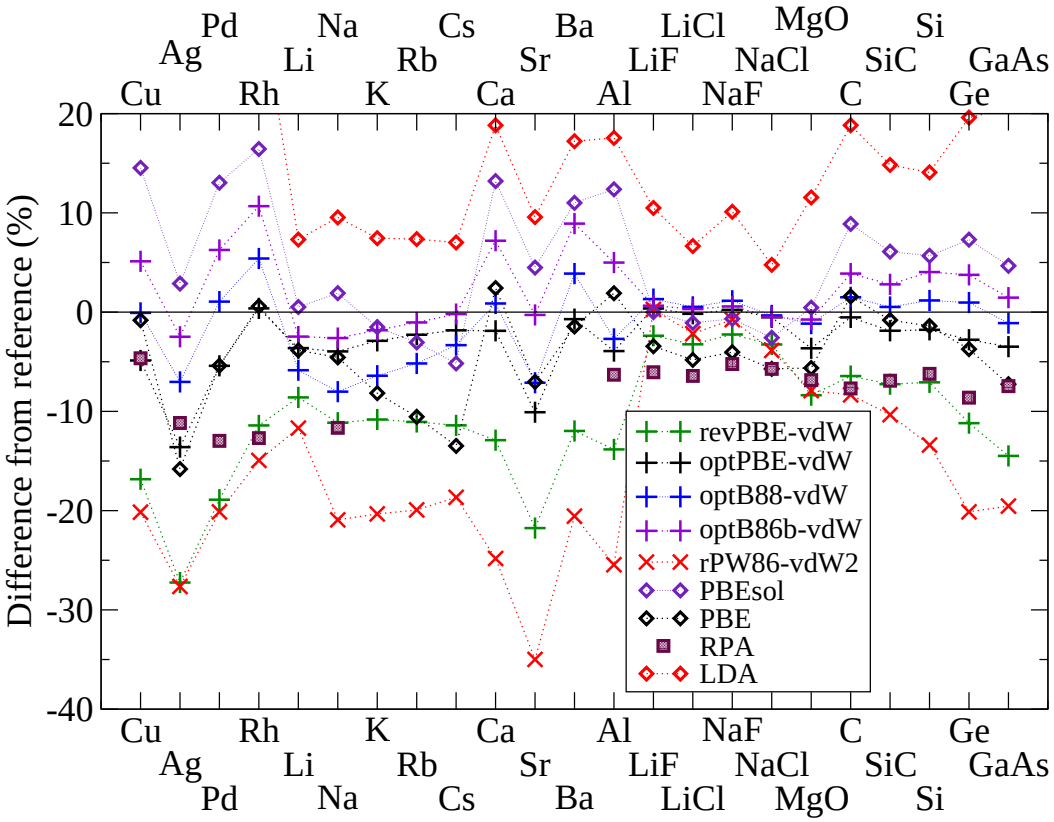

Figure 6.3: Relative errors in atomisation energies calculated using different DFT approaches. Data for LDA, semi-local PBE and PBEsol, various flavours of vdW functionals and the fifth-rung RPA method are shown. The ZPE was subtracted from the experimental data. The optB88-vdW and optB86b-vdW tend to give values between those of PBE and PBEsol for transition metals and semiconductors, in agreement with the behaviour of their exchange enhancement factor. However, they agree better with the reference for alkali halides, where even PBEsol underbinds. Moreover, they give consistent errors for alkali metals where both PBE and PBEsol increasingly underbind with the increasing size of the ion.

compare the effect of adding PBE semi-local or vdW non-local functionals. Let us first present the results for the lattice constants in Figure 6.4. At first sight, the PBEx-PBEc and PBEx-vdWc give rather similar results, consistently decreasing the PBEx-LDAc lattice constant[1]. This means that it is mostly the exchange functional that determines the lattice constant. As we noted before, there is a clear difference for the alkali metals, where the PBEx-PBEc gives progressively worse lattice constants. This is even more pronounced for the atomisation energies, shown in Figure 6.5, where PBEx-PBEc underbinding starts at only -3% for Li but worsens to $\sim -15\%$ for Cs. This trend is clearly reversed by the vdW correlation, although too much. Let us remind the reader that this tendency to underbind larger ions is analogous to the behaviour of semi-local functionals for noble-gas dimers in the gas phase [343]. The interaction energy is

[1] Although LDA is known to give shorter lattice constants, this is because of the exchange part, LDA correlation is underbinding.

Table 6.3: Atomisation energies in eV for various solids calculated using VASP for different exchange-correlation functionals. We show the data of the revPBE-vdW and rPW86-vdW2 functionals, the optimised vdW functionals, and results of LDA, PBEsol, and PBE. The values are compared to the experimental values corrected for zero-point energy effects taken from Ref. [333]. All three optimised functionals give better results than either PBE or PBEsol. The LDA values were taken from Ref. [138] for semiconductors, ionic solids, transition metals, and Al. The atomisation energies of alkali and alkali earth metals were taken from Ref. [88].

Exchange	revPBE	rPW86	optPBE	optB88	optB86b	LDA	PBEsol	PBE	Exp.
Correlation	vdW	vdW2	vdW	vdW	vdW	LDA	PBEsol	PBE	(ZPEC)
Cu	2.93	2.81	3.35	3.52	3.70	4.55	4.04	3.49	3.52
Ag	2.16	2.15	2.57	2.76	2.90	3.64	3.06	2.50	2.97
Pd	3.18	3.13	3.71	3.96	4.16	5.08	4.43	3.71	3.92
Rh	5.12	4.92	5.81	6.10	6.40	7.67	6.73	5.82	5.78
Li	1.52	1.47	1.61	1.57	1.63	1.79	1.68	1.60	1.67
Na	1.01	0.90	1.09	1.04	1.10	1.24	1.15	1.08	1.13
K	0.84	0.75	0.91	0.88	0.92	1.01	0.93	0.86	0.94
Rb	0.76	0.69	0.84	0.81	0.85	0.92	0.83	0.77	0.86
Cs	0.72	0.66	0.80	0.79	0.81	0.87	0.77	0.70	0.81
Ca	1.62	1.40	1.82	1.88	1.99	2.21	2.11	1.90	1.86
Sr	1.36	1.13	1.56	1.61	1.73	1.90	1.81	1.61	1.73
Ba	1.68	1.52	1.90	1.99	2.08	2.24	2.12	1.88	1.91
Al	2.96	2.56	3.30	3.34	3.61	4.04	3.86	3.50	3.44
LiF	4.36	4.48	4.49	4.53	4.50	4.94	4.47	4.32	4.47
LiCl	3.47	3.51	3.58	3.61	3.60	3.83	3.55	3.42	3.59
NaF	3.89	3.95	4.00	4.02	4.00	4.38	3.95	3.82	3.98
NaCl	3.23	3.21	3.32	3.33	3.32	3.50	3.25	3.15	3.34
MgO	4.83	4.85	5.08	5.21	5.23	5.88	5.29	4.97	5.27
C	7.09	6.95	7.54	7.70	7.88	9.01	8.26	7.70	7.58
SiC	6.02	5.82	6.37	6.52	6.67	7.45	6.88	6.44	6.49
Si	4.35	4.05	4.60	4.74	4.87	5.34	4.95	4.62	4.68
Ge	3.43	3.09	3.76	3.90	4.01	4.62	4.15	3.72	3.86
GaAs	2.90	2.73	3.27	3.36	3.44	4.09	3.55	3.15	3.39
ME (eV)	−0.34	−0.46	−0.08	0.00	0.10	0.56	0.20	−0.11	
MAE (eV)	0.34	0.46	0.09	0.07	0.12	0.56	0.22	0.13	
MRE (%)	−11.0	−15.9	−3.0	−1.3	2.1	15.1	4.8	−4.4	
MARE (%)	11.0	16.0	3.1	2.9	3.2	15.1	6.0	5.0	

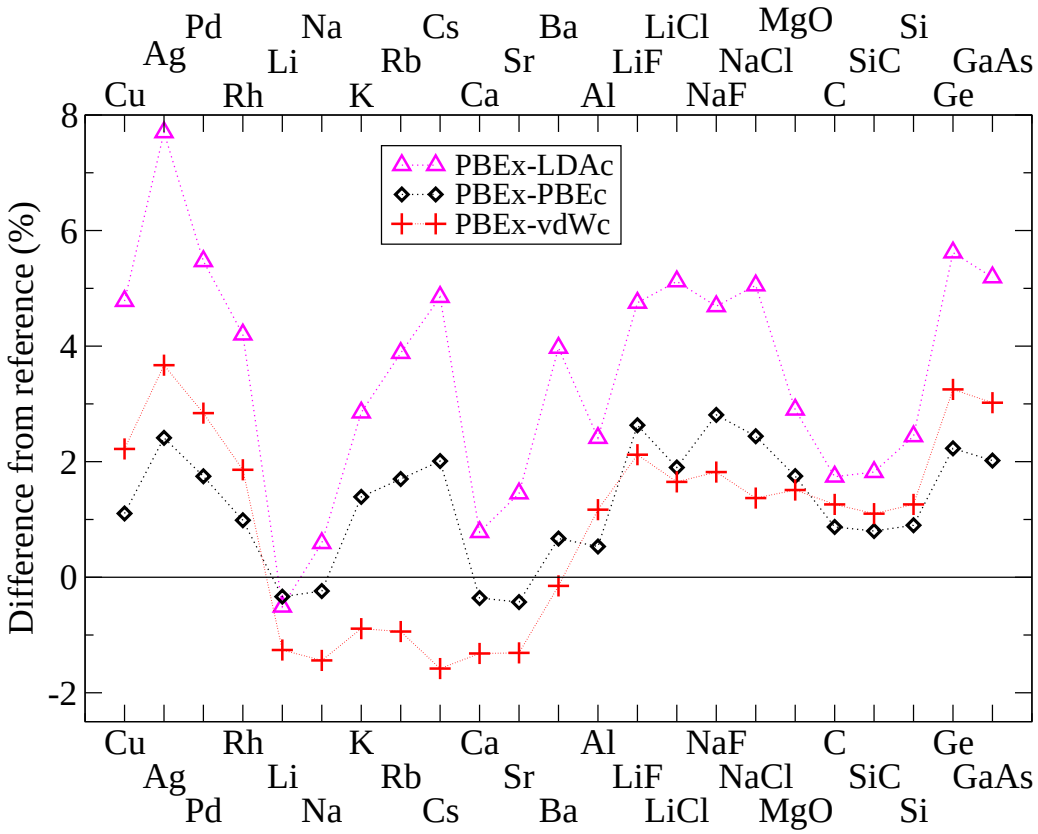

Figure 6.4: Comparison of the relative errors in the lattice constants for the PBE exchange functional with LDA, PBE, and vdW correlation functionals.

obtained only from the region of electron density overlap and therefore does not scale in the same way as the size of the ion.

Careful observation reveals that the differences between PBE and vdW correlations are qualitatively similar for transition metals and semiconductors. With the vdW correlation the lattice constants are larger by ∼1% (except for the smaller semiconductors, where the difference is less) while the atomisation energies have a smaller range of errors. It has been shown [137, 138] using RPA that out of the Rh, Pd, Ag group, electron correlation beyond Hartree-Fock-like exchange is the most important for Ag. With this in mind, it is satisfactory to see the decreased range of errors in atomisation energies for this group, although the trend is not cured completely. Note that the trend in lattice constants is not improved and it would be actually worsened by using a hybrid functional [93]. Thus the semi-local PBE or non-local vdW correlation with semi-local or hybrid exchange seems to be unable to describe the delicate balance of the interactions in the late transition metals. For the semiconductors the vdW correlation clearly lacks the same amount of semi-local attraction as the PBE correlation. However, the PBE worsens the atomisation energies for solids with larger atoms whereas the vdW correlation improves this trend.

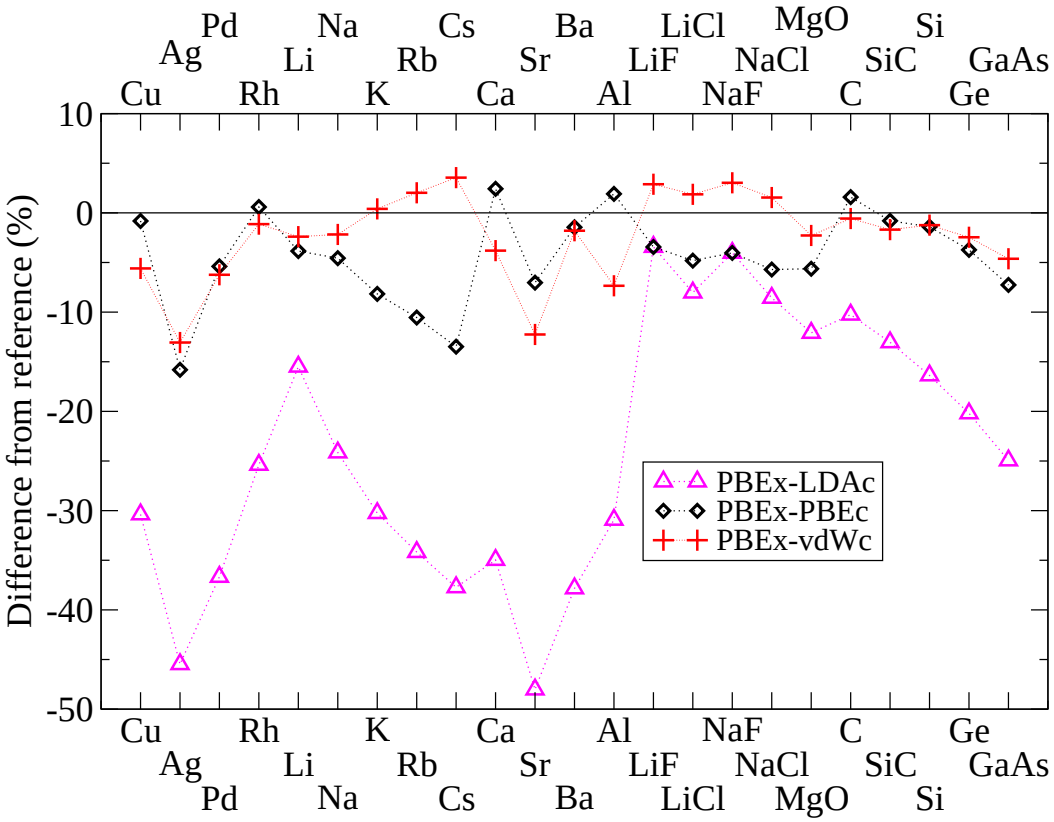

Figure 6.5: Relative errors in the atomisation energies for the PBE exchange functional combined with LDA, PBE, and vdW correlation functionals.

6.7 Discussion and Conclusions

We summarise the results in Table 6.4 and start the discussion by stating that the two functionals from Langreth and Lundqvist and co-workers, revPBE-vdW and rPW86-vdW2 lead to a large overestimation of lattice constants and underestimations of bulk moduli and atomisation energies for most of the solids considered. Moreover, the errors have a wide range, *e.g.*, rPW86-vdW2 underestimates the lattice constant of Li by 1.5% but overestimates value for Ag by 6.7%. The atomisation energies are underestimated by more than 0.3 eV on average. The optimised exchange functionals (optPBE-vdW, optB88-vdW, and optB86b-vdW) improve dramatically over the revPBE-vdW and give lattice constants that are similar to those of PBE. This leads to similar improvements for the bulk moduli. From our study it seems that the vdW correlation functional does not improve dramatically over PBE except for the lattice constants of the alkali metals. Importantly, the atomisation energies seem to be qualitatively improved when a non-local correlation functional is used. This is most notable for the alkali metals, where PBE and PBEsol increasingly underbind with the increasing size of the ion but the vdW functionals suffer no such deficiency. Moreover, the atomisation energies of ionic solids are in very good agreement with the experimental values.

Let us now discuss the results obtained here and in the previous chapter in a broader

Table 6.4: Summary of the results.

	PBE	vdW-DF, vdW-DF2	Optimised exchange
Lattice constants		Worse than PBE	Similar to or better than PBE
MARE	1.4%	2.3% (vdW-DF)	1.4% (optB88-vdW)
Atomisation energies		Worse than PBE	Better than PBE
MARE	5.0%	11.0% (vdW-DF)	2.9% (optB88-vdW)

Table 6.5: The results of the AE6 test of molecular atomisation energies for the functionals considered in this study. The geometries were not optimised which would not affect the results significantly. Negative values mean that the atomisation energy is overestimated relative to the reference [344]. The average atomisation energy of the molecules in AE6 is ~ -500 kcal/mol.

	ME (kcal/mol)	MAE (kcal/mol)
LDA	-77.4	77.4
PBEsol	-34.0	34.0
optB86b-vdW	-24.7	24.7
optB88-vdW	-20.1	20.1
optPBE-vdW	-14.9	14.9
PBE	-11.3	14.3
revPBE-vdW	0.4	4.2

context. First, after the local and semi-local approximations the non-local density functionals are the next logical step before the orbitals are introduced in the exchange-correlation energy such as it is done in the RPA or hybrids. In this sense the non-local correlation functionals offer great promise. However, both revPBE-vdW and rPW86-vdW2 suffer from a too strong repulsion for short distances, a well known feature of revPBE-vdW for systems like the gas phase dimers [16, 157, 154]. In this chapter we have shown that lattice constants of solids are subject to the same errors and overestimations. This is a significant problem since accurate lattice constants are crucial for the predictive power of theory [327]. One possible way to alleviate the problems is to change the exchange functional. In Chapter 5 we have shown that functionals with less steeply rising exchange enhancement factors for small s will improve results on the S22 set and, in this chapter, we have shown similar improvements for the lattice constants of solids. It is known that the solid state functionals decrease the quality of atomisation energies. The optimised exchange functionals also lead to larger errors, for example on the AE6 set [344] (see Table 6.5). However, the worst performer on this test, the optB86b-vdW, gives still much better errors than PBEsol and the MAE of the best performer, optPBE-vdW, is similar to that of PBE.

More profoundly, the question what form of exchange and correlation should be used is still to be resolved. In principle one can try to find an exchange functional compatible with

"dispersionless" interaction energies [345]. Another approach might be to fit a functional to interaction energies based on the so called exact exchange (EXX) or Hartree-Fock-like exchange in the ACFDT formalism. This would allow the correlation part to be compared directly to the ACFDT correlation energy (*e.g.*, in the RPA approximation). However, as we have discussed in the last chapter, this might not be qualitatively that different from trying to reproduce HF binding curves and atomisation energies. Moreover, the EXX energy depends on the single particle orbitals and the correlation part will be just $E_c^{EXX} = E(\text{exact}) - E(\text{EXX})$. Therefore no "exact" correlation energy can be defined in this sense. Even defining E_c^{EXX} using some choice of orbitals will mean that this needs to be reproduced by a given DFT functional which seems to be rather difficult. So far, even the form of semi-local correlation that should be used is a matter of an ongoing debate [16, 346, 316, 315, 292, 325, 154]. This includes the problem of how much of the semi-local correlation energy does the vdW correlation functional recover which we discussed previously. In this light, there is a need for reference systems to help the development, similar to GGA functionals where lattice constants, atomisation energies, bond lengths, and other data have been extremely useful. The doubts and discussions concerning the vdW functionals just highlight the need for accurate reference data for gas phase clusters, adsorbates, solids, and so on. The approach of using quantum chemistry methods for solid state [347, 244, 348, 349] is one that seems very useful and deserves more attention.

To conclude, we have calculated solid state properties of a set of solids using a self-consistent implementation of the vdW-DF method in the VASP code. The lattice constants of solids are, similar to gas phase dimers, too large with the original revPBE-vdW and rPW-vdW2 methods but are improved when optimised exchange functionals are used. The atomisation energies of solids are considerably improved by the use of optimised functionals. The presented results provide some clear reference data as to how the vdW-DF functional and its offspring perform and should be useful in the further development of the method.

Chapter 7

Conclusions and Outlook

In this thesis we have used the density functional theory (DFT) formulation of quantum mechanics both as a method to obtain molecular level information about processes at the nanoscale and as a theory that in practice requires continued refinements in terms of accuracy.

First, we have presented the results of our studies of methods that search for transition states in chemical reactions at surfaces in Chapter 3. For probably the most widely used method, the nudged elastic band (NEB), we found quite surprising results. The calculations showed that less is sometimes more, that is, using the NEB method with a large number of replicas (images) of the system actually decreases the performance, *i.e.*, the number of steps required per replica increases. Moreover, by combining ideas from several of the methods studied, we were able to propose a new method called CI-DHS+GS (this is an abbreviation for "climbing image-Dewar-Healy-Stewart+growing string"). There are several appealing features of this algorithm that make it competitive with other methods. For example, this algorithm, unlike the original DHS method, converges to the transition state. Moreover, in contrast to the NEB method, it does not require an initial guess for the reaction pathway but only information about the initial and final states. This is important as such an initial guess can be problematic to obtain for some processes. Indeed, our new CI-DHS+GS method was found to be superior to the NEB for a complicated water diffusion process on the NaCl(001) surface. Of course in the future it would be interesting to test this method out on a wider variety of problems to really see what potential it has to become a useful and widely used algorithm in surface physics.

As we have demonstrated, current DFT functionals and programmes that harness the power of supercomputers are very useful and can be used to explain basic natural processes at the molecular level. Specifically, in Chapter 4 we studied the initial stages of salt dissolution in water and discovered a rather surprising driving force for this process. The release of ions is caused by the strong interaction of water molecules with the Na ions. However, this does not lead to a preferential release of the Na ions; the Cl ions are released instead. This is because displacing a Cl ion exposes a vacancy with several Na ions which is a favourable adsorption site for water molecules. The next logical step in this study would be to perform molecular dynamics simulations to include temperature effects.

The current state of DFT on the one hand enables large scale studies leading to explanation or increased understanding of natural or industrial processes, as we have shown for salt dissolution. This is due to several factors such as favourable scaling of the method, which allows rather large systems to be tackled. On the other hand we have shown in Chapter 5 that there is a large class of systems where the current exchange-correlation functionals simply fail. This is quite disturbing since this includes many systems that will be important to secure future energy requirements, for example materials for gas storage or separation. The inaccuracy is caused mainly by the lack of describing the physics of non-local electron correlations, which are challenging to describe for basically any electronic structure method. Within DFT, there are methods based on the adiabatic-connection fluctuation-dissipation theorem (ACFDT) which are able to describe dispersion. Although the ACFDT based methods represent a good step towards accurate methods for reference calculations, they are very expensive and will remain too expensive to be used on a daily basis for some time. Therefore it is very useful to study simpler methods, such as the non-local correlation density functionals discussed in Chapter 5. We have tested the original vdW-DF scheme of Dion *et al.* [16] and found that although it improves the interaction energies for dispersion bonded systems, it fails to improve over current standard functionals for systems bound by hydrogen bonds. This is a problem since any DFT functional should be as general as possible so that its use is not restricted to a specific class of systems. We have proposed some new functionals that vastly improve the accuracy compared to the original method, and especially make the method equally accurate for hydrogen and dispersion bonded systems. We also devoted part of Chapter 5 to discussion of the weak points of the non-local correlation functional currently proposed. It needs to be said that compared to the local and semi-local functionals, the non-local correlation functionals add some real physics and thus are a step in a good direction.

Several times throughout this thesis we have noted that there are many exchange-correlation functionals and it is difficult to say which one is "better" based on theoretical reasoning. In this sense it is important to test the proposed functionals on a wide range of available reference systems. Although this might sound empirical, the functionals are designed with the goal that they will be used. Therefore it is useful to know their performance for a wide range of systems and identify their strong and weak points. The algorithmic improvements of the vdW correlation energy evaluation and our self-consistent implementation thereof in the VASP code mean that the vdW functionals can be now tested on a range of systems. We have performed one of the standard tests in Chapter 6 where we applied the vdW functionals to solids. We have found that, rather surprisingly, the results for solids can be related to the results for gas phase dimers. The exchange functional in the generalised-gradient approximation (GGA) basically determines the binding distances in the gas phase, the lengths of molecular bonds, and the equilibrium distances in solid materials. We are currently investigating whether this holds for functionals beyond GGA. Moreover, we have also shown that calculations of some of the

properties still need to be improved, and ways to do this are currently being studied. However, for several systems the improvements made are sufficient to obtain much better agreement with experimental observations, see for example Ref. [319], and other exciting applications are underway. Overall, developments in methods, algorithms, and hardware all looks promising for the future of electronic structure calculations based on DFT and we hope that the developments made in this thesis will help in devising methods for the accurate description of large systems.

Appendix A

Test of the Na^+ H_2O dimer

The binding energy of a water molecule to the NaCl(001) surface as obtained with the PBE functional is too weak. To test if similar error is obtained when water interacts with a single ion we have calculated the binding energies of the Na^+ H_2O dimer using accurate quantum chemistry methods and the PBE and PBE0 functionals. For this system experimental data and previous calculations are available (see, *e.g.*, Refs. [350, 351, 352]) but we decided to obtain our own reference to allow a direct comparison between the methods.

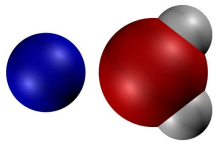

Figure A.1: The structure of the Na^+ H_2O dimer.

In the most stable geometry of the dimer the water molecule points to the sodium ion, the structure is shown in Figure A.1. We used the NWChem 6.0 programme and optimised the structure using MP2 and aug-cc-pVTZ basis set with Na and O 1*s* orbitals frozen. In this geometry we have calculated the interaction energy using HF, MP2, CCSD(T), PBE, and PBE0 and aug-cc-pCVXZ basis sets, where X = D, T, Q. For CCSD(T) X = D, T only. By comparing the interaction energies obtained by MP2 and CCSD(T), shown in Table A.1, one finds that they give almost identical results, to within a meV for aug-cc-pCVDZ and 4 meV for aug-cc-pCVTZ. Therefore the MP2 method gives an accurate estimate of the binding energy and can be used instead of the more expensive CCSD(T). Moreover, the differences between MP2 and the DFT functionals PBE and PBE0 are rather small, indeed PBE interaction energy is within 5 meV of the MP2 for all the basis sets employed. PBE0 tends to give binding energy which is about 30 meV lower than PBE but still in an excellent agreement with the reference. Therefore one can conclude that PBE describes the interaction between a single Na^+ ion and a

Table A.1: Comparison of the interaction energies obtained by different methods for the Na^+ H_2O dimer. PBE gives interaction energies which are within 5 meV of the MP2 reference. All data in eV.

	MP2	CCSD(T)	PBE	PBE0
aug-cc-pCVDZ	−0.996	−0.996	−1.001	−1.032
aug-cc-pCVTZ	−1.016	−1.020	−1.021	−1.049
aug-cc-pCVQZ	−1.031	–	−1.027	−1.054

single water molecule well.

The good agreement of PBE with the reference data for a single water molecule could worsen when more water molecules are added. However, PBE gives rather accurate binding energies of water clusters [300, 114] and thus adding more water molecules should not deteriorate the agreement significantly. For the larger clusters, dispersion needs to be included to recover the trends in relative energies of isomers [114] and dispersion can be expected to also become more important when the water molecule is adsorbed and the electrostatic interactions weaken.

Finally, we calculated the interaction energy for two of the vdW-DF functionals, revPBE-vdW and optB86b-vdW. We used VASP, the same geometry as previously, a 13 Åcubic box and 400 eV plane-wave cut-off. With this set-up PBE gives interaction energy of −1.045 eV which is in a good agreement with the interaction energy obtained with NWChem. The small difference can come from incompleteness of the Gaussian-type basis set in NWChem, periodic boundary conditions or the use of PAW potentials in VASP. The optB86b-vdW gives interaction energy of −1.032 eV, only slightly smaller than the PBE and reference values. The revPBE-vdW functional is generally too repulsive and we find that also here it reduces the binding giving interaction energy of −1.009 eV. Nevertheless, this still agrees quite well with the reference data and is not surprising since the largest contribution to the binding comes from electrostatics. It is worth mentioning that the vdW functionals could become more accurate for interaction of water with larger alkali metal ion. Indeed Glendening and Feller [352] found that altough Hartree-Fock (HF) and MP2 give similar binding energies for Li or Na ions, HF gives too weak binding for Rb and Cs. A potential explanation is the growing importance of dispersion which is not accounted for by HF and would not be accounted for by PBE.

Appendix B

Tests of forcefields for the water-NaCl system

Here we present the results of tests of different forcefield (FF) parametrisations upon which we selected the AMBER and TIP4P parameters to model the water-NaCl interactions. We have tested the properties of NaCl solid, water monomer adsorbed on NaCl surface and energies and geometries of small water clusters. Since in Chapter 4 the FFs are primarily used to generate plausible adsorption structures that are reoptimised by DFT-PBE, we compare to both accurate reference (where available) or experimental data as well as to PBE values. The comparison with PBE is important since we want to use the PBE lattice constant in the FF-MD part and here a system close to optimum is needed to avoid artifacts.

Several properties of NaCl solid calculated with FF parametrisations available in GROMACS [353] are listed in Table B.1. It can be seen that AMBER [275] and OPLS-AA [354] give similar results as well as ENCAD [355] and GROMOS [356] lead to similar lattice constants, bulk moduli, or surface energies. Since the ENCAD and GROMOS lattice constants differ by $\sim$3% from the PBE value, they don't seem to be suitable for our purposes. The AMBER parameters lead to lattice constant which is in best agreement with the PBE one and this is the main reason to select this parametrisation for the FF-MD simulations. However, as is shown in the last line of Table B.1, the vacancy formation energy is overestimated by a large amount. Although the GROMOS parameters agree better, they, however, give adsorption energy of water monomer on the surface which is too large.

One of the reasons that the vacancy formation energy is overestimated seems to be the non-polarisability of the FFs. Therefore, we tested several polarisable NaCl models that can be implemented in GROMACS, *i.e.*, they use the charge-on-spring polarisability model [186]. As is shown in Table B.2, the parametrisations due to Lamoureux *et al.* [278] and Binks [277] agree well with the experimental lattice constant and also give vacancy formation energies in the correct range. The last line in Table B.2 shows the rumpling of the surface: the distance between the Cl and Na atomic planes in the surface layer. This clearly shows that the parameters of Lamoureux *et al.* give too large rumpling. Moreover, this FF suggests that it is easier to remove

Table B.1: Several properties of NaCl solid calculated with FF parametrisations available in GROMACS and compared to PBE and experimental data. The lattice constant, bulk modulus, and surface energy are compared to PBE and experimental values. We also show the adsorption energy of TIP4P water model and compare it to the PBE value and an estimated reference. The last line gives the vacancy formation energies of Cl and NaCl vacancies.

	AMBER	ENCAD	GROMOS	OPLS-AA	PBE	Expt./Theo.
a_0 (Å)	5.75	5.54	5.52	5.77	5.70	5.63
B (GPa)	36	47	47	36	24	27
E_{surf} (meV/Å^2)	13	18	17	13	9	15–20
E_{ads} (eV)	0.41	0.50	0.60	0.43	0.39	0.52 ± 0.06
$E_{\text{vac}}^{\text{NaCl}}$ (eV)	3.4	3.3	2.3	3.4	2.2	–

Table B.2: Several properties of NaCl solid calculated with polarisable FF parametrisations implemented in GROMACS and compared to AMBER, PBE, and experiment.

	AMBER	Lamoureux	Binks	PBE	Expt.
a_0 (Å)	5.75	5.62	5.64	5.70	5.63
B (GPa)	36	40	22	24	27
$E_{\text{vac}}^{\text{Cl}}$ (eV)	3.1	2.4	1.9	2.0	–
$E_{\text{vac}}^{\text{NaCl}}$ (eV)	3.4	2.0	2.2	2.2	–
$\Delta_{1(\text{Cl}-\text{Na})}$ (Å)	0.05	0.44	0.08	0.11	0.14

an ion pair from the surface than a single Cl ion. This disagrees with DFT calculations using PBE or LDA approximations. Overall, the Binks parametrisation seems to offer the best results.

Let us now shortly discuss the tests of different water models on small water clusters. Such test represents a challenge for typical FF water models since they are usually fitted to reproduce bulk properties of liquid water. Thus they include polarisation and quantum nuclear effects implicitly. Polarisable water models should give better results since the isolated monomer is usually fitted to reproduce the dipole of a water molecule. In Figure B.1 we show the cluster formation energies from water dimer to the most stable hexamer. (The total binding energy is divided by the number of hydrogen bonds (HBs) or number of water molecules, these two differ only for the hexamer and dimer.) We have tested the TIP4P model as well as polarisable SW [197], SWM-NDP [280], and SWM-DP [279] parametrisations. We use MP2 values taken from Refs. [300, 114] as a reference and show the PBE values for comparison. It can be seen that all the FFs give stronger binding in dimer compared to trimer, this can be correlated with the too short HB distance predicted for dimer (see Figure B.2). For the larger clusters (three and more waters) the SWM polarisable models give similar energy gains to the MP2 reference. The SW model fails dramatically for the average hydrogen bond lengths, shown in Figure B.2, as well as the binding energies of the water hexamer isomers shown in Figure B.3. The TIP4P

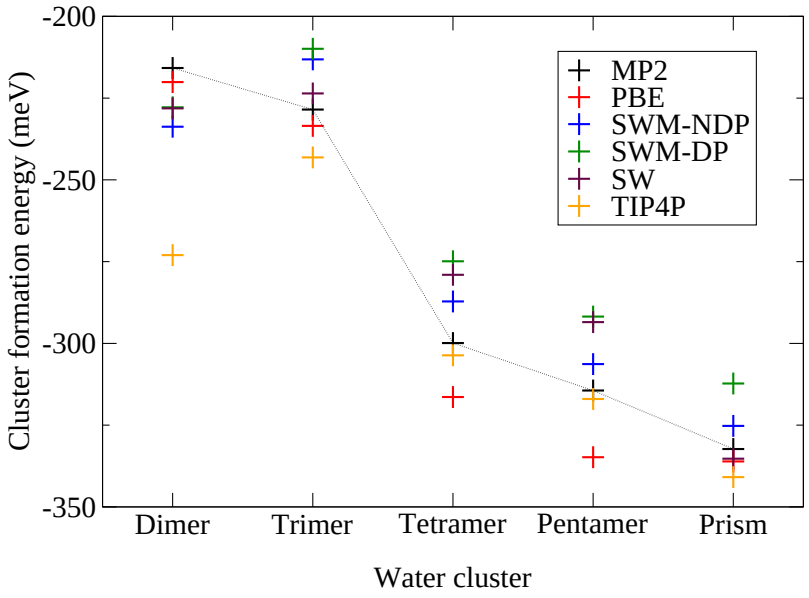

Figure B.1: Cluster formation energy in meV per water molecule or the total formation energy in the case of water dimer. Several methods are compared, non-polarisable TIP4P, polarisable SW, SWM-NDP, and SWM-DP models, DFT-PBE. The MP2 reference energies are shown as well.

model that we have used in the study agrees well with the MP2 reference, that is, except for the dimer, the binding energies are within 20 meV of the reference. The non-polarisability of the model seems to lead to deviations in the average HB lengths, where the HBs for the "cyclic" isomer are too long and HBs for "prism" are too short.

Overall, it seems that, from the models tested, the Binks and SWM-NDP parametrisations are the most suitable to model NaCl and water. However, there are no parameters available to couple the parametrisations together. This would have to be developed which is far beyond the scope of this study. Therefore, we used the AMBER/TIP4P to run the FF simulations.

Let us now briefly mention the effect of the selection of DFT exchange-correlation functional. Specifically we discuss the effect of including the non-local correlation using the vdW-DF method of Dion *et al.* [16] using the optB86b exchange functional introduced in Chapter 5. By comparing the relative stability of several structures we test the dependence of the results on the choice of the functional.

Namely, we compare two different structures for one, four, and five water molecules. The structures are shown in Figure B.4: Na and Cl adjacent monomers, "compact" and "ring" for four water molecules and "ring" and "compact" for five water molecules. As can be seen from the adsorption energies per water molecules collected in Table B.3, the PBE adsorption energies are generally smaller by ∼100 meV per water molecule. The PBE and optB86b-vdW functionals give the same ordering for five water molecules. However, in the case of four water molecules,

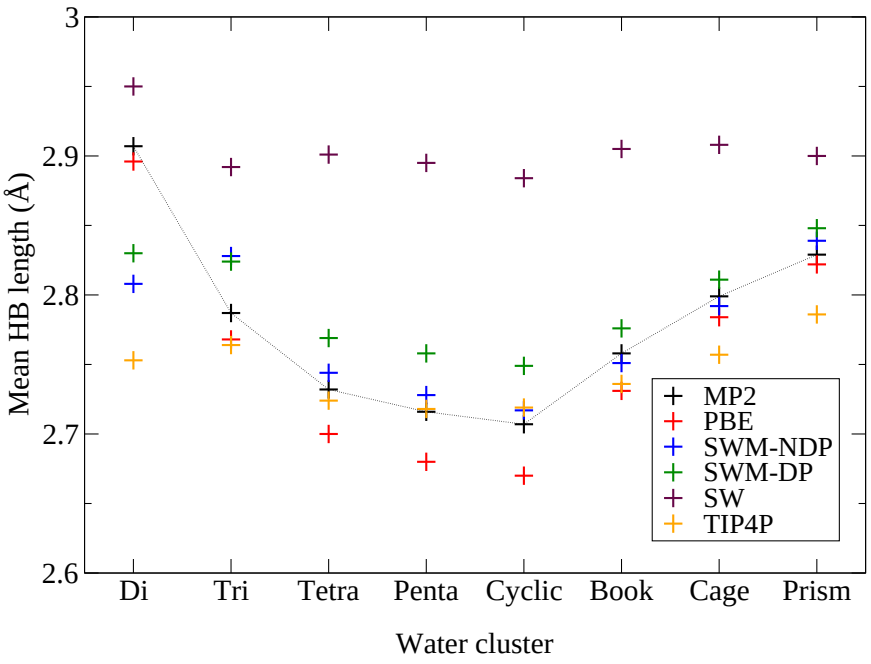

Figure B.2: Average hydrogen bond length (oxygen-oxygen distance) for a dimer (Di), trimer (Tri), tetramer (Tetra), pentamer (Penta), and several low energy isomers of the water hexamer (cyclic, book, cage, prism) calculated using different methods. The methods compared are non-polarisable TIP4P, polarisable SW, SWM-NDP, and SWM-DP models, and DFT-PBE. The MP2 reference distances are shown as well.

the "ring" structure is preferred compared to the "compact" when the optB86b-vdW functional is used. The relative change in energy amounts to 30 meV per water molecule. Interestingly, this structure has been identified as the global minimum for tetramer by Engkvist and Stone [232] using polarisable potentials and they obtained adsorption energy -575 meV. This is slightly less stable than the -612 meV we find, let us mention that they report monomer adsorption energy to be -415 meV, again slightly less stable compared to our -490 meV using optB86b-vdW.

Let us now discuss if this affects the conclusions of this study, *i.e.*, if relative stability of some structures is changed. The two most important cases are the Cl near vacancy at step with 16 water molecules, which was found to be more stable (by $\sim$160 meV) than the step without a defect. The second important energy difference is between the water cluster with 16 water molecules adsorbed on the flat surface and on the NaCl near vacancy. In this case the vacancy is less stable than the surface without a defect by 107 meV. All the structures are shown in Figure B.5. We have used the optB86b-vdW functional and performed geometry optimisation on the systems. Although the adsorption energies change, the relative stability and thus the conclusions don't change: the Cl near is more stable by $\sim$130 meV and therefore it is still preferred to release the ion from the lattice; the NaCl ion pair vacancy is less stable by $\sim$130 meV and we don't observe any dissolution on the flat surface.

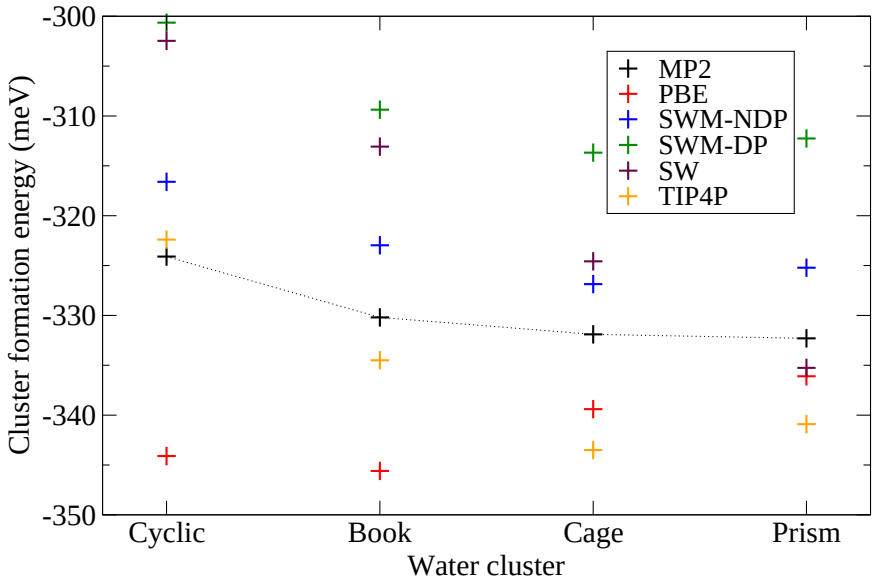

Figure B.3: Cluster formation energy in meV per water molecule of low energy lying water hexamer isomers calculated using different methods. We show data obtained with non-polarisable TIP4P, polarisable SW, SWM-NDP, and SWM-DP models, and DFT-PBE. These are compared to the MP2 reference energies.

Table B.3: Adsorption energies per water molecule in meV for two monomer structures and clusters with four and five water molecules, the geometries are shown in Figure B.4. The "Num. molec." stands for number of molecules. The PBE and optB86b-vdW functionals were used to optimise all the structures. Although the optB86b-vdW adsorption energies are generally lower, most of the energy differences are preserved. The exception is the four water cluster where the "ring" structure gains 30 meV relative to the "compact" geometry.

Num. molec.	1		4		5	
Structure	Na-adjacent	Cl-adjacent	"compact"	"ring"	"ring"	"compact"
PBE	−390	−161	−492	−487	−519	−493
optB86b-vdW	−490	−226	−584	−612	−632	−593

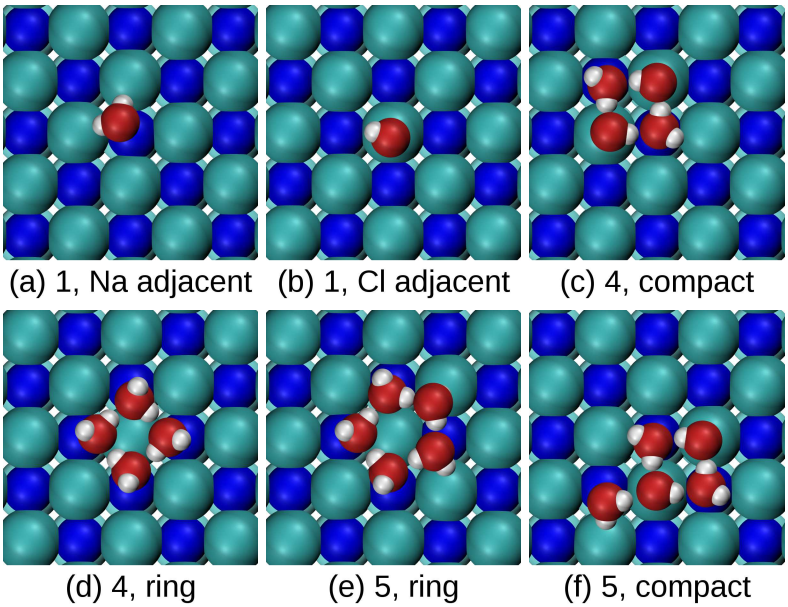

Figure B.4: Low energy water structures on NaCl(001) with one, four, and five water molecules. Adsorption energy for these structures was calculated using the PBE and optB86b-vdW functionals and the effects of including the non-local correlation were compared. Compared to PBE, the optB86b-vdW adsorption energies are lower (*i.e.*, stronger binding). For the monomers and pentamers the relative differences are not affected much. The relative stability of the tetramer is reversed (see Table B.3).

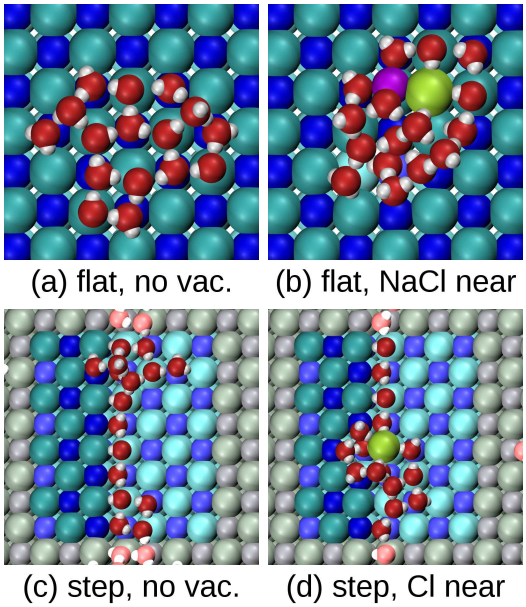

Figure B.5: Water cluster with 16 water molecules on the flat surface (a) without and (b) with "NaCl near" vacancy. The energy ordering given by the PBE functional is preserved when the optB86b-vdW functional is employed. For the surface with a step the "Cl near" vacancy (c) is more stable than the structure without any vacancy (d) when 16 water molecules are present in the simulation cell for both PBE and optB86b-vdW functional.

Appendix C

Implementation of the vdW-DF method in VASP

C.1 Implementation

The vdW-DF is a non-local density functional which means that the exchange-correlation energy contains a term

$$E_{\mathrm{c}}^{\mathrm{nl}} = \int\int \mathrm{d}r_1 \mathrm{d}r_2 \varrho(r_1)\phi(d(r_1), d(r_2))\varrho(r_2)\,. \tag{C.1}$$

This can be evaluated directly but at a high computational cost (evaluation of a water dimer using a reasonable settings and the JuNoLo code [306] takes ∼3 hours using 32 CPUs). Therefore the paper of Román-Pérez and Soler (Ref. [305]) was a breakthrough since it changed the required time from hours to seconds or minutes and allowed the use of self-consistent calculations. For a detailed description of the algorithm we refer the reader to Ref. [305] but we summarise it here. The major observation is that the energy expression given by Equation (C.1) is similar to the Hartree term except the Coulomb interaction is replaced by the kernel ϕ. The Hartree term is readily evaluated in reciprocal space and an analogous transformation is done for the $E_{\mathrm{c}}^{\mathrm{nl}}$ term. Basically the kernel $\phi(d(r_1), d(r_2))$ is interpolated in the two variables and the values of the interpolating functions are obtained for each grid point. This allows the transformation of the energy expression in terms of reciprocal space integration. Inverse FFT transformations are then required to calculated the potential so that a self-consistent procedure can be performed.

In principle, the vdW-DF could be evaluated on the all-electron density within the PAW method. However, this would be very computationally demanding and we decided to implement first the vdW-DF method without the calculation of the all-electron terms. Therefore, $E_{\mathrm{c}}^{\mathrm{nl}}$ is calculated on the sum of the pseudo valence and partial electronic core charge densities, *i.e.*, on the same density that is used to calculate the valence exchange-correlation energy in the PAW method in VASP [176]. We use 30 interpolation points for the q_0 function with a saturation value $q_0^{\mathrm{cut}} = 10$. The vdW kernel uses a hard setting for the kernel short range softening which eliminates the need for the soft correction term (see Ref. [305]). The algorithm utilises the fine FFT grid and, except for the FFTs and summing of the energy, there is no other communication

needed between the MPI processes. The use of the PAW method means that the calculation is all-electron frozen core (with PBE orbitals) for the exchange and LDA correlation part of the exchange-correlation energy and the non-local part is effectively done in a pseudopotential approximation.

In vdW-DF enabled VASP the non-local correlation calculation is invoked by setting `LUSE_VDW = .TRUE.` in INCAR, furthermore, the GGA correlation needs to be removed by setting `AGGAC = 0.000`. The keywords for different exchange functionals are listed in Table C.1. To obtain the vdW2 correlation functional of Lee *et al.* [154], `Zab_vdW = -1.8876` needs to be set.

Table C.1: Keywords used to set different exchange functionals in the INCAR file for a VASP calculation using the GGA, PARAM1, and PARAM2 tags. The PARAM tags are required only for the optB88 and optB86b exchange functionals.

Functional	`GGA`	`PARAM1`	`PARAM2`
revPBE	RE	–	–
optPBE	OR	–	–
optB88	BO	0.1833333	0.220
optB86b	MK	0.1234	1.000
rPW86	ML	–	–

C.2 Interaction energies of the S22 dimers

To test the accuracy of our implementation we have calculated the revPBE-vdW interaction energies of the S22 dimers [41, 295] using several ways to evaluate the vdW correlation. In Table C.2 we compare the interaction energies obtained with JuNoLo which performs the double real space integration, and using the reciprocal space method due to Román-Pérez and Soler with the vdW kernels obtained from Siesta. We use kernels with 20 and 30 interpolation points and q_0^{cut} of 5 and 10, respectively. As can be seen the VASP data with 30 interpolation points agree very well with the all-electron calculations of Vydrov and van Voorhis [307] using a modest aug-cc-pVTZ basis set. We find a very good agreement with the JuNoLo data as well. This confirms that it there is a negligible effect due to the non-self-consistency of the calculations.

Table C.2: Comparison of the S22 interaction energies for the revPBE-vdW functional calculated using different methods. The abbreviations are: HB: hydrogen bonded; PD: parallel displaced; S: stacked; T: T-shape; 2-pyrid. · 2-aminopyr.: 2-pyridoxine · 2-aminopyridine. The column "Reference" shows the interaction energies calculated using accurate post-HF method from Ref. [295] and "Vydrov" shows the data calculated by Vydrov and van Voorhis using an all-electron approach and the aug-cc-pVTZ basis set [307]. The "JuNoLo" column gives the data calculated non-selfconsistently using the JuNoLo code [306] on the pseudo-valence densities. The two "VASP" columns show the self-consistent energies calculated using Siesta kernels with 20 and 30 interpolation points. All data in meV.

	Dimer	Reference	JuNoLo	VASP (20)	VASP (30)	Vydrov
1	Ammonia dimer	-136.4	-103.5	-104.9	-105.1	-104.9
2	Water dimer	-217.0	-170.7	-172.8	-172.9	-172.2
3	Formic acid dimer	-813.1	-655.6	-662.1	-662.5	-662.6
4	Formamide dimer	-696.5	-557.6	-562.5	-562.9	-561.6
5	Uracil dimer HB	-895.1	-745.6	-744.8	-745.6	-756.3
6	2-pyrid. · 2-aminopyr.	-734.5	-615.6	-621.0	-621.7	-622.3
7	Adenine · thymine HB	-717.8	-585.6	-583.7	-584.7	-590.6
8	Methane dimer	-22.9	-34.8	-34.9	-35.0	-34.7
9	Ethene dimer	-64.3	-47.3	-47.0	-47.2	-52.0
10	Benzene · methane	-62.8	-52.7	-52.3	-52.6	-62.0
11	Benzene dimer PD	-115.1	-90.2	-88.4	-89.1	-90.6
12	Pyrazine dimer	-184.6	-136.4	-135.1	-135.9	-135.7
13	Uracil dimer S	-424.2	-369.4	-366.2	-367.6	-369.0
14	Indole benzene S	-196.1	-137.9	-134.4	-135.5	-133.6
15	Adenine · thymine S	-514.2	-389.3	-383.9	-385.7	-376.0
16	Ethene ethyne	-65.2	-65.9	-65.0	-65.1	-64.6
17	Benzene water	-142.2	-113.5	-112.1	-112.4	-112.3
18	Benzene ammonia	-100.6	-81.7	-81.3	-81.6	-82.8
19	Benzene HCN	-196.9	-147.2	-145.0	-145.3	-146.1
20	Benzene dimer T	-117.8	-90.1	-90.3	-90.9	-88.5
21	Indole · benzene T	-244.0	-183.9	-183.3	-184.0	-182.6
22	Phenol dimer	-307.7	-228.0	-229.8	-230.5	-226.8

Appendix D

Comparison of VASP to all-electron calculations for the van der Waals functional

D.1 All electron density based lattice constants

Our tests comparing the vdW approximate evaluation in VASP to all-electron calculations show a very good agreement between both approaches (see Appendix C). However, it is not clear if reference quality calculations can be performed since the vdW energy depends on the PAW potential that is used. To demonstrate this, we show lattice constants of Ge evaluated with three different PAW potentials in Table D.1. We select Ge because of its medium size and the fact that three different PAW potentials are available for it. The potentials are Ge with 4 valence electrons, Ge_d with 14 electrons, and a hard Ge_h with 14 electrons. One can see that the differences between the optB86b-vdW lattice constants cannot be completely attributed to the differences caused by the PAW potential, shown by the optB86b-LDA values. Therefore we decided to obtain all-electron based lattice constants and assess the accuracy of the vdW calculation in VASP against those.

To calculate the all electron vdW energy we use a standalone programme based on the vdW routines in SIESTA. However, the calculation of the AE based lattice constants is not straightforward as several parameters need to be converged. Importantly, the AE density represented on a finite grid leads to numerical errors close to the ionic cores. Therefore we first smoothly cut the electron density around cores and test the convergence of the other parameters. We then study the effect of the cut of the density. Furthermore, we test if the lattice constant can be evaluated using only the valence electron density. We use the lattice constant of Ge with the Ge_h PAW data set for the tests of the parameters.

D.1.1 Convergence tests

The efficient vdW algorithm introduces two basic parameters that control the quality of interpolation of the q_0 function: a cut-off q_0^{cut} and number of interpolation points N_α. The vdW energy

Table D.1: Lattice constants in Å of Ge evaluated using various approximations for the E_c^{nl} for the optB86b-vdW functional. Three PAW potentials were used, Ge has four valence electrons, Ge_d and Ge_h fourteen, and Ge_h has a smaller core radius. The FFT grid contains 120 points in each direction, so that the grid spacing in the cell is ∼0.05 Å. All the calculations used $q_0^{cut} = 10$ and $N_\alpha = 30$ to allow for a comparison between VASP and the all-electron results. The differences in the optB86b-LDA lattice constants represent the error given by the PAW potential. One can see that the all-electron based evaluations of the vdW energy ($\varrho_{ae}^{cut\ 20}$ and $\varrho_{ae}^{no\ soft}$) give almost the same differences in lattice constants between the different PAW potentials as optB86b-LDA. The optB86b-vdW lattice constant calculated with VASP agrees well with the all-electron calculations for the hard potential, the agreement is worse for the Ge and Ge_d potentials. However, in the worst case of the Ge potential this deviation is 0.018 Å, much smaller than the difference of ∼0.07 Å when only the real valence density (ϱ_{val}) is used.

	Ge	Ge_d	Ge_h
optB86b-LDA	5.857	5.842	5.845
optB86b-vdW	5.764	5.714	5.726
ϱ_{val}	5.814	5.735	5.738
$\varrho_{ae}^{cut\ 20}$	5.746	5.729	5.732
$\varrho_{ae}^{no\ soft}$	5.740	5.723	5.726

also depends on the underlying FFT grid and the density cut-off needed to avoid numerical errors close to the cores. The FFT grid is the most straightforward parameter to converge and we find that grid spacing around 0.03 Å can be considered converged, compared to grid spacing of 0.04 Å the lattice constant changes only by 0.002 Å.

Table D.2: Dependence of the Ge lattice constant on the number N_α of q_0 interpolation points and the q_0^{cut}. The electron density was smoothed above 20 a.u. and extremely fine FFT grid with 200 points in each direction (corresponding 0.03 Å spacing) was used.

q_0^{cut}	N_α			
	20	30	40	50
5	5.751	5.749	5.748	5.748
10	5.740	5.734	5.731	5.730
18	7.505	5.733	5.732	5.732

The values of q_0^{cut} and N_α affect the value of the lattice constant more significantly. As can be seen in Table D.2, the lattice constant seems to converge when both q_0^{cut} and N_α are increased. The values of $N_\alpha = 30$, $q_0^{cut} = 10$ give results that are in a very good agreement with the lattice constants obtained with either N_α or q_0^{cut} increased. Moreover, the $q_0^{cut} = 10$ values are almost identical to the values obtained with $q_0^{cut} = 18$. We therefore now set $q_0^{cut} = 10$ and

study how the lattice constant depends on the density cut-off and N_α. Table D.3 shows that the values first converge when N_α is increased up to 40, further increase, to $N_\alpha = 50$ and $N_\alpha = 80$, gives oscillating values. This is more pronounced with higher density cut-offs. This seems to be caused by "overinterpolation" of the q_0 function, which would be probably less severe with an even denser grid. However, there seems to be no point in doing this since the calculations using $N_\alpha = 40$, $q_0^{\mathrm{cut}} = 10$ agree with more stringent settings to within 0.001 Å. Therefore, to obtain the reference lattice constants, we use density cut-off 20 a.u., $N_\alpha = 40$, $q_0^{\mathrm{cut}} = 10$, and FFT grid with fine spacing around 0.03 Å. Since increasing N_α is computationally demanding, we use the values $N_\alpha = 30$, $q_0^{\mathrm{cut}} = 10$ in VASP calculations.

Table D.3: Lattice constant of Ge calculated on the very fine grid with 200 points in each direction for different cut-offs of the all electron density and different N_α interpolation points. The cut-off value for q_0 was set to $q_0^{\mathrm{cut}} = 10$. The change of the lattice constant is small overall when the density cut-off is increased for a constant N_α. The variation is higher for constant cut-off and increasing number of interpolation points. For the highest density cut-off and the highest number of interpolation points the data deviates because of an insufficient real space grid.

ϱ_{cut} (a.u.)	N_α				
	20	30	40	50	80
20	5.740	5.734	5.731	5.730	5.733
100	5.734	5.734	5.731	5.725	5.742
1000	5.738	5.733	5.730	5.728	5.747

Before calculating the lattice constant on the whole solid state test, we present two alternative approaches to the calculation. First, it turns out that the problematic part of the calculation that makes the direct evaluation of the vdW energy impractical is the soft correction term, introduced in Ref [305]. However, the lattice constants calculated with or without this term are virtually identical when the electron density is cut and a "hard" vdW kernel is used (cf. the data in Table D.4 and Table D.3). Therefore one can use the all electron density to evaluate the lattice constant if the soft correction is not added. However, as the data for large N_α in Table D.4 suggest, there is some numerical noise introduced from the interpolation as well. Despite this, the difference in the lattice constants of the all-electron smoothed density and the all-electron density without the soft correction is very small ($< 0.1\%$).

It is also interesting to try to use the real valence density (i.e. not the pseudo valence density) to obtain the lattice constant. In this case the lattice constant converges quickly with all the parameters and, in the case of Ge, the converged value is 5.737 Å, slightly larger than the 5.732 Å obtained with the all electron density. As we shall see, the agreement for other materials strongly depends on the number of electrons included in the valence shell.

Let us now summarize the results and compare the lattice constants obtained using the

Table D.4: Dependence of the Ge lattice constant of the all-electron density cut-off and the number of interpolation points N_α. The soft correction was not added to E_c^{nl}. $q_0^{cut} = 10$ was used. In this case the all-electron density can be used without any cut-off (row ∞) since the contribution from the inner shells is small. The agreement with data in Table D.3 is almost perfect, with the exception of the lattices where $\varrho_{cut} = 1000$ a.u. was used.

ϱ_{cut} (a.u.)	N_α				
	20	30	40	50	80
20	5.736	5.734	5.731	5.730	5.733
100	5.731	5.734	5.731	5.725	5.742
1000	5.732	5.731	5.728	5.726	5.743
∞	5.732	5.731	5.728	5.726	5.743

softer potentials as well. We compare the VASP calculations to the real valence, and all-electron with and without electron density cut-off in Table D.1. Since we want to be able to compare to our VASP implementation we use $N_\alpha = 30$ and $q_0^{cut} = 10$. One can notice that the changes in the all-electron lattice constants ($\varrho_{ae}^{cut\ 20}$ and $\varrho_{ae}^{no\ soft}$) correspond well to the respective changes in the optB86b-LDA values. The real valence calculation (ϱ_{val}) without the d electrons gives too a large lattice constant, the difference is almost halved in the case of the VASP calculation where the partial electronic core charge is added as well. Therefore we can expect a very good agreement of the VASP and all-electron data for PAW potentials that are either hard or contain more than one electronic shell.

D.1.2 Comparison on the whole set

Now we proceed to calculate the lattice constants of the chosen solids using the approaches shown above. This allows us to test if we need to use the quite cumbersome all-electron evaluation or if VASP can be used. We use several ways to estimate the lattice parameter: first, we calculate it directly from VASP using the approximated E_c^{nl}. Second, the real valence density is used, third, the all-electron density without the soft correction. Finally, the vdW energy is calculated on the all-electron density with a density cut-off imposed to avoid numerical errors. The VASP implementation uses $N_\alpha = 30$ interpolation points with $q_0^{cut} = 10$, the real valence and all-electron calculations use $N_\alpha = 40$ interpolation points and $q_0^{cut} = 10$. The number of FFT grid points is set by hand to a large number so that the integration grid spacing is $\sim$0.03 Å.

The lattice constants using optB86b-vdW are collected in Table D.5 and shown in Figure D.1. One can see that the data obtained with VASP (violet +) are in a very good agreement with the all-electron calculations (black +) that use smoothed electron density. The calculations without the soft-correction (green ×) on the all-electron density are generally very similar to the smoothed density calculations. As we have shown earlier, this seems to come more from the representation of the electron density on the finite grid. We find the largest deviations from the AE results for alkali and alkali earth metals, which are very sensitive to the errors in the vdW

correction because of their small bulk moduli. This means that the lattice constant calculated with the all electron density has some error and the very good agreement between the VASP and AE calculations for Cs might be accidental, the trend towards shortening the lattices with the increased size of the ion is not be affected. For the other materials the differences are below 0.1%, i.e. the results differ only at the third decimal place in most cases. This level of accuracy of our VASP calculations is more than sufficient to recover the trends and also similar to or better than the differences for the same solid and functional obtained with different codes [333].

An interesting approach which would circumvent the problematic calculation of the AE vdW correction would be to use the real valence density to calculate E_c^{nl}. However, lattice constants obtained with this approach (blue circles in Figure D.1) are slightly larger than the AE ones. This difference seems to crucially depend on the number of shells included in the valence, this is supported by the fact that the largest errors are observed for Al (3 electrons in valence), Si (4), and As (5). Although the valence electron density based data can't be used to obtain a reliable lattice constant in some cases, they seem to give a good upper bound of the AE based values.

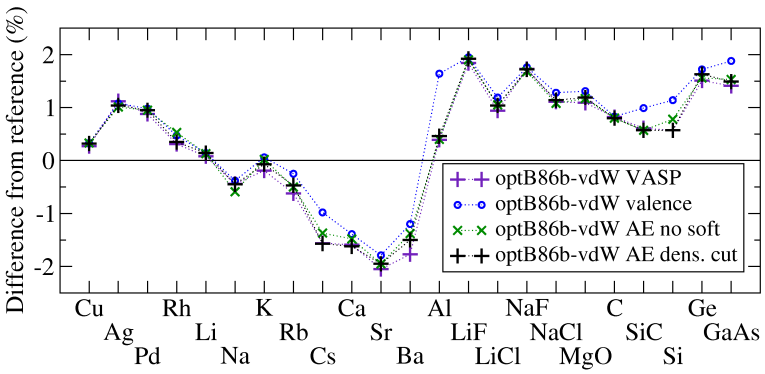

Figure D.1: Lattice constants of various solids calculated with different approximations of the non local van der Waals energy for optB86b-vdW functional. The self-consistent implementation in VASP and non-selfconsistent calculations based on the same density are reported. These use the real valence density ("valence") and the all-electron density without ("AE no soft") and with ("AE dens. cut") the soft correction. The VASP calculations tend to give better agreement with the AE calculations because of the partial electronic core charge density added to the pseudo valence density.

D.2 All electron atomisation energies

To assess the validity of our implementation and to evaluate its accuracy we calculate the atomisation energies of the solids within VASP and with the all-electron post-processing correction. A self-consistent calculation using optB86b-vdW is done for the solid close to the energy minimum and the respective atom or atoms in a large rectangular box (with approximately two times larger sides). From this calculation we obtain the approximate E_c^{nl}. In the next step, the all-electron

density from the VASP calculation is used to evaluate $E_c^{nl,ae}$. By subtracting the solid energies per atom from the atomic ones, we obtain the non-local contribution to the atomisation energy for these two approaches which we can compare. The results are summarised in Table D.6 where we show the E_c^{nl} contribution to binding from VASP and from the all-electron calculations with and without the soft-correction, along with the total atomisation energy. The agreement is very good overall with the errors in the total atomisation energies below 2%. The soft-correction is not calculated in VASP, however, its effect on the atomisation energies is negligible.

As was shown in the case of lattice constants the all-electron density based $E_c^{nl,ae}$ strongly depends on the underlying grid and high density regions need to be cut. The problem is less severe in the case of atomisation energies where we use exactly the same grid spacing for the solid and atomic calculations so that numerical inaccuracies subtract out. In most of the cases the calculations with cut density gives the same vdW contribution to the atomisation energy (to within a meV). In a few cases the contribution slightly differs (by up to 30 meV for Pd), and therefore we give the results calculated with the electron density cut above 100 a.u. in Table D.6.

Table D.5: Lattice constants in Å calculated with the optB86b-vdW functional using different approaches and compared to the zero point energy corrected experimental value. Self-consistent calculation using the sum of the pseudo valence density and the soft core density ("VASP"), post-processing calculations using the real valence density ("ϱ_{val}"), all-electron density with ϱ_{ae} and without $\varrho_{\mathrm{ae}}^{\mathrm{no\ soft}}$ the soft correction are given.

Solid	VASP	ϱ_{val}	$\varrho_{\mathrm{ae}}^{\mathrm{no\ soft}}$	ϱ_{ae}	Exp.(ZPEC)
N_α	30	40	40	40	–
q_0^{cut}	10	10	10	10	–
ϱ_{cut}	∞	∞	∞	20	–
Cu	3.605	3.607	3.607	3.606	3.595
Rh	3.805	3.811	3.813	3.806	3.793
Pd	3.909	3.913	3.912	3.912	3.875
Ag	4.101	4.100	4.097	4.098	4.056
Li	3.452	3.454	3.454	3.454	3.449
Na	4.191	4.194	4.185	4.191	4.210
K	5.202	5.215	5.213	5.208	5.212
Rb	5.541	5.562	5.548	5.550	5.576
Cs	5.945	5.980	5.956	5.944	6.039
Ca	5.465	5.476	5.471	5.463	5.553
Sr	5.921	5.937	5.927	5.927	6.045
Ba	4.906	4.935	4.926	4.920	4.995
Al	4.036	4.086	4.036	4.038	4.020
LiF	4.037	4.041	4.039	4.040	3.964
LiCl	5.103	5.116	5.109	5.109	5.056
NaF	4.658	4.660	4.656	4.658	4.579
NaCl	5.627	5.636	5.625	5.628	5.565
MgO	4.230	4.239	4.233	4.234	4.184
C	3.572	3.573	3.571	3.571	3.543
SiC	4.369	4.385	4.367	4.367	4.342
Si	5.447	5.478	5.458	5.447	5.416
Ge	5.725	5.737	5.728	5.731	5.640
GaAs	5.717	5.744	5.724	5.722	5.638

Table D.6: Total atomisation energy from VASP ($E_{\mathrm{at,total}}$) using optB86b-vdW and contribution of the non-local correlation term ($E_{\mathrm{c}}^{\mathrm{nl}}$) to the atomisation energies for a set of solids. The non-local correlation has been calculated with VASP self-consistently, and using the Siesta routine on the all-electron density with and without the soft-correction. All data in eV.

	$E_{\mathrm{at,total}}$	$E_{\mathrm{at}}^{\mathrm{nl}}$		
		VASP	ae	ae, no soft
Cu	3.679	0.941	0.933	0.935
Ag	2.887	1.097	1.063	1.065
Pd	4.160	1.309	1.259	1.261
Rh	6.385	1.498	1.430	1.433
Li	1.203	0.155	0.153	0.155
Na	0.923	0.221	0.221	0.222
K	0.832	0.281	0.275	0.276
Rb	0.762	0.314	0.301	0.303
Cs	0.743	0.355	0.340	0.342
Ca	1.940	0.584	0.569	0.571
Sr	1.691	0.638	0.616	0.617
Ba	2.036	0.739	0.711	0.713
Al	3.488	0.799	0.750	0.752
LiF	4.410	0.273	0.267	0.268
LiCl	3.489	0.375	0.369	0.370
NaF	7.918	0.270	0.268	0.269
NaCl	3.239	0.359	0.356	0.357
MgO	5.189	0.533	0.523	0.524
C	7.910	0.772	0.745	0.747
SiC	6.669	0.767	0.737	0.738
Si	4.836	0.741	0.712	0.714
Ge	4.003	0.752	0.733	0.734
GaAs	3.442	0.741	0.717	0.718

Bibliography

[1] D. M. Eigler and E. K. Schweizer. Positioning single atoms with a scanning tunneling microscope. *Nature*, 344:524, 1990.

[2] K. E. Drexler. *Engines of Creation: The Coming Era of Nanotechnology.* Anchor Books, New York, USA, 1986.

[3] M. J. Gillan, D. Alfe, J. Brodholt, L. Vocadlo, and G. D. Price. First-principles modelling of Earth and planetary materials at high pressures and temperatures. *Rep. Prog. Phys.*, 69:2365, 2006.

[4] C. J. Pickard and R. J. Needs. Stable phases of iron at terapascal pressures. *J. Phys.: Cond. Matt.*, 21:452205, 2009.

[5] S Curtarolo, D Morgan, K Persson, J Rodgers, and G Ceder. Predicting crystal structures with data mining of quantum calculations. *Phys. Rev. Lett.*, 91:135503, 2003.

[6] J. K. Norskov, T. Bligaard, J. Rossmeisl, and C. H. Christensen. Towards the computational design of solid catalysts. *Nature Chem.*, 1:37, 2009.

[7] W. Kohn. Nobel Lecture: Electronic structure of matter—wave functions and density functionals. *Rev. Mod. Phys.*, 71:1253, 1999.

[8] D. R. Bowler and T. Miyazaki. Calculations for millions of atoms with density functional theory: linear scaling shows its potential. *J. Phys.: Cond. Matt.*, 22:074207, 2010.

[9] A. R. Leach. *Molecular modelling: Principles and applications.* Pearson Education, Harlow, UK, 2001.

[10] S. J. Marrink, H. J. Risselada, S. Yefimov, D. P. Tieleman, and A. H. de Vries. The MARTINI force field: Coarse grained model for biomolecular simulations. *J. Phys. Chem. B*, 111:7812, 2007.

[11] P. J. Feibelman. Pinning of graphene to Ir(111) by flat Ir dots. *Phys. Rev. B*, 77:165419, 2008.

[12] A. Michaelides, Z.-P. Liu, C. J. Zhang, A. Alavi, D. A. King, and P. Hu. Identification of general linear relationships between activation energies and enthalpy changes for dissociation reactions at surfaces. *J. Am. Chem. Soc.*, 125:3704, 2003.

[13] A. J. Cohen, P. Mori-Sanchez, and W. Yang. Insights into current limitations of density functional theory. *Science*, 321:792, 2008.

[14] J. F. Dobson and B. P. Dinte. Constraint satisfaction in local and gradient susceptibility approximations: Application to a van der waals density functional. *Phys. Rev. Lett.*, 76:1780, 1996.

[15] Y. Zhang and R. Tsu. Binding graphene sheets together using silicon: Graphene/silicon superlattice. *Nanoscale Res. Lett.*, 5:805, 2010.

[16] M. Dion, H. Rydberg, E. Schröder, D. C. Langreth, and B. I. Lundqvist. Van der Waals density functional for general geometries. *Phys. Rev. Lett.*, 92:246401, 2004.

[17] C. D. Sherrill. *A Brief Review of Elementary Quantum Chemistry*. Georgia Institute of Technology, Atlanta, USA, 2001.

[18] W. M. C. Foulkes, L. Mitas, R. J. Needs, and G. Rajagopal. Quantum Monte Carlo simulations of solids. *Rev. Mod. Phys.*, 73:33, 2001.

[19] S. Pisana, M. Lazzeri, C. Casiraghi, K. S. Novoselov, A. K. Geim, A. C. Ferrari, and F. Mauri. Breakdown of the adiabatic Born-Oppenheimer approximation in graphene. *Nature Mater.*, 6:198, 2007.

[20] J. D. White, J. Chen, D. Matsiev, D. J. Auerbach, and A. M. Wodtke. Conversion of large-amplitude vibration to electron excitation at a metal surface. *Nature*, 433:503, 2005.

[21] B. G. Walker, C. Molteni, and N. Marzari. Ab initio molecular dynamics of metal surfaces. *J. Phys.: Cond. Matt.*, 16:S2575, 2004.

[22] M. J. Gillan. Quantum classical crossover of the transition rate in the damped double well. *J. Phys. C-Solid State Phys.*, 20:3621, 1987.

[23] D. Marx and M. Parrinello. Ab-initio path-integral molecular-dynamics. *Z. Phys. B*, 95:143, 1994.

[24] M. E. Tuckerman, D. Marx, M. L. Klein, and M. Parrinello. On the quantum nature of the shared proton in hydrogen bonds. *Science*, 275:817, 1997.

[25] J. A. Morrone and R. Car. Nuclear quantum effects in water. *Phys. Rev. Lett.*, 101:017801, 2008.

[26] M. Tachikawa and Y. Osamura. Isotope effect of hydrogen and lithium hydride molecules. Application of the dynamic extended molecular orbital method and energy component analysis. *Theo. Chem. Acc.*, 104:29, 2000.

[27] S. P. Webb, T. Iordanov, and S. Hammes-Schiffer. Multiconfigurational nuclear-electronic orbital approach: Incorporation of nuclear quantum effects in electronic structure calculations. *J. Chem. Phys.*, 117:4106, 2002.

[28] M. V. Pak and S. Hammes-Schiffer. Electron-proton correlation for hydrogen tunneling systems. *Phys. Rev. Lett.*, 92:103002, 2004.

[29] C. Swalina, M. V. Pak, A. Chakraborty, and S. Hammes-Schiffer. Explicit dynamical electron-proton correlation in the nuclear-electronic orbital framework. *J. Phys. Chem. A*, 110:9983, 2006.

[30] A. Chakraborty, M. V. Pak, and S. Hammes-Schiffer. Inclusion of explicit electron-proton correlation in the nuclear-electronic orbital approach using Gaussian-type geminal functions. *J. Chem. Phys.*, 129:014101, 2008.

[31] A. Chakraborty and S. Hammes-Schiffer. Density matrix formulation of the nuclear-electronic orbital approach with explicit electron-proton correlation. *J. Chem. Phys.*, 129:204101, 2008.

[32] R. M. Martin. *Electronic structure: Basic theory and practical methods.* Cambridge University Press, Cambridge, UK, 2004.

[33] R. N. Barnett and U. Landman. Born-Oppenheimer molecular-dynamics simulations of finite systems: Structure and dynamics of $(H_2O)_2$. *Phys. Rev. B*, 48:2081, 1993.

[34] A. Szabo and N. S. Ostlund. *Modern quantum chemistry: Introduction to advanced electronic structure theory.* Dover Publications, New York, USA, 1996.

[35] W. D. Laidig, P. Saxe, and R. J. Bartlett. The description of N_2 and F_2 potential-energy surfaces using multireference coupled cluster theory. *J. Chem. Phys.*, 86:887, 1987.

[36] X. Li and J. Paldus. Full potential energy curve for N_2 by the reduced multireference coupled-cluster method. *J. Chem. Phys.*, 129:054104, 2008.

[37] R. J. Bartlett and M. Musiał. Coupled-cluster theory in quantum chemistry. *Rev. Mod. Phys.*, 79:291, 2007.

[38] K. Raghavachari, G. W. Trucks, J. A. Pople, and M. Head-Gordon. A fifth-order perturbation comparison of electron correlation theories. *Chemical Physics Letters*, 157:479, 1989.

[39] C. Møller and M. S. Plesset. Note on an approximation treatment for many-electron systems. *Phys. Rev.*, 46:618, 1934.

[40] M. O. Sinnokrot and C. D. Sherrill. Highly accurate couple cluster potential energy curves for the benzene dimer: Sandwich, t-shaped, and parallel-displaced configurations. *J. Phys. Chem. A*, 108:10200, 2004.

[41] P. Jurečka, J. Šponer, J. Černý, and P. Hobza. Benchmark database of accurate (MP2 and CCSD(T) complete basis set limit) interaction energies of small model complexes, DNA base pairs, and amino acid pairs. *Phys. Chem. Chem. Phys.*, 8:1985, 2006.

[42] K. E. Riley, M. Pitoňák, P. Jurečka, and P. Hobza. Stabilization and structure calculations for noncovalent interactions in extended molecular systems based on wave function and density functional theories. *Chem. Rev.*, 110:5023, 2010.

[43] M. Marsman, A. Grueneis, J. Paier, and G. Kresse. Second-order Moller-Plesset perturbation theory applied to extended systems. I. Within the projector-augmented-wave formalism using a plane wave basis set. *J. Chem. Phys.*, 130:184103, 2009.

[44] A. Grueneis, M. Marsman, and G. Kresse. Second-order Moller-Plesset perturbation theory applied to extended systems. II. Structural and energetic properties. *J. Chem. Phys.*, 133:074107, 2010.

[45] C. D. Sherrill. Frontiers in electronic structure theory. *J. Chem. Phys.*, 132:110902, 2010.

[46] W. A. de Jong, E. Bylaska, N. Govind, C. L. Janssen, K. Kowalski, T. Mueller, I. M. B. Nielsen, H. J. J. van Dam, V. Veryazov, and R. Lindh. Utilizing high performance computing for chemistry: parallel computational chemistry. *Phys. Chem. Chem. Phys.*, 12:6896, 2010.

[47] J. Ma, A. Michaelides, and D. Alfè. Binding of hydrogen on benzene, coronene, and graphene from quantum Monte Carlo calculations. *J. Phys. Chem.*, 134:134701, 2011.

[48] G. H. Booth, A. J. W. Thom, and A. Alavi. Fermion Monte Carlo without fixed nodes: A game of life, death, and annihilation in Slater determinant space. *J. Chem. Phys.*, 131:054106, 2009.

[49] D. Cleland, G. H. Booth, and A. Alavi. Communications: Survival of the fittest: Accelerating convergence in full configuration-interaction quantum Monte Carlo. *J. Chem. Phys.*, 132:041103, 2010.

[50] R. G. Parr and W. Yang. *Density-functional theory of atoms and molecules.* Oxford University Press, New York, USA, 1994.

[51] P. Hohenberg and W. Kohn. Inhomogeneous electron gas. *Phys. Rev. B*, 136:B864, 1964.

[52] W. Kohn and L. J. Sham. Self-consistent equations including exchange and correlation effects. *Phys. Rev.*, 140:1133, 1965.

[53] C. Huang and E. A. Carter. Nonlocal orbital-free kinetic energy density functional for semiconductors. *Phys. Rev. B*, 81:045206, 2010.

[54] K. Husimi. Some formal properties of the density matrix. *Proc. Phys. Soc. Jpn.*, 22:264, 1940.

[55] P. Löwdin. Quantum theory of many-particle systems. I. physical interpretations by means of density matrices, natural spin-orbitals, and convergence problems in the method of configurational interaction. *Phys. Rev.*, 97:1474, 1955.

[56] J. E. Mayer. Electron correlation. *Phys. Rev.*, 100:1579, 1955.

[57] R. H. Tredgold. Density matrix and the many-body problem. *Phys. Rev.*, 105:1421, 1957.

[58] Y. Mizuno and T. Izuyama. Remarks on mayers reduced density matrix method. *Prog. Theo. Phys.*, 18:33–38, 1957.

[59] R. U. Ayres. Variational approach to the many-body problem. *Phys. Rev.*, 111:1453, 1958.

[60] F. Bopp. Ableitung der bindungsenergie von n-teilchen-systemen aus 2-teilchen-dichtematrizen. *Z. Phys.*, 156:348–359, 1959.

[61] A. J. Coleman. Structure of fermion density matrices. *Rev. Mod. Phys.*, 35:668, 1963.

[62] M. Nakata, H. Nakatsuji, M. Ehara, M. Fukuda, K. Nakata, and K. Fujisawa. Variational calculations of fermion second-order reduced density matrices by semidefinite programming algorithm. *J. Chem. Phys.*, 114:8282–8292, 2001.

[63] D. A. Mazziotti. Realization of quantum chemistry without wave functions through first-order semidefinite programming. *Phys. Rev. Lett.*, 93:213001, 2004.

[64] J. Harris and R. O. Jones. Surface-energy of a bounded electron-gas. *J. Phys. F Metal Phys.*, 4:1170, 1974.

[65] E. Apra, E. Stefanovich, R. Dovesi, and C. Roetti. An abinitio Hartree-Fock study of silver-chloride. *Chem. Phys. Lett.*, 186:329, 1991.

[66] F. Kirchhoff, J. M. Holender, and M. J. Gillan. Energetics and electronic structure of silver chloride. *Phys. Rev. B*, 49:17420, 1994.

[67] B. Y. Tong. Exchange- and correlation-energy calculations in finite systems. *Phys. Rev. A*, 4:1375, 1971.

[68] Y. S. Kim and R. G. Gordon. Study of electron-gas approximation. *J. Chem. Phys.*, 60:1842, 1974.

[69] J. P. Perdew and A. Zunger. Self-interaction correction to density-functional approximations for many-electron systems. *Phys. Rev. B*, 23:5048, 1981.

[70] A. D. Becke. Density functional calculations of molecular bond energies. *J. Chem. Phys.*, 84:4524, 1986.

[71] K. Laasonen, F. Csajka, and M. Parrinello. Water dimer properties in the gradient-corrected density functional theory. *Chemical Physics Letters*, 194:172, 1992.

[72] B. G. Johnson, C. A. Gonzales, P. M. W. Gill, and J. A. Pople. A density functional study of the simplest hydrogen abstraction reaction. Effect of self-interaction correction. *Chem. Phys. Lett.*, 221:100, 1994.

[73] D. Porezak and M. R. Pederson. Density functional based studies of transition states and barriers for hydrogen exchange and abstraction reactions. *J. Chem. Phys.*, 102:9345, 1995.

[74] G. I. Csonka and B. G. Johnson. Inclusion of exact exchange for self-interaction corrected h3 density functional potential energy surface. *Theo. Chem. Acc.*, 99:158, 1998.

[75] M. Boero. Excess electron in water at different thermodynamic conditions. *J. Phys. Chem. A*, 111:12248, 2007.

[76] O. Marsalek, T. Frigato, J. VandeVondele, S. E. Bradforth, B. Schmidt, C. Schuette, and P. Jungwirth. Hydrogen forms in water by proton transfer to a distorted electron. *J. Phys. Chem. B*, 114:915, 2010.

[77] J. VandeVondele and M. Sprik. A molecular dynamics study of the hydroxyl radical in solution applying self-interaction-corrected density functional methods. *Phys. Chem. Chem. Phys*, 7:1363, 2005.

[78] M d'Avezac, M Calandra, and F Mauri. Density functional theory description of hole-trapping in SiO_2: A self-interaction-corrected approach. *Phys. Rev. B*, 71:205210, 2005.

[79] D. M. Ceperley and B. J. Alder. Ground state of the electron gas by a stochastic method. *Phys. Rev. Lett.*, 45:566, 1980.

[80] J. P. Perdew and Y. Wang. Accurate and simple analytic representation of the electron-gas correlation energy. *Phys. Rev. B*, 45:13244, 1992.

[81] S. H. Vosko, L. Wilk, and M. Nusair. Accurate spin-dependent electron liquid correlation energies for local spin-density calculations – a critical analysis. *Can. J. Phys.*, 58:1200, 1980.

[82] V. N. Staroverov, G. E. Scuseria, J. Tao, and J. P. Perdew. Tests of a ladder of density functionals for bulk solids and surfaces. *Phys. Rev. B*, 69:075102, 2004.

[83] J. P. Perdew, K. Burke, and M. Ernzerhof. Generalized gradient approximation made simple. *Phys. Rev. Lett.*, 77:3865, 1996. *ibid*, 78:1396, 1997.

[84] J. P. Perdew. *Electronic Structure of Solids '91.* edited by P. Ziesche and H. Eschrig (Akademie Verlag, Berlin), 1991.

[85] A. D. Becke. Density-functional exchange-energy appoximation with correct asymptotic behavior. *Phys. Rev. A*, 38:3098, 1988.

[86] C. Lee, W. Yang, and R. G. Parr. Development of the Colle-Salvetti correlation-energy formula into a functional of the electron density. *Phys. Rev. B*, 37:785, 1988.

[87] J. P. Perdew. Density-functional approximation for the correlation energy of the inhomogeneous electron gas. *Phys. Rev. B*, 33:8822, 1986.

[88] J. P. Perdew, A. Ruzsinszky, G. I. Csonka, L. A. Constantin, and J. Sun. Workhorse similocal density functional for condensed matter physics and quantum chemistry. *Phys. Rev. Lett.*, 103:026403, 2009.

[89] J. P. Perdew, J. A. Chevary, S. H. Vosko, K. A. Jackson, M. R. Pederson, D. J. Singh, and C. Fiolhais. Accurate and simple analytic representation of the electron-gas correlation energy. *Phys. Rev. B*, 46:6671, 1992.

[90] R. Q. Hood, M. Y. Chou, A. J. Williamson, G. Rajagopal, R. J. Needs, and W. M. C. Foulkes. Quantum Monte Carlo investigation of exchange and correlation in silicon. *Phys. Rev. Lett.*, 78:3350, 1997.

[91] A. D. Becke. Density-functional thermochemistry. III. The role of exact exchange. *J. Chem. Phys.*, 98:5648, 1993.

[92] K. Kim and K. D. Jordan. Comparison of density-functional and MP2 calculations on the water monomer and dimer. *J. Phys. Chem.*, 98:10089, 1994.

[93] J. Paier, M. Marsman, K. Hummer, G. Kresse, I. C. Gerber, and J. G. Ángyán. Screened hybrid density functionals applied to solids. *J. Chem. Phys.*, 124:154709, 2006.

[94] C. Adamo and V. Barone. Toward reliable density functional methods without adjustable parameters: The PBE0 model. *J. Chem. Phys.*, 110:6158, 1999.

[95] J. Heyd, G. E. Scuseria, and M. Ernzerhof. Hybrid functionals based on a screened Coulomb potential. *J. Chem. Phys.*, 118:8207, 2003.

[96] J. Heyd, G. E. Scuseria, and M. Ernzerhof. Hybrid functionals based on a screened Coulomb potential (vol 118, pg 8207, 2003). *J. Chem. Phys.*, 124, 2006.

[97] B. G. Janesko. Rung 3.5 density functionals. *J. Chem. Phys.*, 133, 2010.

[98] V. Peuckert. Microscopic theory of some surface effects in a dense electron gas. *Z. Phys. A*, 241:191, 1971.

[99] M. Rasolt and S. H. Vosko. Investigations of nonlocal exchange and correlation effects in metals via the density-functional formalism. *Phys. Rev. B*, 10:4195, 1974.

[100] D. C. Langreth and J. P. Perdew. Exchange-correlation energy of a metallic surface. *Solid State Commun.*, 17:1425, 1975.

[101] D. C. Langreth and J. P. Perdew. Exchange-correlation energy of a metallic surface - wave-vector analysis. *Phys. Rev. B*, 15:2884, 1977.

[102] Y. Zhao, N. E. Schultz, and D. G. Truhlar. Exchange-correlation functional with broad accuracy for metallic and nonmetallic compounds, kinetics, and noncovalent interactions. *J. Chem. Phys.*, 123:161103, 2005.

[103] Y. Zhao and D. G. Truhlar. Density functionals for noncovalent interaction energies of biological importance. *J. Chem. Theory Comput.*, 3:289, 2007.

[104] L. F. Molnar, X. He, B. Wang, and K. M. Merz. Further analysis and comparative study of intermolecular interactions using dimers from the S22 database. *J. Chem. Phys.*, 131:065102, 2009.

[105] C. Douketis, G. Scoles, S. Marchetti, M. Zen, and A. J. Thakkar. Intermolecular forces via hybrid Hartree-Fock SCF plus damped dispersion (HFD) energy calculations - an improved spherical model. *J. Chem. Phys.*, 76:3057, 1982.

[106] M. Elstner, P. Hobza, T. Frauenheim, S. Suhai, and E. Kaxiras. Hydrogen bonding and stacking interactions of nucleic acid base pairs: A density-functional-theory based treatment. *J. Chem. Phys.*, 114:5149, 2001.

[107] X. Wu, M. C. Vargas, S. Nayak, V. Lotrich, and G. Scoles. Towards extending the applicability of density functional theory to weakly bound systems. *J. Chem. Phys.*, 115:8748–8757, 2001.

[108] J. Antony and S. Grimme. Density functional theory including dispersion corrections for intermolecular interactions in a large benchmark set of biologically relevant molecules. *Phys. Chem. Chem. Phys.*, 8:5287, 2006.

[109] P. Jurečka, J. Černý, P. Hobza, and D. R. Salahub. Density functional theory augmented with an empirical dispersion term. interaction energies and geometries of 80 noncovalent complexes compared with *ab initio* quantum mechanics calculations. *J. Comput. Chem.*, 28:555, 2006.

[110] S. Grimme, J. Antony, T. Schwabe, and C. Mück-Lichtenfeld. Density functional theory with dispersion corrections for supramolecular structures, aggregates, and complexes of (bio)organic molecules. *Org. Biomol. Chem.*, 5:741, 2007.

[111] A. Tkatchenko and M. Scheffler. Accurate molecular van der Waals interactions from ground-state electron density and free-atom reference data. *Phys. Rev. Lett.*, 102:073005, 2009.

[112] S. Grimme, J. Antony, S. Ehrlich, and H. Krieg. A consistent and accurate ab initio parametrization of density functional dispersion correction (DFT-D) for the 94 elements H–Pu. *J. Chem. Phys.*, 132:154104, 2010.

[113] H. B. G. Casimir and D. Polder. The influence of retardation on the London-van der Waals forces. *Phys. Rev.*, 73:360–372, 1948.

[114] B. Santra, A. Michaelides, M. Fuchs, A. Tkatchenko, C. Filippi, and M. Scheffler. On the accuracy of density-functional theory exchange-correlation functionals for H bonds in small water clusters II: The water hexamer and van der Waals interactions. *J. Chem. Phys.*, 129:194111, 2008.

[115] F. Hanke. Sensitivity analysis and uncertainty calculation for dispersion corrected density functional theory. *J. Comput. Chem.*, 32:1424, 2011.

[116] A. Savin and H. Flad. Density functionals for the Yukawa electron-electron interaction. *Int. J. Quant. Chem.*, 56:327, 1995.

[117] A. Savin. *Recent Developments and Applications of Modern Density Functional Theory.* edited by J.M. Seminario (Elsevier, Amsterdam), 1996.

[118] S. Paziani, S. Moroni, P. Gori-Giorgi, and G. B. Bachelet. Local-spin-density functional for multideterminant density functional theory. *Phys. Rev. B*, 73:155111, 2006.

[119] H. Iikura, T. Tsuneda, T. Yanai, and K. Hirao. A long-range correction scheme for generalized-gradient-approximation exchange functionals. *J. Chem. Phys.*, 115:3540, 2001.

[120] J. G. Ángyán, I. C. Gerber, A. Savin, and J. Toulouse. van der Waals forces in density functional theory: Perturbational long-range electron-interaction corrections. *Phys. Rev. A*, 72:012510, 2005.

[121] E. Goll, H. Werner, H. Stoll, T. Leininger, P. Gori-Giorgi, and A. Savin. A short-range gradient-corrected spin density functional in combination with long-range coupled-cluster methods: Application to alkali-metal rare-gas dimers. *Chem. Phys.*, 329:276, 2006.

[122] B. G. Janesko, T. M. Henderson, and G. E. Scuseria. Long-range-corrected hybrid density functionals including random phase approximation correlation. *J. Chem. Phys.*, 130:081105, 2009.

[123] B. G. Janesko, T. M. Henderson, and G. E. Scuseria. Long-range-corrected hybrid density functionals including random phase approximation correlation: Application to noncovalent interactions. *J. Chem. Phys.*, 131:034110, 2009.

[124] S. Grimme. Semiempirical hybrid density functional with perturbative second-order correlation. *J. Chem. Phys.*, 124:034108, 2006.

[125] J. Chai and M. Head-Gordon. Long-range corrected double-hybrid density functionals. *J. Chem. Phys.*, 131:174105, 2009.

[126] O. Gunnarsson and B. I. Lundqvist. Exchange and correlation in atoms, molecules, and solids by spin-density functional formalism. *Phys. Rev. B*, 13:4274, 1976.

[127] F. Furche. Molecular tests of the random phase approximation to the exchange-correlation energy functional. *Phys. Rev. B*, 64:195120, 2001.

[128] M. Fuchs and X. Gonze. Accurate density functionals: Approaches using the adiabatic-connection fluctuation-dissipation theorem. *Phys. Rev. B*, 65:235109, 2002.

[129] F. Furche and T. Van Voorhis. Fluctuation-dissipation theorem density-functional theory. *J. Chem. Phys.*, 122:164106, 2005.

[130] T. Miyake, F. Aryasetiawan, T. Kotani, M. van Schilfgaarde, M. Usuda, and K. Terakura. Total energy of solids: An exchange and random-phase approximation correlation study. *Phys. Rev. B*, 66:245103, 2002.

[131] A. Marini, P. Garcia-Gonzalez, and A. Rubio. First-principles description of correlation effects in layered materials. *Phys. Rev. Lett.*, 96:136404, 2006.

[132] Deyu Lu, Yan Li, Dario Rocca, and Giulia Galli. Ab initio calculation of van der Waals bonded molecular crystals. *Phys. Rev. Lett.*, 102:206411, 2009.

[133] J. F. Dobson, A. White, and A. Rubio. Asymptotics of the dispersion interaction: Analytic benchmarks for van der Waals energy functionals. *Phys. Rev. Lett.*, 96:073201, 2006.

[134] S. Lebègue, J. Harl, Tim Gould, J. G. Ángyán, G. Kresse, and J. F. Dobson. Cohesive properties and asymptotics of the dispersion interaction in graphite by the random phase approximation. *Phys. Rev. Lett.*, 105:196401, 2010.

[135] W. Zhu, J. Toulouse, A. Savin, and J. G. Ángyán. Range-separated density-functional theory with random phase approximation applied to noncovalent intermolecular interactions. *J. Chem. Phys.*, 132:244108, 2010.

[136] J. Harl and G. Kresse. Cohesive energy curves for noble gas solids calculated by adiabatic connection fluctuation-dissipation theory. *Phys. Rev. B*, 77:045136, 2008.

[137] J. Harl and G. Kresse. Accurate bulk properties from approximate many-body techniques. *Phys. Rev. Lett.*, 103:056401, 2010.

[138] J. Harl, L. Schimka, and G. Kresse. Assessing the quality of the random phase approximation for lattice constants and atomization energies of solids. *Phys. Rev. B*, 81:115126, 2010.

[139] A. Grueneis, M. Marsman, J. Harl, L. Schimka, and G. Kresse. Making the random phase approximation to electronic correlation accurate. *J. Chem. Phys.*, 131:154115, 2009.

[140] J. Jung, P. García-González, J. F. Dobson, and R. W. Godby. Effects beyond the random-phase approximation in calculating the interaction between metal films. *Phys. Rev. B*, 70:205107, 2004.

[141] P. J. Feibelman, B. Hammer, J. K. Norskov, F. Wagner, M. Scheffler, R. Stumpf, R. Watwe, and J. Dumesic. The CO/Pt(111) puzzle. *J. Phys. Chem. B*, 105:4018, 2001.

[142] L. Schimka, J. Harl, A. Stroppa, A. Grueneis, M. Marsman, F. Mittendorfer, and G. Kresse. Accurate surface and adsorption energies from many-body perturbation theory. *Nature Mater.*, 9:741, 2010.

[143] J. F. Dobson. Prospects for a van der Waals density functional. *Int. J. Quantum Chem.*, 69:615, 1998.

[144] K. Rapcewicz and N. W. Ashcroft. Fluctuation attraction in condensed matter – a nonlocal functional-approach. *Phys. Rev. B*, 44:4032, 1991.

[145] Y. Andersson, D. C. Langreth, and B. I. Lundqvist. van der Waals interactions in density-functional theory. *Phys. Rev. Lett.*, 76:102, 1996.

[146] R. K. Nesbet. Local response model of the generalized polarization potential. *Phys. Rev. A*, 56:2778, 1997.

[147] O. A. Vydrov and T. Van Voorhis. Dispersion interactions from a local polarizability model. *Phys. Rev. A*, 81:062708, 2010.

[148] D. C. Langreth, M. Dion, H. Rydberg, E. Schroder, P. Hyldgaard, and B. I. Lundqvist. Van der Waals density functional theory with applications. *Int. J. Quant. Chem.*, 101:599, 2005.

[149] E. Hult, H. Rydberg, B. I. Lundqvist, and D. C. Langreth. Unified treatment of asymptotic van der Waals forces. *Phys. Rev. B*, 59:4708, 1999.

[150] H. Rydberg, B. I. Lundqvist, D. C. Langreth, and M. Dion. Tractable nonlocal correlation density functionals for flat surfaces and slabs. *Phys. Rev. B*, 62:6997, 2000.

[151] H. Rydberg. Long- and medium-ranged nonlocal correlations in density functional theory, 2001. http://fy.chalmers.se/ hery/Thesis/pdf/PaperVI.pdf.

[152] O. A. Vydrov and T. Van Voorhis. Improving the accuracy of the nonlocal van der Waals density functional with minimal empiricism. *J. Chem. Phys.*, 130:104105, 2009.

[153] D. Lu, H. Nguyen, and G. Galli. Power series expansion of the random phase approximation correlation energy: The role of the third- and higher-order contributions. *J. Chem. Phys.*, 133:154110, 2010.

[154] K. Lee, É. D. Murray, L. Kong, B. I. Lundqvist, and D. C. Langreth. Higher-accuracy van der Waals density functional. *Phys. Rev. B*, 82:081101, 2010.

[155] Y. Zhang and W. Yang. Comment on "Generalized gradient approximation made simple". *Phys. Rev. Lett.*, 80:890, 1998.

[156] O. A. Vydrov and T. Van Voorhis. Nonlocal van der Waals density functional made simple. *Phys. Rev. Lett.*, 103:063004, 2009.

[157] A. Puzder, M. Dion, and D. C. Langreth. Binding energies in benzene dimers: Nonlocal density functional calculations. *J. Chem. Phys.*, 124:164105, 2006.

[158] T. Thonhauser, A. Puzder, and D. C. Langreth. Interaction energies of monosubstituted benzene dimers via nonlocal density functional theory. *J. Chem. Phys.*, 124:164106, 2006.

[159] T. Gould, E. Gray, and J. F. Dobson. van der Waals dispersion power laws for cleavage, exfoliation, and stretching in multiscale, layered systems. *Phys. Rev. B*, 79:113402, 2009.

[160] J. M. Soler, E. Artacho, J. D. Gale, A. Garca, J. Junquera, P. Ordejn, and D. Snchez-Portal. The Siesta method for ab initio order-N materials simulation. *J. Phys.: Cond. Matt.*, 14:2745, 2002.

[161] D. R. Bowler, R. Choudhury, M. J. Gillan, and T. Miyazaki. Recent progress with large-scale ab initio calculations: the CONQUEST code. *Phys. Status Solidi B*, 243:989–1000, 2006.

[162] V. Blum, R. Gehrke, F. Hanke, P. Havu, V. Havu, X. G. Ren, K. Reuter, and M. Scheffler. Ab initio molecular simulations with numeric atom-centered orbitals. *Comput. Phys. Commun.*, 180:2175, 2009.

[163] C. Schwartz. Importance of angular correlations between atomic electrons. *Phys. Rev.*, 126:1015, 1962.

[164] W. Kutzelnigg and J. D. Morgan. Rates of convergence of the partial-wave expansions of atomic correlation energies. *J. Chem. Phys.*, 96:4484, 1992.

[165] D. Feller. The use of systematic sequences of wave-functions for estimating the complete basis set, full configuration-interaction limit in water. *J. Chem. Phys.*, 98:7059, 1993.

[166] A. K. Wilson and T. H. Dunning. Benchmark calculations with correlated molecular wave functions. X. Comparison with "exact" MP2 calculations on Ne, HF, H_2O, and N_2. *J. Chem. Phys.*, 106:8718, 1997.

[167] M. C. Payne, M. P. Teter, D. C. Allan, T. A. Arias, and J. D. Joannopoulos. Iterative minimization techniques for *ab initio* total-energy calculations: molecular dynamics and conjugate gradients. *Rev. Mod. Phys.*, 64:1045, 1992.

[168] F. Gygi and A. Baldereschi. Self-consistent Hartree-Fock and screened-exchange calculations in solids - application to silicon. *Phys. Rev. B*, 34:4405, 1986.

[169] E. Hernandez, M. J. Gillan, and C. M. Goringe. Linear-scaling density-functional-theory technique: The density-matrix approach. *Phys. Rev. B*, 53:7147, 1996.

[170] S. Goedecker. Linear scaling electronic structure methods. *Rev. Mod. Phys.*, 71:1085, 1999.

[171] J. J. Mortensen, L. B. Hansen, and K. W. Jacobsen. Real-space grid implementation of the projector augmented wave method. *Phys. Rev. B*, 71:035109, 2005.

[172] L. Genovese, A. Neelov, S. Goedecker, T. Deutsch, S. A. Ghasemi, A. Willand, D. Caliste, O. Zilberberg, M. Rayson, A. Bergman, and R. Schneider. Daubechies wavelets as a basis set for density functional pseudopotential calculations. *J. Chem. Phys.*, 129:014109, 2008.

[173] H. J. Monkhorst and J. D. Pack. Special points for Brillouin-zone integrations. *Phys. Rev. B*, 13:5188, 1976.

[174] D. Vanderbilt. Soft self-consistent pseudopotentials in a generalized eigenvalue formalism. *Phys. Rev. B*, 41:7892, 1990.

[175] P. E. Blöchl. Projector augmented-wave method. *Phys. Rev. B*, 50:17953, 1994.

[176] G. Kresse and J. Joubert. From ultrasoft pseudopotentials to the projector augmented wave method. *Phys. Rev. B*, 59:1758, 1999.

[177] M. Marsman and G. Kresse. Relaxed core projector-augmented-wave method. *J. Chem. Phys.*, 125:104101, 2006.

[178] G. Kresse and J. Furthmüller. Efficiency of ab-initio total energy calculations for metals and semiconductors using a plane-wave basis set. *Comp. Mater. Sci.*, 6:15, 1996.

[179] S. J. Clark, M. D. Segall, C. J. Pickard, P. J. Hasnip, M. J. Probert, K. Refson, and M. C. Payne. First principles methods using CASTEP. *Z. Kristallogr.*, 220:567, 2005.

[180] J. VandeVondele, M. Krack, F. Mohamed, M. Parrinello, T. Chassaing, and J. Hutter. QUICKSTEP: Fast and accurate density functional calculations using a mixed Gaussian and plane waves approach. *Comput. Phys. Commun.*, 167:103, 2005.

[181] P. Giannozzi, S. Baroni, N. Bonini, M. Calandra, R. Car, C. Cavazzoni, D. Ceresoli, G. L. Chiarotti, M. Cococcioni, I. Dabo, A. Dal Corso, S. de Gironcoli, S. Fabris, G. Fratesi, R. Gebauer, U. Gerstmann, C. Gougoussis, A. Kokalj, M. Lazzeri, L. Martin-Samos,

N. Marzari, F. Mauri, R. Mazzarello, S. Paolini, A. Pasquarello, L. Paulatto, C. Sbraccia, S. Scandolo, G. Sclauzero, A. P. Seitsonen, A. Smogunov, P. Umari, and R. M. Wentzcovitch. QUANTUM ESPRESSO: a modular and open-source software project for quantum simulations of materials. *J. Phys.: Cond. Matt.*, 21:395502, 2009.

[182] W. A. Goddard, T. H. Dunning, W. J. Hunt, and P. J. Hay. Generalized valence bond description of bonding in low-lying states of molecules. *Acc. Chem. Res.*, 6:368, 1973.

[183] J. C. Slater and G. F. Koster. Simplified LCAO method for the periodic potential problem. *Phys. Rev.*, 94:1498, 1954.

[184] J. P. Stewart. Optimization of parameters for semiempirical methods IV: extension of MNDO, AM1, and PM3 to more main group elements. *J. Mol. Model.*, 10:155, 2004.

[185] B. G. Dick and A. W. Overhauser. Theory of dielectric constants of alkali halide crystals. *Phys. Rev.*, 112:90, 1958.

[186] N. H. de Leeuw and S. C. Parker. Molecular-dynamics simulation of MgO surfaces in liquid water using a shell-model potential for water. *Phys. Rev. B*, 58:13901, 1998.

[187] S. Patel and C. L. Brooks. CHARMM fluctuating charge force field for proteins: I parameterization and application to bulk organic liquid simulations. *J. Comp. Chem.*, 25:1, 2004.

[188] H. J. C. Berendsen, J. R. Grigera, and T. P. Straatsma. The missing term in effective pair potentials. *J. Phys. Chem.*, 91:6269, 1987.

[189] W. L. Jorgensen, J. Chandrasekhar, J. D. Madura, R. W. Impey, and M. L. Klein. Comparison of simple potential functions for simulating liquid water. *J. Chem. Phys.*, 79:926, 1983.

[190] J. L. F. Abascal and C. Vega. A general purpose model for the condensed phases of water: TIP4P/2005. *J. Chem. Phys.*, 123:234505, 2005.

[191] W. L. Jorgensen and J. D. Madura. Temperature and size dependence for Monte Carlo simulations of TIP4P water. *Mol. Phys.*, 56:1381, 1985.

[192] M. W. Mahoney and W. L. Jorgensen. A five-site model for liquid water and the reproduction of the density anomaly by rigid, nonpolarizable potential functions. *J. Phys. Chem.*, 112:8910, 2000.

[193] F. H. Stillinger and C. W. David. Polarization model for water and its ionic dissociation products. *J. Chem. Phys.*, 69:1473, 1978.

[194] P. Barnes, J. L. Finney, J. D. Nicholas, and J. E. Quinn. Cooperative effects in simulated water. *Nature*, 282:459, 1979.

[195] M. Sprik and M. L. Klein. A polarizable model for water using distributed charge sites. *J. Chem. Phys.*, 89:7556, 1988.

[196] C. J. Burnham, J. C. Li, S. S. Xantheas, and M. Leslie. The parametrization of a Thole-type all-atom polarizable water model from first principles and its application to the study of water clusters (n=2-21) and the phonon spectrum of ice Ih. *J. Chem. Phys.*, 110:4566, 1999.

[197] P. J. van Maaren and D. van der Spoel. Molecular dynamics simulations of water with novel shell-model potentials. *J. Phys. Chem. B*, 105:2618, 2001.

[198] Y. Wu, H. L. Tepper, and G. A. Voth. Flexible simple point-charge water model with improved liquid state properties. *J. Chem. Phys.*, 124:024503, 2006.

[199] M. P. Hodges, A. J. Stone, and S. S. Xantheas. Contribution of many-body terms to the energy for small water clusters: A comparison of ab initio calculations and accurate model potentials. *J. Phys. Chem. A*, 101:9163, 1997.

[200] G. C. Groenenboom, E. M. Mas, R. Bukowski, K. Szalewicz, P. E. S. Wormer, and A. van der Avoird. Water pair and three-body potential of spectroscopic quality from ab initio calculations. *Phys. Rev. Lett.*, 84:4072, 2000.

[201] G. S. Fanourgakis, G. K. Schenter, and S. S. Xantheas. A quantitative account of quantum effects in liquid water. *J. Chem. Phys.*, 125:141102, 2006.

[202] S. Habershon, T. E. Markland, and D. E. Manolopoulos. Competing quantum effects in the dynamics of a flexible water model. *J. Chem. Phys.*, 131:024501, 2009.

[203] P. L. Freddolino, F. Liu, M. Gruebele, and K. Schulten. Ten-microsecond molecular dynamics simulation of a fast-folding WW domain. *Biophys. J.*, 94:L75, 2008.

[204] D. E. Shaw, P. Maragakis, K. Lindorff-Larsen, S. Piana, R. O. Dror, M. P. Eastwood, J. A. Bank, J. M. Jumper, J. K. Salmon, Y. Shan, and W. Wriggers. Atomic-level characterization of the structural dynamics of proteins. *Science*, 330:341, 2010.

[205] A Laio and M Parrinello. Escaping free-energy minima. *Proc. Natl. Acad. Sci. U. S. A.*, 99:12562, 2002.

[206] H. Metiu. *Physical Chemistry: Statistical mechanics*. Taylor & Francis, New York, USA, 2006.

[207] D. G. Truhlar and B. C. Garrett. Variational transition-state theory. *Acc. Chem. Res.*, 13:440, 1980.

[208] H. A. Kramers. Brownian motion in a field of force and the diffusion model of chemical reactions. *Physica*, 7:284, 1940.

[209] J. A. Montgomery, D. Chandler, and B. J. Berne. Trajectory analysis of a kinetic-theory for isomerization dynamics in condensed phases. *J. Chem. Phys.*, 70:4056, 1979.

[210] J. E. Straub, D. A. Hsu, and B. J. Berne. On determining reaction kinetics by molecular dynamics using absorbing barriers. *J. Phys. Chem.*, 89:5188, 1985.

[211] A. F. Voter and J. D. Doll. Dynamical corrections to transition-state theory for multistate systems - surface self-diffusion in the rare-event regime. *J. Chem. Phys.*, 82:80, 1985.

[212] G. H. Vineyard. Frequency factors and isotope effects in solid state rate processes. *J. Phys. Chem. Solids*, 3:121, 1957.

[213] G. Henkelman, G. Jóhannesson, and H. Jónsson. *Progress on Theoretical Chemistry and Physics*. edited by S. Schwartz, Kluwer Academic, New York, 2000.

[214] H. B. Schlegel. Exploring potential energy surfaces for chemical reactions: An overview of some practical methods. *J. Comput. Chem.*, 24:1514, 2003.

[215] G. Mills, H. Jónsson, and G. K. Schenter. Reversible work transition-state theory - application to dissociative adsorption of hydrogen. *Surf. Sci.*, 324:305, 1995.

[216] G. Henkelman and H. Jónsson. Improved tangent estimate in the nudged elastic band method for finding minimum energy paths and saddle points. *J. Chem. Phys.*, 113:9978, 2000.

[217] S. A. Trygubenko and D. J. Wales. A doubly nudged elastic band method for finding transition states. *J. Chem. Phys.*, 120:2082, 2004. *ibid*, 120:7820, 2004.

[218] M. J. S. Dewar, E. F. Healy, and J. J. P. Stewart. Location of transition-states in reaction-mechanisms. *J. Chem. Soc.-Faraday Trans. II*, 80:227, 1984.

[219] G. Henkelman and H. Jónsson. A dimer method for finding saddle points on high dimensional potential surfaces using only first derivatives. *J. Chem. Phys.*, 111:7010, 1999.

[220] B. Peters, A. Heyden, A. T. Bell, and A. Chakraborty. A growing string method for determining transition states: Comparison to the nudged elastic band and string methods. *J. Chem. Phys.*, 120:7877, 2004.

[221] A. Heyden, A. T. Bell, and F. J. Keil. Efficient methods for finding transition states in chemical reactions: Comparison of improved dimer method and partitioned rational function optimization method. *J. Chem. Phys.*, 123:224101, 2005.

[222] Y. Tateyama, T. Ogitsu, K. Kusakabe, and S. Tsuneyuki. Constant-pressure first-principles studies on the transition states of the graphite-diamond transformation. *Phys. Rev. B*, 54:14994, 1996.

[223] G. T. Barkema and N. Mousseau. Event-based relaxation of continuous disordered systems. *Phys. Rev. Lett.*, 77:4358, 1996.

[224] B. J. Finlayson-Pitts. The tropospheric chemistry of sea salt: A molecular-level view of the chemistry of NaCl and NaBr. *Chem. Rev.*, 103:4801, 2003.

[225] E. N. Korol and O. Y. Posudievsky. Adsorption on the surface of ionic-crystals and the effect of applied electric-field. *Surf. Sci.*, 169:104, 1986.

[226] B. Wassermann, S. Mirbt, J. Reif, J. C. Zink, and E. Matthias. Clustered water-adsorption on the NaCl(100) surface. *J. Chem. Phys.*, 98:10049, 1993.

[227] E. V. Stefanovich and T. N. Truong. Embedded density functional approach for calculations of adsorption on ionic crystals. *J. Chem. Phys.*, 104:2946, 1996.

[228] K. Jug and G. Geudtner. Comparative studies on the adsorption of small molecules at NaCl and MgO surfaces. *J. Mol. Catal. A-Chem.*, 119:143, 1997.

[229] D. P. Taylor, W. P. Hess, and M. I. McCarthy. Structure and energetics of the water/NaCl(100) interface. *J. Phys. Chem. B*, 101:7455, 1997.

[230] A. Allouche. Water adsorption on NaCl(100): a quantum ab-initio cluster calculation. *Surf. Sci.*, 406:279, 1998.

[231] E. Stöckelmann and R. Hentschke. A molecular-dynamics simulation study of water on NaCl(100) using a polarizable water model. *J. Chem. Phys.*, 110:12097, 1999.

[232] O. Engkvist and A. J. Stone. Adsorption of water on NaCl(001). I. intermolecular potentials and low temperature structures. *J. Chem. Phys.*, 110:12089, 1999.

[233] H. Meyer, P. Entel, and J. Hafner. Physisorption of water on salt surfaces. *Surf. Sci.*, 488:177, 2001.

[234] J. M. Park, J. H. Cho, and K. S. Kim. Atomic structure and energetics of adsorbed water on the NaCl(001) surface. *Phys. Rev. B*, 69:233403, 2004.

[235] P. Cabrera-Sanfelix, A. Arnau, G. R. Darling, and D. Sanchez-Portal. Water adsorption and diffusion on NaCl(100). *J. Phys. Chem. B*, 110:24559, 2006.

[236] Y. Yang, S. Meng, and E. G. Wang. Water adsorption on a NaCl (001) surface: A density functional theory study. *Phys. Rev. B*, 74:245409, 2006.

[237] P. Cabrera-Sanfelix, A. Arnau, G. R. Darling, and D. Sanchez-Portal. On the structure of the first hydration layer on NaCl(100): Role of hydrogen bonding. *J. Chem. Phys.*, 126:214707, 2007.

[238] P. B. Barraclough and P. G. Hall. Adsorption of water-vapor by lithium-fluoride, sodium-fluoride and sodium-chloride. *Surf. Sci.*, 46:393, 1974.

[239] S. Fölsch, A. Stock, and M. Henzler. 2-dimensional water condensation on the NaCl(100) surface. *Surf. Sci.*, 264:65, 1992.

[240] L. W. Bruch, A. Glebov, J. P. Toennies, and H. Weiss. A helium atom scattering study of water-adsorption on the NaCl(100) single-crystal surface. *J. Chem. Phys.*, 103:5109, 1995.

[241] G. E. Ewing and S. J. Peters. Adsorption of water on NaCl. *Surf. Rev. Lett.*, 4:757, 1997.

[242] S. J. Peters and G. E. Ewing. Water on salt: An infrared study of adsorbed H_2O on NaCl(100) under ambient conditions. *J. Phys. Chem. B*, 101:10880, 1997.

[243] Q. Dai, J. Hu, and M. Salmeron. Adsorption of water on NaCl(001) surfaces: Role of atomic steps. *J. Phys. Chem. B*, 101:1994, 1997.

[244] B. Li, A. Michaelides, and M. Scheffler. How strong is the bond between water and salt? *Surf. Sci.*, 602:L135, 2008.

[245] R. A. Olsen, G. J. Kroes, G. Henkelman, A. Arnaldsson, and H. Jónsson. Comparison of methods for finding saddle points without knowledge of the final states. *J. Chem. Phys.*, 121:9776, 2004.

[246] E. F. Koslover and D. J. Wales. Comparison of double-ended transition state search methods. *J. Chem. Phys.*, 127:134102, 2007.

[247] D. Sheppard, R. Terrell, and G. Henkelman. Optimization methods for finding minimum energy paths. *J. Chem. Phys.*, 128:134106, 2008.

[248] Y. Abashkin and N. Russo. Transition-state structures and reaction profiles from constrained optimization procedure - implementation in the framework of density-functional theory. *J. Chem. Phys.*, 100:4477, 1994.

[249] G. Henkelman, B. P. Uberuaga, and H. Jónsson. A climbing image nudged elastic band method for finding saddle points and minimum energy paths. *J. Chem. Phys.*, 113:9901, 2000.

[250] M. J. Rothman and L. L. Lohr. Analysis of an energy minimization method for locating transition states on potential energy hypersurfaces. *Chem. Phys. Lett.*, 70:405, 1980.

[251] G. T. Barkema and N. Mousseau. The activation-relaxation technique: an efficient algorithm for sampling energy landscapes. *Comp. Mater. Sci.*, 20:285, 2001.

[252] A. Michaelides and P. Hu. Hydrogenation of S to H_2S on Pt(111): A first-principles study. *J. Chem. Phys.*, 115:8570, 2001.

[253] G. Kresse and J. Hafner. Ab initio molecular dynamics for liquid metals. *Phys. Rev. B*, 47:558, 1993.

[254] B. Li, A. Michaelides, and M. Scheffler. Density functional theory study of flat and stepped NaCl(001). *Phys. Rev. B*, 76:075401, 2007.

[255] B. Santra *et al.* In preparation.

[256] A. Verdaguer, G. M. Sacha, M. Luna, D. Frank Ogletree, and M. Salmeron. Initial stages of water adsorption on NaCl (100) studied by scanning polarization force microscopy. *J. Chem. Phys.*, 123, 2005.

[257] S. J. Peters and G. E. Ewing. Thin film water on NaCl(100) under ambient conditions: An infrared study. *Langmuir*, 13:6345, 1999.

[258] M. C. Foster and G. E. Ewing. Adsorption of water on the NaCl(001) surface. ii. an infrared study at ambient temperatures. *J. Chem. Phys.*, 112:6817, 2000.

[259] S. Fölsch and M. Henzler. Water adsorption on the NaCl(100) surface. *Surf. Sci.*, 264:65, 1992.

[260] H. Shindo, M. Ohashi, O. Tateishi, and A. Seo. Atomic force microscopic observation of step movements on NaCl(001) and NaF(001) with the help of adsorbed water. *J. Chem. Soc. Faraday Trans.*, 93:1169, 1997.

[261] H. Shindo and M. Ohashi. In-situ AFM observation of crystal growth of NaCl in an aqueous solution. *Appl. Phys. A*, 66:S487, 1998.

[262] M. Luna, F. Rieutord, N. A. Melman, Q. Dai, and M. Salmeron. Adsorption of water on alkali halide surfaces studied by scanning polarization force microscopy. *J. Phys. Chem. A*, 102:6793, 1998.

[263] A. Verdaguer, J. J. Segura, J. Fraxedas, H. Bluhm, and M. Salmeron. Correlation between charge state of insulating NaCl surfaces and ionic mobility induced by water adsorption: A combined ambient pressure X-ray photoelectron spectroscopy and scanning force microscopy study. *J. Phys. Chem. C*, 112:16898, 2008.

[264] S. Yamabe, H. Kouno, and K. Matsumura. A mechanism of the ion separation of the NaCl microcrystal via the association of water clusters. *J. Phys. Chem. B*, 104:10242, 2000.

[265] P. Jungwirth. How many waters are necessary to dissolve a rock salt molecule? *J. Phys. Chem. A*, 104:145, 2000.

[266] H. Ohtaki, N. Fukushima, E. Hayakawa, and I. Okada. Dissolution process of sodium chloride crystal in water. *Pure & Appl. Chem.*, 60:1321, 1988.

[267] R. Bahadur, L. M. Russell, S. Alavi, S. T. Martin, and P. R. Buseck. Void-induced dissolution in molecular dynamics simulations of NaCl and water. *J. Chem. Phys.*, 124:154713, 2006.

[268] A. Y. Zasetsky, J. J. Sloan, and I. M. Svishchev. Dissolution of solid NaCl nanoparticles embedded in supersaturated water vapor probed by molecular dynamic Simulations. *J. Phys. Chem. A*, 112:3114, 2008.

[269] Y. Yang, S. Meng, L. F. Xu, E. G. Wang, and S. Gao. Dissolution dynamics of NaCl nanocrystal in liquid water. *Phys. Rev. E*, 72:012602, 2005.

[270] L. Liu, M. Krack, and A. Michaelides. Density oscillations in a nanoscale water film on salt: Insight from ab initio molecular dynamics. *J. Am. Chem. Soc.*, 130:8572, 2008.

[271] L. Liu, M. Krack, and A. Michaelides. Interfacial water: A first principles molecular dynamics study of a nanoscale water film on salt. *J. Chem. Phys.*, 130:234702, 2009.

[272] L. Liu, A. Laio, and A. Michaelides. Initial stages of salt crystal dissolution determined with ab initio molecular dynamics. *Phys. Chem. Chem. Phys.*, 2011. *in press.*

[273] E. Lindahl, B. Hess, and D. van der Spoel. Gromacs 3.0: A package for molecular simulation and trajectory analysis. *J. Mol. Mod.*, 7:306, 2001.

[274] B. Hess, C. Kutzner, D. van der Spoel, and E. Lindahl. Gromacs 4: Algorithms for highly efficient, load-balanced, and scalable molecular simulation. *J. Chem. Theory Comput.*, 4:435, 2008.

[275] J. Wang, P. Cieplak, and P. A. Kollman. How well does a restrained electrostatic potential (resp) model perform in calculating conformational energies of organic and biological molecules? *J. Comput. Chem.*, 21:1049, 2000.

[276] E. J. Sorin and V. S. Pande. Exploring the helix-coil transition via all-atom equilibrium ensemble simulations. *Biophys. J.*, 88:2472 – 2493, 2005.

[277] D. J. Binks. PhD thesis, University of Surrey, 1994.

[278] G. Lamoureux and B. Roux. Absolute hydration free energy scale for alkali and halide ions established from simulations with a polarizable force field. *J. Phys. Chem. B*, 110:3308, 2006.

[279] G. Lamoureux, A. D. MacKerell, and B. Roux. A simple polarizable model of water based on classical drude oscillators. *J. Chem. Phys.*, 119:5185, 2003.

[280] G. Lamoureux, E. Harder, I. V. Vorobyov, B. Roux, and A. D. MacKerell. A polarizable model of water for molecular dynamics simulations of biomolecules. *Chem. Phys. Lett.*, 418:245, 2006.

[281] D. J. Wales. *Energy Landscapes: with applications to clusters, biomolecules and glasses.* Cambridge University Press, Cambridge, UK, 2003.

[282] C. Ignatius. Master's thesis, University College London, 2010.

[283] P. Cabrera-Sanfelix and G. R. Darling. Dissociative adsorption of water at vacancy defects in graphite. *J. Phys. Chem. C*, 111:18258, 2007.

[284] B. Ahlswede and K. Jug. MSINDO study of the adsorption of water molecules at defective NaCl(100) surfaces. *Surf. Sci.*, 439:86, 1999.

[285] T. Otsuka, T. Miyazaki, T Ohno, D. R. Bowler, and M. J. Gillan. Accuracy of order-N density-functional theory calculations on DNA systems using CONQUEST. *J. Phys.: Cond. Matt.*, 20:294201, 2008.

[286] L. Grill, M. Dyer, L. Lafferentz, M. Persson, M. V. Peters, and S. Hecht. Nano-architectures by covalent assembly of molecular building blocks. *Nature Nanotechnol.*, 2:687, 2007.

[287] O. M. Yaghi and H. L. Li. Hydrothermal synthesis of a metal-organic framework containing large rectangular channels. *J. Am. Chem. Soc.*, 117:10401, 1995.

[288] D. N. Dybtsev, H. Chun, S. H. Yoon, D. Kim, and K. Kim. Microporous manganese formate: A simple metal-organic porous material with high framework stability and highly selective gas sorption properties. *J. Am. Chem. Soc.*, 126:32, 2004.

[289] T. Schwabe and S. Grimme. Double-hybrid density functionals with long-range dispersion corrections: higher accuracy and extended applicability. *Phys. Chem. Chem. Phys.*, 9:3397, 2007.

[290] D. C. Langreth, B. I. Lundqvist, S. D. Chakarova-Käck, V. R. Cooper, M. Dion, P. Hyldgaard, A. Kelkkanen, J. Kleis, L. Kong, S. Li, P. G. Moses, É. Murray, A. Puzder, H. Rydberg, E. Schroder, and T. Thonhauser. A density functional for sparse matter. *J Phys.: Cond. Matt.*, 21:084203, 2009.

[291] A. K. Kelkkanen, B. I. Lundqvist, and J. K. Nørskov. Density functional for van der Waals forces accounts for hydrogen bond in benchmark set of water hexamers. *J. Chem. Phys.*, 131:046102, 2009.

[292] A. Gulans, M. J. Puska, and R. M. Nieminen. Linear-scaling self-consistent implementation of the van der Waals density functional. *Phys. Rev. B*, 79:201105(R), 2009.

[293] L. Gráfová, M. Pitoňák, J. Řezáč, and P. Hobza. Comparative study of selected wave function and density functional methods for noncovalent interaction energy calculations using the extended S22 data set. *J. Chem. Theory Comput.*, 6:2365, 2010.

[294] T. Takatani, E. G. Hohenstein, M. Malagoli, M. S. Marshall, and C. D. Sherrill. Basis set consistent revision of the S22 test set of noncovalent interaction energies. *J. Chem. Phys.*, 132:144104, 2010.

[295] R. Podeszwa, K. Patkowski, and K. Szalewicz. Improved interaction energy benchmarks for dimers of biological relevance. *Phys. Chem. Chem. Phys.*, 12:5974, 2010.

[296] T. P. Tauer, M. E. Derrick, and C. D. Sherrill. Estimates of the ab initio limit for sulfur–π interactions: The H_2S–benzene dimer. *J. Phys. Chem. A*, 109:191, 2005.

[297] A. L. Ringer, M. S. Figgs, M. O. Sinnokrot, and C. D. Sherrill. Aliphatic C–H/π interactions: Methane–benzene, methane–phenol, and methane–indole complexes. *J. Phys. Chem. A*, 110:10822, 2006.

[298] J. Ma, D. Alfe, A. Michaelides, and E. Wang. The water-benzene interaction: Insight from electronic structure theories. *J. Chem. Phys.*, 130:154303, 2009.

[299] E. E. Dahlke, R. M. Olson, H. R. Leverentz, and D. G. Truhlar. Assessment of the accuracy of density functionals for prediction of relative energies and geometries of low-lying isomers of water hexamers. *J. Phys. Chem. A*, 112:3976–3984, 2008.

[300] B. Santra, A. Michaelides, and M. Scheffler. On the accuracy of density-functional theory exchange-correlation functionals for H bonds in small water clusters: Benchmark approaching the complete basis set limit. *J. Chem. Phys.*, 127:184104, 2007.

[301] S. Brunauer, P. H. Emmett, and E. Teller. Adsorption of gases in multimolecular layers. *J. Am. Chem. Soc.*, 60:309, 1938.

[302] E. Zaremba and W. Kohn. Van der Waals interaction between an atom and a solid surface. *Phys. Rev. B*, 13:2270, 1976.

[303] D. Rocca, R. Gebauer, F. De Angelis, M. K. Nazeeruddin, and S. Baroni. Time-dependent density functional theory study of squaraine dye-sensitized solar cells. *Chem. Phys. Lett.*, 475:49, 2009.

[304] M. S. Dyer, A. Robin, S. Haq, R. Raval, M. Persson, and J. Klimeš. Understanding the interaction of the porphyrin macrocycle to reactive metal substrates: Structure, bonding and adatom capture. *ACS Nano*, 5:1831, 2011.

[305] G. Román-Pérez and J. M. Soler. Efficient implementation of a van der Waals density functional: Application to double-wall carbon nanotubes. *Phys. Rev. Lett.*, 103:096102, 2009.

[306] P. Lazić, N. Atodiresei, M. Alaei, V. Calciuć, and S. Blügel. JuNoLo - Jülich nonlocal code for parallel post-processing evaluation of vdW-DF correlation energy. *Comput. Phys. Commun.*, 181:371, 2010.

[307] O. A. Vydrov and T. Van Voorhis. Implementation and assessment of a simple nonlocal van der Waals density functional. *J. Chem. Phys.*, 132:164113, 2010.

[308] D. J. Lacks and R. G. Gordon. Pair interactions of rare-gas atoms as a test of exchange-energy-density functionals in regions of large density gradients. *Phys. Rev. A*, 47:4681, 1993.

[309] A. D. Becke. On the large-gradient behavior of the density functional exchange energy. *J. Chem. Phys.*, 85:7184, 1986.

[310] J. P. Perdew and W. Yue. Accurate and simple density functional for the electronic exchange energy: Generalized gradient approximation. *Phys. Rev. B*, 33:8800, 1986.

[311] B. Hammer, L. B. Hansen, and J. K. Nørskov. Improved adsorption energetics within density-functional theory using revised Perdew-Burke-Ernzerhof functionals. *Phys. Rev. B*, 59:7413, 1999.

[312] G. K. H. Madsen. Functional form of the generalized gradient approximation for exchange: The PBEα functional. *Phys. Rev. B*, 75:195108, 2007.

[313] J. P. Perdew, A. Ruzsinszky, G. I. Csonka, O. A. Vydrov, G. E. Scuseria, L. A. Constantin, X. Zhou, and K. Burke. Restoring the density-gradient expansion for exchange in solids and surfaces. *Phys. Rev. Lett.*, 100:136406, 2008.

[314] F. O. Kannemann and A. D. Becke. Van der Waals interactions in density-functional theory: Rare gas diatomics. *J. Chem. Theory Comput.*, 5:719, 2009.

[315] É. D. Murray, K. Lee, and D. C. Langeth. Investigation of exchange energy density functional accuracy for interacting molecules. *J. Chem. Theo. Comput.*, 5:2754, 2009.

[316] O. A. Vydrov, Q. Wu, and T. Van Voorhis. Self-consistent implementation of a nonlocal van der Waals density functional with a Gaussian basis set. *J. Chem. Phys.*, 129:014106, 2008.

[317] L. Romaner, X. Ren, C. Ambrosch-Draxl, and M. Scheffler. Role of non-local correlations for the cohesive properties of the coinage metals. submitted.

[318] J. Carrasco, A. Michaelides, M. Forster, S. Haq, R. Raval, and A. Hodgson. A one-dimensional ice structure built from pentagons. *Nature Mater.*, 8:427, 2009.

[319] J. Carrasco, B. Santra, J. Klimeš, and A. Michaelides. To wet or not to wet? Dispersion forces tip the balance for water-ice on metals. *Phys. Rev. Lett.*, 106:026101, 2011.

[320] Y. Muto. Force between nonpolar molecules. *J. Phys. Math. Soc. Japan*, 17:629, 1943.

[321] B. M. Axilrod. Interaction of the van der Waals type between three atoms. *J. Chem. Phys.*, 11:299, 1943.

[322] A. J. Misquitta, J. Spencer, A. J. Stone, and A. Alavi. Dispersion interactions between semiconducting wires. *Phys. Rev. B*, 82:075312, 2010.

[323] G. Jansen, R. Liu, and J. G. Ángyán. On the equivalence of ring-coupled cluster and adiabatic connection fluctuation-dissipation theorem random phase approximation correlation energy expressions. *J. Chem. Phys.*, 133:154106, 2010.

[324] O. A. von Lilienfeld and A. Tkatchenko. Two- and three-body interatomic dispersion energy contributions to binding in molecules and solids. *J. Chem. Phys.*, 132:234109, 2010.

[325] J. Klimeš, D. R. Bowler, and A. Michaelides. Chemical accuracy for the van der Waals density functional. *J. Phys.: Cond. Matt.*, 22:022201, 2010.

[326] V. R. Cooper. Van der waals density functional: An appropriate exchange functional. *Phys. Rev. B*, 81:161104, 2010.

[327] P. J. Feibelman. Lattice match in density functional calculations: ice Ih vs. β-AgI. *Phys. Chem. Chem. Phys.*, 10:4688, 2008.

[328] J. Friedel. The absorption of light by noble metals and its relation to the van der Waals contribution to the cohesive energy. *Proc. Phys. Soc. B*, 65:769, 1952.

[329] J. J. Rehr, E. Zaremba, and W. Kohn. van der Waals forces in the noble metals. *Phys. Rev. B*, 12:2062, 1975.

[330] D. D. Richardson and J. Mahanty. van der Waals contribution to the binding energy of noble metals. *J. Phys. C: Solid State Phys.*, 10:3971, 1977.

[331] J. C. Upadhyaya and S. Wang. Effect of van der Waals forces on the crystal structure of heavy alkali metals. *Phys. Lett.*, 73A:238, 1979.

[332] J. Tao, J. P. Perdew, and A. Ruzsinszky. Long-range van der Waals attraction and alkali-metal lattice constants. *Phys. Rev. B*, 81:233102, 2010.

[333] G. I. Csonka, J. P. Perdew, A. Ruzsinszky, P. H. T. Philipsen, S. Lebègue, J. Paier, O. A. Vydrov, and J. G. Ángyán. Assessing the performance of recent density functionals for bulk solids. *Phys. Rev. B*, 79:155107, 2009.

[334] P. Haas, F. Tran, and P. Blaha. Calculation of the lattice constant of solids with semilocal functionals. *Phys. Rev. B*, 79:085104, 2009.

[335] A. E. Mattsson, R. Armiento, J. Paier, G. Kresse, J. M. Wills, and T. R. Mattsson. The AM05 density functional applied to solids. *J. Chem. Phys.*, 128:084714, 2008.

[336] J. Paier, R. Hirschl, M. Marsman, and G. Kresse. The Perdew-Burke-Ernzerhof exchange-correlation functional applied to the G2-1 test set using a plane-wave basis set. *J. Chem. Phys.*, 122:234102, 2005.

[337] R. Armiento and A. E. Mattsson. Functional designed to include surface effects in self-consistent density functional theory. *Phys. Rev. B*, 72:085108, 2005.

[338] Z. Wu and R. E.. Cohen. More accurate generalized gradient approximation for solids. *Phys. Rev. B*, 73:026403, 2006.

[339] S. D. Chakarova-Käck, E. Schröder, B. I. Lundqvist, and D. C. Langreth. Application of van der Waals density functional to an extended system: Adsorption of benzene and naphthalene on graphite. *Phys. Rev. Lett.*, 96:146107, 2006.

[340] E. Ziambaras, J. Kleis, E. Schröder, and P. Hyldgaard. Potassium intercalation in graphite: A van der Waals density-functional study. *Phys. Rev. B*, 76:155425, 2007.

[341] F. Tran, R. Laskowski, P. Blaha, and K. Schwarz. Performance on molecules, surfaces, and solids of the Wu-Cohen GGA exchange-correlation energy functional. *Phys. Rev. B*, 75:115131, 2007.

[342] A. E. Mattsson and T. R. Mattsson. AM05 density functional applied to the water molecule, dimer, and bulk liquid. *J. Chem. Theory Comput.*, 5:887, 2009.

[343] T. van Mourik and R. J. Gdanitz. A critical note on density functional theory studies on rare-gas dimers. *J. Chem. Phys.*, 116:9620, 2002.

[344] B. J. Lynch and D. G. Truhlar. Small representative benchmarks for thermochemical calculations. *J. Phys. Chem. A*, 107:8996, 2003.

[345] K. Pernal, R. Podeszwa, K. Patkowski, and K. Szalewicz. Dispersionless density functional theory. *Phys. Rev. Lett.*, 103:263201, 2009.

[346] T. Thonhauser, V. R. Cooper, L. Shen, A. Puzder, P. Hyldgaard, and D. C. Langreth. Van der Waals density functional: Self-consistent potential and the nature of the van der Waals bond. *Phys. Rev. B*, 76:125112, 2007.

[347] K. Rościszewski, B. Paulus, P. Fulde, and H. Stoll. Ab initio calculation of ground-state properties of rare-gas crystals. *Phys. Rev. B*, 60:7905, 1999.

[348] S. J. Nolan, M. J. Gillan, D. Alfè, N. L. Allan, and F. R. Manby. Accurate calculation of properties of crystalline lithium hydride using correlated wavefunction theory. *Phys. Rev. B*, 80:165109, 2009.

[349] S. Tosoni and J. Sauer. Accurate quantum chemical energies for the interaction of hydrocarbons with oxide surfaces: CH_4/MgO(001). *Phys. Chem. Chem. Phys.*, 12:14330, 2010.

[350] C. W. Bauschlicher, S. R. Langhoff, H. Partridge, J. E. Rice, and A. Komornicki. A theoretical study of $Na(H_2O)_n^+$ ($n = 1$–4). *J. Chem. Phys.*, 95:5142, 1991.

[351] K. Hashimoto and K. Morokuma. Ab initio molecular orbital study of $Na(H_2O)_n$ ($n = 1$–6) clusters and their ions. Comparison of electronic structure of the "surface" and "interior" complexes. *J. Phys. Chem.*, 114:11436, 1994.

[352] E. D. Glendening and D. Feller. Cation–water interactions: The $M^+(H_2O)_n$ clusters for alkali metals, M = Li, Na, K, Rb, and Cs. *J. Phys. Chem.*, 99:3060, 1995.

[353] H. J. C. Berendsen, D. van der Spoel, and R. van Drunen. Gromacs: A message-passing parallel molecular dynamics implementation. *Comp. Phys. Comm.*, 91:43, 1995.

[354] W. L. Jorgensen, D. S. Maxwell, and J. Tirado-Rives. Development and testing of the OPLS all-atom force field on conformational energetics and properties of organic liquids. *J. Am. Chem. Soc.*, 118:11225, 1996.

[355] M. Levitt, M. Hirshberg, R. Sharon, and V. Daggett. Potential energy function and parameters for simulations of the molecular dynamics of proteins and nucleic acids in solution. *Comp. Phys. Commun.*, 91:215, 1995.

[356] W. R. P. Scott, P. H. Hunenberger, I. G. Tironi, A. E. Mark, S. R. Billeter, J. Fennen, A. E. Torda, T. Huber, P. Kruger, and W. F. van Gunsteren. The GROMOS biomolecular simulation program package. *J. Phys. Chem. A*, 103:3596, 1999.

Acknowledgements

I would like to thank to all those who supported me during my doctoral studies. The work presented would not be possible without the kind support of my supervisor, Prof. Angelos Michaelides and benefited greatly from our discussions. I appreciate deeply the improvements of various of my skills that I have obtained during my stay with his group as well as for supporting me in attending scientific conferences and meeting scientists in the field. I also thank my second supervisor, Dr. David Bowler for useful discussions.

I also thank the members of the ICE group for creating a nice environment, namely Dr. Limin Liu, Dr. Xiaoliang Hu, Dr. Xinzheng Li, Dr. Bo Li, Dr. Changjun Zhang, Dr. Ding Pan, and Dr. Jie Ma not only for discussions about physics and chemistry but also about Chinese. Erlend Davidson for any computer related matter, most of all our compilation of VASP on the Cray-X2, which enabled the salt dissolution study. Dr. Brent Walker for a lot of help, fun, and finding nice places where to eat. Dr. Biswajit Santra and Dr. Javier Carrasco for lots of exciting results. Dr. Anna Kimmel as well as the new colleagues Stephen Cox, Gabriella Graziano, and Gabriele Tocci for interesting discussions.

I would like to thank my family for all that they have done in allowing me to reach this point. And finally, I'd like to thank Eva (my sweetie) for everything.

Publications

The work presented in this thesis has lead to the following publications:

J. Klimeš, D.R. Bowler, A. Michaelides, A critical assessment of theoretical methods for finding reaction pathways and transition states of surface processes. J. Phys.: Cond. Mat., **22**, 074203 (2010). Part of the special issue in celebration of Prof. Michael Gillan's birthday.

J. Klimeš, D.R. Bowler, A. Michaelides, Chemical accuracy for the van der Waals density functional. J. Phys.: Cond. Mat. **22**, 022201 (2010). Accepted as a fast track communication and awarded Publication Price of UCL Chemistry department.

J. Klimeš, D.R. Bowler, and A. Michaelides, Van der Waals density functionals applied to solids. Phys. Rev. B *accepted*, arXiv:1102.1358.

I contributed with the methods developed in this thesis to the publications:

X. L. Hu, J. Klimeš, A. Michaelides, Proton transfer in adsorbed water dimers. Phys. Chem. Chem. Phys. **12**, 3953 (2010).

J. Carrasco, B. Santra, J. Klimeš, J. and A. Michaelides, To wet or not to wet? Dispersion forces tip the balance for water-ice on metals. Phys. Rev. Lett. **106**, 026101 (2011).

M. Dyer, A. Robin, S. Haq, R. Raval, M. Persson, and J. Klimeš, Understanding the interaction of the porphyrin macrocycle to reactive metal substrates: Structure, bonding and adatom capture. ACS Nano **5**, 1831 (2011).

X. L. Hu, J. Carrasco, J. Klimeš, A. Michaelides, Towards a general understanding of water monomer adsorption on flat insulating surfaces, Phys. Chem. Chem. Phys., *accepted*.